Quaternary Dating Studies using ESR Signals, with Emphasis on Shell, Coral, Tooth Enamel and Quartz

A thesis submitted for the degree of

DOCTOR OF PHILOSOPHY

of

THE AUSTRALIAN NATIONAL UNIVERSITY

by

HIROYUKI YOSHIDA
吉田 裕之

B.Sc. (Yamagata)

RESEARCH SCHOOL OF CHEMISTRY

April 1996

CERTIFICATE OF ORIGINALITY

The work presented herein has not been submitted to any other university or institution for a higher degree and, unless acknowledged, is my own original work.

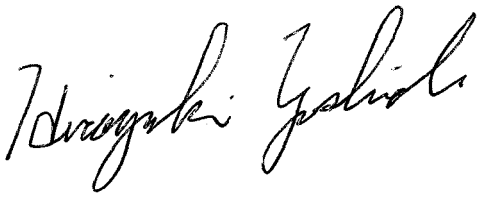

Hiroyuki Yoshida

18th April 1996

Acknowledgements

This study would not have been possible without the advice and assistance of several organisations and many individuals. First of all, I am particularly grateful to Dr Steven Brumby, Professor Athelstan L. J. Beckwith (Research School of Chemistry), Dr Peter S. Roy (Geological Survey of New South Wales) and Professor Robin F. Warner (Sydney University) for initiating a great opportunity to study in Australia and for their long-standing support. Much useful information relating to ESR dating has been provided by Dr Rainer Grün at the Quaternary Dating Research Centre. Professor John Chappell at the Division of Archaeology and Natural History, Research School of Pacific and Asian Studies, has given useful advice and information and provided the opportunity for drilling at Lake George, New South Wales. I would like to thank Dr Richard G. Roberts and Dr Nigel A. Spooner, Division of Archaeology and Natural History, Research School of Pacific and Asian Studies, for providing quartz samples, encouraging advice, and information concerning TL and OSL dating. The targets for AMS ^{14}C dating were prepared by Mr John Head at the Quaternary Dating Research Centre, Research School of Pacific and Asian Studies and the isotope ratios were measured by Dr Keith Fifield at the Research School of Physical Sciences, and Engineering. I am grateful to Dr Andrew Murray and Ms. Jacquie Olley at the Division of Water Resources, CSIRO, for instructions on sample preparation for high-resolution γ-ray spectroscopy and making the spectrometer available. Ms. Robin Westcott, Department of Geology, generously granted access to an X-ray diffraction spectrometer to analyse mineral components in the shell samples. Uranium contents of shell samples were determined using an ICP-MS by Ms. Pat Oswald-Sealy at the Research School of Earth Sciences, and Ms. Lois Taylor at the Quaternary Dating Research Centre. ^{60}Co γ-source irradiations of the samples were carried out using the facility of Dr Tony Pryor at the Division of Plant Industry, CSIRO. Professor John E. Parkington and Dr Duncan E. Miller at the Department of Archaeology, University of Cape Town, initiated the field trip to Elands Bay, South Africa, and supplied geological information on the sampling sites.

Abstract

In this study, the electron spin resonance (ESR) method is examined as a suitable dating tool to estimate the age of Quaternary materials. Although ESR dating has contributed substantially to earth science and archaeological studies, a standard procedure has not yet been developed for mollusc shell. Also, there has not been any practical application of ESR to the dating of sediments using solar-reset quartz. In this study, recently published and newly developed ESR methods are tested and compared with independent age controls (e.g. obtained by ^{14}C, U-series, thermoluminescence and optically stimulated luminescence) for mollusc shell, coral and quartz.

Annealing experiments on Q-band spectra suggest that the g=2.0006 signal in aragonite shell contains thermally unstable components but these appear to be removed by annealing at 150°C for 14-15 hours. For both aragonite and calcite-containing shells, D_E-values based on the ESR signals at g=2.0006 (X-band, 200 mW, aragonite shells), g=2.0006 (Q-band, aragonite shells), g=2.0006 (X-band, calcite-containing shells) and g=2.0014 (X-band, aragonite shells) appear to be comparable after annealing at 150°C for 14-15 hours. In contrast, the g=2.0007 signals observed in the X-band (microwave power of 5 mW and 200 mW) and Q-band in coral samples appear to yield comparable D_E-values both before and after annealing; these signals thus may not include thermally unstable components.

For the coral samples examined, the ESR ages based on the annealed g=2.0058 signal and the g=2.0007 signal (before and after annealing) are in agreement with the independent age controls; both signals appear to be suitable for dating. However, the ESR ages based on the annealed g=2.0058 signal in aragonite and calcite-containing shells are often much greater than those based on the g=2.0006 and g=2.0014 signals. At this stage, it has not been determined which, if any, signal yields the most reliable estimate of age.

Three new light-sensitive ESR signals in quartz have been discovered in this study. These signals are observed at g=1.9870, 1.9842 and 1.9162 at liquid nitrogen temperature (≈ 77K) with an X-band spectrometer. Sunlight bleaching experiments using an orange filter (> 510 nm wavelength transmission) suggest that the bleaching behaviour of these signals is comparable to the bleaching response of the 375°C TL signal, but is unlike that of the 325°C TL and OSL signal. The ESR ages based on these signals are in close accord with independent age estimates obtained by ^{14}C, TL and OSL. The D_0 values (the characteristic saturation doses) based on the light-sensitive ESR signals are much greater than those indicated by OSL. This implies that these signals have potential application to the dating of quartz sediments deposited as long ago as 1-2 Ma (given an environmental dose rate of 0.5-1 Gy ka^{-1}, typical of many Australian sandy deposits), a time period beyond the range of ^{14}C, U-series, TL and OSL dating.

Table of contents

List of tables

List of figures

Part I

BACKGROUND

Chapter 1 INTRODUCTION

1.1 ESR dating in the earth and archaeological sciences

The ESR method has been widely applied to dating in Quaternary research, since Ikeya (1975) demonstrated its potential to date stalactite. ESR dating is still in its developmental stage, but various kinds of material have been dated, such as speleothem, mollusc shell, coral, tooth enamel, bone and quartz. Using these samples, it is possible to obtain dates ranging from a few hundred years to over 1 Ma (fossil carbonates), perhaps even to 100 Ma for quartz. These ranges are beyond the upper limit of ^{14}C, uranium-series and luminescence methods. The ESR method utilises zeroing processes such as heat, pressure, shock and bleaching by sunlight, which allow the dating of a wide variety of geological and archaeological events in the Quaternary period. Environmental changes associated with prehistoric human activities, the origins and spread of modern and archaic humans, and global changes in climate and tectonism have been investigated using ESR. To obtain these the most reliable ages for these events, methodological improvements are continually being sought. In this study, the application of ESR to the dating of Quaternary marine and terrestrial deposits is investigated, with the aim being to improve the accuracy of the ESR ages obtained from materials incorporated within these deposits.

1.2 Marine sedimentation in southeastern Australia: an example of a dating problem

This study was prompted by a practical example of a chronological problem in marine geology which ESR had the potential to resolve.

In 1990, a joint research project between the New South Wales Department of Mineral Resources and Picon Explorations Pty Ltd (now Cable Sands Holdings Pty Ltd) was carried out in the Forster-Tuncurry area, on the east coast of New South Wales. The aim

of this project was to investigate the marine geology of placer minerals on the New South Wales continental shelf. To this end, geological data were collected from drilling and vibrocore samples, high-resolution marine seismic and ground-penetrating radar surveys were made, and sedimentological and mineralogical analyses were accomplished.

Sedimentation patterns on the southeastern Australian margin had previously been studied extensively (e.g. Roy and Crawford, 1977; Bryant *et al.*, 1988; Roy and Thom, 1981, 1991). Since these depositional environments are dominated by coastal and shallow water marine processes, it was essential to obtain data on sea level changes, one of the most important elements in interpreting past depositional environments. Published sea level curves reconstructed for the Pleistocene (Chappell and Shackelton, 1986; Chappell *et al.*, 1994a) and a modified curve for the Holocene, based on local data (Thom and Roy, 1985; Chappell and Polach, 1991), were adopted for this purpose.

Because late Quaternary deposits in coastal environments in southeastern Australia are comprised mainly of quartz and biogenic carbonate, ^{14}C dating has been employed widely to estimate the age and rate of coastal sedimentation using broken shell fragments (shell 'hash'). However, marine sediments, along with the carbonate remains, can be reworked biologically and/or physically after initial deposition. This could result in bulk ^{14}C samples consisting of a mixture of shells of different ages, which is likely to affect significantly the accuracy of shell 'hash' ^{14}C dates (e.g. Nielsen and Roy, 1982). Walbran *et al.* (1989) dated individual fragments of *Acanthaster planci* in sediment cores from the Great Barrier Reef in Queensland using the accelerator mass spectrometry (AMS) ^{14}C method, and found that bulk samples consisted of a mixture of shell fragments of various ages.

To understand the mixing mechanism of marine sediments, some simple models have been developed previously (e.g. Berger and Heath, 1968; Guinasso and Schink, 1975; Carney, 1981). These models were developed for deep sea sediments, where the accumulation rates and mixing depths are relatively small. The same models are inappropriate for high-energy wave-dominated environments, such as the southeastern Australian shelf, where

reworking is likely to be episodic and mixing rates may greatly exceed accumulation rates (Dott, 1983). Roy (1991) described several mixing models that could cause distortion effects to shell hash ^{14}C dates, and he suggested that depositional environments in southeastern Australia are probably too complicated to be explained in terms of simple mathematical models. It is, therefore, not possible to make a ^{14}C age-correction based on such mixing models to estimate the true age of sediment deposition. This implies that ^{14}C dating using bulk carbonate samples will not yield reliable estimates of the age of sedimentation unless the sample contains no reworked carbonate. To distinguish the presence of reworked shells in bulk samples, direct dating of individual shell fragments is required: this can be accomplished either by AMS ^{14}C dating or by ESR dating, the latter being the principal subject of this study.

1.3 Absolute dating of Quaternary deposits

Several methods are available that can be used to determine the ages of geological and archaeological events in the Quaternary. These techniques are based on the rate of growth of specific radioactive isotopes (e.g. $^{40}K/^{40}Ar$, $^{39}Ar/^{40}Ar$, $^{230}Th/^{234}U$), the rate of decay of cosmogenically-produced radionuclides (e.g. ^{14}C), the rate of accumulation of radiation damage in crystals (e.g. thermoluminescence, optically stimulated luminescence, electron spin resonance, fission tracks), global time markers (e.g. palaeomagnetism, stable oxygen isotopes) and the rate of chemical alteration of organic and inorganic materials (e.g. amino-acid racemization, obsidian hydration, cation-ratio). Among these methods, only a few can be utilised for the types of materials found typically in Quaternary deposits.

1.3.1 The ^{14}C method and its problems

Coastal deposits in southeastern Australia consist mainly of quartz sediment and shell hash. Because no other material is generally available for dating, carbonate composites made up of shell fragments have been dated extensively by ^{14}C to determine the age of

deposition of marine sediment (Thom *et al.*, 1978; Thom *et al.*, 1981; Chapman *et al.*, 1982; Thom, 1983). In general, a minimum of 30 g of shell sample is required to obtain enough carbon for ^{14}C analysis (Gupta and Polach, 1985). Alternatively, it is now possible to date milligram-size samples by AMS, which enables individual shell fragments to be dated directly. This is not considered a practical routine method, however, because of the high cost of AMS dating. Furthermore, a problem for both conventional and AMS ^{14}C methods is their limited dating range. The half-life of ^{14}C is 5730 ± 40 years, permitting age determinations for the past 40,000-50,000 years, in theory. Recent developments in the AMS method have extended this theoretical limit to 70,000 years. In practice, however, the limit is often substantially lower (30,000-40,000 years) due to *in situ* contamination of old samples by modern carbon (see Aitken, 1990). Also, ^{14}C ages require calibration for past changes in the production rate of ^{14}C in the upper atmosphere. Reliable calibration data are available for the last 11,000 years (Stuiver and Reimer, 1993), and with less reliability back to 30,000 years (Bard *et al.*, 1993). The 30,000 year-working limit of ^{14}C dating is too short to cover the series of geological and archaeological events that have occurred during the ≈ 2 Ma Quaternary period.

1.3.2 Other absolute dating methods and their problems

In addition to the ^{14}C method, marine carbonates can be dated by uranium-series or amino-acid racemization techniques. Alternatively, quartz grains have been used to estimate the age of sediment deposition, by both thermoluminescence (TL) and optically stimulated luminescence (OSL) methods. Electron spin resonance (ESR) also has the potential to date both carbonates and quartz grains. The ESR technique is the focus of this study, but a short description will be given of the other techniques which are referred to elsewhere in this thesis.

Uranium-series methods

The most common form of uranium-series dating is the method based on disequilibrium in the ^{238}U decay series, which involves the activity ratio between two radioactive daughter products, ^{234}U and ^{230}Th. This method can be used to determine ages up to about 400 ka (Ivanovich and Harmon, 1992), and has been applied most successfully to fossil corals (e.g. Omura *et al.*, 1979, 1994; Ashby *et al.*, 1987; Bard *et al.*, 1993) which appear to have behaved as chemically-closed systems since the time of their formation. On the other hand, the dating of fossil molluscs and sea urchins has not been satisfactory because these materials do not form closed systems with respect to ^{238}U and its daughter products (Kaufman *et al.*, 1971; Szabo and Vedder, 1971; Muhs and Kennedy, 1985). The late Quaternary sediments in southeastern Australia incorporate mainly fossil molluscs and these are most likely to behave as open systems. As it is not currently possible to determine a history of U-uptake or loss for these shells, uranium-series dating cannot be applied at this stage to these deposits. However, alpha spectrometric and mass spectrometric U-series ages have been obtained from the raised coral reef terraces on the Huon Peninsula, Papua New Guinea, one of the study sites discussed in this thesis.

Luminescence methods

Thermoluminescence (TL) and optically stimulated luminescence (OSL) methods have been widely used to date archaeological and geological events in the Quaternary, using minerals such as quartz, feldspar and zircon. The upper age limit for quartz appears to be in excess of 800 ka (Huntley *et al.*, 1993). Luminescence methods utilise the time-dependent accumulation of trapped electrons and holes, produced by natural radiation. Radiative recombination (accompanied by the emission of photons) is induced by heating (TL) or illumination (OSL). Both techniques provide an estimate of the elapsed time since the mineral grains were last exposed to sunlight (e.g. Wintle and Huntley, 1979; Singhvi *et al.*, 1982; Huntley *et al.*, 1985). The basis of the method is that the luminescence signal is zeroed by exposure to sunlight and grows steadily once the mineral grain becomes

buried. Water-lain sediments are, however, unsuitable for some TL methods because sunlight bleaching is less effective beneath a cover of water. Sediment transport patterns and reworking of deposits in coastal and near-shore environments in southeastern Australia suggest that such sediments may not be sufficiently well bleached to reset the TL signal before sample burial. In contrast, OSL methods should be suitable for dating water-lain as well as wind-blown sediments, because the OSL signal is bleached completely and rapidly by wavelengths transmitted even through a column of water (Spooner, 1994; Rendell *et al.*, 1994).

Electron spin resonance methods

Electron spin resonance (ESR) dating has been developed relatively recently and has great potential for widespread application. The ESR technique is based on the measurement of the number of paramagnetic centres produced by natural radiation in a mineral. ESR has been widely applied to date geological and archaeological events in the Quaternary (e.g. Ikeya, 1975; Grün and Stringer, 1991) and a variety of materials (e.g. mollusc shell, coral, tooth enamel, bone, speleothem and quartz) has been investigated (e.g. Grün, 1989; Schwarcz, 1994). The dating range for these materials could extend to more than 1 Ma or even to 100 Ma (Odom and Rink, 1988). Another advantage of the ESR method is that only small amounts of material (20-250 mg) are required for analysis. It is therefore possible to date individual mollusc shells using this technique. However, a standard procedure for ESR measurement of mollusc shell has not been fully developed yet, with different research groups using different ESR signals and instrument settings for the intensity measurements. Also, Katzenberger and Willems (1988) found inflexion points in the dose response curves of molluscs and suggested that this material was unsuitable for ESR dating. Rather better results have been obtained recently from corals (e.g. Radtke and Grün, 1988; Grün, *et al.*, 1992) and tooth enamel (e.g. Schwarcz, 1985; Grün *et al.*, 1987), but ESR dating of solar-reset quartz remains an intractable problem (Schwarcz, 1994).

1.4 Study objectives

The initial impetus for this project was provided by marine geologists in their desire to avoid unreliable age estimates caused by the reworking of fossil shells. This problem appears to bedevil ^{14}C dates based on bulk shell samples. To address this problem, it was necessary to examine the prospects for dating individual fossil shells. Considering all available dating techniques, the ESR method was chosen as the most suitable procedure for. This thesis, therefor, has the following broad aims:

a) to test existing and develop new ESR dating techniques to provide reliable age estimates for a variety of biogenic carbonate materials found in sedimentary, especially marine, deposits;

b) to test published develop new ESR methods for dating Australian quartz sediments deposited by wind and, in particular, water;

c) to demonstrate the reliability of existing and newly developed dating procedures by means of comparison with independent age estimates (e.g. by ^{14}C, U-series, TL and OSL).

These objectives have been accomplished in the following ways:

1) Test published ESR dating methods

There is no standard procedure used routinely in the ESR dating of molluscs (or marine carbonates), and different protocols have been recommended by several research groups. Since ESR ages may vary according to the dating procedures employed, it is necessary to test existing ESR dating methods for shell, coral, tooth enamel and quartz, and examine the consistency of their results.

2) Examine the suitability of dose response functions in shell

Katzenberger and Willems (1988) reported that mollusc shell was unsuitable for ESR dating because their samples exhibited inflexion points in the dose response curves. However, the existence and magnitude of this phenomenon may vary between different shell species. It is thus essential to examine different Australian shell species for the occurrence of inflexion points and the most appropriate curve-fitting function.

3) Investigate annealing effects on the accumulated dose (D_E) in shell and coral

The behaviour of shell and coral samples to various annealing procedures has received little attention in previous studies. The thermally unstable components in the ESR signals used for dating are, however, a great concern for age estimates, so it is important to examine the effects of annealing on D_E-values derived from the ESR dating signals in shell and coral.

4) Seek new light-sensitive ESR signals in quartz

Despite the presence of several light-sensitive signals in the related trapped-electron dating methods of TL and OSL, no such signals in ESR have been found which can be used for dating. As Australian quartz samples exhibit particularly strong TL and OSL signals, these samples may provide an opportunity to discover similarly enhanced light-sensitive ESR signals.

5) Develop new ESR dating methods for shell, coral and quartz

Using the knowledge gained above, new ESR dating methods for shell, coral and quartz shall be developed and the reliability of their age estimates tested by means of independent age control.

1.5 Thesis framework

This thesis is divided into four parts:

Part I : Background;
Part II : Dating using published methods;
Part III : Development of new methods;
Part IV : Dating using new methods.

In Part I, some problems concerning the dating methods used for Quaternary deposits are described in Chapter 1, while the principles of ESR dating and the feasibility of dating shell, coral, tooth and quartz are discussed in Chapter 2. Sampling sites and details of sample preparation are described in Chapter 3. In Part II, published ESR dating methods are examined for shell (Chapter 4), coral (Chapter 5), tooth enamel (Chapter 6) and quartz (Chapter 7). The ESR ages obtained are compared with independent age controls (such as ^{14}C, U-series, TL and OSL) in Chapter 8. Based on the results in Part II, some methodological developments for ESR dating are established in Part III. An examination of dose response functions using shell samples is discussed in Chapter 9, while annealing effects on the ESR signals in shell are examined for X-band and Q-band in Chapter 10. Changes observed in ESR signals in quartz upon bleaching by sunlight are given in Chapter 11, and newly discovered ESR light-sensitive signals in quartz are also reported in this Chapter. In Part IV, newly developed ESR dating methods are tested for shell (Chapter 12), coral (Chapter 13) and quartz (Chapter 14). This is followed by a concluding Chapter discussing the progress made in dating of biogenic carbonate and quartz by ESR, and the prospects for future fruitful research in ESR dating.

Chapter 2 ESR DATING METHODS

2.1 Introduction

ESR dating was first applied to corals by Duchesne *et al.* (1961), but not until Ikeya (1975) dated a stalactite from Akiyoshi Cave in Japan was ESR demonstrated to be a practical dating method. Since then, the ESR method has been applied widely and has established an important role in Quaternary geochronology and archaeometry. ESR dating has been applied to speleothems, spring deposited travertine, mollusc shells, corals, and tooth enamel (e.g. Grün, 1989). Also, its application to quartz has been attempted to estimate the age of formation of heated ceramics, volcanic rocks, and intra-fault material and the age of deposition of wind-blown sediments (e.g. Grün, 1989).

ESR utilises lattice defects in minerals, which act as 'traps' for unpaired electrons or holes produced by natural radiation (α-particles, β-particles and γ-rays) from the decay of radioactive nuclides, and cosmic rays. The trapped-electron population accumulates steadily with time at paramagnetic centres, once a mineral has formed (mineralization) or the antecedent ESR signal has been zeroed by processes such as heating, shear stress or sunlight. The paramagnetic centres can be detected using an ESR spectrometer, as microwaves induce transitions between the spin states of unpaired electrons, the Zeeman effect, in certain magnetic fields. The ESR intensity is proportional to the number of centres produced. The total accumulated dose may be estimated by the additive-dose method (e.g. Grün, 1989), where the ESR signal intensity versus additive dose curve is back-extrapolated as shown in Figure 2.1. The ESR age (T) can be estimated on the basis of the following equation:

$$D_E = \int_0^T D(t)\, dt \qquad (2.1)$$

where D_E is the total accumulated dose since the last zeroing process, and $D(t)$ is the dose rate. Usually the dose rate is assumed to be a constant, D, determined from *in situ* dosimetry or from laboratory analysis of the radioactive elements in the minerals and

surrounding material. This dose rate is the sum of doses due to ionizing radiation from α-particles, β-particles, γ-rays and cosmic rays. Under these simplifying assumptions, the estimation of an ESR age therefore involves the assessment of two parameters, the accumulated dose (D_E) and the dose rate (D):

$$\text{T, Age} = \frac{D_E\text{-value}}{\text{D, Dose rate } (\alpha, \beta, \gamma + \text{cosmic rays})} \qquad (2.2)$$

Since different types of materials exhibit unique ESR spectra and distinct dose rates, the evaluations of D_E and D require different procedures. The remainder of this Chapter is concerned with the methods which have been used to estimate D_E and D for shell, coral, tooth and quartz.

2.2 Shell

There has been a considerable volume of literature concerned with ESR dating of mollusc shell, since Ikeya and Ohmura (1981) first dated fossil shells by ESR. Several different ways of estimating the D_E-value have been proposed by various groups. Generally, aragonitic mollusc shell exhibits five lines in the ESR spectra, namely the signals at g=2.0058, 2.0032, 2.0020, 2.0012 and 1.9976 (Molodkov and Hütt, 1985; Hütt *et al.*, 1985). These signals each yield different D_E-values. Use of the g=2.0020 signal is recommended by Molodkov and Hütt (1985) (see Figure 10.1(a)), but Radtke *et al.* (1985) determined that this signal had insufficient thermal stability to be used for dating; the latter authors recommended the signal intensity at g=2.0014. On the other hand, Tsuji *et al.* (1985) used the g=2.0010 signal for dating, while Ninagawa *et al.* (1985) used the g=2.0004 signal for dating of calcite shells.

Currently, there remains no convincing evidence indicating which signal should be used for dating. There appear to be three main schools of thought on this matter. First, several groups (e.g. Kai and Ikeya, 1989; Huang *et al.*, 1989; Peng *et al.*, 1989) have been regularly using the signals at g=2.0006-2.0010. Second, Grün (1989) suggested that the g=2.0014 signal should be used for dating, to eliminate the effect of the g=2.0020 signal.

However, Katzenberger and Willems (1988) found that inflexion points occasionally appeared in the dose response curves based on the g=2.0014 signal. Katzenberger *et al.* (1989) also considered that the g=2.0014 signal consisted of at least three overlapping signals, and was therefore unsuitable for dating. Most recently, Barabas *et al.* (1992a) proposed the use of the g=2.0006 signal at high microwave power (> 20 mW), but indicated the considerable limitations for its application to dating.

For dose rate determinations, analysis of radioactive elements (uranium, thorium and potassium) is required for both the sample and the surrounding material. For marine mollusc shells, an initial $^{234}U/^{238}U$ ratio of 1.14 ± 0.01 is usually assumed for sea water (following Chen *et al.*, 1986, who determined a present sea water value of 1.144 ± 0.002). The *k*-value, the effectiveness of defect production by α-particles compared to defect production by β-particles and γ-rays, was determined by Grün (1985a) and DeCanniere *et al.* (1986) to be 0.1 and 0.2, respectively. The dose rate for a mollusc shell can be calculated using the following equation given by Grün (1989):

$$\begin{aligned} D = {} & C_{U(I)} (k\, D_\alpha + S_{U\text{-}\beta}\, D_\beta + S_\gamma\, D_\gamma) \\ & + C_{U(SED)} (W_{\beta(SED)}\, G_{U\text{-}\beta}\, D_\beta + W_{\gamma(SED)}\, G_\gamma\, D_\gamma) \\ & + C_{Th(SED)} (W_{\beta(SED)}\, G_{Th\text{-}\beta}\, D_\beta + W_{\gamma(SED)}\, G_\gamma\, D_\gamma) \\ & + C_{K(SED)} (W_{\beta(SED)}\, G_{K\text{-}\beta}\, D_\beta + W_{\gamma(SED)}\, G_\gamma\, D_\gamma) \\ & + G_{COS}\, D_{COS}. \end{aligned} \qquad (2.3)$$

where $G_{\beta,\gamma,COS}$ are the attenuation factors for α-, β-, γ- and cosmic rays; $S_{\beta,\gamma}$ are the self-absorption factors for α-, β- and γ- rays; $W_{\beta,\gamma}$ are the correction factors for water content for α-, β- and γ- rays; $D_{\alpha,\beta,\gamma}$ are the dose rates per unit concentration; D_{COS} is the cosmic ray dose rate; *k* is the effective α-efficiency; and $C_{U,Th,K}$ are the concentrations of uranium, thorium and potassium. In the above equation, the suffix 'SED' relates to the sediment and the suffices 'U, Th, K' relate to uranium, thorium and potassium, respectively. The reduction in β-particle contributions due to attenuation and acid etching was corrected using equation (3) of Grün (1986). Since uranium in the sample is in disequilibrium, the dose contribution from the uranium decay chain, $AD_U(T)$, can be obtained using the following equation given by Grün (1989):

$$AD_U(T) = C_U \int_0^T D_U(t)\, dt \qquad (2.4)$$

2.3 Coral

Dating of coral has great potential in studies of the tectonic and sea level history during the Quaternary (e.g. Radtke *et al.*, 1987; Radtke and Grün, 1988; Grün *et al.*, 1992). Coral was first dated by Ikeya and Ohmura (1983), focusing on sites in southern Japan. This study was followed by others on corals in Haiti (Skinner, 1985, 1986), Barbados and the New Hebrides (Radtke and Grün, 1988) and the Huon Peninsula, Papua New Guinea (Grün *et al.*, 1992). Unlike mollusc shells, corals have been dated successfully by ESR because corals behave almost as a closed system with respect to radioactive elements, so that the dose rate determinations are more reliable. Also, corals exhibit a clear signal at g=2.0007 (due to the rapidly rotating CO_2^- centre), often called the 'dating signal' (e.g. Barabas *et al.*, 1992a, 1992b) (see Figure 5.3(a)).

For the dose rate determinations, analysis of the radioactive elements (U, Th and K) is required for the sample. As with marine mollusc shells, an initial $^{234}U/^{238}U$ ratio of 1.14 ± 0.01 is generally assumed for sea water (following Chen *et al.*, 1986). The *k*-value was determined by Radtke *et al.* (1988) and Grün *et al.* (1992) to be 0.06 ± 0.01 and 0.05 ± 0.01, respectively. The dose rate for coral can be calculated using the following equation given by Grün (1989):

$$D = C_{U(I)} (k D_\alpha + D_\beta + D_\gamma) + G_{COS} D_{COS} [+ (MD_\gamma - C_{U(I)} D_{\gamma(t)})]. \qquad (2.5)$$

Here G_{COS} is the attenuation factor for cosmic rays; $D_{\alpha,\beta,\gamma}$ are the dose rates per unit concentration; D_{COS} is the cosmic ray dose rate; *k* is the effective α-efficiency; $C_{U(I)}$ is the concentration of U in the sample; and MD_γ is the measured γ-dose rate. The final expression in square brackets relates to the measured γ-dose rate with the internal γ-disequilibrium dose rate at time t. As for shell samples, uranium disequilibrium in corals should also be considered (e.g. by using equation (A-6) of Grün (1989)).

2.4 Tooth enamel

Tooth samples are found at many archaeological sites that are too old to be dated by conventional methods (e.g. ^{14}C). The mineral in tooth enamel exploited in ESR dating is hydroxyapatite, $Ca_{10}(PO_4)_6(OH)_2$, which exhibits ESR peaks at g=2.0036, 2.0018 and 2.0009 due to organic radicals (Ikeya, 1981; Grün *et al.*, 1987). The g=2.0018 signal, believed to be due to CO_3^{2-} centres (Gilinskaya *et al.*, 1971; Cevc *et al.*, 1972), has been used for dating and appears to be useful up to at least 1-2 Ma (Henning and Grün, 1983; Schwarcz, 1985).

It has been recognised that teeth behave as open systems and accumulate significant amounts of uranium after burial. The uranium concentrations in dentine and cement are about 10 times higher than in enamel (Grün, 1989), so it is important to consider different models of uranium uptake for the dose rate assessment. Two models of uranium migration, early and linear uranium uptakes, are routinely considered in the dose rate calculation (Ikeya, 1982; Grün *et al.*, 1987). Enamel, dentine and cement are usually free of thorium and potassium (Grün, 1989), so analysis of only the uranium contents in those materials are required. A *k*-value of 0.15 was determined by Grün (1985a) and De Canniere *et al.* (1986). The dose rate for a tooth enamel sample can be obtained using the following equation given by Grün (1989):

$$\begin{aligned} D = {} & C_{U(I)} (k\, D_\alpha + S_{U\text{-}\beta}\, D_\beta + D_\beta) \\ & + C_{U(DE1)} (W_{\beta(DE1)}\, G_{U\text{-}\beta(DE1)}\, D_\beta) \\ & + C_{U(DE2)} (W_{\beta(DE2)}\, G_{U\text{-}\beta(DE2)}\, D_\beta) \\ & + C_{U(SED)} (W_{\gamma(SED)}\, D_\gamma + W_{\beta(SED)}\, G_{U\text{-}\beta}\, D_\beta) \\ & + C_{Th(SED)} (W_{\gamma(SED)}\, D_\gamma + W_{\beta(SED)} + G_{Th\text{-}\beta}\, D_\beta) \\ & + C_{K(SED)} (W_{\gamma(SED)}\, D_\gamma + W_{\beta(SED)} + G_{K\text{-}\beta}\, D_\beta) \\ & + G_{COS}\, D_{COS}. \end{aligned} \qquad (2.6)$$

The symbols are as explained in section 2.2 (equation 2.3) except DE1 and DE2 which relate to the each side of dentine. Disequilibrium in the uranium decay chain in the sample

should be considered when an early uranium uptake model is used (e.g. by employing equation (A-6) given by Grün (1989)). In the case of linear uranium uptake, equation (A-6) has to be substituted by equation (A-9) of Grün (1989).

2.5 Quartz

Dating of quartz has enormous potential in Quaternary geochronology and archaeometry because quartz grains are widely distributed and found in almost every kind of sediment or deposit, such as deep-sea sediments, marine deposits, terrestrial landforms and archaeological sites. In previous studies, five different types of ESR centres have been observed: the OHC centre at g=2.011, the E' centre at g=2.0001 and the Ge centre at g=1.997 can be observed at room temperature, while the Al and Ti centres may be detected at liquid nitrogen temperature (≈77K). Dating of quartz by ESR is still in its infancy and the prospects of dating using these signals have been concerned mainly with four different 'zeroing' mechanisms to release trapped electrons or holes: crystallisation, heating, hydrostatic pressure and sunlight. Using these zeroing mechanisms, a wide variety of events can be dated, such as incidents associated with volcanic activity, geological fault activity, human activity, (e.g. pottery sherds, burned bricks and flints), and the natural or anthropogenic deposition of quartz sediments.

Among these zeroing events, zeroing by sunlight can be applied to estimate the elapsed time since sediments were last exposed to sunlight. However, only a few studies have reported ESR dating of solar-reset sediments (e.g. Yokoyama *et al.*, 1985a; Tanaka *et al.*, 1995). This is because the observed ESR signals are not as light-sensitive as TL and OSL signals (e.g. Buhay *et al.*, 1988) and it is believed that none of the ESR signals in quartz can be reset completely by sunlight in the natural environment (Schwarcz, 1994). Under such circumstances, dating of sun-bleached sediments by ESR is not practical unless new light-sensitive ESR signals are discovered.

For the dose rate determinations, the radioactivity and water contents of the sediment samples have to be analysed. The alpha-efficiency in quartz is assumed to be around 0.1 (as indicated for TL; Zimmerman, 1971). The dose rate for quartz can be derived from the following equation given by Grün (1989):

$$\begin{aligned} D = {} & C_{U(I)} (k\, D_\alpha\, S_{U\text{-}\alpha} + D_\beta\, S_{U\text{-}\beta}) \\ & + C_{U(SED)} (k\, W_{\alpha(SED)}\, G_{U\text{-}\alpha(SED)}\, D_\alpha \\ & + W_{\beta(SED)}\, G_{U\text{-}\beta(SED)}\, D_\beta + W_{\gamma(SED)}\, D_\gamma) \\ & + C_{Th(SED)} (k\, W_{\alpha(SED)}\, G_{Th\text{-}\alpha}\, D_\alpha + W_{\beta(SED)}\, G_{Th\text{-}\beta}\, D_\beta + W_{\gamma(SED)}\, D_\gamma) \\ & + C_{K(SED)} (W_{\beta(SED)}\, D_\gamma\, G_{K\text{-}\beta}\, D_\beta + W_{\gamma(SED)}\, D_\gamma) \\ & + G_{COS}\, D_{COS}. \end{aligned} \qquad (2.7)$$

The symbols are as explained in section 2.2 (equation 2.3).

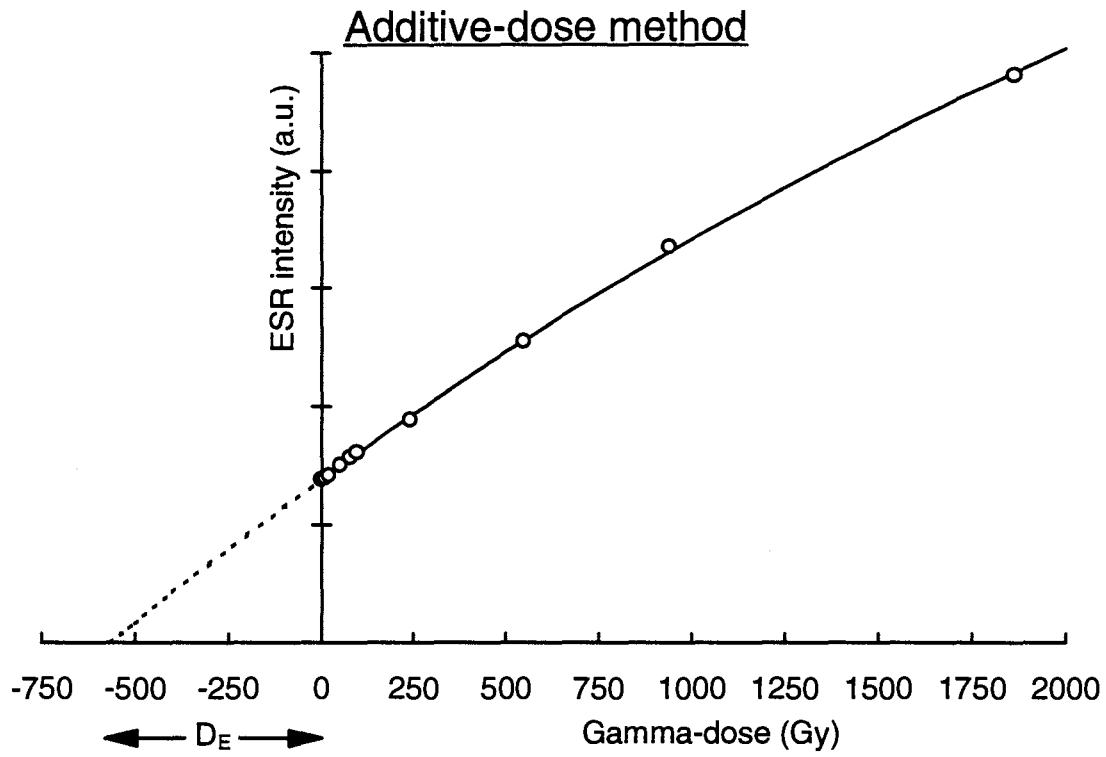

Figure 2.1. Evaluation of the total accumulated dose (D_E-value) by the additive-dose method. The D_E-value (Gy) is determined by the back-extrapolation of the ESR signal intensity curve to the zero ordinate. The intensity of the ESR signal is enhanced by laboratory γ-irradiation of the natural ('as collected') sample.

Chapter 3 STUDY SITES & SAMPLE PREPARATION

3.1 Criteria for site selection

In this study, materials such as shell, coral, tooth enamel and quartz have been investigated to estimate the age of formation of marine, freshwater and terrestrial cave deposits. To compare dating methods for materials in different depositional environments, seven sites were selected for study. Locations of sample sites are shown in Figure 3.1.

To estimate the age of marine deposits, fossil shells and quartz sediments were collected from drill cores. In the Forster-Tuncurry region, on the east coast of New South Wales, ninety-two vibrocores (Roy *et al.*, 1992) were taken to study the details of the geomorphology and chronology at this site. Several radiocarbon (^{14}C) and thermoluminescence (TL) dates have been obtained previously (Roy *et al.*, 1992). This prior study was a joint research project between the New South Wales Department of Mineral Resources (DMR) and Picon Explorations Pty Ltd (currently Cable Sands Holdings Pty Ltd), and was initiated by Dr. P. S. Roy at the Geological Survey of New South Wales (GSNSW). The main objectives of the project were to understand marine mineral occurrences in continental shelf environments and evaluate the potential for heavy mineral concentration and preservation in shelf sediments. For the dating work reported here, Dr. Roy gave permission to access all of his sample and data collections.

While working with the fossil shell samples from Forster-Tuncurry, it was found that the samples were not ideal for ESR dating because of reworking of the sediment and associated shell on the continental shelf. Additional shell samples from other sites were therefore required to assess the validity of dating shell by ESR. To this end, a large number of fossil marine shells were collected from four archaeological sites in Elands Bay (Yates *et al.*, 1986), on the west coast of South Africa, during field work in 1993. At the same time, modern shells of the same species were taken from the coast near one of the South African sites to examine the effects of possible calcite recrystallisation in the fossil

shells. It is believed that the sediments at Elands Bay have not been substantially reworked, and that the shells have been exposed to an approximately constant dose rate throughout the period of burial. Furthermore, the shells from Elands Bay were believed to cover a wide range of ages, from less than 1,000 years to more than 125,000 years. This enabled the suitability of the ESR dating method to be examined for shells of widely varying ages, and permitted the results to contribute to the debate concerning mid-Holocene sea-level changes in southern Africa (Miller *et al.*, 1993).

Unlike marine molluscs, corals exhibit well-defined ESR dating signals and have been dated successfully by ESR (e.g. Ikeya and Ohmura, 1983; Radtke *et al.*, 1988; Skinner, 1988; Jones *et al.*, 1993). To this end, well-studied coral samples from Huon Peninsula in north-eastern Papua New Guinea were used to examine the validity of newly developed ESR methods for biocarbonate materials. The Huon Peninsula corals have excellent independent chronologies from alpha spectrometric and mass spectrometric uranium-series methods (Grün *et al.*, 1992; Chappell *et al.*, 1994a, 1994b; Omura *et al.*, 1994). Also, geological ages for this raised coral reef terrace sequence have been derived by Chappell *et al.*, (1994b) from the uplift rate at three sections and the measured height of the raised terraces.

To test the validity of ESR dating for materials found at terrestrial sites, measurements on enamel from four teeth of *Bovidae* have been carried out as a collaborative project with the Quaternary Dating Research Centre, Research School of Pacific and Asian Studies, Australian National University (ANU). The teeth were obtained by Dr. R. Grün from the archaeological site of Tham Khuyen Cave in Vietnam (Bao and Kha, 1966; Schwartz *et al.*, 1994).

Finally, sedimentary quartz from four Australian sites was examined by ESR to determine whether or not this ubiquitous mineral could be dated by ESR. Unlike the shell, coral and tooth enamel samples, for which the ESR signal is initiated at the time of formation, quartz was examined for evidence of one or more ESR signals which could be reset by a

brief exposure to sunlight, in the same manner as for TL and optically-stimulated luminescence (OSL) dating. Like the shell samples, the quartz samples from Forster-Tuncurry Shelf are assumed to have been reworked physically during sedimentation or bioturbated subsequently. Mixing might cause problems for luminescence and ESR dating as a result of incomplete zeroing of either signal by sunlight or because of a variable post-depositional dose rate. To avoid these complications, lake sediments were examined as a sub-aqueous depositional environment better suited to dating due to negligible mixing. Professor J. Chappell in the Division of Archaeology and Natural History, Research School of Pacific and Asian Studies, ANU, suggested drill cores from Lake George in the Southern Tablelands of New South Wales. Several cores have been taken from this site and palaeomagnetic stratigraphy, fossil pollen and plant microfossils have been studied by several researchers (Bowler *et al.*, 1976; Churchill *et al.*, 1978; Singh *et al.*, 1981a).

An earlier drill core from Lake George (Singh *et al.*, 1981b) had been dated by ^{14}C, providing an independent check on the ESR dates back to *circa* 35 ka B.P. Preliminary studies revealed, however, that the quartz samples from Lake George showed a poorly-defined ESR signal. Quartz samples from other sites were therefore examined also. Dr. R. G. Roberts from the Division of Archaeology and Natural History, Research School of Pacific and Asian Studies, ANU, provided quartz samples from two important archaeological sites in Australia. One site is Allen's Cave on the Nullarbor Plain in South Australia (Roberts *et al.*, 1994a), and the other is a rock shelter in Deaf Adder Gorge, Northern Territory (Roberts *et al.*, 1994b). The sub-aerially deposited samples are from well-bleached quartzose sediments, and both sites have been dated by TL, OSL and ^{14}C techniques. The ages obtained by TL and OSL methods are in good agreement and, for samples in the time range 10-30 ka, are independently supported by calibrated ^{14}C ages.

3.2 Shell sites and sample preparation

3.2.1 Forster-Tuncurry, New South Wales

Forty-eight fossil shells were collected from vibrocores taken from the Forster-Tuncurry offshore region (32°05'-32°20'S latitude), on the east coast of New South Wales. A large number of ^{14}C dates have been obtained previously from bulk shell samples. The ^{14}C ages of selected shell samples are shown in Table 3.1 and the details of shell species (Wells, 1984; Shepherd and Thomas, 1989) are given in Table 3.2. Some of the ^{14}C ages obtained are reported to be 'too old' with respect to sea level changes based on the local data of Thom and Roy (1985) and the Huon Peninsula data reported by Chappell and Polach (1991). Further details are provided by Roy *et al.* (1992).

For the ESR analyses, all shell samples were washed with tap water and etched with 10 % acetic acid for up to 90 minutes to remove the outer 150-200 μm irradiated by α particles. The shells were then gently crushed and particles of 64-250 μm diameter were obtained by dry sieving. These particles were etched with 5 % acetic acid for a few minutes, rinsed with distilled water several times, then allowed to dry at room temperature. For the ESR measurements, 7 to 10 aliquots, each weighing 200 mg, were prepared for the each shell sample, and selected doses were administered using a ^{60}Co γ-source (dose rate of ≈ 10 Gy min^{-1}) at the Division of Plant Industry, CSIRO. The selected shell samples were analysed by X-ray diffraction at the Department of Geology, ANU, to examine the effects of possible recrystallisation to calcite.

For the internal dose rate evaluation, the shell samples were analysed by inductively-coupled plasma mass spectrometry (ICP-MS) at the Research School of Earth Sciences, ANU, and flame photometry. To determine the external dose rate, the sediment samples were analysed using high-resolution γ-ray spectrometry at the Division of Water Resources, CSIRO, following the procedures described in Murray *et al.* (1987).

3.2.2 Elands Bay, South Africa

Fossil shells were collected from four locations in Elands Bay on the west coast of South Africa: Borrew Pit Midden, Malkappan Elandas, Hoedjiespunt 1 and Hoedjiespunt 2. A total of 16 shells, four shells from each site, were selected for the ESR studies. Details of the collected samples (Kilburn and Rippey, 1982) are given in Tables 3.3 and 3.4. A radiocarbon age of *circa* 900 years B.P. has been obtained from bones excavated from Borrew Pit Midden, and deposits at the other locations are believed to be last interglacial in age (D. E. Miller and J. E. Parkington, pers. comm., 1993), but no independent age control is available. This work is a collaborative project with Professor J. E. Parkington and Dr. D. E. Miller of the Department of Archaeology, University of Cape Town, South Africa. The shell samples were prepared for ESR analyses in the same way as described in section 3.2.1. The fossil shell samples, and modern shells of the same species collected at the beach near the sampling sites, were checked by X-ray diffraction at the Department of Geology, ANU.

The environmental gamma dose rates were measured *in situ* at the sampling sites by Dr. R. Grün using a portable γ-ray spectrometer. For the external β-dose rate evaluation, the sediment samples were analysed by ICP-MS at the Research School of Earth Sciences, ANU, and atomic absorption spectrophotometry. To estimate the internal dose rate, the shell samples were analysed by ICP-MS and flame photometry.

3.3 Coral site and sample preparation

Ten coral samples from Huon Peninsula, Papua New Guinea, previously studied by Grün *et al.* (1992), were obtained for analysis. Huon Peninsula represents one of the most detailed natural archives of late Quaternary sea levels. The raised coral reef terraces at this site have been dated by alpha spectrometric and mass spectrometric U/Th methods and ESR. Recent reports indicate that sea levels estimated from the Huon Peninsula

terrace sequence (Chappell *et al.*, 1994a) and from deep sea cores (Shackleton, 1987) are in agreement throughout the last glacial cycle. Also, geological ages of the terraces have been derived by Chappell (1990) and Chappell *et al.* (1994b) from the average uplift rate at three transects across the terrace sequence and the measured heights of the platforms. The estimated geological ages, U/Th ages and previously determined ESR ages are shown in Table 3.5. The time period covered by these samples is *circa* 40-70 ka.

For ESR analysis, the samples had been ground and sieved to 125-250 μm in 1992 by R. Grün, and several aliquots were γ-dosed at this time also. The same analytical data for the environmental dose rate assessments reported by Grün *et al.* (1992) were used in this study. The ≤ 125 μm fraction was used for uranium analysis by delayed neutron activation. The alpha efficiency (*k*-value) of all samples was determined with an ^{241}Am α-source.

3.4 Tooth enamel site and sample preparation

Twelve enamel samples were obtained from four teeth of *Bovidae*. The teeth were excavated by Dr. R. Grün from the archaeological site of Tham Khuyen Cave in Vietnam, one of the most important fossil sites in Asia, first excavated in 1965 (Bao and Kha, 1966; Schwartz *et al.*, 1994). The site is located in the northern Province of Lang Son, near the Chinese border. The tooth samples were taken from a pocket of sediments (corresponding to units 1-3 on the main outcrop) located five meters north of the cave. From this pocket, the *Hylobates* skull (Tham Khuyen no. 267) was excavated. Units 1-3 also contained the remains of the giant ape *Gigantopithecus blacki* (Cuong, 1985), *Homo erectus* (Cuong, 1984) and other primate fossils.

As an independent age control, a U/Th age of 117 ka (Ciochon *et al.*, in press) was obtained from calcite crystals in unit T2 (between units 8 and 9 on the main outcrop), located stratigraphically above the ESR sampling site. A sandy/silty conglomerate (breccia) underlying the ESR sampling site has been studied and the findings of lithological and pollen analyses (Huong *et al.*, 1975) was consistent with the faunal

analyses (Bao and Kha, 1966). Comparisons with southern Chinese faunas suggested a late middle Pleistocene age (about 300-250 ka). The ESR age was, therefore, expected to lie between 117 ka and the late middle Pleistocene.

For ESR analyses, dental enamel and dentine were separated using a dentist's drill. For internal dose rate determinations, the enamel and dentine were then dissolved in 50 % nitric acid and taken to a final weight of 100 g in 2 % nitric acid. For the external dose rate, the sediment was dissolved in concentrated hydrofluoric acid and concentrated nitric acid by high temperature microwaving. The sediment was eventually dissolved in 2 % nitric acid and taken to a final weight of 100 g. Samples were assayed using ICP-MS to estimate the internal and external dose rates.

3.5 Quartz sites and sample preparation

3.5.1 Forster-Tuncurry, New South Wales

Two samples composed of quartzose sediments, Q13 and Q18, were collected for ESR studies from a location close to where the TL samples had been taken previously. The latter samples were TL dated (Roy *et al.*, 1992) by Mr. D. M. Price at the University of Wollongong. The TL ages and details of the samples are given in Table 3.6. Sample Q13 consists of uniformly fine-grained and well-sorted quartz and is presumed to represent a Holocene transgressive back-barrier deposit or a Pleistocene barrier depositional environment. Sample Q18 is comprised of fine to coarse grained quartz, from a presumed Pleistocene barrier depositional environment. Further details of the cores are reported by Roy *et al.* (1992).

The sediments used for ESR analyses were initially washed with tap water to remove clays and separate almost pure quartz grains. Then quartz samples Q13 and Q18 were treated with 40 % HF acid for 2 hours, rinsed with distilled water several times, and allowed to dry at room temperature. Particles of 75-250 μm diameter were isolated by

dry sieving, and aliquots weighing 200 mg were serially irradiated using a ^{60}Co γ-source (dose rate of ≈ 3 Gy min^{-1}). The samples were prepared under yellow laboratory illumination conditions and were not exposed to direct sunlight when collected in the field.

The same environmental dose rates reported by Roy *et al.* (1992) were used in this study. The sediment samples were analysed by means of thick-source alpha counting over a 42 mm ZnS scintillation screen. Potassium contents were determined by atomic emission spectrometry (AES).

3.5.2 Lake George, New South Wales

Lake George is located about 40 km north-east of Canberra at an elevation of 673 m above sea level (latitude 35°05'S, longitude 149°25'E), on the Southern Tablelands of New South Wales. During field work in 1993, three holes were drilled and 32 cores were taken from the northern part of the lake using 50 cm long barrels and PVC pipes. This location is close to that of core LG4 taken by Singh *et al.* (1981b). The cores have been stored in the dark to prevent possible bleaching by light. Samples LG-A and LG-B were obtained from Core 2-6 (hole No. 2, sub-bottom depth 300-334 cm). These samples were dark grey in colour and contained fine to very fine grained sand, with around 50 % of the sample composed of mud.

For ESR analyses, the sediments were initially washed with tap water to remove clays and separate almost pure quartz grains. The separated quartz grains were then treated with 10 % HCl acid for 2 hours, followed by 40 % HF acid for 2 hours, rinsed with distilled water several times, and allowed to dry at room temperature. Particles of 75-250 μm diameter were isolated by dry sieving, and aliquots weighing 200 mg were serially irradiated using a ^{60}Co γ-source (dose rate of ≈ 3 Gy min^{-1}). The samples were prepared under yellow laboratory illumination conditions and were not exposed to sunlight when collected in the field.

3.5.3 Allen's Cave, South Australia

Samples $Ox_{OD}AC390$ and $Ox_{OD}AC150$ (Roberts *et al.*, 1994a) were selected for ESR studies, using the quartz grains isolated during luminescence sample pretreatment. These samples had been recovered from a small rock shelter known as Allen's Cave, located in a doline on the limestone Nullarbor Plain. The independent age controls for these two samples are given in Table 3.7. Sample $Ox_{OD}AC390$ has been studied by OSL and dated to 38.2 ± 3.1 ka. Sample $Ox_{OD}AC150$ has been dated by OSL and TL methods, yielding ages of 9.7 ± 0.6 ka and 10.7 ± 0.9 ka, respectively. Also, charcoal samples collected from a hearth immediately overlying $Ox_{OD}AC150$ were dated by ^{14}C to 9.0-11.0 ka after calibration (using the computer program CALIB 3.0; Stuiver and Reimer, 1993). The good agreement obtained between the TL and OSL ages and the independent ^{14}C ages indicates that the quartz grains were well-bleached prior to deposition in the cave, and this inference is supported by the near-modern OSL age obtained for a near-surface sample (Roberts *et al.*, 1996). The luminescence/^{14}C age correspondence provides a firm chronology against which to compare ESR age determinations for sun-bleached quartz.

Sample preparation was conducted in subdued red (> 590 nm) light. Samples were treated with hydrogen peroxide, hydrochloric acid, fluorosilicic acid and fluoboric acid to separate the quartz and heavy minerals. Heavy minerals with a density greater than 2.7 g cm^{-3} were removed using sodium polytungstate solution. Quartz grains of 90-125 μm diameter were isolated by dry sieving and then etched in 40 % hydrofluoric acid for 45 minutes. For ESR analyses, the quartz grains were weighed into aliquots of 200 mg mass and irradiated using a ^{60}Co γ-source (dose rate of ≈ 10.7 Gy min^{-1}).

For the environmental dose rate evaluation, the sediment samples were analysed using high-resolution γ and α spectrometry at the Division of Water Resources, CSIRO (following the procedures described in Murray *et al.*, 1987; Roberts *et al.*, 1996). The

internal dose rates were estimated from instrumental neutron activation analyses of the etched quartz grains.

3.5.4 Deaf Adder Gorge, Northern Territory

Samples Ox_{OD}K166 and Ox_{OD}K172 (Roberts *et al.*, 1994b) had been collected previously from a rock shelter site in Deaf Adder Gorge, tropical northern Australia. Both samples have been dated by OSL and TL methods, and associated charcoal fragments have been dated by ^{14}C (see Table 3.8). Good agreement among these age estimates, and the young OSL age obtained for a near-surface sample (Roberts *et al.*, 1994b), indicates that the quartz grains are a reliable luminescence dosimeter and were well-bleached prior to burial. They are therefore considered well suited to ESR analysis for the purpose of identifying light-sensitive ESR signals in sun-bleached deposits. The samples were prepared in the same manner, and under the same subdued red illumination, as described in section 3.5.3. The environmental dose rate was deduced in the same manner as described in section 3.5.3 and the internal dose rate was estimated from thick-source alpha counting of the etched quartz grains (see Roberts *et al.*, 1994b).

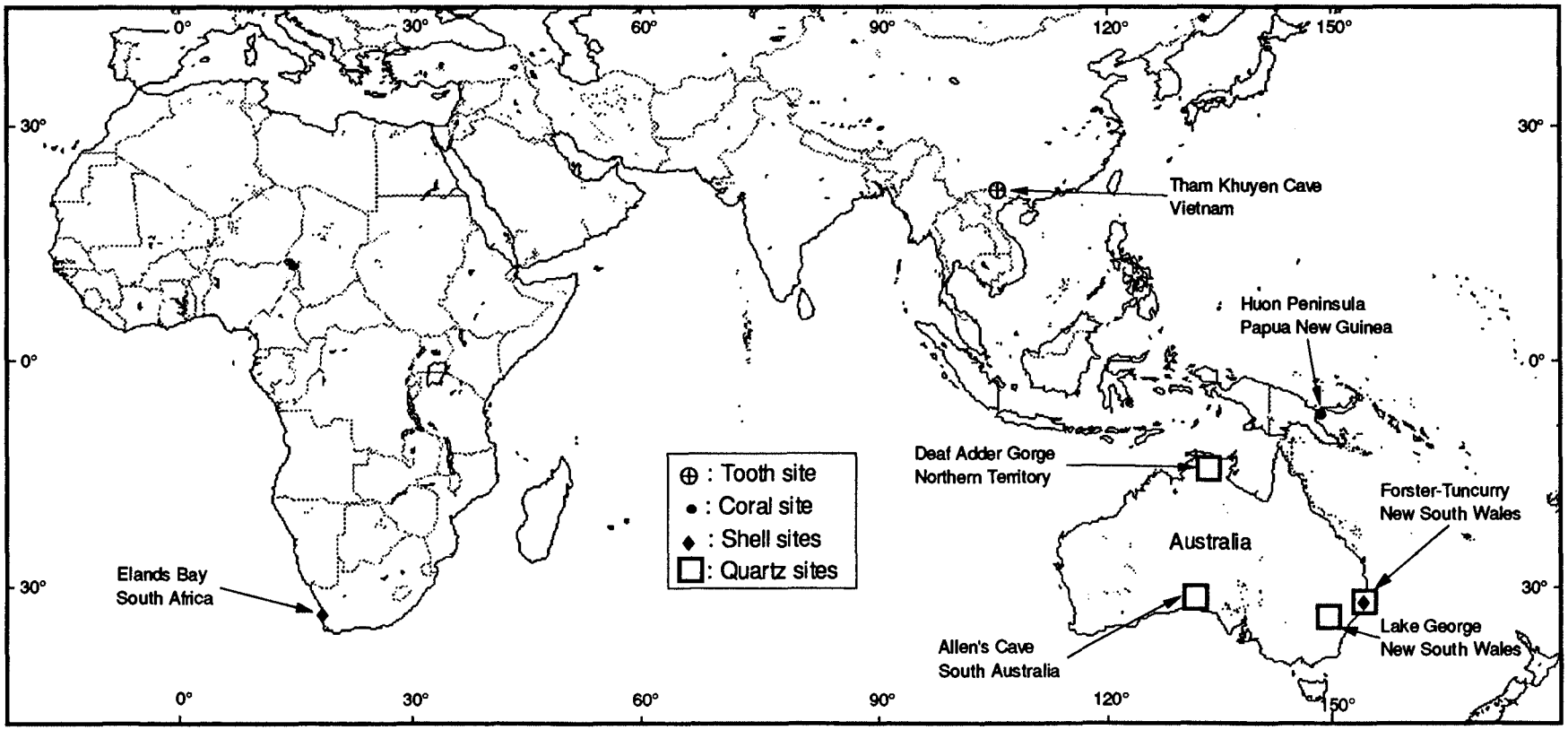

Figure 3.1. Location map of sample sites.

Table 3.1. Selected shell samples from Forster-Tuncurry Shelf, New South Wales, and radiocarbon dates (after Roy *et al.*, 1992).

Core number	Water depth (m)	Sub-bottom (cm)	Depositional environment	^{14}C age (years B.P.)	(Lab. no.)	No.	Shell species
FT 13-1	14.0	321-321	Holocene shoreface	6690 ± 103	Beta 45166	2	*Anadara trapezia*
		560-565	Holocene estuary	-		3	-
FTC 13-2	20.0	30-45	Holocene shoreface	-		4	*Linga carnosa*
						5	*Anadara trapezia*
		98-115	Holocene estuary	-		6	*Dosinia sculpta*
						7	*Dosinia sculpta*
FTC 13-3	23.5	30-70	Holocene inner shelf	-		8	*Linga carnosa*
FTC 13-5	30.4	90-103	Holocene inner shelf	2020 ± 65	Beta 45167	9	*Placamen*
						10	*Placamen*
FT 13-7	38.0	30-35	Holocene inner shelf	3070 ± 74	Beta 45168	11	*Anadara trapezia*
FT 13-8	43.0	145-150	Holocene mid shelf	6430 ± 83	Beta 45169	12	*Anadara trapezia*
FTC 13-10	53.0	120-140	Holocene mid shelf	12690 ± 83	Beta 45170	13	*Linga carnosa*
						14	*Anadara trapezia*
						15	*Linga carnosa*
						16	Oyster
						17	*Anadara trapezia*
						18	*Anadara trapezia*
						19	Oyster
		165-170	Pleistocene estuary	-		20	*Pyrazus ebeninus*
FT 14-1	20.0	435-445	Holocene back-barrier	8510 ± 93	Beta 45432	21	-
						22	*Anadara trapezia*
						23	*Anadara trapezia*
						24	-
						25	*Anadara trapezia*
						26	*Anadara trapezia*
						27	*Anadara trapezia*
						28	*Anadara trapezia*
						29	*Anadara trapezia*
						30	*Anadara trapezia*
						31	*Anadara trapezia*
FT/BMRC 19-4	29.0	223-227	Holocene mid shelf	-		32	-
						33	*Chlamys lividus*
						34	*Chlamys lividus*
						35	Oyster
						36	Oyster
						37	*Uber aulacoglossa*
						38	*Anadara trapezia*
						39	-
						40	*Anadara trapezia*
						41	-
						42	*Chlamys lividus*
FT/BMR 19-3A	90.9	290-300	Holocene mid shelf	17640 ± 113	Beta 45437	43	*Anadara trapezia*
				18420 ± 281	Beta 45438	44	*Anadara trapezia*
						45	*Anadara trapezia*
FT/BMRC 22-5	77.6	128-145	Late Pleistocene marine transgressive reworked zone	12510 ± 123	Beta 45180	46	Oyster
FTC 43-7	48.2	340-360	Holocene mid shelf	-		47	*Linga carnosa*
						48	*Linga carnosa*
						49	*Linga carnosa*

Radiocarbon ages are based on isotopic fractionation corrected ^{14}C depletion with respect to 95% of the activity of NBS oxalic acid using the ^{14}C half-life of 5570 years and assuming a δ^{13}C value of -1 ± 2‰ with respect to PDB. The ages are corrected for an Oceanic Reservoir Apparent Age of -450 ± 35 years (Gillespie and Polach, 1979).

Table 3.2. Descriptions of shell samples from Forster-Tuncurry Shelf, New South Wales (after Wells, 1984; Shepherd and Thomas, 1989).

Shell species	Habitat	Distribution
Anadara trapezia	mud flats, estuary, beaches	southern Queensland to eastern Victoria
Chlamys lividus	subtidal in areas of moderate tidal influence	New South Wales to Western Australia
Dosinia sculpta	seagrass beds	all mainland states
Linga carnosa	sand pockets among rocks below low-tide level on the open shore	?
Placamen molimen	shallow water in sand or sandy mud	New South Wales to South Australia
Pyrazus ebeninus	lives with *Pyrazus australis* in muddy foreshores usually among *Zostera* weed	New South Wales to southern Queensland
Uber aulacoglossa	sandy mud flats	southern Queensland to southern Australia

Table 3.3. Sites and shell samples from Elands Bay, South Africa, and age estimates.

Sample site	Age estimate	No.	Shell species
Borrew Pit Midden (Elands 1)	900 years B.P. (radiocarbon age of bones)	E 1	*Patella granatina apices*
		E 2	*Patella argenvillei*
		E 3	*Choromytilus meridionalis*
		E 4	*Argobuccinum argus*
Malkappan Elandas (Elands 2)	< last interglacial?	E 5	*Choromytilus meridionalis*
		E 6	*Patella granatina*
		E 7	*Burnupena papyracea*
		E 8	*Nucella cingulata*
Hoedjiespunt 1 (Elands 3)	≈ last interglacial?	E 9	*Tellina madagascariensis*
		E10	*Tellina madagascariensis*
		E11	*Dosinia lupinus*
		E12	*Dosinia lupinus*
Hoedjiespunt 2 (Elands 4)	< last interglacial?	E13	*Choromytilus meridionalis*
		E14	*Patella granatina*
		E15	*Patella granularis*
		E16	*Patella argenvillei*

Table 3.4. Descriptions of shell samples from Elands Bay, South Africa.

Shell species	Habitat	Distribution
Argobuccinum argus	lives entirely intratidally, down to about 50 m	South Africa, from East London to Namibia; also various subantarctic islands
Burnupena papyracea	pools along the low spring-tide level and down to about 37 m	Namibia to Hermanus
Choromytilus meridionalis	lives in large colonies on exposed rocks, harbour piles, etc., in the lower mid-tidal region, often in sandy areas	Namibia to Algoa Bay
Dosinia lupinus	open coast, burrowing in clean sand at depths of 8-16 m	Europe to Namibia and around the Cape to East London
Nucella cingulata	rocks along the low-water margin, and down to about 20m	Namibia to False Bay
Patella argenvillei	exposed rocks in a belt at about low-water spring-tide level, especially where these are encrusted with calcareous algae (*Lithothamnion*)	Namibia to western Transkei
Patella granatina *Patella granatina apices*	largely restricted to the cold Atlantic coast, where it clings to mid-tidal rocks, often in pools	Namibia to Danger Point (just east of False Bay)
Patella granularis	intertidal rocks, from just below high-water spring-tide level to below low-water neap-tide level	Namibia to Zululand
Tellina madagascariensis	open coast, chiefly below tide limits and down to about 3 m	around the Cape during the Pleistocene (now extinct)

Table 3.5. Age estimates for corals from Huon Peninsula, Papua New Guinea (after Grün *et al.*, 1992; Chappell *et al.*, 1994b and Omura *et al.*, 1994).

Reef	Geological estimate (ka)	Field no. (Lab. no.)	$(^{234}U/^{238}U)_0$ (activity ratio)	U (ppm)	Alpha spectrometric U-series age ± 1σ (years)	Mass spectrometric U-series age ± 2σ (years)	ESR Lab. no.	ESR age ± 1σ (years)
terrace II	29	KWA I1 (KK-08)	1.137 ± 0.015	3.002 ± 0.047	44,000 ± 1,400	41,120 ± 500	670	49,000 ± 5,400
		KWA N1 (AO344)	1.138 ± 0.015	2.743 ± 0.035	50,500 ± 1,300	52,860 ± 440	671	54,400 ± 5,600
terrace IIIb	40	KWA J1 (KK-10)	1.116 ± 0.012	4.150 ± 0.058	(38,200 ± 1,100)[1,2]	-	666	56,200 ± 4,900
		KAN C2 (KK-11)	1.119 ± 0.017	2.417 ± 0.038	(46,400 ± 1,600)[2]	-	664	38,900 ± 4,200
		KWA K1 (AO347)	1.150 ± 0.017	2.972 ± 0.043	56,000 ± 1,500	53,160 ± 430	665	50,900 ± 5,500
terrace IIIa	44 - 53	KAN D4 (AO345)	1.149 ± 0.013	4.429 ± 0.056	(42,300 ± 1,100)[1]	-	669	52,600 ± 6,500
		KAN D4 (AO359)	1.138 ± 0.016	4.570 ± 0.060	(42,800 ± 1,100)[1]	-	-	-
		KWA Q1 (AO346)	1.145 ± 0.015	3.356 ± 0.044	57,500 ± 1,500	48,970 ± 590	667	55,300 ± 6,900
		KAN D5 (AO360)	1.160 ± 0.015	3.211 ± 0.039	(57,800 ± 1,400)[2]	(46,360 ± 710)[2]	668	54,900 ± 6,600
		KAN D5 (KK-09)	1.111 ± 0.015	3.155 ± 0.048	(61,600 ± 2,000)[2]	-	-	-
terrace IV	70	SIAL E1 (AO369)	1.125 ± 0.016	3.108 ± 0.040	(65,800 ± 1,800)[2]	(59,120 ± 1,290)[2]	663	68,000 ± 8,400
		FRT F1 (AO349)	1.147 ± 0.014	2.728 ± 0.029	72,800 ± 2,200	69,130 ± 730	662	74,600 ± 7,800

Notes: $^{230}Th/^{234}U$ ages in parentheses are considered to be unreliable since those samples do not meet the following criteria:
(1) The uranium concentration should be the same as in present-day counterparts (2 to 4 ppm).
(2) The initial $^{234}U/^{238}U$ activity ratio, $(^{234}U/^{238}U)_0$, should be consistent with that in modern sea water, 1.13 to 1.16 (mean = 1.144 ± 0.002; Chen *et al.*, 1986).
(3) The sample should be free (i.e. contain < 0.02 ppm) of initial ^{230}Th, incorporated at its living stage, and/or secondary ^{230}Th, introduced by contamination during diagenesis.

Table 3.6. Thermoluminescence details for quartz samples from Forster-Tuncurry Shelf, New South Wales (after Roy *et al.*, 1992).

Sample code	Core number	Water depth (m)	Sub-bottom (cm)	Laboratory number	Plateau region (°C)	Palaeodose (Gy)	K content (% by AES)	Moisture content (% by weight)	U + Th specific activity (Bq kg^{-1})	Annual radiation dose (μGy $year^{-1}$)	TL age (ka)
Q13	FT 13-3	23.5	190-195	W1130	325 - 500	130.9 ± 17.2	0.580 ± 0.005	19.6 ± 3	48.8 ± 1.5	1368 ± 45	95.7 ± 13.0
Q18	FT 13-7	38.3	120-125	W1131	300 - 500	55.4 ± 7.3	0.732 ± 0.005	21.0 ± 3	17.3 ± 0.7	1044 ± 41	53.1 ± 7.3

Notes:
1. The specific activity of these samples was measured by means of thick-source alpha counting over a 42 mm ZnS scintillation screen. The values shown assume secular equilibrium in both the U and Th decay chains. Uncertainty levels represent one standard deviation.
2. Palaeodose analysis temperatures are 375°C.
3. A Rb content of 50 ± 25 ppm is assumed.
4. A cosmic ray dose rate contribution of 150 ± 50 μGy $year^{-1}$ is assumed.

Table 3.7. Ages of samples $Ox_{OD}AC150$ and $Ox_{OD}AC390$ from Allen's Cave, South Australia, estimated by ^{14}C, OSL and TL (Roberts *et al.*, 1994a, 1996).

Sample code	Dating method	Equivalent dose (Gy)	Age (ka)
$Ox_{OD}AC150$	^{14}C	-----	9.65 ± 0.65 (ANU-8077) $10.2 \pm \frac{0.6}{0.3}$ (ANU-6850) 10.5 ± 0.5 (ANU-6849)
	OSL	23.5 ± 0.6	9.7 ± 0.6
	TL	25.9 ± 1.4	10.7 ± 0.9
$Ox_{OD}AC390$	OSL	66.6 ± 2.3	38.2 ± 3.1

Notes: 1. OSL samples were preheated for 5 min at 220°C.
2. TL age is determined from the 265-380°C plateau region.
3. ^{14}C ages are calibrated according to Stuiver and Reimer (1993).

Table 3.8. Ages of samples $Ox_{OD}K166$ and $Ox_{OD}K172$ from Deaf Adder Gorge, Northern Territory, estimated by ^{14}C, OSL and TL (Roberts *et al.*, 1994b).

Sample code	Dating method	Equivalent dose (Gy)	Age (ka)
$Ox_{OD}K172$	^{14}C	---	8.3 - 8.6 (ANU-8652) 8.7 - 9.3 (ANU-8653) 10.5 - 11.3 (ANU-8677) 11.1 - 12.9 (ANU-8654) 12.5 - 13.5 (ANU-8676) 12.6 - 13.0 (ANU-8678) 15.0 - 16.2 (SUA-236)
	OSL	11.2 ± 0.3	13.5 ± (0.5, 0.9)
	TL	12.1 ± 0.6	14.6 ± (0.9, 1.2)
$Ox_{OD}K166$	^{14}C	---	~ 24 (SUA-237) ~ 27 (ANU-3182)
	OSL	24.6 ± 0.7	30.0 ± (1.7, 2.4)
	TL	23.1 ± 1.0	28.1 ± (1.9, 2.4)

Notes: 1. Equivalent doses are given as mean ± standard error. The total uncertainty associated with laboratory β doses is estimated as 4% at the 2σ level and is included as a systematic uncertainty in the age determination. OSL samples were preheated for 5 min at 220°C.
2. OSL and TL ages are given as mean ± (random uncertainty, total uncertainty). TL ages of $Ox_{OD}K172$ and $Ox_{OD}K166$ are determined from the 275-375°C and 270-430°C plateau regions, respectively.
3. ^{14}C ages are calibrated according to Stuiver and Reimer (1993) and Bard *et al.* (1993).

Part II

DATING USING PUBLISHED METHODS

Chapter 4 SHELL SAMPLES

To estimate the age of marine deposits, marine fossil shells, corals and quartz sediments were dated by ESR. The time range of these samples was expected to be as young as Holocene to as old as last interglacial in age, which is far beyond the upper limit of the ^{14}C dating method. For the fossil shells, individual shell fragments were used for the ESR analyses. The most widely accepted procedures used in the early 1990's were chosen for initial ESR examination, and these measurements are reported in this chapter.

4.1 Forster-Tuncurry, New South Wales

4.1.1 Methods used

ESR measurements were carried out initially for all shell samples and signal intensities at g=2.0014, the g-value recommended by Radtke *et al.* (1985), were used to determine values of accumulated dose (the D_E-values). Further ESR studies, using a higher microwave power and signal intensities at g=2.0006 (after Barabas *et al.*, 1992a, 1992b), were made using 14 shell samples from three cores, FT13-10, FT14-1 and FT/BMR19-3A. Radiocarbon dates, obtained using an accelerator mass spectrometer (AMS), provided independent age control. Targets for AMS ^{14}C dating were prepared by Mr John Head at the Quaternary Dating Research Centre (QDRC), Research School of Pacific and Asian Studies at the ANU, and the isotope ratios were measured by Dr. Keith Fifield at the Research School of Physical Sciences and Engineering, ANU. Typical ESR spectra of marine molluscs, and the methods used to measure the signal intensities, are shown in Figure 4.1.

For each sample, seven to ten aliquots, each weighing 200 mg, were irradiated using a ^{60}Co γ-source; one aliquot was kept unirradiated (the 'natural') and the others were given doses of up to $\approx$ 135 Gy. More than 10 weeks after the irradiation, ESR measurements

were carried out at room temperature (≈ 22°C) by X-band ESR spectrometers (Jeol JES-PE, Bruker ER 200D-SRC and Bruker ESP 300E); Grün (1989) suggested that ESR measurements should be made at least two weeks after irradiation. ESR spectra were recorded with a modulation frequency of 100 kHz, a modulation amplitude of 0.5 Gpp, a scan range of 30 G, and a scan speed of 2 G min^{-1} with a time constant of 500 ms. The ESR signals at g=2.0014 and g=2.0006 were recorded using microwave powers of 2 mW and 200 mW, respectively. D_E-values were estimated by constructing dose response curves of ESR intensity versus added dose, and obtaining the D_E-values by the extrapolation of a single saturating exponential or a saturating-exponential-plus-linear curve fitted to the data points; the choice of curve was made on the basis of the goodness-of-fit to the data sets, as described later in this thesis (Chapter 9). Each aliquot was weighted by the inverse square of its ESR signal intensity, using the 'DOSE' program reported by Brumby (1992).

To determine the natural dose rate, the concentrations of radioactive elements in the shell samples and the sediments of the cores were analysed. For the internal dose rate analysis, uranium contents of the shell samples were determined by inductively-coupled plasma mass spectrometry (ICP-MS) at the Research School of Earth Sciences, ANU. Although mollusc shells are usually free of thorium, rubidium and potassium (Grün, 1989), potassium contents were checked by flame photometry. To determine the external dose rates, sediment samples were analysed using high-resolution γ-ray spectrometry at the Division of Water Resources, CSIRO (following the procedures described in Murray *et al.*, 1987). Since a common habitat of *Anadara trapezia* species is muddy flats or estuaries, two estuarine sediments from cores FT13-2 and FT14-1 (containing 10 % and 50 % mud, respectively) were also analysed.

The saturated water contents (W (%) = (mass of water / mass of dry sediment) × 100) of the sediments were determined by heating the water-saturated sediments at 105°C; an error term of ± 5 % was attached to each water content determination. W was calculated from the difference in mass between the water-saturated sediments and their fully dried

counterparts. Since the sediments have never been above sea level, the fraction of time spent at saturation (F) is assumed to be 1 for all sediments. Water correction factors for β and γ attenuation were made using the equations given by Aitken (1985). The reduction in β-particle contributions due to attenuation and acid etching was corrected using equation (3) of Grün (1986). The cosmic ray dose rates were estimated using the equations reported in Prescott and Hutton (1988, 1994); the time-averaged water depths (estimated from the sea level curve of Thom and Roy (1985), as modified by Roy *et al.* (1992) on the basis of additional ^{14}C dates), were taken into account. The significance to the dose rate of any unsupported excess of ^{230}Th with respect to ^{234}U was examined using the method described in Huh and Kadko (1992). The shell samples from cores FT13-10, FT14-1 and FT/BMR19-3A were checked for possible recrystallisation from aragonite to calcite using X-ray diffraction (XRD) at the Department of Geology, ANU; such recrystallisation may cause underestimation of the D_E-values (e.g. Grün, 1989).

For the ESR age calculations, an initial $^{234}U/^{238}U$ ratio of 1.14 ± 0.01 was assumed for sea water (following Chen *et al.*, 1986, who determined a present sea water value of 1.144 ± 0.002), and a *k*-value of 0.1 ± 0.05 (Grün, 1985a) was used. Since mollusc shells behave as open systems in respect to uranium (Kaufman *et al.*, 1971), ESR ages of the samples with uranium concentrations > 0.5 ppm were estimated for both early and linear uranium-uptake models, based on the equations described in section 2.2.

4.1.2 ESR ages obtained

ESR results of all shell samples, based on the signal at g=2.0014, are given in Table 4.1; a natural dose rate (internal plus external) of 1 mGy $year^{-1}$ is assumed for ESR age calculations. Unfortunately, D_E-values of five samples (numbers 19, 33, 36, 39 and 41) were not obtained because the signal at g=2.0014 overlapped with the Mn^{2+} signal. Additional ESR results, based on the signals at g=2.0006, of 14 shell samples from cores FT13-10, FT14-1 and FT/BMR19-3A are given in Table 4.2(a). In this table, analytical data were used to estimate the natural dose rates and these are given in Table 4.2(b).

Some examples of ESR spectra and dose response curves are shown in Figures 4.2(a)-(d). All shell samples shown in Tables 4.2(a) and (b) were found to consist of more than 95 % aragonite, suggesting that little recrystallisation has occurred.

In Figure 4.3, D_E-values based on the signals at g=2.0014 are compared with those obtained at g=2.0006. For samples 15 and 29, the D_E-values based on the signal at g=2.0014 agree at the 1σ level with those based on the g=2.0006 signal. For the other samples, D_E-values based on the signal at g=2.0014 are always smaller than those based on the g=2.0006 signal (Table 4.2(a)). Barabas *et al.* (1992a, 1992b) proposed that the signal at g=2.0006 was a dating signal probably associated with a rapidly rotating CO_2^- centre. This suggests, therefore, that the signal intensity at g=2.0014 does not represent the CO_2^- centre but may be associated with other overlapping paramagnetic centres such as g=2.0032 and g=2.0020 signals.

From the determined radionuclide data (Table 4.2(b)), all sediments show disequilibrium within the ^{238}U decay chain, with a deficit of ^{226}Ra (and daughters) with respect to ^{238}U. Radium desorption from sediments is commonly encountered in saline waters, such as estuaries and oceans (Ivanovich and Harmon, 1992). The estuary sediments containing about 50 % mud exhibit much higher dose rates ($\approx$ 2 times) than the other, sandy, sediments. Unexpectedly (cf. Grün, 1989), some shell samples contained substantial amounts of potassium (>0.4 %) and its contribution to the natural dose rates was considerable. Rubidium concentrations, however, were too low to be detected by atomic absorption spectrophotometry and thus made a negligible contribution to the dose rates. The uranium concentrations of the shell samples were very low, so the ESR ages show little difference between the early-uptake and linear-uptake uranium models.

The possibility of a significant unsupported excess of ^{230}Th was examined using equation 13.3 of Huh and Kadko (1992): $A_0=\lambda[U]L/DS$, where λ is the decay constant ($year^{-1}$) of ^{230}Th, [U] is the concentration (dpm cm^{-3}) of the parent U isotope (^{234}U) in sea water, L is the water depth (cm), D is the dry bulk sediment density (g cm^{-3}) and S is the

sedimentation rate (cm year^{-1}). By assuming a mean concentration of ^{238}U and the ^{234}U/^{238}U ratio in sea water as 3.3 μg l^{-1} and 1.14, respectively, 0.0028 dpm cm^{-3} is obtained for [U]. Using *L*, *D* and *S* values of 3000 cm, 1.5 g cm^{-3} and 2 cm year^{-1}, respectively, a ^{230}Th excess of 0.00043 Bq kg^{-1} is obtained. This is equivalent to 6.7 × 10^{-3} μGy year^{-1}, uncorrected for β-attenuation. Huh and Kadko (1992) reported the ^{230}Th/^{231}Pa activity ratio as 10.8, so the unsupported excess of ^{231}Pa can be assumed to be around 6.2 × 10^{-4} μGy year^{-1}. These values, however, are likely to be maxima because: (a) ^{230}Th and ^{231}Pa are incompletely removed from the water column in the open ocean (Huh and Kadko, 1992); and (b) there is likely to be ^{226}Ra disequilibrium (loss of ^{226}Ra) from the unsupported ^{230}Th component, as observed in the sediment samples. The addition of 0.00043 Bq kg^{-1} ^{230}Th may therefore give much less excess of ^{226}Ra and daughters, from where most of the dose rate is derived in the uranium chain. Thus, the unsupported excess of ^{230}Th and ^{231}Pa is likely to provide a negligible addition to the dose rate (< 7.3 × 10^{-3} μGy year^{-1}) in these coastal deposits.

These results suggest that the total dose rates are dominated by the dose rates of the sediments. There may be a possibility, therefore, that the ESR ages of *Anadara trapezia* shells will be overestimated if the dose rate of the sandy sediments where the shell samples were collected is used to represent the dose rate for the entire period of shell burial. The degree of overestimation will depend on the period over which the shell samples were buried initially in a muddy (higher dose rate) sediment, compared to the period during which the shells were buried subsequently in sandy sediments.

4.1.3 Comparisons with independent age controls

The estimated ages from bulked shell radiocarbon assays, AMS radiocarbon determinations on individual shells, and the ESR ages are compared in Table 4.3. ESR ages based on the signals at g=2.0014 and g=2.0006 are compared with AMS ^{14}C ages in Figure 4.4.

The AMS results for the three cores show a wide range of ages: 9,000-36,000 years (FT13-10), 6,000-9,000 years (FT14-1) and 10,000-16,000 years (FT/BMR19-3A), indicating that the shells consist of a mixture of reworked fossil shells. If the youngest AMS dates represent the age of deposition of the sediments, then the shell hash ages yield substantial overestimates of the date of sedimentation: ≈ 3,000, 2,000 and 8,000 years too old for FT13-10, FT14-1 and FT/BMR19-3A, respectively. This indicates that fossil shells represent a mixture of shells of various ages and that bulk (shell hash) ^{14}C age determinations are liable to greatly overestimate the age of the most recent period of sediment and shell deposition. It should be noted that the ^{14}C ages discussed here are not calibrated for changes in initial ^{14}C concentrations over time (Bard *et al.*, 1993) but are corrected for the marine reservoir effect (Roy *et al.*, 1992). Calibration of the AMS ^{14}C ages would increase those at ≈ 6, 10, and 30 ka B.P. by around 0.8, 1.5 and 3-4 ka, respectively (Stuiver and Reimer, 1993; Bard *et al.*, 1993).

While inconclusive, the AMS ^{14}C dates appear closer to the ESR ages based on the signal at g=2.0014 than the ESR ages based on the g=2.0006 signal. For five samples (14, 17, 21, 29 and 43), ESR ages based on the signal at g=2.0014 agree at the 1σ error level with the AMS ^{14}C dates, while the ESR ages of the other samples are underestimated. ESR ages of samples 23, 29 and 45 based on the g=2.0006 signal are in agreement with their AMS ^{14}C counterparts at the 1σ error level, while the ESR ages of the other samples are overestimated, with one exception. Since the shell uranium concentrations were very low, and had a minimal effect on the ESR ages, it is not possible to distinguish between the linear-uptake and early-uptake ages to infer the correct uptake model. For some samples, the discrepancies between the ESR ages, based on the signals at g=2.0014 and g=2.0006, and the AMS ^{14}C ages are significant and this may not simply be explained by the effect of sediment reworking on the natural dose rates. The question arises as to whether or not these ESR signals are suitable for dating. Further studies were carried out on these shell samples using a Q-band spectrometer and the results are discussed in Chapter 12.

4.2 Elands Bay, South Africa

4.2.1 Methods used

For the ESR measurements on each sample, 10 aliquots, each weighing 100 mg, were irradiated using a ^{60}Co γ-source; one aliquot was kept unirradiated (the 'natural') and the other nine aliquots were given doses of 6.5, 15.2, 30.5, 63.8, 134.8, 305.4, 524.8, 722.0 and 1039.4 Gy. More than 8 weeks after the irradiation, the ESR intensities at g=2.0014 were measured with Jeol JES-PE and Bruker ESP 300E spectrometers at room temperature (≈ 20°C). The same instrument settings as described in section 4.1.1 were used, except for a scan speed of 5.4 G min^{-1} with a time constant of 655 ms. D_E-values were estimated by extrapolation of additive-dose dose response curves using the 'DOSE' curve-fitting program (Brumby, 1992), as described in section 4.1.1.

The environmental gamma dose rates were measured *in situ* at the sampling sites by Dr. R. Grün using a portable γ-ray spectrometer. To estimate the β dose rates in the sediments, uranium and thorium contents were analysed by ICP-MS at the Research School of Earth Sciences, ANU, and potassium and rubidium contents were determined by atomic absorption spectrophotometry (AAS). To estimate the internal dose rates, the uranium, thorium and rubidium contents of the shell samples were measured by ICP-MS and the potassium contents were determined by flame photometry. Aragonite to calcite mass ratios of the fossil shell samples, as well as the ratios for modern shells of the same species collected from the beach near the sampling sites, were determined by XRD at the Department of Geology, ANU.

ESR ages were calculated in the same manner as described in section 4.1.1, except that a time-averaged water content (W×F: W(%) = (mass of water / mass of dry sediment) × 100; F = fraction of burial time spent at saturation) of 10 ± 5 % was assumed for the sediments. Cosmic ray dose rates were estimated by using the equations described in

Prescott and Hutton (1988, 1994) and by assuming burial depths of 1 ± 0.5 m for Borrew Pit Midden and 3 ± 1 m for the other sites.

4.2.2 ESR ages obtained

The ESR results based on the signal at g=2.0014 are shown in Table 4.4(a). The XRD data and analytical data used to estimate the natural dose rates are shown in Table 4.4(b). Selected XRD spectra are shown in Figure 4.5. The shell samples containing calcite did not show an ESR signal at g=2.0014. XRD results indicate that shell species of *Argobuccinum argus* (sample E4), *Burnupena papyracea* (sample E7), *Tellina madagascariensis* (samples E9 and E10) and *Dosinia lupinus* (samples E11 and E12) are aragonite-dominated shells (>99 % by mass). For these samples, D_E-values were estimated using the signal at g=2.0014; ESR spectra and dose response curves for these species are shown in Figures 4.6(a)-(d). Modern shells of *Choromytilus meridionalis*, *Nucella cingulata*, *Patella argenvillei*, *Patella granatina* and *Patella granularis* were found to be rich in calcite, and to have similar ratios of aragonite to calcite as their fossil shell counterparts. This suggests that in the fossil shells containing calcite, the calcite is not the result of recrystallisation and, thus, that these shell samples may be suitable for ESR dating. Further studies on the shell samples containing calcite were carried out after a preheating treatment and the results are presented in Chapter 12. Shells of species *Choromytilus meridionalis* (samples E3, E5 and E13) contained Mn^{2+} signals which interfered with the dating signal at g=2.0014; D_E-values for these samples were therefore not obtained.

The analytical data of the shell samples indicate that the uranium and thorium contents of the shells may be influenced by those of the surrounding sediments and by the particular species of shell. The shell species (*Dosinia lupinus* and *Tellina madagascariensis*) and the sediment at the Hoedjiespunt 1 site are high in uranium (0.8-1.6 ppm and 6.4 ppm for the shells and sediment, respectively) and thorium (23-402 ppb and 24.0 ppm for the shells and sediment, respectively), with a γ-dose rate of 581.0 μGy $year^{-1}$ determined from

the portable gamma-spectrometer readings. Among these shell samples, the uranium and thorium concentrations in *Dosinia lupinus* (1.6 ppm and 70-400 ppb, respectively) are much higher than those in *Tellina madagascariensis* (0.8-1.0 ppm and 20-40 ppb, respectively). Similar observations were made at the sampling sites of Borrew Pit Midden and Hoedjiespunt 2. Rubidium contents in the shell samples were negligible.

The natural dose rates were dominated by the contribution from sediments and cosmic rays, rather than by the uranium and thorium contents of the shell samples. There are, therefore, insignificant differences between the ESR ages based on the early and linear uranium-uptake models. ESR ages obtained for Hoedjiespunt 1 vary from around 17 ka to 80 ka. *Dosinia lupinus* shells give ages of about 60-80 ka, whereas *Tellina madagascariensis* shells indicate much younger ages of about 17-40 ka. Since the sediments at Hoedjiespunt 1 have probably not been extensively reworked or mixed, the considerable ESR age variation among the fossil shells, as observed also for the Forster-Tuncurry shell samples, implies that the ESR dates cannot be used to infer the correct age of the deposit. Alternatively, the deposit may have been reworked more than is suspected.

4.2.3 Comparisons with independent age controls

The ESR ages for the shell samples are poorly constrained by independent age estimates, and no independent age is available for each of the shells. The ESR age of sample E4 from Borrew Pit Midden (3.1 ± 0.4 ka) is much older than the radiocarbon age of ≈ 900 years B.P. obtained from bones excavated at this site. The shell sample E4, however, may have been reworked and the ESR age obtained may not correspond to the most recent phase of sediment deposition. Four ESR ages obtained for Hoedjiespunt 1 indicate a very wide age range (16.7-78.2 ka) and preclude a firm age estimate for this site. The ESR ages obtained indicate a Pleistocene age that is younger than last interglacial, which was the age previously ascribed to this unit on the basis of geological expectations (see section 3.2.2). Clearly, the validity of using ESR signals to date shell samples at Elands Bay and Forster-Tuncurry is not proven using published ESR dating methods. Further

methodological developments are described in Chapters 10 and 12 that are intended to resolve some of the uncertainties in dating shells by ESR.

Table 4.1. ESR results based on the signal at g=2.0014 for shell samples from Forster-Tuncurry Shelf, New South Wales.

Core number	Water depth (m)	Sub-bottom (cm)	No.	Shell species	^{14}C age (years B.P.)	ESR D_E (Gy)	ESR Age (years)
FT 13-1	14.0	321-321	2	*Anadara trapezia*	6690 ± 103	5.2 ± 0.6	5200 ± 600
		560-565	3	-	-	2.5 ± 2.2	2500 ± 2200
FTC 13-2	20.0	30-45	4	*Linga carnosa*	-	1.7 ± 0.2	1700 ± 200
			5	*Anadara trapezia*		2.9 ± 0.4	2900 ± 400
		98-115	6	*Dosinia sculpta*	-	6.4 ± 0.5	6400 ± 500
			7	*Dosinia sculpta*		7.9 ± 1.0	7900 ± 1000
FTC 13-3	23.5	30-70	8	*Linga carnosa*	-	3.4 ± 2.4	3400 ± 2400
FTC 13-5	30.4	90-103	9	*Placamen molimen*	2020 ± 65	3.7 ± 0.8	3700 ± 800
			10	*Placamen molimen*		3.3 ± 1.1	3300 ± 1100
FT 13-7	38.0	30-35	11	*Anadara trapezia*	3070 ± 74	7.0 ± 2.9	7000 ± 2900
FT 13-8	43.0	145-150	12	*Anadara trapezia*	6430 ± 83	4.3 ± 0.6	4300 ± 600
FTC 13-10	53.0	120-140	13	*Linga carnosa*	12690 ± 83	29.0 ± 2.0	29000 ± 2000
			14	*Anadara trapezia*		7.0 ± 0.4	7000 ± 400
			15	*Linga carnosa*		35.5 ± 3.4	35500 ± 3400
			16	Oyster		12.9 ± 2.1	12900 ± 2100
			17	*Anadara trapezia*		5.9 ± 0.7	5900 ± 700
			18	*Anadara trapezia*		5.5 ± 0.6	5500 ± 600
			19	Oyster		Mn^{2+}	-
		165-170	20	*Pyrazus ebeninus*	-	5.9 ± 0.3	5900 ± 300
FT 14-1	20.0	435-445	21	-	8510 ± 93	3.4 ± 0.2	3400 ± 200
			22	*Anadara trapezia*		1.7 ± 0.1	1700 ± 100
			23	*Anadara trapezia*		0.68 ± 0.06	680 ± 60
			24	-		2.1 ± 1.2	2100 ± 1200
			25	*Anadara trapezia*		5.6 ± 1.3	5600 ± 1300
			26	*Anadara trapezia*		4.2 ± 0.9	4200 ± 900
			27	*Anadara trapezia*		2.5 ± 0.1	2500 ± 100
			28	*Anadara trapezia*		2.0 ± 0.3	2000 ± 300
			29	*Anadara trapezia*		3.8 ± 0.8	3800 ± 800
			30	*Anadara trapezia*		2.3 ± 1.5	2300 ± 1500
			31	*Anadara trapezia*		2.3 ± 1.8	2300 ± 1800
FT/BMRC 19-4		223-227	32	-	-	13.9 ± 2.5	13900 ± 2500
			33	*Chlamys lividus*		Mn^{2+}	-
			34	*Chlamys lividus*		1.5 ± 0.4	1500 ± 400
			35	Oyster		2.4 ± 1.6	2400 ± 1600
			36	Oyster		Mn^{2+}	-
			37	*Uber aulacoglossa*		2.9 ± 1.0	2900 ± 1000
			38	*Anadara trapezia*		5.0 ± 0.7	5000 ± 700
			39	-		Mn^{2+}	-
			40	*Anadara trapezia*		4.9 ± 0.5	4900 ± 500
			41	-		Mn^{2+}	-
			42	*Chlamys lividus*		5.0 ± 0.5	5000 ± 500
FT/BMR 19-3A	90.9	290-300	43	*Anadara trapezia*	17640 ± 113	4.6 ± 0.4	4600 ± 400
			44	*Anadara trapezia*	18420 ± 281	4.0 ± 0.3	4000 ± 300
			45	*Anadara trapezia*		4.2 ± 0.4	4200 ± 400
FT/BMRC 22-5	77.6	128-145	46	Oyster	12510 ± 123	3.8 ± 0.6	3800 ± 600
FTC 43-7	48.2	340-360	47	*Linga carnosa*	-	15.3 ± 4.3	15300 ± 4300
			48	*Linga carnosa*		17.1 ± 4.1	17100 ± 4100
			49	*Linga carnosa*		15.2 ± 2.4	15200 ± 2400

Notes: 1. A dose rate of 1 mGy $year^{-1}$ is assumed for ESR age calculations.

2. Mn^{2+}: The dating signal (g=2.0014) was not observed because of an overlapping Mn^{2+} signal.

3. Radiocarbon ages are based on isotopic fractionation corrected ^{14}C depletion with respect to 95% of the activity of NBS oxalic acid using the ^{14}C half-life of 5570 years and assuming a $\delta^{13}C$ value of -1 ± 2‰ with respect to PDB. The ages are corrected for an Oceanic Reservoir Apparent Age of -450 ± 35 years (Gillespie and Polach, 1979).

Table 4.2(a). ESR ages based on the signals at g=2.0014 (microwave power of 2 mW) and g=2.0006 (200 mW) for shell samples from Forster-Tuncurry Shelf, New South Wales.

Core number (Water depth)	Sub-bottom (cm)	Sample number	ESR analysis (g=2.0014, 2 mW)			ESR analysis (g=2.0006, 200 mW)		
			Internal dose rate (μGy year^{-1})	D_E-value (Gy)	Age (years)	Internal dose rate (μGy year^{-1})	D_E-value (Gy)	Age (years)
FT13-10 (43 m)	120-140	13	245 ± 15	29.0 ± 2.0	42,200 ± 3,200	247 ± 15	35.4 ± 1.2	51,400 ± 2,500
		14	336 ± 25 (303 ± 29)	7.0 ± 0.4	9,600 ± 600 (10,100 ± 600)	345 ± 28 (307 ± 29)	15.3 ± 0.4	20,900 ± 900 (22,000 ± 800)
		15	276 ± 21	35.5 ± 3.4	49,400 ± 5,100	281 ± 22	46.5 ±11.7	64,200 ± 16,400
		17	130 ± 11	5.9 ± 0.7	11,400 ± 1,300	133 ± 12	9.1 ± 0.3	17,500 ± 900
		18	100 ± 12	5.5 ± 0.6	11,300 ± 1,300	106 ± 14	11.8 ± 0.3	23,700 ± 1,200
FT14-1 (19 m)	435-445	21	83 ± 13	3.4 ± 0.2	7,000 ± 500	89 ± 15	8.8 ± 0.1	18,000 ± 800
		22	232 ± 21 (202 ± 20)	1.7 ± 0.1	2,700 ± 200 (2,800 ± 200)	235 ± 22 (203 ± 20)	4.0 ± 0.1	6,300 ± 300 (6,600 ± 300)
		23	121 ± 23 (85 ± 13)	0.68 ± 0.06	1,300 ± 100 (1,400 ± 100)	128 ± 26 (88 ± 13)	4.1 ± 0.1	7,700 ± 500 (8,300 ± 400)
		27	79 ± 18 (51 ± 9)	2.5 ± 0.1	5,100 ± 400 (5,400 ± 400)	82 ± 18 (52 ± 9)	4.2 ± 0.2	8,600 ± 600 (9,200 ± 500)
		28	64 ± 13	2.0 ± 0.3	4,300 ± 600	69 ± 14	5.6 ± 0.1	12,000 ± 600
		29	64 ± 14	3.8 ± 0.8	8,200 ± 1,800	64 ± 15	4.2 ± 0.2	8,900 ± 700
FT/BMR19-3A (90 m)	290-300	43	57 ± 12	4.6 ± 0.4	11,400 ± 1,100	60 ± 13	7.2 ± 0.3	17,700 ± 1,200
		44	48 ± 12	4.0 ± 0.3	10,000 ± 900	50 ± 13	5.8 ± 0.2	14,600 ± 900
		45	82 ± 18 (52 ± 9)	4.2 ± 0.4	9,800 ± 1,100 (10,500 ± 1,200)	86 ± 19 (54 ± 9)	6.6 ± 0.2	15,200 ± 1,000 (16,400 ± 900)

Note: ESR ages without and with parentheses are based on early and linear uranium-uptake models, respectively.

Table 4.2(b). Analytical data for shells and sediments from Forster-Tuncurry Shelf, New South Wales.

Core number (water depth)	Sub-bottom (cm)	Sample number	Shell				Sediment							Cosmic ray dose rate (μGy year^{-1})	External γ-ray dose rate (μGy year^{-1})
			Shell thickness (μm)	Removed outer layer (μm)	U (ppm)	K (%)	^{238}U (Bq kg^{-1})	^{226}Ra (Bq kg^{-1})	^{210}Pb (Bq kg^{-1})	^{232}Th (Bq kg^{-1})	^{228}Ra (Bq kg^{-1})	^{40}K (Bq kg^{-1})	W (%)		
FT13-10 (43m)	120-140	13	1000 ± 100	150 ± 15	0.19	0.42	18.2 ± 4.5	6.9 ± 0.4	2.9 ± 3.4	9.5 ± 1.1	9.5 ± 1.1	123.4 ± 7.8	20.9 ± 1.0	33.1 ± 3.8	260.2 ± 8.1
		14	1500 ± 150	200 ± 20	0.58	0.44									
		15	1000 ± 100	150 ± 15	0.32	0.44									
		17	1500 ± 150	200 ± 20	0.28	0.16									
		18	1500 ± 150	200 ± 20	0.34	0.10									
FT14-1 (19m)	435-445	21	1500 ± 150	200 ± 20	0.38	0.07	22.6 ± 2.5	6.0 ± 0.2	5.7 ± 15.8	9.1 ± 0.3	8.5 ± 0.6	116.1 ± 2.5	16.8 ± 0.8	49.0 ± 5.3	271.5 ± 7.2
		22	1500 ± 150	200 ± 20	0.59	0.28									
		23	1500 ± 150	200 ± 20	0.74	0.08									
		27	1500 ± 150	200 ± 20	0.53	0.04									
		28	1500 ± 150	200 ± 20	0.39	0.03									
		29	1500 ± 150	200 ± 20	0.42	0.03									
FT/BMR19-3A (90m)	290-300	43	1500 ± 150	200 ± 20	0.34	0.03	15.7 ± 2.7	9.5 ± 0.2	37.2 ± 17.1	9.2 ± 0.5	8.3 ± 0.6	70.2 ± 2.1	24.0 ± 1.2	18.3 ± 0.5	219.4 ± 5.2
		44	1500 ± 150	200 ± 20	0.33	0.02									
		45	1500 ± 150	200 ± 20	0.52	0.04									
FT13-2 (20m)	200-205	-	-	-	-	-	14.0 ± 2.3	7.8 ± 0.2	7.0 ± 1.7	9.1 ± 0.2	9.6 ± 0.5	95.5 ± 3.5	24.6 ± 1.2	61.4 ± 6.0	265.7 ± 7.1
FT14-1 (19m)	540-545	-	-	-	-	-	29.4 ± 5.8	17.5 ± 0.6	16.9 ± 4.5	23.9 ± 0.6	22.5 ± 1.5	214.4±10.3	32.8 ± 1.6	46.5 ± 5.0	501.6 ± 13.0

Notes:
1. All shells are composed of more than 95% aragonite.
2. The water correction factors for β and γ attenuations were made using the equations listed in Aitken (1985):
   W (saturated water content) = (mass of water / mass of dry sediment) × 100.
   Fraction of time at saturation (F) was estimated as 1.
3. The cosmic ray dose rates were obtained using the equations given in Prescott and Hutton (1988, 1994).

Table 4.3. Age estimates by beta-counting radiocarbon, AMS radiocarbon, and ESR for shell samples from Forster-Tuncurry Shelf, New South Wales.

Core number (Water depth)	Sub-bottom (cm)	Sample number	Radiocarbon		ESR age (years)	
			Shell-hash age (years B.P.)	AMS age (years B.P.)	g=2.0014 (microwave power: 2 mW)	g=2.0006 (microwave power: 200 mW)
FT13-10 (43 m)	120-140	14	12,690 ± 83 (Beta 45170)	9,280 ± 400	9,600 ± 600 (10,100 ± 600)	20,900 ± 900 (22,000 ± 800)
		18		9,905 ± 400	11,300 ± 1,300	23,700 ± 1,200
		17		11,390 ± 350	11,400 ± 1,300	17,500 ± 900
		15		32,800 ± 800	49,400 ± 5,100	64,200 ± 16,400
		13		35,500 ± 1,100	42,200 ± 3,200	51,400 ± 2,500
FT14-1 (19 m)	435-445	28	8,510 ± 93 (Beta 45432)	6,380 ± 450	4,300 ± 600	12,000 ± 600
		21		7,010 ± 400	7,000 ± 500	18,000 ± 800
		27		7,520 ± 400	5,100 ± 400 (5,400 ± 400)	8,600 ± 600 (9,200 ± 500)
		23		8,365 ± 400	1,300 ± 100 (1,400 ± 100)	7,700 ± 500 (8,300 ± 400)
		22		8,460 ± 400	2,700 ± 200 (2,800 ± 200)	6,300 ± 300 (6,600 ± 300)
		29		9,090 ± 340	8,200 ± 1,800	8,900 ± 700
FT/BMR19-3A (90 m)	290-300	43	17,640 ± 113 (Beta 45437)	10,400 ±450	11,400 ± 1,100	17,700 ± 1,200
		44		12,390 ± 450	10,000 ± 900	14,600 ± 900
		45	18,420 ± 281 (Beta 45438)	15,570 ± 470	9,800 ± 1,100 (10,500 ± 1,200)	15,200 ± 1,000 (16,400 ± 900)

Notes: 1. ESR ages without and with parentheses are based on early and linear uranium-uptake models, respectively.
2. Radiocarbon ages are based on isotopic fractionation corrected ^{14}C depletion with respect to 95% of the activity of NBS oxalic acid using the ^{14}C half-life of 5570 years and assuming a $\delta^{13}C$ value of -1 ± 2‰ with respect to PDB. The ages are corrected for an Oceanic Reservoir Apparent Age of -450 ± 35 years (Gillespie and Polach, 1979).

Table 4.4(a). ESR results based on the signal at g=2.0014 (microwave power of 2 mW) for aragonite shell samples from Elands Bay, South Africa.

Sample site	Sample number	Shell species	D_E-value (Gy)	Early uranium uptake		Linear uranium uptake	
				Internal dose rate (μGy year^{-1})	Age (years)	Internal dose rate (μGy year^{-1})	Age (years)
Borrew Pit Midden (Elands 1)	E 1	*Patella granatina apices*	-	-	-	-	-
	E 2	*Patella argenvillei*	-	-	-	-	-
	E 3	*Choromytilus meridionalis*	Mn^{2+}	-	-	-	-
	E 4	*Argobuccinum argus*	1.9 ± 0.2	22 ± 4	2,900 ± 300	-	-
Malkappan Elandas (Elands 2)	E 5	*Choromytilus meridionalis*	Mn^{2+}	-	-	-	-
	E 6	*Patella granatina*	-	-	-	-	-
	E 7	*Burnupena papyracea*	19.4 ± 1.0	126 ± 16	38,900 ± 3,100	-	-
	E 8	*Nucella cingulata*	-	-	-	-	-
Hoedjiespunt 1 (Elands 3)	E 9	*Tellina madagascariensis*	21.8 ± 9.7	106 ± 32	16,600 ± 7,500	53 ± 16	17,300 ± 7,800
	E10	*Tellina madagascariensis*	56.8 ± 3.0	172 ± 53	39,200 ± 3,200	85 ± 24	41,600 ± 3,300
	E11	*Dosinia lupinus*	106.5 ± 12.9	326 ± 100	68,200 ± 9,900	155 ± 46	76,500 ± 10,500
	E12	*Dosinia lupinus*	84.3 ± 5.0	335 ± 92	56,900 ± 5,600	174 ± 44	63,700 ± 5,600
Hoedjiespunt 2 (Elands 4)	E13	*Choromytilus meridionalis*	Mn^{2+}	-	-	-	-
	E14	*Patella granatina*	-	-	-	-	-
	E15	*Patella granularis*	-	-	-	-	-
	E16	*Patella argenvillei*	-	-	-	-	-

Notes: 1. Mn^{2+}: The dating signal (g=2.0014) was not observed because of an overlapping Mn^{2+} signal.
2. - : D_E-values were not obtained because these samples were calcite-dominated shells and did not show the g=2.0014 signal.

Table 4.4(b). Analytical data for shell samples from Elands Bay, South Africa.

Sample site	Sample number	XRD analysis			Shell					Sediment			Cosmic ray dose rate (μGy year^{-1})	External γ-dose rate (μGy year^{-1})
		Shell species	Aragonite mass (%)	Calcite mass (%)	Shell thickness (μm)	Removed outer layer (μm)	U (ppb)	Th (ppb)	K (%)	U (ppb)	Th (ppb)	K (%)		
Borrew Pit Midden (Elands 1)	E 1	*Patella granatina apices*	1.9 ± 0.4	98.1 ± 0.4	2000 ± 300	250 ± 50	3	16	0.02	3125	12255	0.79	183 ± 13	260.7
	E 2	*Patella argenvillei*	35.1 ± 0.2	64.9 ± 0.2	3200 ± 300	150 ± 50	16	4	0.02					
	E 3	*Choromytilus meridionalis*	56.0 ± 0.2	44.0 ± 0.2	3000 ± 300	100 ± 50	47	19	0.01					
	E 4	*Argobuccinum argus*	99.0 ± 0.2	1.0 ± 0.2	2500 ± 500	250 ± 50	139	6	0.01					
Malkappan Elandas (Elands 2)	E 5	*Choromytilus meridionalis*	25.6 ± 0.2	74.4 ± 0.2	2500 ± 300	100 ± 50	148	2	0.01	1167	5573	0.46	141 ± 18	80.8
	E 6	*Patella granatina*	5.0 ± 0.2	95.0 ± 0.2	2500 ± 500	250 ± 50	46	< 0.5	0.06					
	E 7	*Bumupena papyracea*	99.0 ± 0.2	1.0 ± 0.2	2100 ± 100	150 ± 50	231	1	0.13					
	E 8	*Nucella cingulata*	47.0 ± 0.2	53.0 ± 0.2	1700 ± 200	100 ± 50	216	1	0.11					
Hoedjiespunt 1 (Elands 3)	E 9	*Tellina madagascariensis*	99.4 ± 0.1	0.6 ± 0.1	2200 ± 200	100 ± 50	792	23	0.01	6371	23975	1.24	141 ± 18	581.0
	E10	*Tellina madagascariensis*	99.9 ± 0.1	0.1 ± 0.1	2000 ± 100	50 ± 25	1032	43	0.02					
	E11	*Dosinia lupinus*	99.4 ± 0.1	0.6 ± 0.1	2150 ± 100	100 ± 50	1644	402	0.01					
	E12	*Dosinia lupinus*	98.8 ± 0.1	1.2 ± 0.1	2600 ± 100	100 ± 25	1614	66	0.06					
Hoedjiespunt 2 (Elands 4)	E13	*Choromytilus meridionalis*	6.4 ± 0.3	93.6 ± 0.3	1800 ± 100	50 ± 25	77	1	0.01	1284	2634	0.36	141 ± 18	184.1
	E14	*Patella granatina*	0.0 ± 0.3	100.0 ± 0.3	2500 ± 100	100 ± 50	135	< 0.5	0.04					
	E15	*Patella granularis*	2.2 ± 0.2	97.8 ± 0.2	2300 ± 100	100 ± 25	110	< 0.5	0.01					
	E16	*Patella argenvillei*	25.8 ± 0.2	74.2 ± 0.2	4000 ± 300	250 ± 50	116	2	0.07					
Modern shells from beach (Elands Bay)	EM1	*Patella granatina*	0.0 ± 0.4	100.0 ± 0.4										
	EM2	*Patella argenvillei*	17.2 ± 0.2	82.8 ± 0.2										
	EM3	*Choromytilus meridionalis*	25.8 ± 0.1	74.2 ± 0.1										
	EM4	*Nucella cingulata*	26.2 ± 0.2	73.8 ± 0.2										
	EM5	*Patella granularis*	30.8 ± 0.2	69.2 ± 0.2										

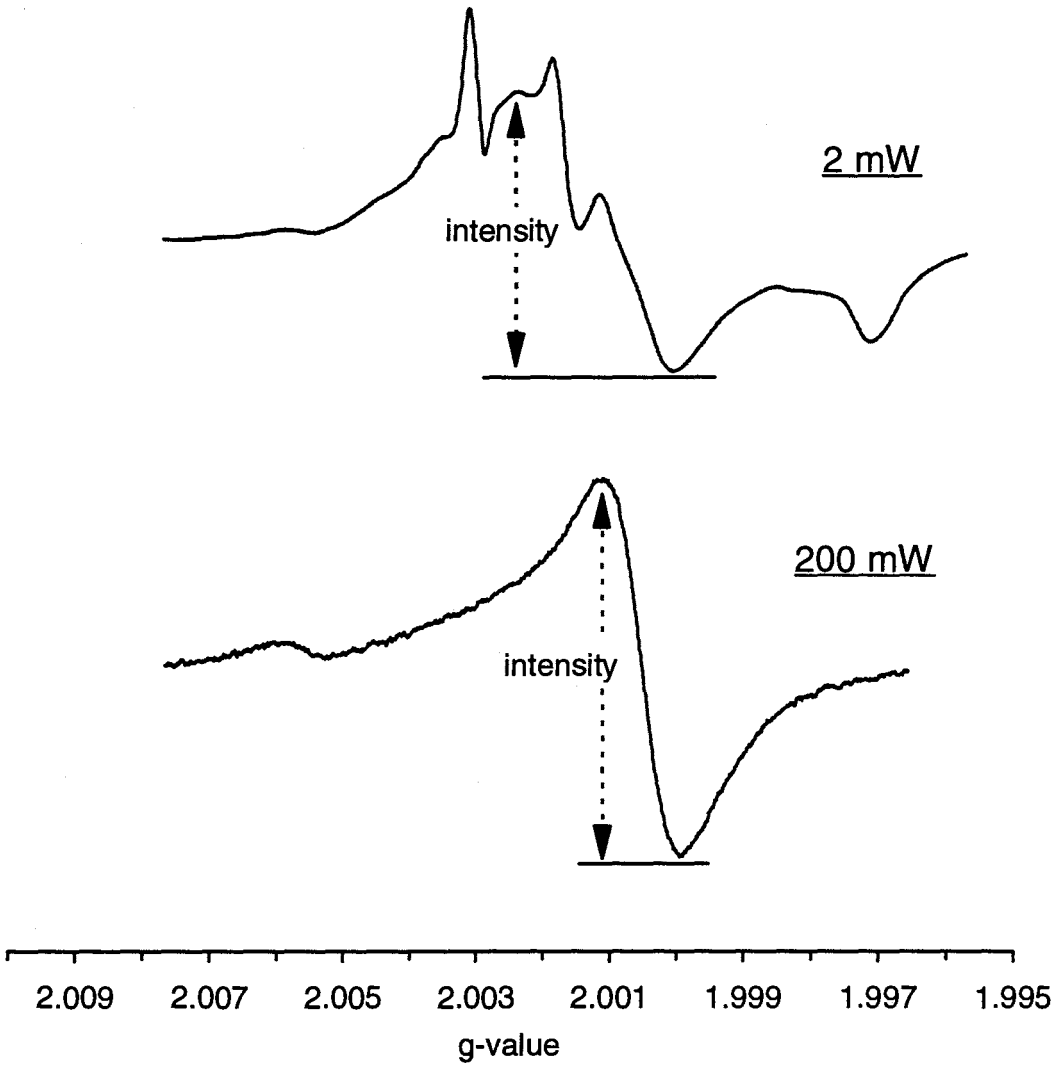

Figure 4.1. ESR spectra of *Anadara trapezia* shell with microwave powers of 2 mW (g=2.0014) and 200 mW (g=2.0006), and the methods used to measure the signal intensities.

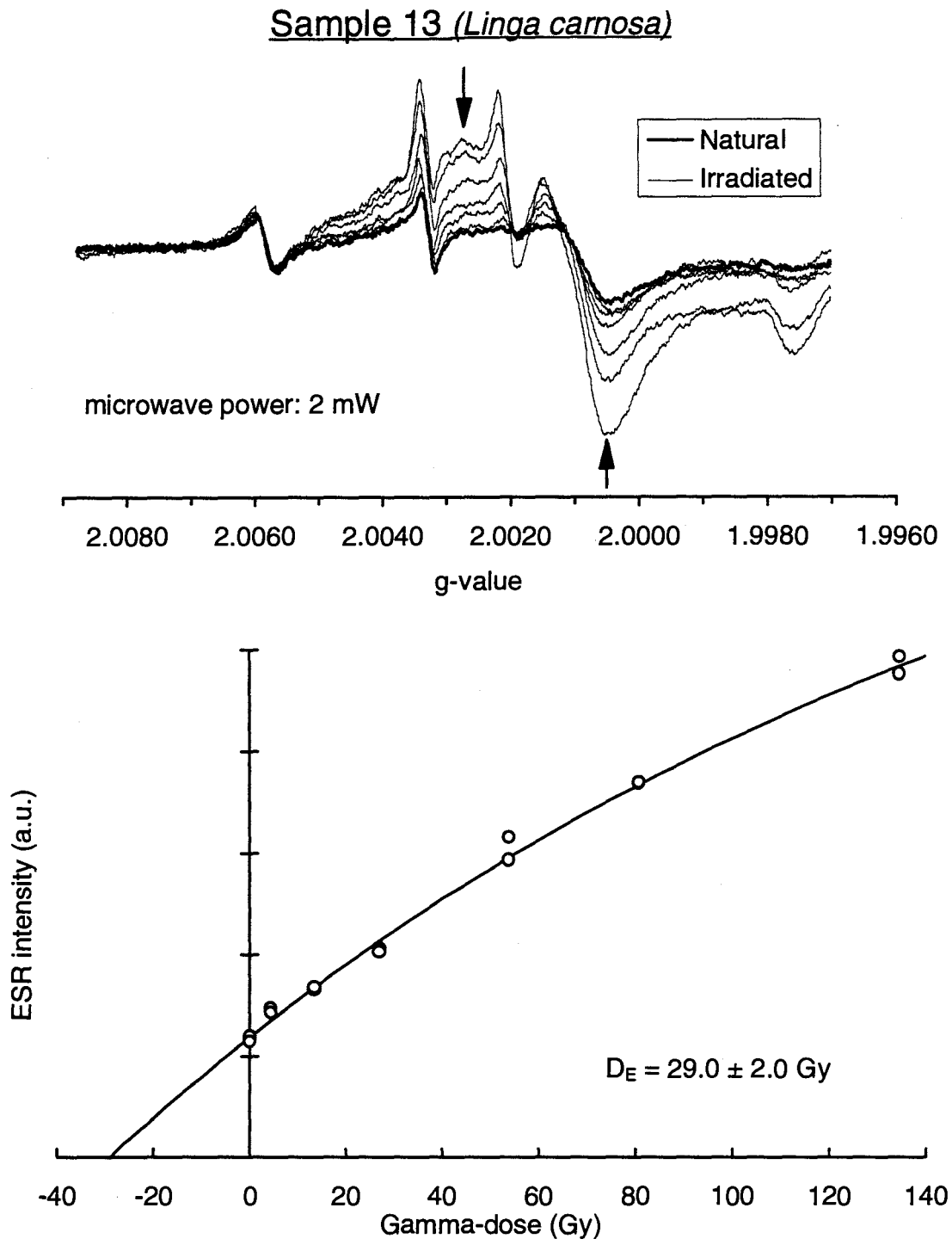

Figure 4.2(a). ESR spectra (Natural and N+irradiated) and dose response curve based on the signal at g=2.0014 (microwave power of 2 mW) for shell sample 13 *(Linga carnosa)* from Forster-Tuncurry Shelf, New South Wales. The arrows indicate the method used to estimate the peak-to-peak signal height intensity. A D_E-value of 29.0 ± 2.0 Gy was estimated from a single saturating exponential fit.

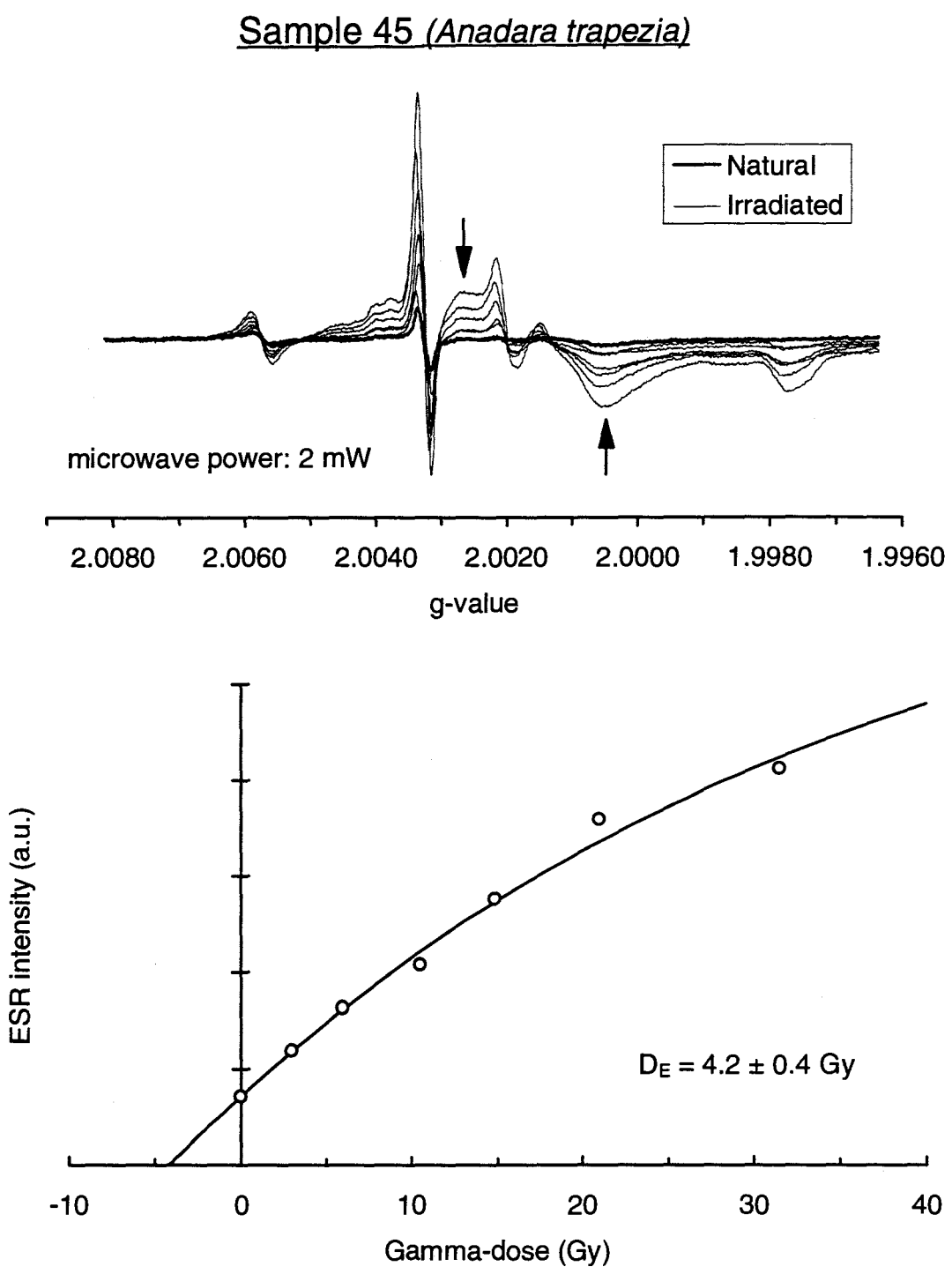

Figure 4.2(b). ESR spectra (Natural and N+irradiated) and dose response curve based on the signal at g=2.0014 (microwave power of 2 mW) for shell sample 45 *(Anadara trapezia)* from Forster-Tuncurry Shelf, New South Wales. The arrows indicate the method used to estimate the peak-to-peak signal height intensity. A D_E-value of 4.2 ± 0.4 Gy was estimated from a single saturating exponential fit.

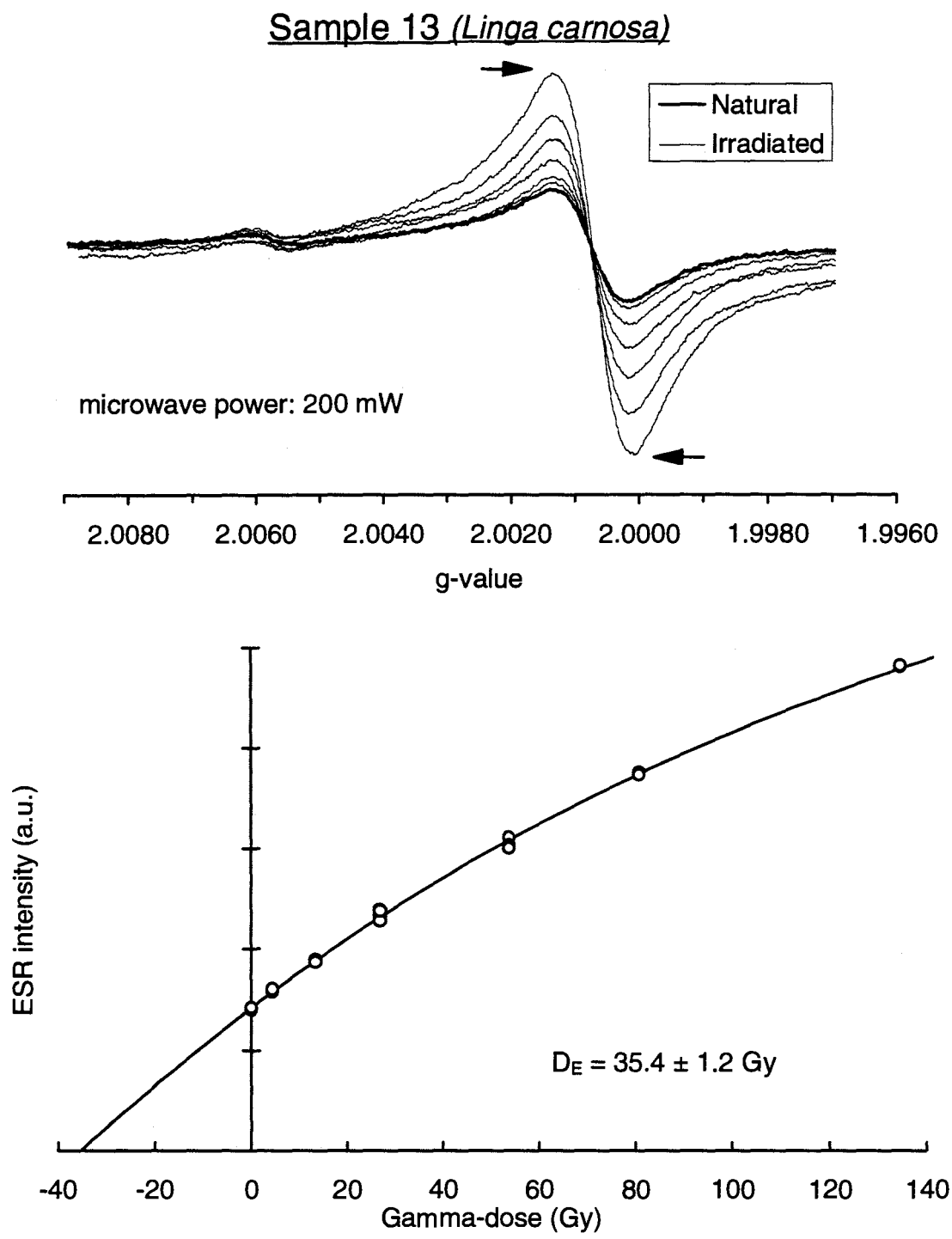

Figure 4.2(c). ESR spectra (Natural and N+irradiated) and dose response curve based on the signal at g=2.0006 (microwave power of 200 mW) for shell sample 13 *(Linga carnosa)* from Forster-Tuncurry Shelf, New South Wales. The arrows indicate the method used to estimate the peak-to-peak signal height intensity. A D_E-value of 35.4 ± 1.2 Gy was estimated from a single saturating exponential fit.

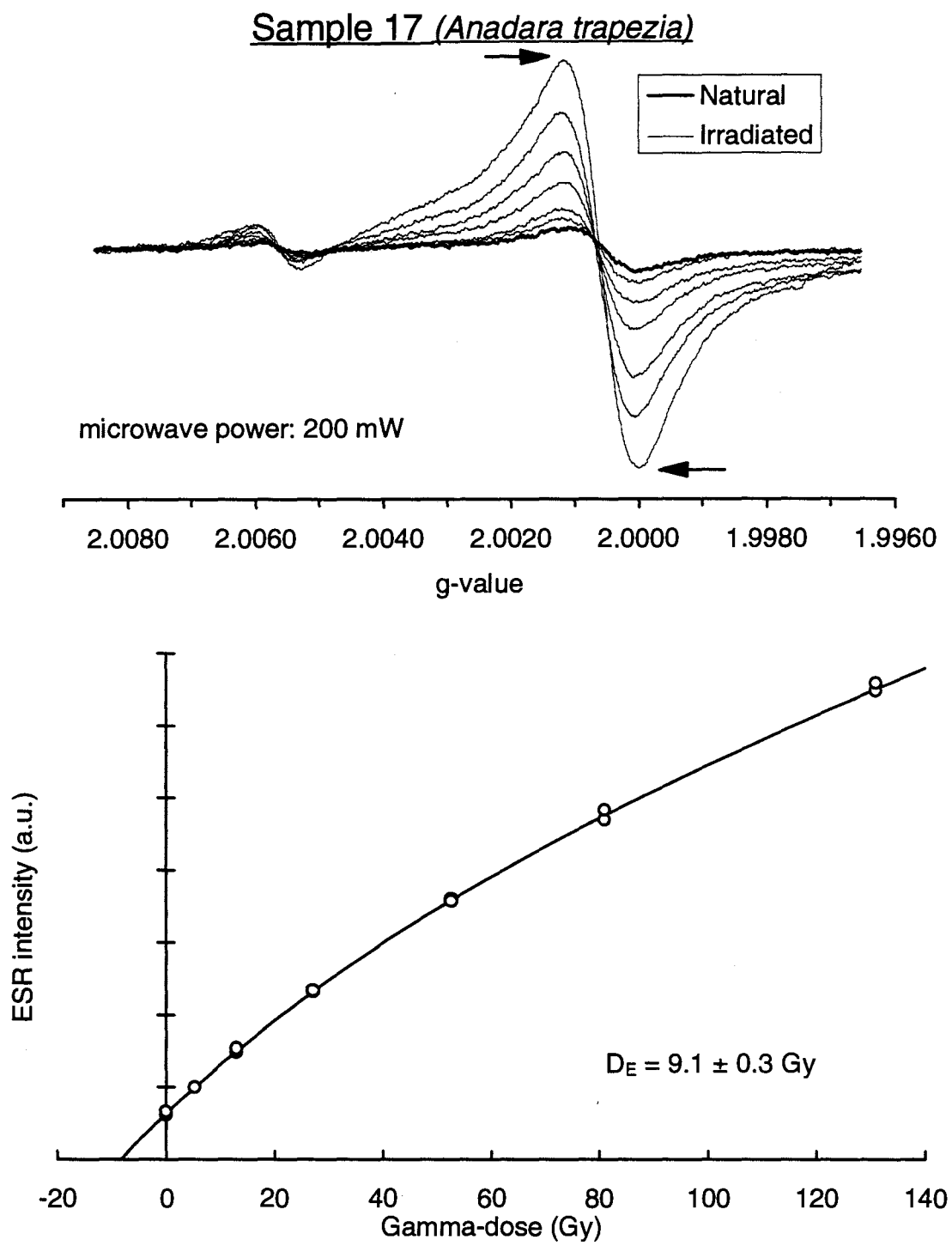

Figure 4.2(d). ESR spectra (Natural and N+irradiated) and dose response curve based on the signal at g=2.0006 (microwave power of 200 mW) for shell sample 17 *(Anadara trapezia)* from Forster-Tuncurry Shelf. The arrows indicate the method used to estimate the peak-to-peak signal height intensity. A D_E-value of 9.1 ± 0.3 Gy was estimated from a saturating-exponential-plus-linear fit.

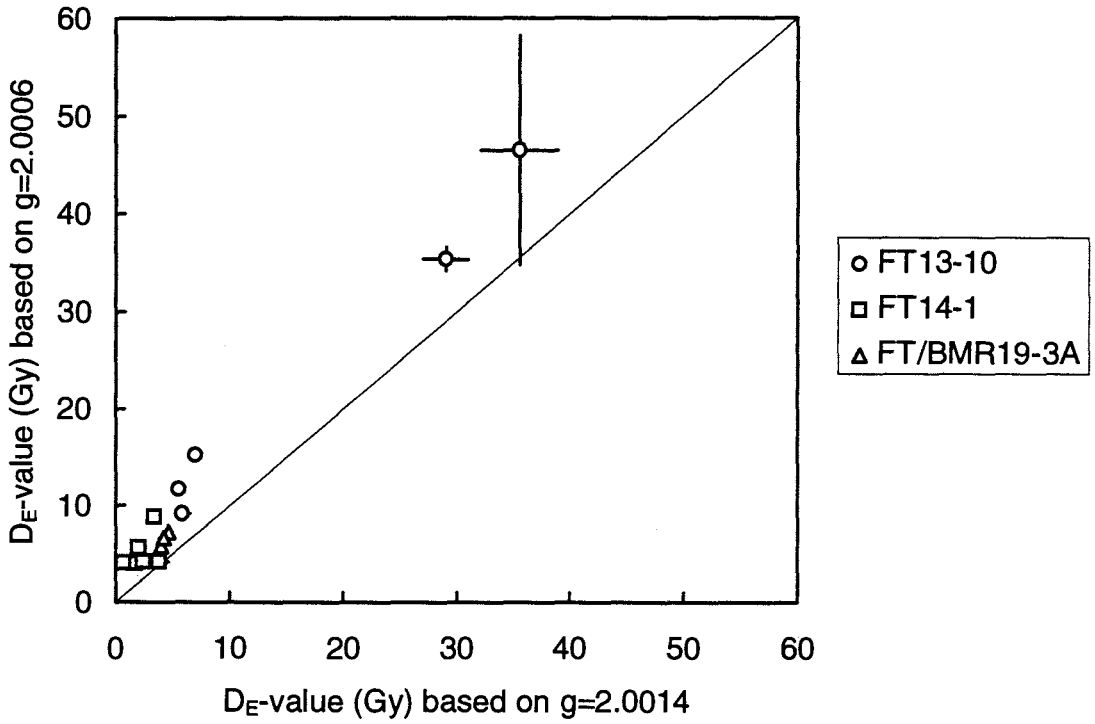

Figure 4.3. D_E-values based on the signals at g=2.0014 and g=2.0006 using microwave powers of 2 mW and 200 mW, respectively, for shell samples from Forster-Tuncurry Shelf, New South Wales.

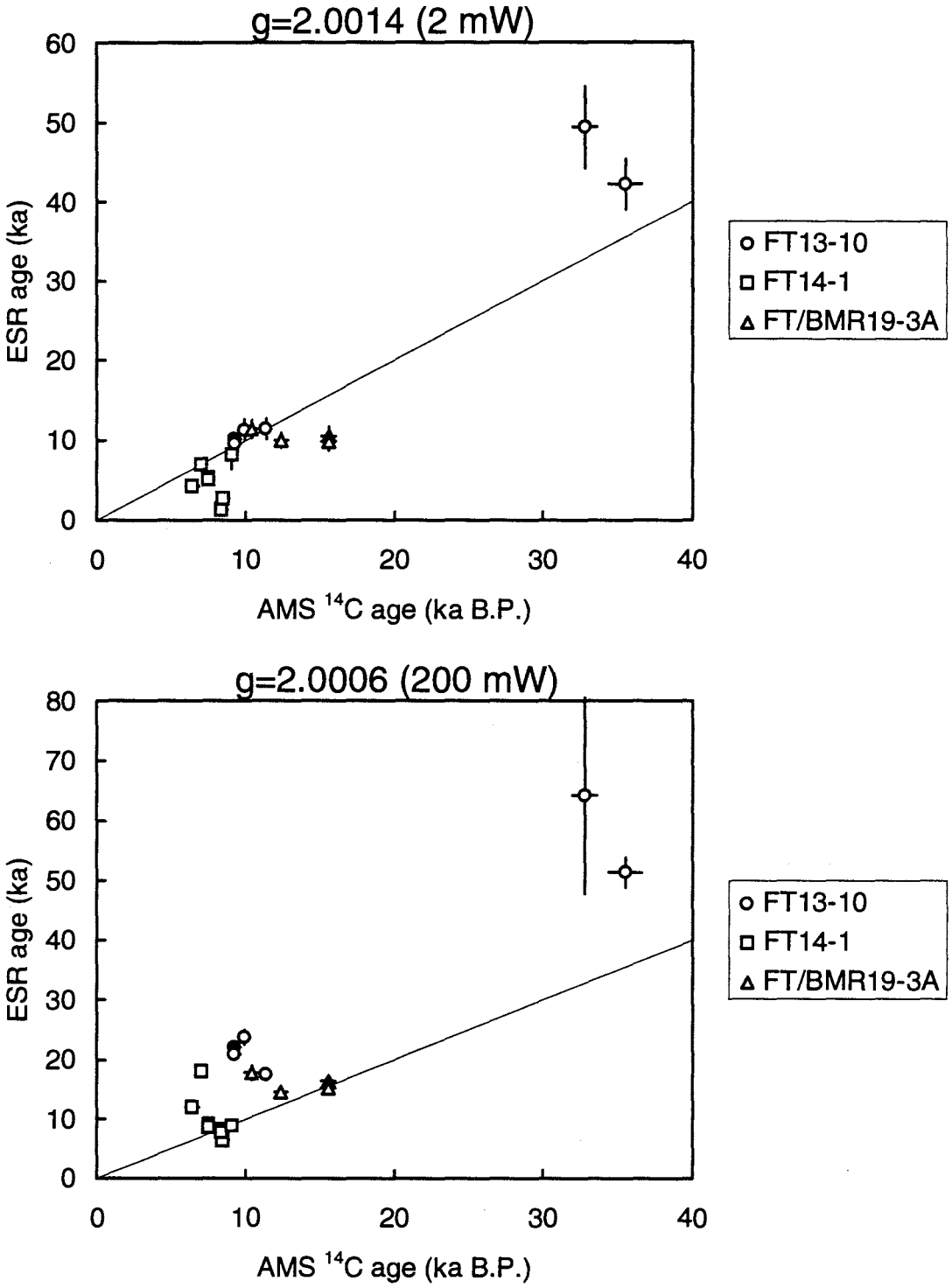

Figure 4.4. Plots of AMS ^{14}C age versus ESR age based on the signals at g=2.0014 (above) and g=2.0006 (below) using microwave powers of 2 mW and 200 mW, respectively, for shell samples from Forster-Tuncurry Shelf, New South Wales. Open and solid symbols represent ESR ages based on uranium early-uptake and linear-uptake models, respectively.

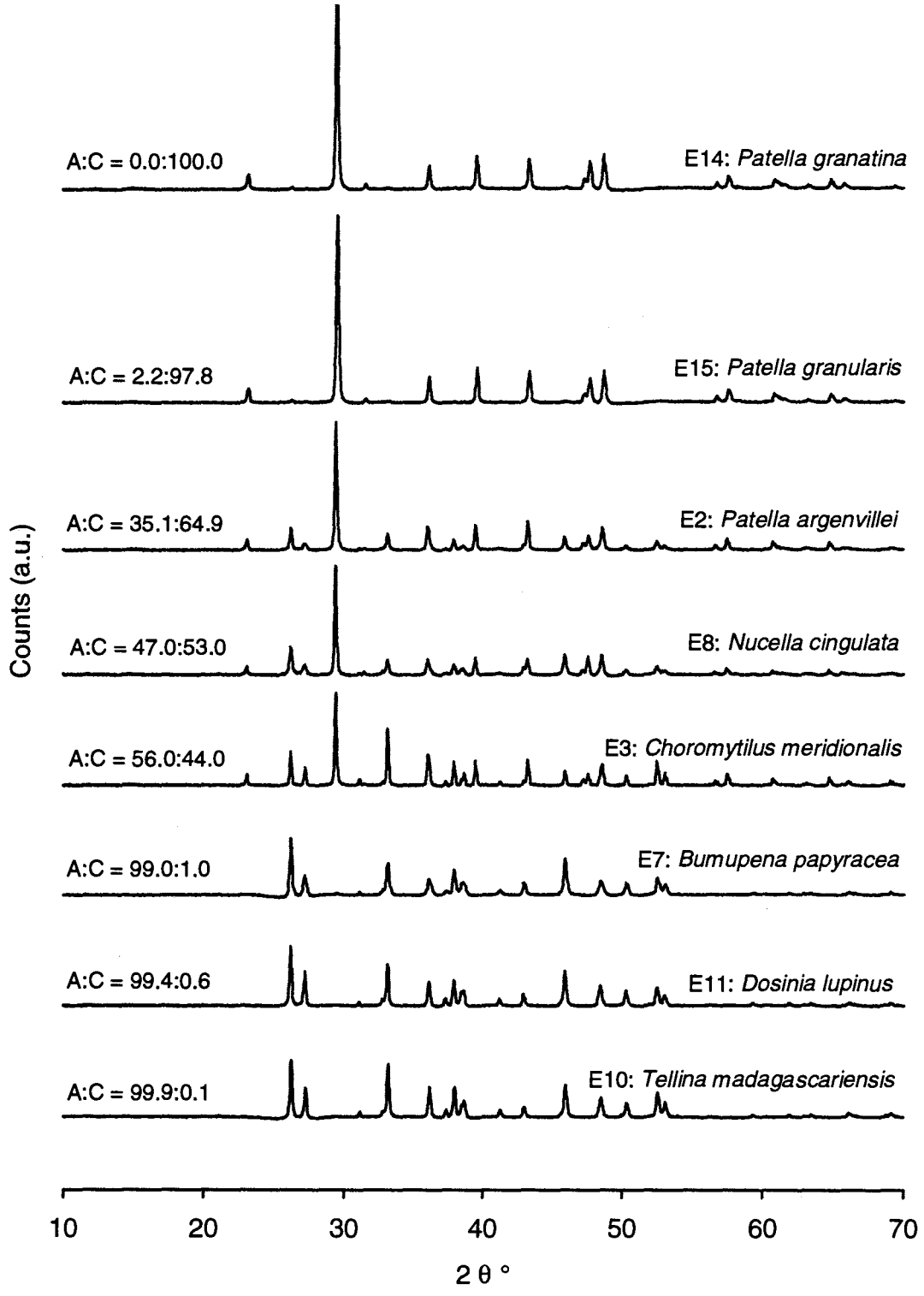

Figure 4.5. XRD spectra of shell samples from Elands Bay, South Africa. 'A:C' represents the mass ratio of aragonite to calcite.

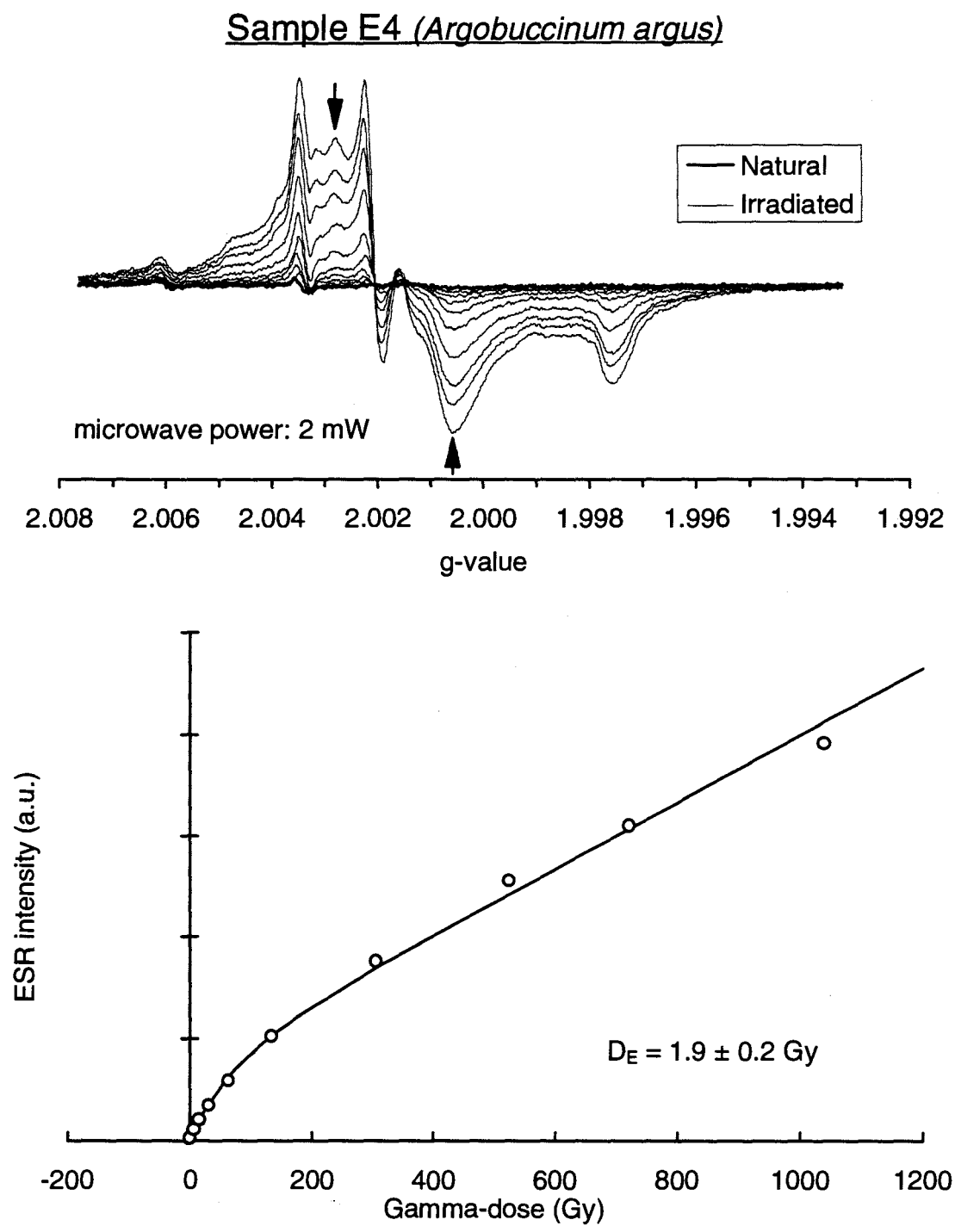

Figure 4.6(a). ESR spectra (Natural and N+irradiated) and dose response curve based on the signal at g=2.0014 (microwave power of 2 mW) for sample E4 (*Argobuccinum argus*) from Elands Bay, South Africa. The arrows indicate the method used to estimate the peak-to-peak signal height intensity. A D_E-value of 1.9 ± 0.2 Gy was estimated from a saturating-exponential-plus-linear fit.

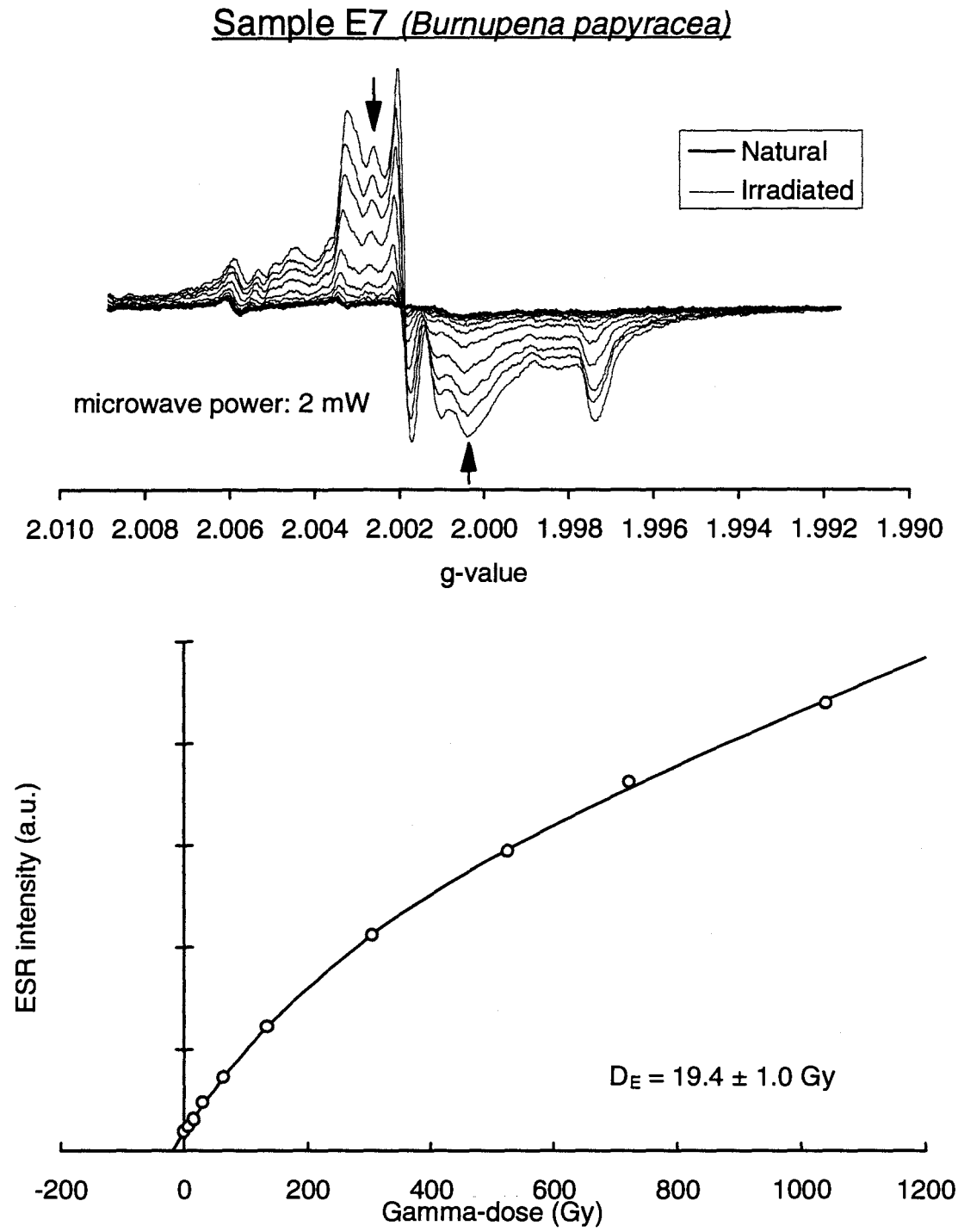

Figure 4.6(b). ESR spectra (Natural and N+irradiated) and dose response curve based on the signal at g=2.0014 (microwave power of 2 mW) for sample E7 (*Burnupena papyracea*) from Elands Bay, South Africa. The arrows indicate the method used to estimate the peak-to-peak signal height intensity. A D_E-value of 19.4 ± 1.0 Gy was estimated from a saturating-exponential-plus-linear fit.

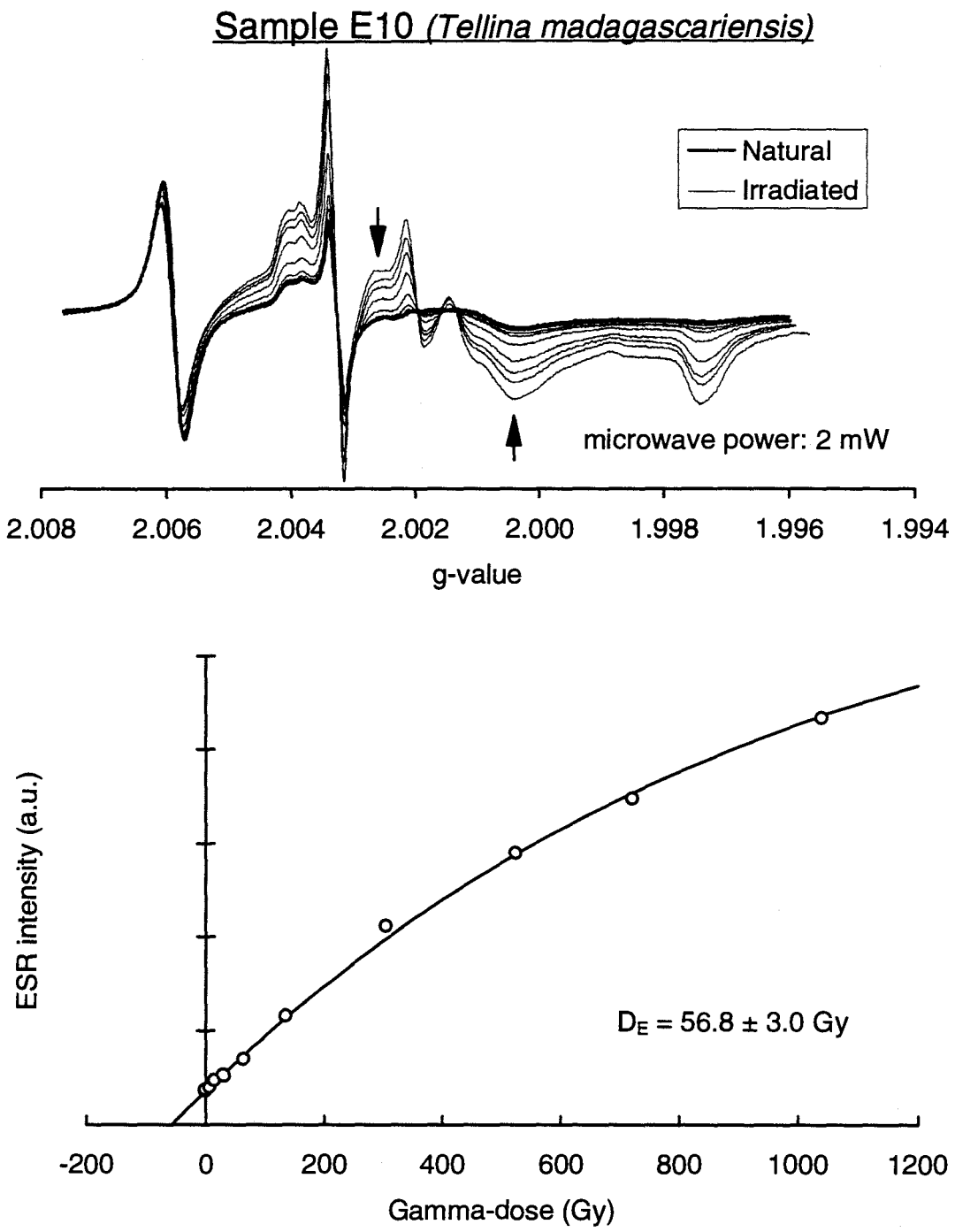

Figure 4.6(c). ESR spectra (Natural and N+irradiated) and dose response curve based on the signal at g=2.0014 (microwave power of 2 mW) for sample E10 (*Tellina madagascariensis*) from Elands Bay, South Africa. The arrows indicate the method used to estimate the peak-to-peak signal height intensity. A D_E-value of 56.8 ± 3.0 Gy was estimated from a saturating exponential fit.

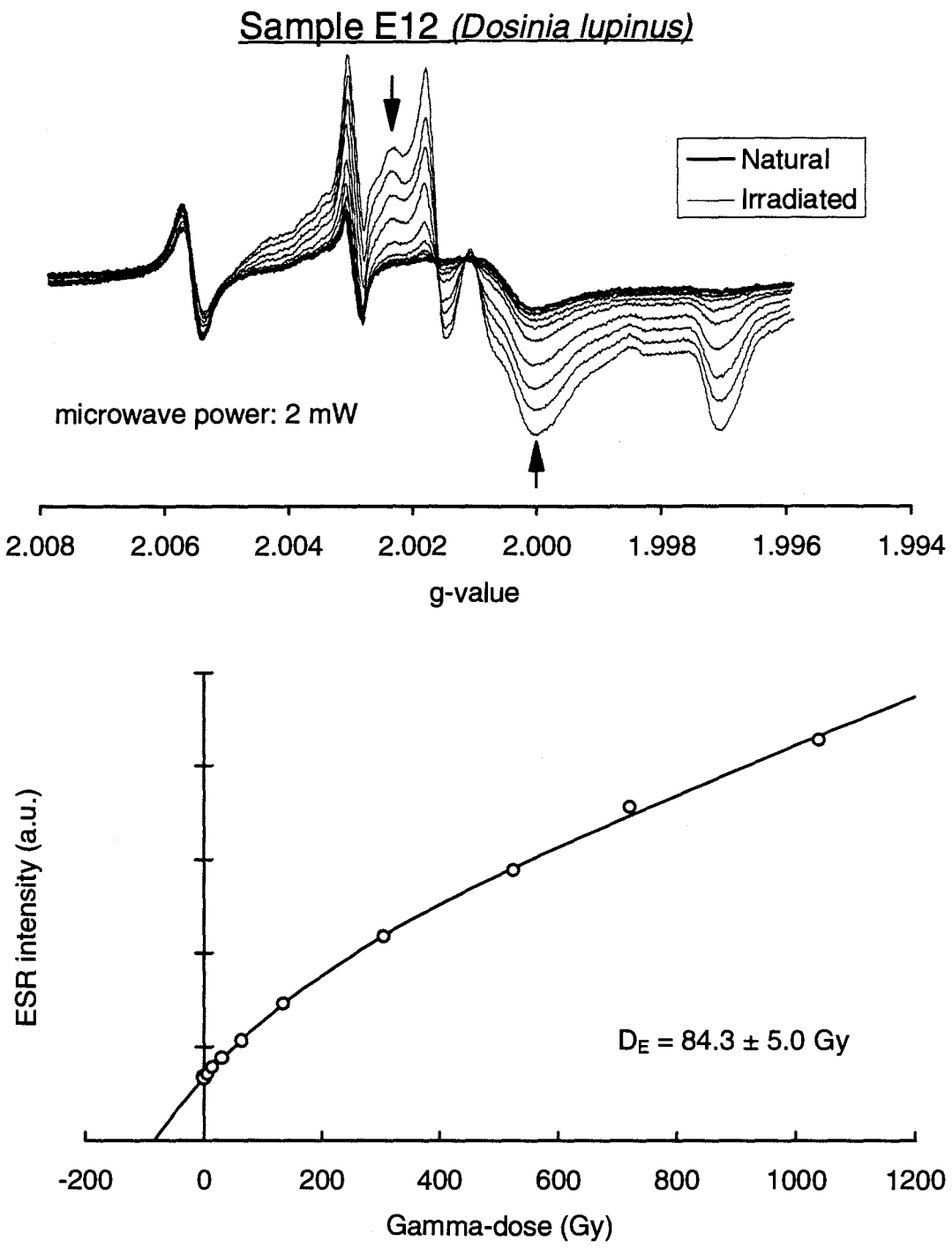

Figure 4.6(d). ESR spectra (Natural and N+irradiated) and dose response curve based on the signal at g=2.0014 (microwave power of 2 mW) for sample E12 (*Dosinia lupinus*) from Elands Bay, South Africa. The arrows indicate the method used to estimate the peak-to-peak signal height intensity. A D_E-value of 84.3 ± 5.0 Gy was estimated from a saturating-exponential-plus-linear fit.

Chapter 5 CORAL SAMPLES

Coral samples from only one site were dated by ESR during this study. These samples were collected from the Huon Peninsula, Papua New Guinea, and have been previously studied by Dr. R. Grün. They provide a suite of well-dated samples against which to test the validity of some recently developed ESR dating methods. The same natural and N+γ samples used by Grün *et al.* (1992) were used also in this study.

5.1 Methods used

The aragonitic coral samples were originally dated by ESR by Grün *et al.* (1992). The same methods described in that study, plus some additional analyses (see below), were employed here. For each sample, thirteen aliquots, each of 100 mg mass, had been irradiated in 1992 using a ^{60}Co source with 5.7, 11.4, 22.8, 45.5, 91.0, 182.1, 313.0, 455.2, 620.2, 771.0, 916.1 or 1029.9 Gy. The signals at g=2.0007 were measured with an X-band (9.70 GHz) Bruker ESP 300E spectrometer at room temperature (≈ 20°C), with a modulation frequency of 100 kHz, a microwave power of 5 mW, a modulation amplitude of 0.5 Gpp, a scan range of 30 G, a scan speed of 5.4 G min^{-1} with a time constant of 655 ms. Additional measurements were carried out for samples 669, 670 and 671 using a higher microwave power of 200 mW, all other settings being identical to those used for the 5 mW measurements. D_E-values were estimated in the same manner for both microwave powers, the data for each aliquot being weighted in proportion to the inverse square of the ESR intensity, as described in section 4.1.1.

Since potassium contents as estimated by flame photometry were found to be negligible, the uranium content data analysed by delayed neutron activation (as described in Grün *et al.*, 1992) were used to determine the environmental dose rates. The dose rates were calculated based on the equations described in section 2.3. An initial $^{234}U/^{238}U$ ratio of 1.14 ± 0.01 as measured for modern sea water (Chen *et al.*, 1986) was adopted. A cosmic

ray dose rate of 140 ± 30 μGy $year^{-1}$, corresponding to a depth of about 3 ± 2 m below the ground surface, was assumed (after Prescott and Hutton, 1988).

5.2 ESR ages obtained

The ESR results based on the signals at g=2.0007 (microwave powers of 5 mW and 200 mW) obtained in this study and by Grün *et al.* (1992) are compared in Table 5.1 and Figure 5.1. ESR spectra and dose response curves for samples 663, 665, 668 (microwave power 5 mW) and 670 (microwave powers of 5 mW and 200 mW) are shown in Figures 5.3(a), 5.3(b), 5.3(c), 5.3(d) and 5.3(e), respectively. The ESR signal at g=2.0058 is considered to be radiation-insensitive (e.g. Grün, 1989). However, the signals observed at g=2.0058, g=2.0032, g=2.0020 and g=2.0007 were all increased by γ-irradiation in all the samples examined here.

The D_E-values obtained by Grün *et al.* (1992) and by this study are expected to be comparable for the 5 mW microwave power setting, because the same samples were being examined under identical ESR measurement conditions. Most samples show close agreement between the D_E-values obtained in both studies. However, the D_E-values for samples 663, 665 and 667 differ significantly (at the 1σ level), with larger D_E-values being obtained in this study (about 21 %, 30 % and 22 % larger, respectively). It is believed that the discrepancies in the D_E-values (and hence the ESR ages) for these three samples are not caused by errors such as instrument settings or a packing error; the degree of sample packing was consistent between samples. The ESR spectra recorded by Grün *et al.* (1992) and the spectra measured in this study were made more than 6 weeks and 3 years, respectively, after the γ-irradiation. Since Templer (1986) reported 'anomalous fading' of ESR signals in carbonates (that is, a decrease in intensity after a laboratory irradiation), this could be a possible explanation for the disagreements. If this is the case, then the results suggest that some corals contain thermally unstable components in the g=2.0007 signal. Despite some differences in the D_E-values, the calculated ESR ages in both studies

are in good agreement at the 1σ level, except for sample 665 whose age estimates are in accordance at the 2σ level.

At the higher microwave power setting (200 mW), the signals at g=2.0032 and g=2.0020 appear to be saturated, whereas the signals at g=2.0058 and g=2.0007 have not reached saturation. The D_E-values based on the signal at g=2.0007 using microwave powers of 5 mW and 200 mW are in good agreement at the 1σ level for samples 670 and 671, and at the 2σ level for sample 669. The calculated ESR ages all agree at the 1σ level. This result suggests that the use of high or low microwave power has a negligible effect on the dose response, and hence D_E-value, of the signal at g=2.0007 in corals.

5.3 Comparisons with independent age controls

The age estimates obtained by alpha spectrometric and mass spectrometric uranium-series methods, geological expectations, and the ESR methods employed in this study and by Grün *et al.* (1992) are compared in Table 5.2. The $^{230}Th/^{234}U$ ages in parentheses are not considered for age comparisons since these samples are regarded as providing unreliable data (see Table 5.2). In this table, new dates estimated by alpha spectrometric uranium-series (Omura *et al.*, 1994) are included. Chappell *et al.* (1994a) reported that these new dates provided more accurate sea level estimates for the period between 70 ka and 30 ka and are close to Shackleton's (1987) sea levels determined using oxygen isotopes. The ESR ages obtained in this study are compared with alpha spectrometric and mass spectrometric uranium-series ages in Figure 5.2.

The ages of terrace II estimated by alpha spectrometric and mass spectrometric uranium-series methods and by the ESR methods (microwave powers of 5 mW and 200 mW) for samples 670 and 671 are in good agreement at 40-55 ka. These ages are, however, much greater than the geological estimate of 29 ka. Similar results are observed for samples 665 and 666 (terrace IIIb): uranium-series and ESR ages agree at about 45-60 ka, which is slightly older than the geological estimate (40 ka). For this terrace, ESR ages of sample

664 (≈ 39 ka) are in good agreement with the geological estimate. The uranium-series and ESR ages of samples 667, 668 and 669 (terrace IIIa) are in good agreement (50-60 ka), except for the ESR age of sample 667 (≈ 64 ka) obtained in this study. The estimated ESR and uranium-series ages of samples 662 and 663 are all in close accordance at about 70-80 ka. In Figure 5.2, there is a suggestion that the ESR ages systematically slightly exceed their uranium-series counterparts. For several samples, however, the ESR age uncertainties overlap the uranium-series age determinations, so no firm conclusions can be drawn on this matter; further attention is warranted.

5.4 Conclusions

With one exception, ESR ages based on the signal at g=2.0007 using microwave powers of 5 mW and 200 mW concur with alpha spectrometric and mass spectrometric uranium-series ages within the 1σ or 2σ age uncertainties. The use of high or low microwave power has a negligible effect on the dose response and D_E-value of the signal at g=2.0007 in corals. By using a higher microwave power (200 mW), the signals at g=2.0032 and g=2.0020 appear to be saturated. These observations support previous studies (e.g. Barabas *et al.*, 1992a, 1992b), which suggested the use of the g=2.0007 (g=2.0006 in their reports) signal with higher microwave power for the dating of carbonate materials. The signal at g=2.0007 in corals appears, therefore, to be a reliable signal for dating using high or low microwave power.

Close agreement between the D_E-values obtained by Grün *et al.* (1992) and by this study is attained under identical ESR measurement conditions. Samples 663, 665 and 667, however, gave much larger D_E-values in this study. This may indicate that 'anomalous fading' of the ESR signal at g=2.0007 has occurred in the 3 year period since laboratory γ-irradiation. If this is the case, it is essential to remove thermally unstable defects associated with the g=2.0007 signal after the laboratory γ-irradiation. The same requirement may also be necessary for other carbonate materials such as mollusc shell and

foraminifera, for which the signal at g=2.0007 (or g=2.0006; Barabas *et al.*, 1992a, 1992b) is used for dating.

For samples from terrace II and IIIb, the age estimates obtained by alpha spectrometric and mass spectrometric uranium-series methods and the ESR methods are much greater than the geological estimates. Two possible reasons for this discrepancy are that: (a) the uranium-series and ESR dates are overestimates; and/or (b) the geological assessment (i.e. sample collection in the field and/or the sea level model of Chappell (1990) and Chappell *et al.* (1994a)) was inappropriate. Since good concordances between the uranium-series dates, the ESR dates and the geological age estimates are observed for the other terraces, the geological evaluation of terraces II and IIIb may be in error.

To further develop reliable ESR dating procedures for corals, D_E-values based on the signal at g=2.0007 are estimated using higher and lower microwave powers after a selected annealing procedure. Also, the dating potential of the signal at g=2.0058 after the annealing procedure is examined and compared with the results obtained from the g=2.0007 signal. Further details of these experiments are given in Chapters 10 and 13.

Table 5.1. ESR analyses of corals from Huon Peninsula, Papua New Guinea (after Grün *et al.*, 1992; Chappell *et al.*, 1994a, 1994b and Omura *et al.*, 1994).

Lab. no.	Reef	Field no. (Lab. no.)	U (ppm)	ext. D (μGy a^{-1})	ESR (Grün *et al.*, 1992) 5 mW			ESR (This study) 5 mW			ESR (This study) 200 mW		
					int. D (μGy a^{-1})	D_E (Gy)	Age (years)	int. D (μGy a^{-1})	D_E (Gy)	Age (years)	int. D (μGy a^{-1})	D_E (Gy)	Age (years)
670	terrace II	KWA I1 (KK-08)	3.12	140 ± 30	503 ± 28	31.5 ± 2.8	49,000 ± 5,400	500 ± 27	30.8 ± 2.0	48,200 ± 4,300	487 ± 27	28.1 ± 0.9	44,800 ± 3,200
671	(29 ka)	KWA N1 (AO344)	2.64	140 ± 30	443 ± 24	31.7 ± 2.5	54,400 ± 5,600	444 ± 25	32.1 ± 1.4	55,000 ± 4,300	439 ± 24	30.8 ± 1.4	53,200 ± 4,300
666		KWA J1 (KK-10)	3.12	140 ± 30	529 ± 29	37.6 ± 2.3	56,200 ± 4,900	515 ± 28	34.3 ± 2.8	52,300 ± 5,300	-	-	-
664	terrace IIIb	KAN C2 (KK-11)	3.16	140 ± 30	469 ± 27	23.7 ± 2.0	38,900 ± 4,200	469 ± 26	23.6 ± 1.3	38,800 ± 3,300	-	-	-
665	(40 ka)	KWA K1 (AO347)	2.93	140 ± 30	479 ± 26	31.5 ± 2.7	50,900 ± 5,500	517 ± 28	40.8 ± 1.7	62,100 ± 4,600	-	-	-
669		KAN D4 (AO345)	3.81	140 ± 30	630 ± 35	40.5 ± 4.4	52,600 ± 6,500	647 ± 35	44.3 ± 1.2	56,300 ± 3,600	625 ± 34	39.4 ± 1.5	51,500 ± 3,600
667	terrace IIIa	KWA Q1 (AO346)	3.17	140 ± 30	535 ± 29	37.3 ± 4.0	55,300 ± 6,900	567 ± 30	45.4 ± 2.5	64,200 ± 5,200	-	-	-
668	(44 - 53 ka)	KAN D5 (AO360)	3.68	140 ± 30	619 ± 34	41.7 ± 4.4	54,900 ± 6,600	626 ± 33	43.2 ± 1.7	56,400 ± 4,000	-	-	-
663	terrace IV	SIAL E1 (AO369)	3.26	140 ± 30	596 ± 32	50.1 ± 5.4	68,000 ± 8,400	632 ± 33	60.4 ± 2.0	78,300 ± 5,200	-	-	-
662	(70 ka)	FRT F1 (AO349)	2.70	140 ± 30	513 ± 28	48.7 ± 4.1	74,600 ± 7,800	519 ± 28	50.6 ± 3.2	76,800 ± 6,800	-	-	-

Notes:
1. Abbreviations: ext. D = external dose rate; int. D = internal dose rate.
2. An initial $^{234}U/^{238}U$ ratio of 1.14 ± 0.01 was assumed. Modern sea water has a mean value of 1.144 ± 0.002 (Chen *et al.*, 1986).
3. An alpha efficiency value (k) of 0.05 ± 0.01 was used, following Grün *et al.* (1992).
4. A cosmic ray dose rate of 140 ± 30 μGy a^{-1}, corresponding to a depth of about 3 ± 2 m below the surface, was assumed (after Prescott and Hutton, 1988).

Table 5.2. Age estimates for corals from Huon Peninsula, Papua New Guinea (after Grün *et al.*, 1992; Chappell *et al.*, 1994a, 1994b and Omura *et al.*, 1994).

Lab. no.	Reef	Field no. (Lab no.)	Alpha spectrometric U-series age (years)	Mass spectrometric U-series age (years)	ESR (Grün *et al.*, 1992) 5 mW Age (years)	ESR (This study) 5 mW Age (years)	ESR (This study) 200 mW Age (years)
-	terrace IIc	BOBO U21 (KS-15)	33,400 ± 600	-	-	-	-
-	terrace IIa	KANZ U14	34,800 ± 130	-	-	-	-
-		BOBO U10	37,800 ± 250	-	-	-	-
-		KANZ U9 (AO403)	41,800 ± 600	-	-	-	-
670	terrace II	KWA I1 (KK-08)	44,000 ± 1,400	41,120 ± 500	49,000 ± 5,400	48,200 ± 4,300	44,800 ± 3,200
671	(29 ka)	KWA N1 (AO344)	50,500 ± 1,300	52,860 ± 440	54,400 ± 5,600	55,500 ± 4,300	53,200 ± 4,300
666	terrace IIIb	KWA J1 (KK-10)	(38,200 ± 1,100)[a,b]	-	56,200 ± 4,900	52,300 ± 5,300	-
-		KANZ 34 ((KS-12)	44,500 ± 700	-	-	-	-
664		KAN C2 (KK-11)	(46,400 ± 1,600)[b]	-	38,900 ± 4,200	38,800 ± 3,300	-
665	(40 ka)	KWA K1 (AO347)	56,000 ± 1,500	53,160 ± 430	50,900 ± 5,500	62,100 ± 4,600	-
669	terrace IIIa	KAN D4 (AO345)	(42,300 ± 1,100)[a]	-	52,600 ± 6,500	56,300 ± 3,600	51,500 ± 3,600
-		KAN D4 (AO359)	(42,800 ± 1,100)[a]	-	-	-	-
667		KWA Q1 (AO346)	57,500 ± 1,500	48,970 ± 1,590	55,300 ± 6,900	64,200 ± 5,200	-
668	(44 - 53 ka)	KAN D5 (AO360)	(57,800 ± 1,400)[b]	(46,360 ± 710)[b]	54,900 ± 6,600	56,400 ± 4,000	-
-		KAN D5 (KK-09)	(61,600 ± 2,000)[b]	-	-	-	-
-	terrace $IIIa_l$	KANZ 33 (KS-17)	45,800 ± 700	-	-	-	-
-	terrace $IIIa_m$	KANZ 4 (KS-16)	51,200 ± 800	-	-	-	-
-	terrace $IIIa_u$	KANZ 3 (KS-11)	51,800 ± 800	-	-	-	-
-	terrace $IIIa_{u+}$	KANZ 1	61,000 ± 550	-	-	-	-
663	terrace IV	SIAL E1 (AO369)	(65,800 ± 1,800)[b]	(59,120 ± 1,290)[b]	68,000 ± 8,400	78,300 ± 5,200	-
662	(70 ka)	FRT F1 (AO349)	72,800 ± 2,200	69,130 ± 730	74,600 ± 7,800	76,800 ± 6,800	-

Notes: $^{230}Th/^{234}U$ ages in parentheses are considered to be unreliable since those samples do not meet the following criteria:
(a) The uranium concentration should be the same as in present-day counterparts (2 to 4 ppm).
(b) The initial $^{234}U/^{238}U$ activity ratio, $(^{234}U/^{238}U)_0$, should be consistent with that in modern sea water, 1.13 to 1.16 (mean = 1.144 ± 0.002; Chen *et al.*, 1986).
(c) The sample should be free (i.e. contain < 0.02 ppm) of initial ^{230}Th incorporated at its living stage, and/or secondary ^{230}Th, introduced by contamination during diagenesis.

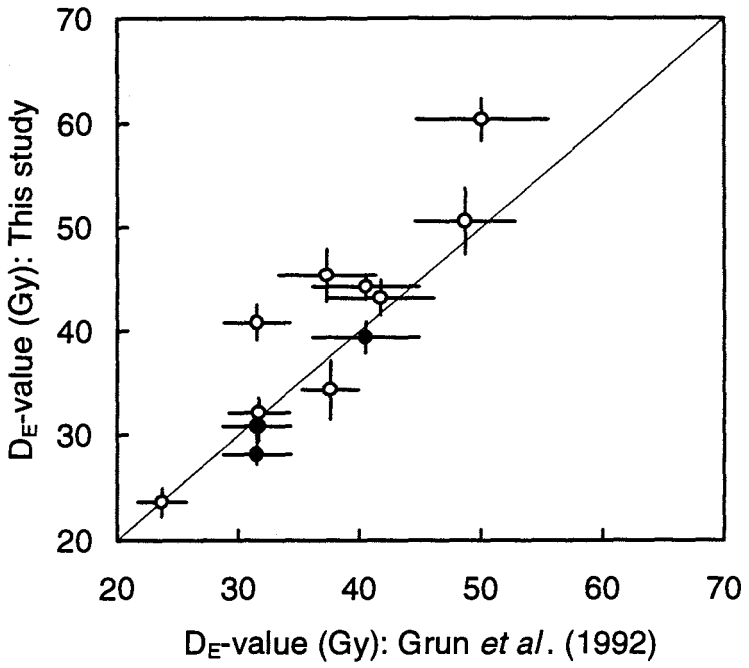

Figure 5.1. Comparisons of D_E-values based on the signal at g=2.0007 obtained by Grün *et al.* (1992) using a microwave power of 5 mW and this study using microwave powers of 5 mW (open circles) and 200 mW (solid circles).

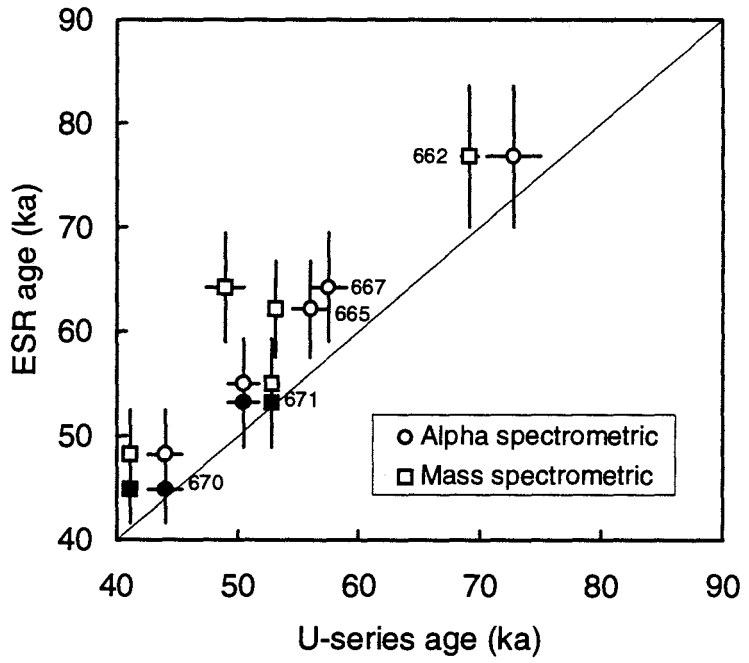

Figure 5.2. ESR ages, based on the signal at g=2.0007 using microwave powers of 5 mW (open symbols) and 200 mW (solid symbols), versus alpha spectrometric and mass spectrometric U-series ages.

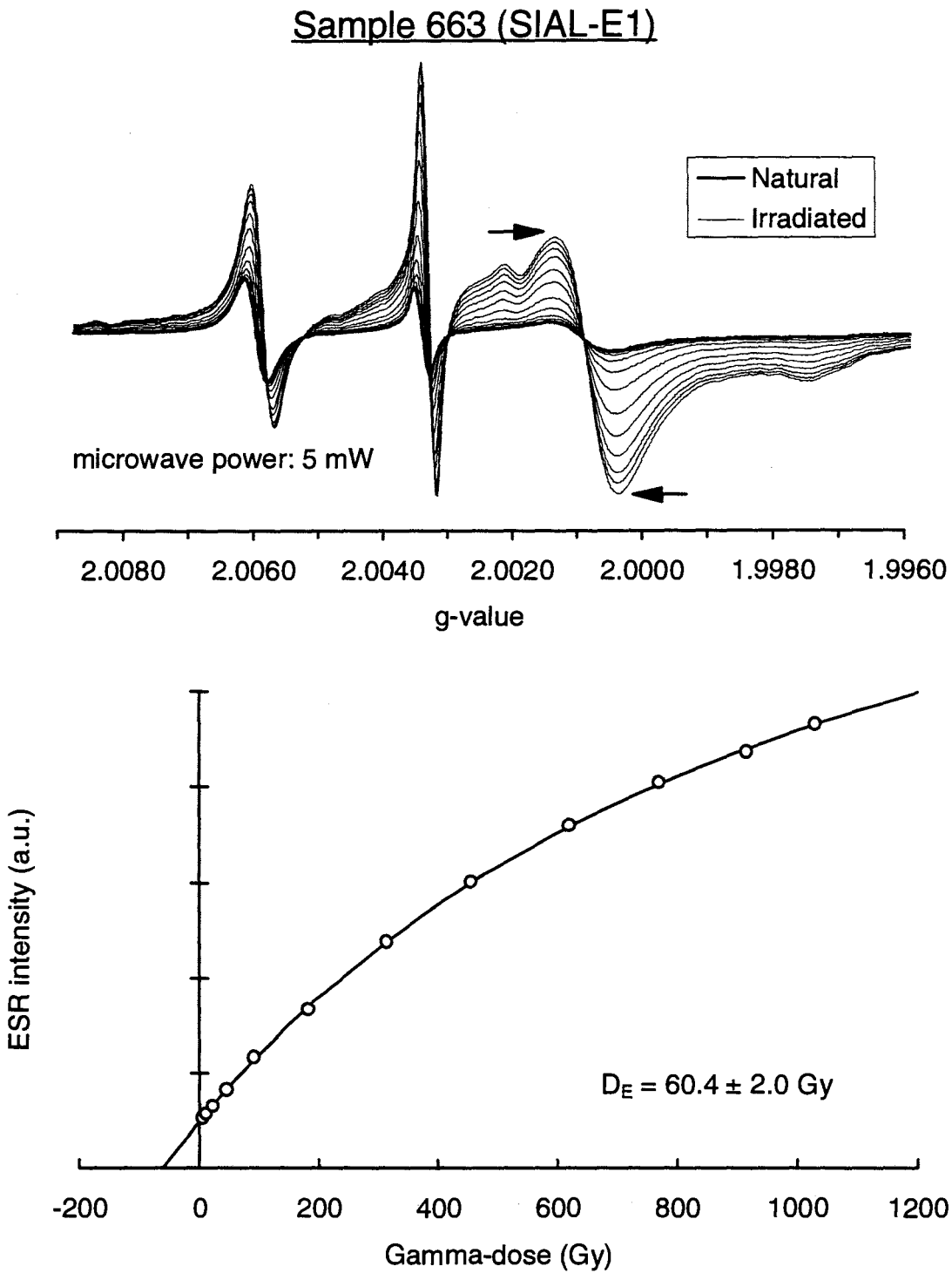

Figure 5.3(a). ESR spectra and dose response curve of coral sample 663 (SIAL-E1). The arrows indicate the method used to estimate the peak-to-peak height intensity at g=2.0007 (microwave power of 5 mW). A D_E-value of 60.4 ± 2.0 Gy was estimated by a single-saturating-exponential-plus-linear fit.

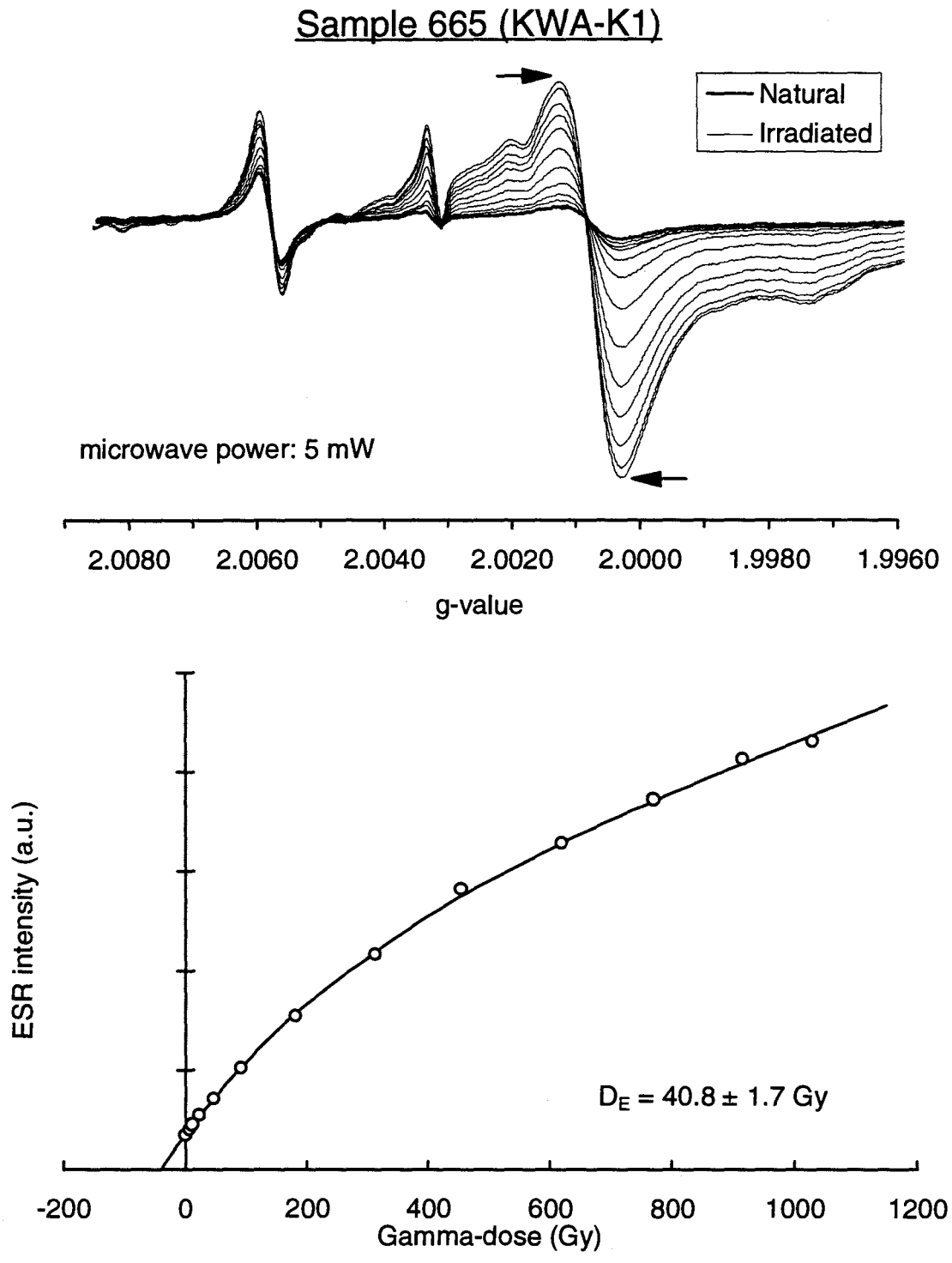

Figure 5.3(b). ESR spectra and dose response curve of coral sample 665 (KWA-K1). The arrows indicate the method used to estimate the peak-to-peak height intensity at g=2.0007 (microwave power of 5 mW). A D_E-value of 40.8 ± 1.7 Gy was estimated by a single-saturating-exponential-plus-linear fit.

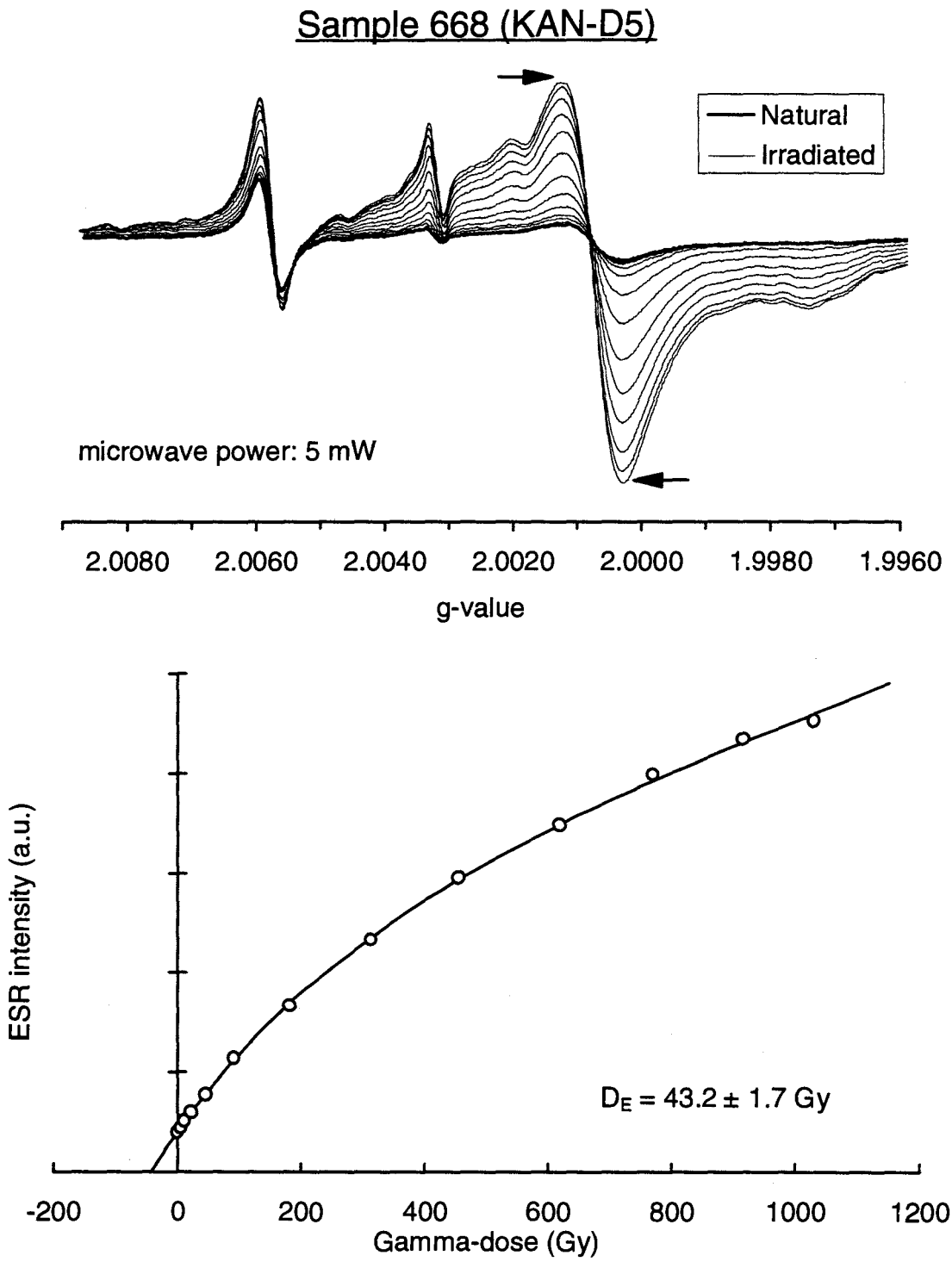

Figure 5.3(c). ESR spectra and dose response curve of coral sample 668 (KAN-D5). The arrows indicate the method used to estimate the peak-to-peak height intensity at g=2.0007 (microwave power of 5 mW). A D_E-value of 43.2 ± 1.7 Gy was estimated by a single-saturating-exponential-plus-linear fit.

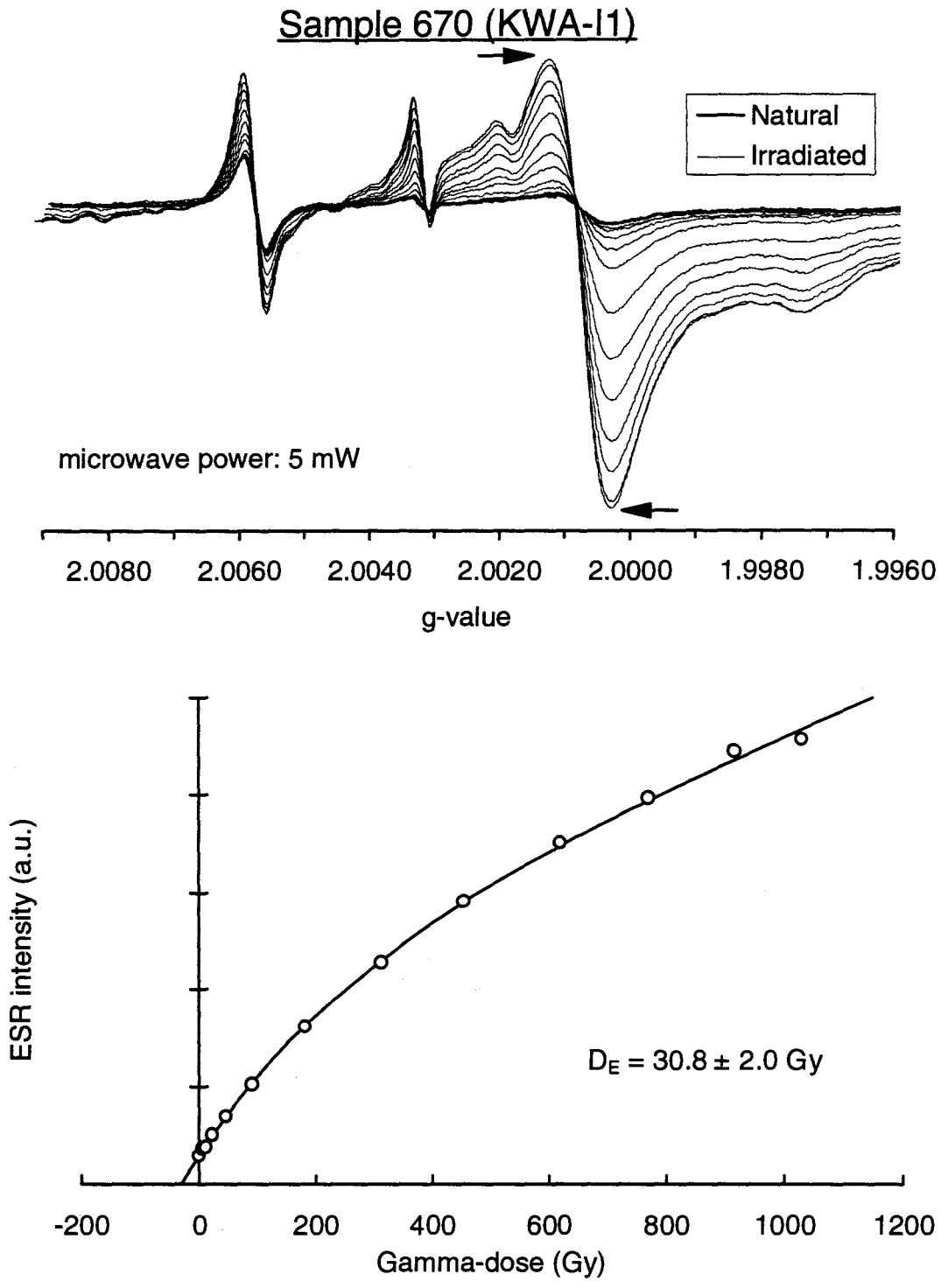

Figure 5.3(d). ESR spectra and dose response curve of coral sample 670 (KWA-I1). The arrows indicate the method used to estimate the peak-to-peak height intensity at g=2.0007 (microwave power of 5 mW). A D_E-value of 30.8 ± 2.0 Gy was estimated by a single-saturating-exponential-plus-linear fit.

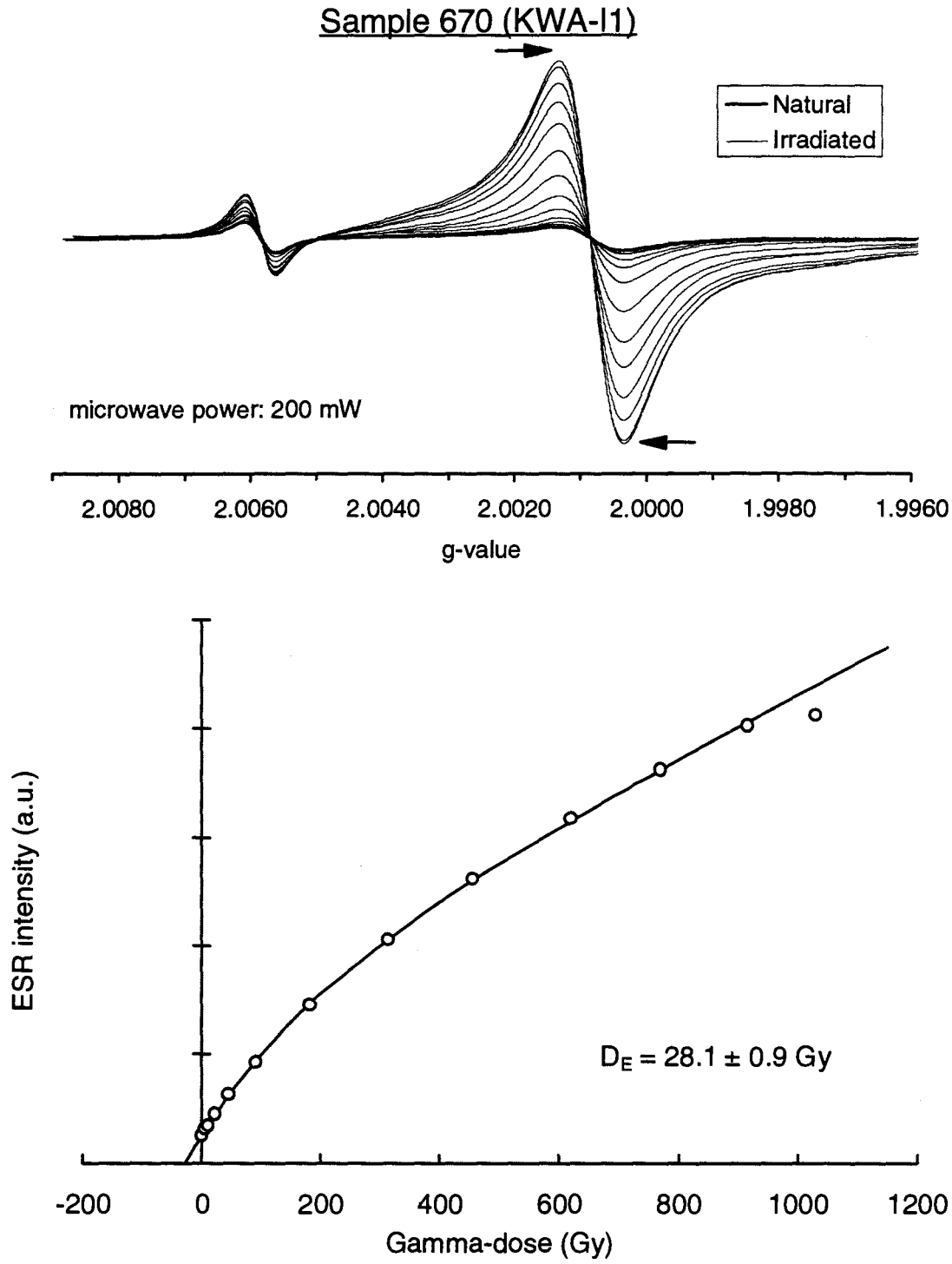

Figure 5.3(e). ESR spectra and dose response curve of coral sample 670 (KWA-I1). The arrows indicate the method used to estimate the peak-to-peak height intensity at g=2.0007 (microwave power of 200 mW). A D_E-value of 28.1 ± 0.9 Gy was estimated by a single-saturating-exponential-plus-linear fit.

Chapter 6 TOOTH SAMPLES

Samples of tooth enamel from Tham khuyen Cave, Vietnam, were examined by ESR. These samples were collected by Dr R. Grün, who also carried out the *in situ* γ-spectrometry measurements at the site.

6.1 Methods used

The sample preparations and dose rate analyses were carried out at the Quaternary Dating Research Centre, ANU, following the procedures of Grün (1989). For ESR dating, a total of 13 enamel samples were separated from four teeth of *Bovidae*, V78, V79, V80 and V81. ESR signals at g=2.0018 were used to determine D_E-values, based on the method proposed by Grün *et al.* (1987). The ESR spectra were measured with an X-band (9.60 GHz) Bruker ESP 300E spectrometer at room temperature (≈ 20°C) with a modulation frequency of 100 kHz, a microwave power of 2 mW, a modulation amplitude of 5 Gpp, a scan range of 50 G, a scan speed of 18 G min^{-1} with a time constant of 41 ms. The D_E-values and associated statistical errors were determined by the additive-dose method (Brumby, 1992; Grün and Brumby, 1994). Further details of the site and the context of the samples are given by Ciochon *et al.* (in press).

For the environmental dose rate assessment, uranium (enamel, dentine and sediment) and thorium (sediment) contents were determined by ICP-MS and neutron activation. The potassium content of the sediment was determined by neutron activation. The β attenuation factors were calculated using equation (3) of Grün (1986) and the average water content of 10.5 % ((mass of water / mass of dry sediment) × 100), with an error term of ± 5 %, was incorporated in the dose rate determination.

6.2 ESR ages obtained

The analytical data for the dose rate assessment and the estimated ages for the tooth enamel samples are given in Tables 6.1(a) and 6.1(b), respectively. Some examples of ESR spectra and dose response curves are shown in Figures 6.1(a)-(c). The uranium contents in enamel and dentine for sub-samples of individual teeth appear to be consistent, except for samples V79B and V80A. The D_E-values obtained are similarly compatible between sub-samples, agreeing at 1σ or 2σ error limits. The contribution of the internal dose rates to the total dose rates are substantial, so that differences between the ESR ages based on early and linear uranium-uptake models are significant (Grün, 1989). To determine the most suitable model for correct age estimation, however, requires further detailed uranium analyses (e.g. McDermott *et al.*, 1993). The ESR ages obtained are in agreement within the 1σ error limits, except for sample V81, with the early and linear uranium-uptake models yielding average ESR ages of 404 ± 51 ka and 534 ± 87 ka, respectively. Assuming the correct age lies between these estimates (cf. Grün and Stringer, 1991; McDermott *et al.*, 1993), the Tham Khuyen specimen is therefore probably in the region of 475 ± 125 ka in age.

6.3 Comparisons with independent age controls

There is no independent age control available for the unit dated by ESR. The nearby unit T2 (between units 8 and 9 on the main outcrop), located in the upper units of the ESR sampling site, yielded a U/Th age of 117 ka (Ciochon *et al.*, in press) from calcite crystals. Lithological and pollen analyses (Huong *et al.*, 1975) and faunal studies suggest that the sandy/silty conglomerate (breccia) underlying the ESR sampling site is late middle Pleistocene in age (≈ 300-250 ka). The ESR age estimate of 475 ± 125 ka is therefore slightly greater than these age evaluations, although the early uranium-uptake model age estimate (404 ± 51 ka) provides a closer match than the linear uranium-uptake ESR age to these independent age estimates.

Table 6.1(a). Analytical data for tooth samples from Tham Khuyen Cave, Vietnam (Ciochon *et al.*, in press).

Tooth	Sample number	Teeth		Sediment			Enamel		Sediment	
		U (EN) (ppm)	U (DE) (ppm)	U (ppm)	Th (ppm)	K (%)	Thickness (μm)	Removed (μm)	γ dose rate (μGy year^{-1})	β dose rate (μGy year^{-1})
1	V78A	0.27 ± 0.03	26.1 ± 2.6	3.48 ± 0.28	12.45 ± 0.45	0.17 ± 0.05	3400 ± 300	100 ± 50	948 ± 95	64 ± 9
	V78B	0.27 ± 0.03	27.3 ± 2.7				3400 ± 300	100 ± 50		
	V78C	0.35 ± 0.04	26.8 ± 2.7				3400 ± 300	100 ± 50		
2	V79A	0.37 ± 0.04	45.4 ± 4.5	2.73 ± 0.57	12.83 ± 0.37	0.19 ± 0.05	1540 ± 100	180 ± 50		112 ± 16
	V79B	0.83 ± 0.08	43.8 ± 4.4				1540 ± 100	180 ± 50		
	V79C	0.36 ± 0.04	45.5 ± 4.6				1540 ± 100	180 ± 50		
3	V80A	0.75 ± 0.08	26.5 ± 2.7	3.07 ± 0.50	13.70 ± 0.50	0.15 ± 0.05	4120 ± 300	500 ± 150		34 ± 7
	V80B	1.23 ± 0.12	24.9 ± 2.5				3560 ± 300	250 ± 100		50 ± 9
	V80C	1.30 ± 0.13	23.5 ± 2.4				4120 ± 300	500 ± 150		34 ± 7
4	V81-1A	0.82 ± 0.08	33.3 ± 3.3	3.75 ± 0.10	14.70 ± 0.42	0.29 ± 0.05	1100 ± 150	100 ± 50		197 ± 25
	V81-1B	0.95 ± 0.10	37.3 ± 3.7				1100 ± 150	100 ± 50		
	V81-2A	0.26 ± 0.03	30.5 ± 3.1	2.43 ± 0.50	10.40 ± 0.10	0.13 ± 0.05	900 ± 150	50 ± 30		144 ± 24
	V81-2B	0.22 ± 0.02	32.0 ± 3.2				900 ± 150	50 ± 30		

Note: 1. Abbreviations: EN = enamel; DE = dentine.

Table 6.1(b). ESR age estimates for tooth samples from Tham Khuyen Cave, Vietnam.

Tooth	Sample number	D_E-value (Gy)	Sediment		Early uranium-uptake				Linear uranium-uptake			
			γ-D (μGy year^{-1})	β-D (μGy year^{-1})	β-D (DE) (μGy year^{-1})	Internal D (μGy year^{-1})	Total D (μGy year^{-1})	Age (ka)	β-D (DE) (μGy year^{-1})	Internal D (μGy year^{-1})	Total D (μGy year^{-1})	Age (ka)
1	V78A	566 ± 21	948 ± 95	64 ± 9	297 ± 43	140 ± 23	1449 ± 107	391 ± 32	141 ± 20	65 ± 11	1218 ± 98	465 ± 41
	V78B	552 ± 36			309 ± 45	139 ± 23	1460 ± 108	378 ± 37	146 ±21	64 ± 12	1222 ± 98	451 ± 47
	V78C	515 ± 55			300 ± 43	179 ± 31	1491 ± 109	345 ± 45	142 ± 21	82 ± 16	1236 ± 99	417 ± 56
2	V79A	1043 ± 76		112 ± 16	999 ± 125	189 ± 32	2248 ± 161	464 ± 47	484 ± 62	90 ± 16	1634 ± 166	638 ± 65
	V79B	1023 ± 55			954 ± 121	418 ± 68	2432 ± 169	421 ± 37	463 ± 59	200 ± 33	1723 ± 118	549 ± 52
	V79C	965 ± 37			995 ± 126	182 ± 31	2237 ± 162	431 ± 35	482 ± 61	87 ± 15	1629 ± 115	592 ± 48
3	V80A	656 ± 32		34 ± 7	180 ± 35	402 ± 65	1564 ± 121	419 ± 38	86 ± 16	188 ± 32	1256 ± 102	522 ± 49
	V80B	718 ± 35		50 ± 9	238 ± 41	640 ± 98	1876 ± 143	383 ± 35	115 ± 20	302 ± 48	1415 ± 109	507 ± 46
	V80C	770 ± 28		34 ± 7	155 ± 31	694 ± 109	1831 ± 148	420 ± 37	75 ± 15	328 ± 52	1385 ± 110	556 ± 48
4	V81-1A	1288 ± 63		197 ± 25	967 ± 137	408 ± 68	2520 ± 182	511 ± 45	470 ± 67	196 ± 32	1811 ± 123	711 ± 60
	V81-1B	1149 ± 97			1067 ± 151	467 ± 79	2679 ± 197	429 ± 48	518 ± 74	224 ± 38	1887 ± 129	609 ± 66
	V81-2A	734 ± 41		144 ± 24	970 ± 138	119 ± 23	2181 ± 171	336 ± 32	466 ± 67	56 ± 11	1614 ± 119	455 ± 42
	V81-2B	702 ± 48			1010 ± 142	102 ± 17	2204 ± 173	318 ±33	485 ± 70	48 ± 8	1625 ± 121	431 ± 44
	Average							404 ± 51				534 ± 87

Notes:
1. Analytical and dose rate data from Ciochon *et al.* (in press).
2. Abbreviations: D = dose rate; DE = dentine.
3. The ^{60}Co-gamma source was calibrated by alanine dosimetry by A. Wieser, GSF, Munich. The calibration error of 2 % is included in the D_E-value error term.
4. The errors associated with the bottom line "average" ages represent the standard errors on the mean for the 13 individual determinations. They therefore reflect the degree of scatter about the mean ages.

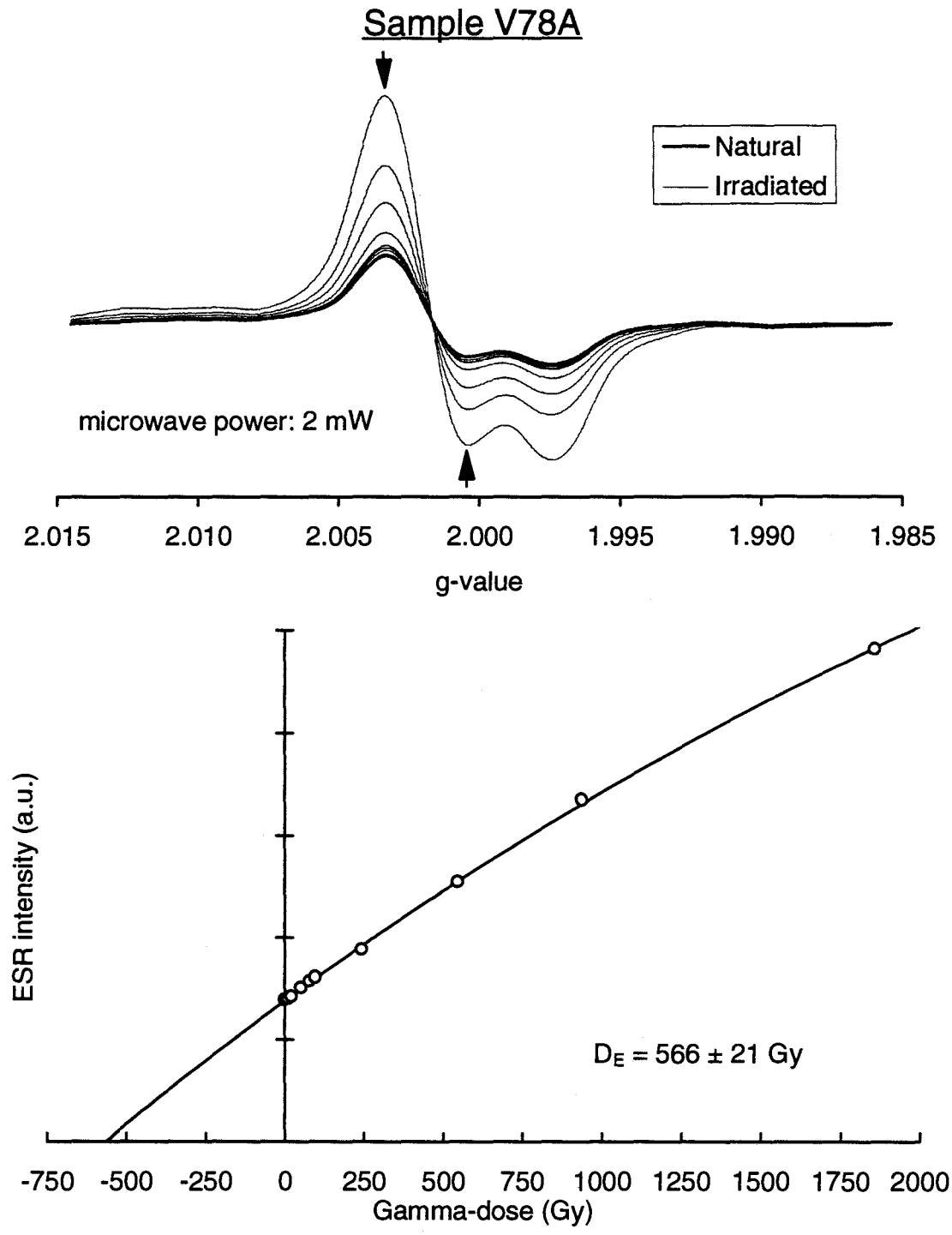

Figure 6.1(a). ESR spectra (Natural and N+irradiated) and dose response curve based on the signal at g=2.0018 (microwave power of 2 mW) for tooth sample V78A from Tham Khuyen Cave, Vietnam. The arrows indicate the method used to estimate the peak-to-peak signal height intensity. A D_E-value of 566 ± 21 Gy was estimated from a single saturating exponential fit.

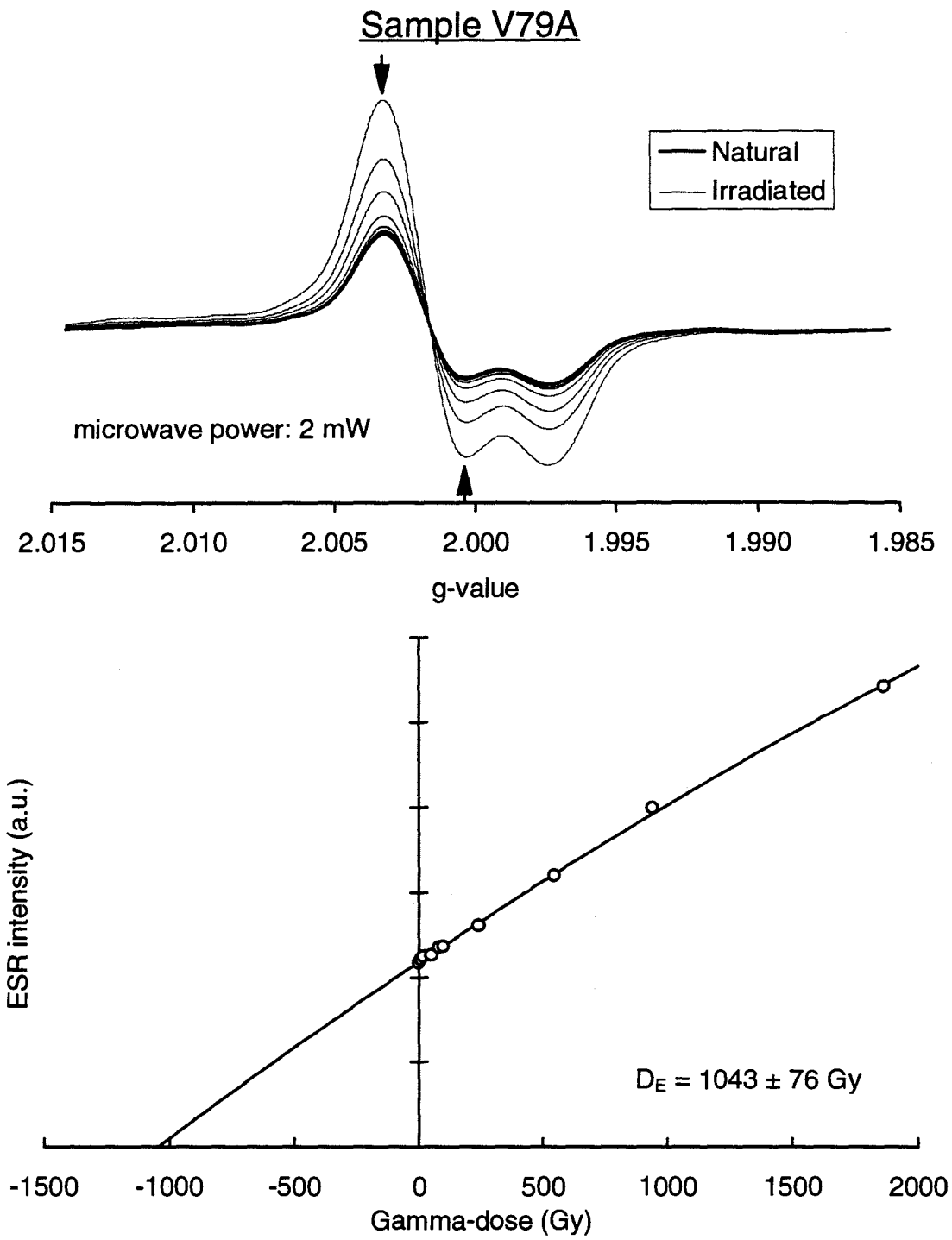

Figure 6.1(b). ESR spectra (Natural and N+irradiated) and dose response curve based on the signal at g=2.0018 (microwave power of 2 mW) for tooth sample V79A from Tham Khuyen Cave, Vietnam. The arrows indicate the method used to estimate the peak-to-peak signal height intensity. A D_E-value of 1043 ± 76 Gy was estimated from a single saturating exponential fit.

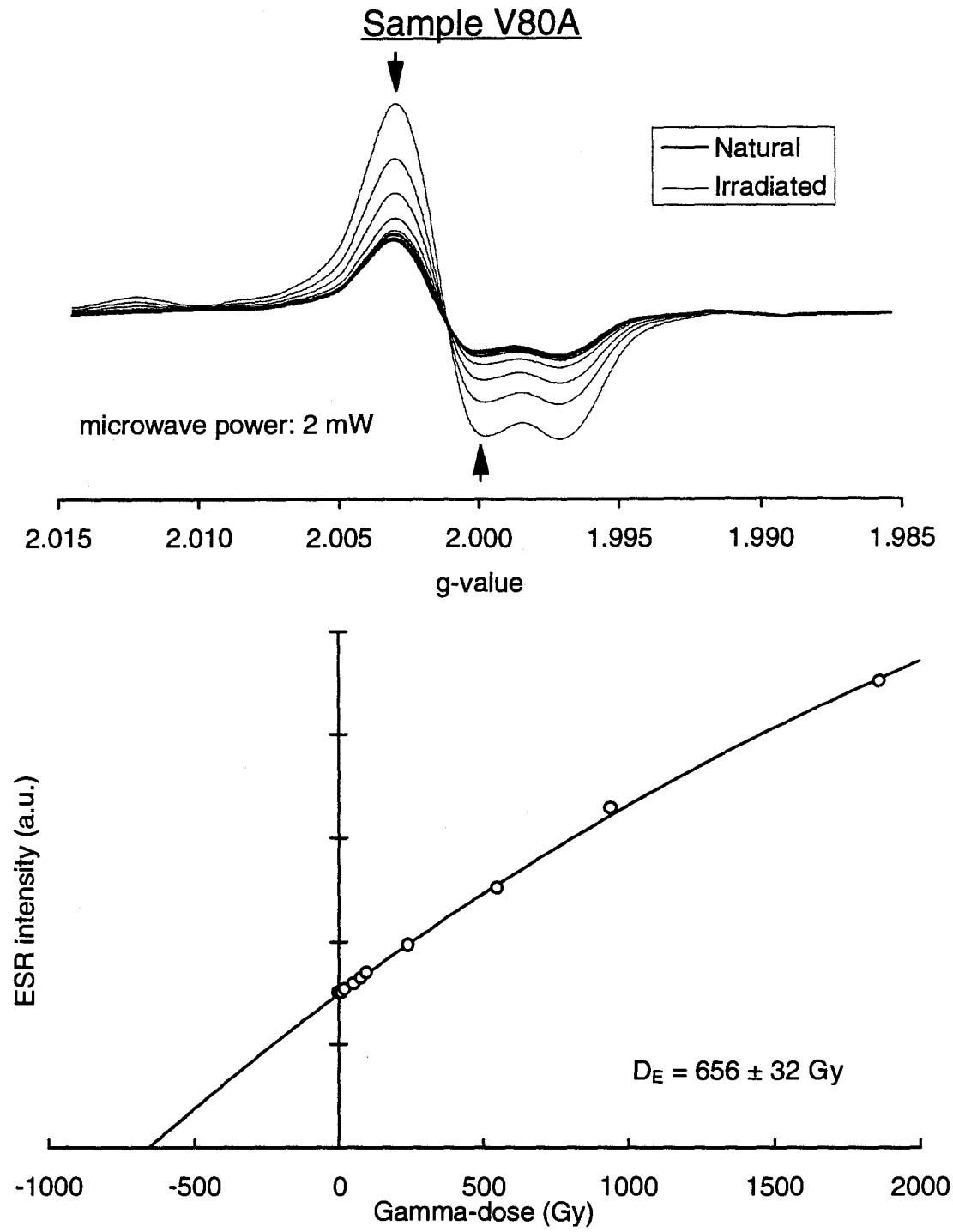

Figure 6.1(c). ESR spectra (Natural and N+irradiated) and dose response curve based on the signal at g=2.0018 (microwave power of 2 mW) for tooth sample V80A from Tham Khuyen Cave, Vietnam. The arrows indicate the method used to estimate the peak-to-peak signal height intensity. A D_E-value of 656 ± 32 Gy was estimated from a single saturating exponential fit.

Chapter 7 QUARTZ SAMPLES

7.1 Methods used

All samples were examined initially for the dating signals of OHC (g=2.0011), E' (g=2.0001) and Ge (g=1.997) centres at room temperature, as the Ge centre, in particular, has been reported by Tanaka *et al.* (1985) as yielding light-sensitive ESR signals. In the samples examined, however, none of these centres gave detectable ESR signals. Subsequently, ESR measurements were made of the Al and Ti signals recorded at liquid nitrogen temperature (≈ 77K).

For the Forster-Tuncurry samples, nine aliquots, each weighing 200 mg, were prepared and then subjected to a selection of gamma doses (up to ≈ 1260 Gy) using a ^{60}Co source (dose rate ≈ 3.6 Gy min^{-1}). A similar approach, described in detail in section 14.1, was used for the Deaf Adder Gorge sample (Ox_{OD}K166) and for sample Ox_{OD}AC150 from Allen's Cave. Since the quantity of sample Ox_{OD}AC390 from Allen's Cave was limited, only one aliquot (200 mg) was used for ESR measurements. The sample was given a selected dose using a ^{60}Co source (dose rate ≈ 10.7 Gy min^{-1}) followed by ESR measurements. A second dose was then administered, and the ESR signal remeasured. This procedure was repeated a further 20 times resulting in the sample receiving a total dose of 1720 Gy. This sample was then used for the sunlight bleaching experiments described in section 11.2.1. The methods used to estimate the intensities of the Al and Ti signals are shown in Figure 7.1. The D_E-values were determined using the same methods as described in section 4.1.1.

ESR spectra were measured at both room (≈ 20°C) and liquid nitrogen temperature (≈ 77K; with a quartz dewar) using X-band ESR spectrometers (Jeol JES-PE and Bruker ESP 300E). The room temperature spectra were measured with a modulation frequency of 100 kHz, a microwave power of 0.63 mW, a modulation amplitude of 0.5 Gpp, a scan

range of 10 Gpp, and a scan speed of 1.8 min^{-1} with a time constant of 2621 ms. The low temperature spectra were measured with a modulation frequency of 100 kHz, a microwave power of 1 mW, a modulation amplitude of 0.5 Gpp, a scan range of 100 G, and a scan speed of 17.9 Gy min^{-1} with a time constant of 655 ms.

For the environmental dose rate assessment of the Forster-Tuncurry samples, the specific activity of uranium and thorium was measured by means of thick-source alpha counting over a 42 mm ZnS scintillation screen. Potassium contents were determined by AES. The dose rates obtained (Roy *et al.*, 1992) assume secular equilibrium in both the uranium and thorium decay chains. The rubidium content and the cosmic ray dose rate contribution are assumed to be 50 ± 25 ppm and 150 ± 50 μGy $year^{-1}$, respectively (Roy *et al.*, 1992).

The environmental dose rates at the Deaf Adder Gorge site in the Northern Territory were deduced from high-resolution γ-ray spectrometry determinations, and the internal dose rates were estimated from thick-source alpha counting of the acid-etched quartz grains, as described by Roberts *et al.* (1994b). At Allen's Cave in South Australia, field gamma spectrometry measurements were also made, while the internal dose rates were estimated from neutron activation analyses of the etched quartz grains (see details in Roberts *et al.*, 1996).

7.2 ESR ages obtained

7.2.1 Forster-Tuncurry, New South Wales

ESR results and dose response curves for samples Q13 and Q18, based on the Al and Ti centres, are given in Table 7.1 and Figure 7.2, respectively. The dose rate data used for the TL age determinations (Roy *et al.*, 1992) were used also to calculate the ESR ages. For both samples, the ESR ages based on the Al centre are much older (3.0 times for sample Q18 and 3.7 times for sample Q13) than the Ti ages. At this point, it is not clear whether the Al and Ti signals had been bleached completely before deposition but the

results suggest that these signals have different light sensitivities. The Ti centre appears to be bleached more rapidly, and more completely before sediment deposition, than the Al centre.

7.2.2 Lake George, New South Wales

The samples from this site unfortunately exhibited undetectably weak ESR signals from the Ti centre (see Figure 7.3), so no further dating work was done. Sunlight bleaching experiments on these samples are described in Chapter 11.

7.2.3 Allen's Cave, South Australia

ESR spectra and dose response curves of samples $Ox_{OD}AC150$ and $Ox_{OD}AC390$, based on the Al and Ti signals, are shown in Figures 7.4(a), (b) and Figures 7.5(a), (b), respectively. ESR ages based on the Al and Ti signals are given in Table 7.2, together with the dose rates given by Roberts *et al.* (1996). Similar results to the Forster-Tuncurry samples (Q13 and Q18) were observed for sample $Ox_{OD}AC150$: the ESR age based on the Al centre is much greater (3.6 times) than its Ti-centre age. On the other hand, the ESR ages based on the Al and Ti signals in $Ox_{OD}AC390$ are in good agreement at the 1σ level. However, the dose response curve based on the Ti signal of sample $Ox_{OD}AC390$ (Fig. 7.5(b)) is half-way to saturation at the 'natural' ESR intensity (i.e. at zero gamma dose). The estimated D_E-value of 440.4 ± 21.6 Gy could, therefore, be an overestimate due to the lengthy extrapolation of the dose response curve. Unlike the Forster-Tuncurry samples, which are water-lain, the wind-blown sediments at Allen's Cave are apt to be well-bleached before burial. These D_E-value discrepancies between the Al and Ti signals in $Ox_{OD}AC150$ again suggest, therefore, that the two centres have different light sensitivities, with the Ti centre being more light-sensitive than the Al centre.

7.2.4 Deaf Adder Gorge, Northern Territory

Sample Ox_{OD}K166 from this site (see Roberts *et al.*, 1994b, for site details) exhibited weak ESR signals for both the Al and Ti centres in the natural (unirradiated) quartz (Fig. 7.6). It was possible, however, to obtain an ESR age estimate using the Al signal. As this D_E-value is likely to be an overestimate, as observed for the Al signal in the Forster-Tuncurry and Allen's Cave samples, no further investigations were made using Ox_{OD}K166.

7.3 Comparisons with independent age controls

ESR results and the TL ages for samples from Forster-Tuncurry Shelf (Q13 and Q18) and Allen's Cave (Ox_{OD}AC150 and Ox_{OD}AC390) are compared in Table 7.3(a), (b) and Table 7.4(a), (b), respectively. No agreement was observed between the ESR ages based on the Al and Ti centres and the independent ages, estimated by ^{14}C, OSL and TL. In all cases, the ESR dates are much older than the independent ages. Among the ESR estimates, the Al signals produce the oldest ages, 3.0-3.7 times greater than the Ti signal ages (except for sample Ox_{OD}AC390). The Ti-centre age of sample Ox_{OD}AC150 (14.2 ± 1.1 ka) is reasonably close to the OSL, TL and calibrated ^{14}C ages (9-11 ka), but the Al-centre age (50.7 ± 3.3 ka) is substantially greater. Since this sample is believed to have been well-bleached before burial, the results suggest that neither the Al nor Ti signals had been completely zeroed by sunlight exposure. The discrepancy between the Al and Ti signal ages, and the TL age determinations for the Forster-Tuncurry samples, provides further evidence of inadequate bleaching of these ESR signals prior to sample burial. As a consequence, new ESR signals were sought that had greater sensitivity to light; these signals are discussed in Chapters 11 and 14.

Table 7.1. ESR results based on the Al and Ti centres of samples Q13 and Q18 from Forster-Tuncurry Shelf, New South Wales.

Sample number	Lab. no. for TL	Specific activity (U + Th Bq kg^{-1})	K (%)	Moisture (%)	Dose rate (μGy $year^{-1}$)	Al centre		Ti centre	
						D_E (Gy)	Age (ka)	D_E (Gy)	Age (ka)
Q13	W1130	48.8 ± 1.5	0.580 ± 0.005	19.6 ± 3	1368 ± 45	1099 ± 249	803 ± 184	298 ± 46	218 ± 34
Q18	W1131	17.3 ± 0.7	0.732 ± 0.005	21.0 ± 3	1044 ± 41	462 ± 31	443 ± 34	154 ± 5	148 ± 8

Note: Dose rate and moisture values from Roy *et al.* (1992).

Table 7.2. ESR results based on the Al and Ti centres of samples $Ox_{OD}AC390$ and $Ox_{OD}AC150$ from Allen's Cave, South Australia.

Sample code	Dose rate (Gy ka^{-1})	Al centre		Ti centre	
		D_E-value (Gy)	Age (ka)	D_E-value (Gy)	Age (ka)
$Ox_{OD}AC150$	2.32 ± 0.09	117.7 ± 6.1	50.7 ± 3.3	32.9 ± 2.2	14.2 ± 1.1
$Ox_{OD}AC390$	1.67 ± 0.09	456.0 ± 18.9	273.1 ± 18.6	440.4 ± 21.6	263.7 ± 19.2

Note: Dose rate values from Roberts *et al.* (1996).

Table 7.3(a). ESR and TL results for sample Q13 from Forster-Tuncurry Shelf, New South Wales.

Sample number	Dating method (Lab. no.)		Dose rate (μGy year^{-1})	D_E-value (Gy)	Age (ka)
Q13	TL (W1130)		1368 ± 45	130.9 ± 17.2	95.7 ± 13.0
	ESR	Al signal		1099 ± 249	803 ± 184
		Ti signal		298 ± 46	218 ± 34

Note: TL and dose rate data from Roy *et al.* (1992).

Table 7.3(b). ESR and TL results for sample Q18 from Forster-Tuncurry Shelf, New South Wales.

Sample number	Dating method (Lab. no.)		Dose rate (μGy year^{-1})	D_E-value (Gy)	Age (ka)
Q18	TL (W1131)		1044 ± 41	55.4 ± 7.3	53.1 ± 7.3
	ESR	Al signal		462 ± 31	443 ± 34
		Ti signal		154 ± 5	148 ± 8

Note: TL and dose rate data from Roy *et al.* (1992).

Table 7.4(a). ESR results and ^{14}C, OSL and TL dates for sample $Ox_{OD}AC150$ from Allen's Cave, South Australia.

Sample code	Dating method		Dose rate (Gy ka^{-1})	D_E-value (Gy)	Age (ka)
$Ox_{OD}AC150$	^{14}C		2.32 ± 0.09	-----	9.65 ± 0.65 (8.70 ± 0.30 B.P.; ANU-8077) $10.2 \pm \frac{0.6}{0.3}$ (9.27 ± 0.14 B.P.; ANU-6850) 10.5 ± 0.5 (9.53 ± 0.19 B.P.; ANU-6849)
	OSL			23.5 ± 0.6	9.7 ± 0.6
	TL			25.9 ± 1.4	10.7 ± 0.9
	ESR	Al signal		117.7 ± 6.1	50.7 ± 3.3
		Ti signal		32.9 ± 2.2	14.2 ± 1.1

Notes: 1. ^{14}C, OSL, TL and dose rate data from Roberts *et al.* (1996).
2. OSL samples were preheated for 5 min at 220°C.
3. TL age is determined from the 265-380°C plateau region.
4. ^{14}C ages (with 2σ uncertainty) are calibrated according to Stuiver and Reimer (1993). The conventional ages are given in parentheses, with the laboratory code.

Table 7.4(b). ESR and OSL results for sample $Ox_{OD}AC390$ from Allen's Cave, South Australia.

Sample code	Dating method		Dose rate (Gy ka^{-1})	D_E-value (Gy)	Age (ka)
$Ox_{OD}AC390$	OSL		1.67 ± 0.09	66.6 ± 2.3	38.2 ± 3.1
	ESR	Al signal		456.0 ± 18.9	273.1 ± 18.6
		Ti signal		440.4 ± 21.6	263.7 ± 19.2

Notes: 1. OSL and dose rate data from Roberts *et al.* (1994a, 1996).
2. OSL samples were preheated for 5 min at 220°C.

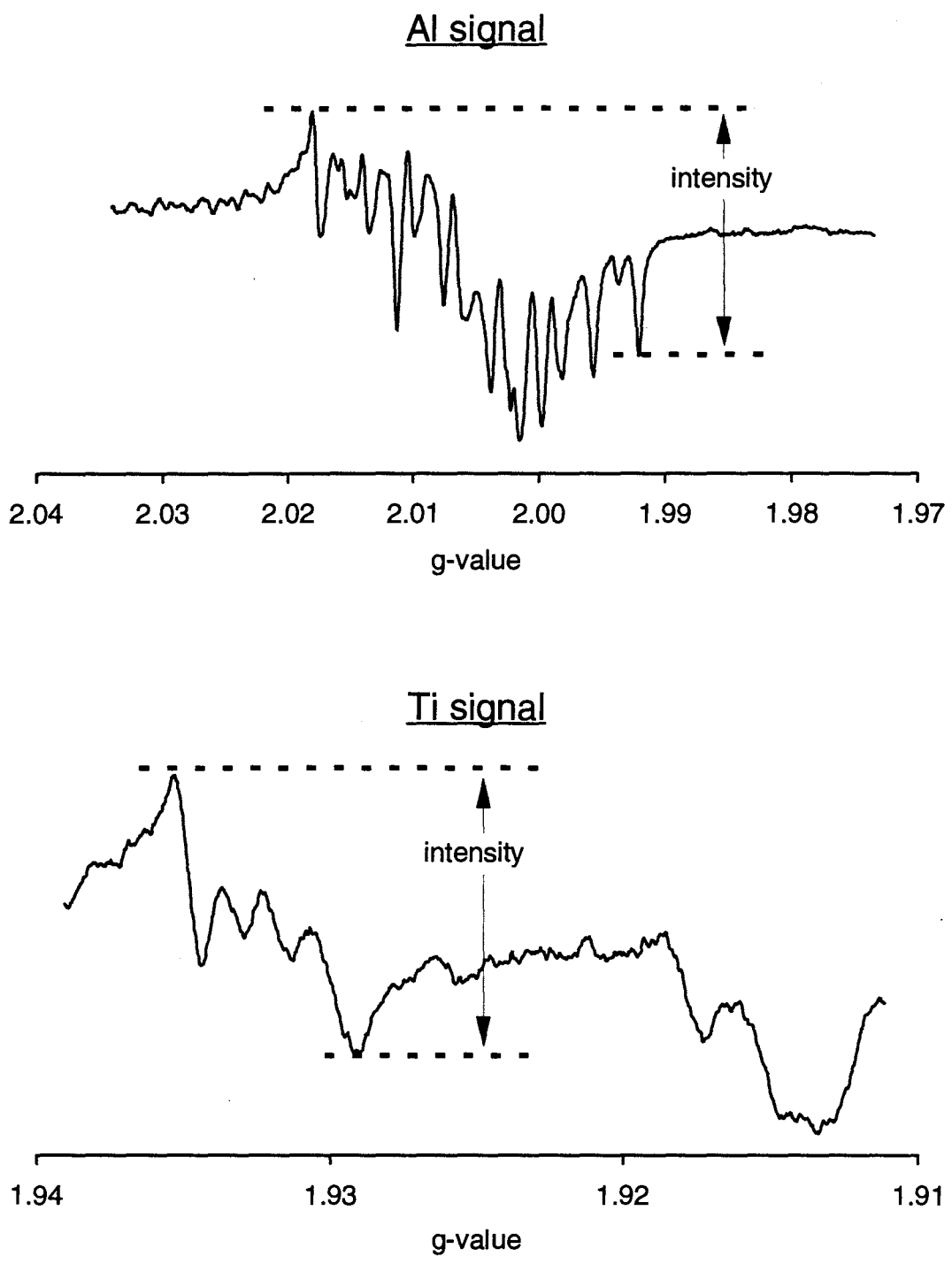

Figure 7.1. ESR spectra of Al and Ti signals for sample Q13 from Forster-Tuncurry, New South Wales, and the methods used to estimate their intensities.

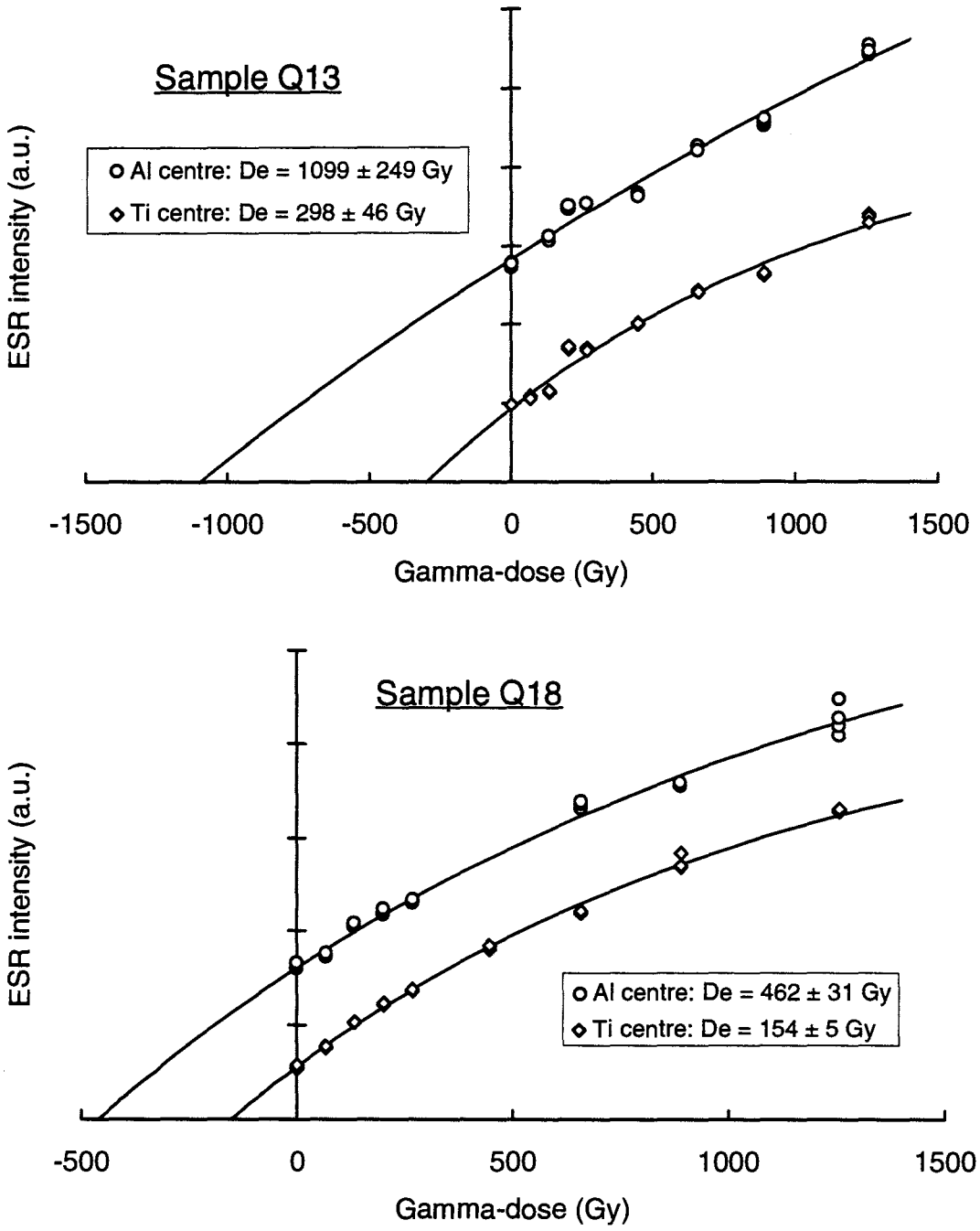

Figure 7.2. Dose response curves of samples Q13 and Q18 from Forster-Tuncurry, New South Wales, based on the Al and Ti signals. All curves are single saturating exponential fits.

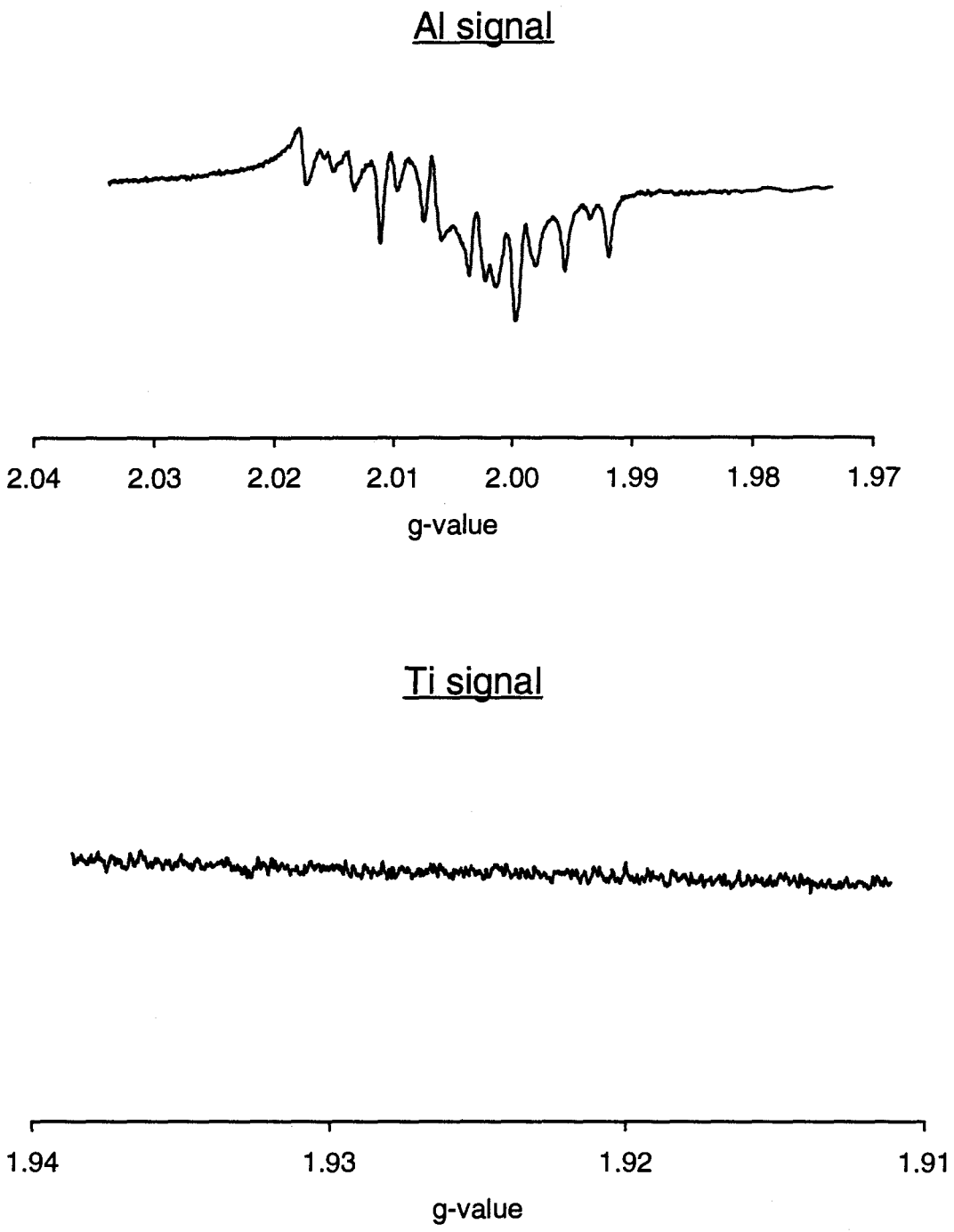

Figure 7.3. ESR spectra of Al and Ti signals for sample LG-A (natural) from Lake George, New South Wales.

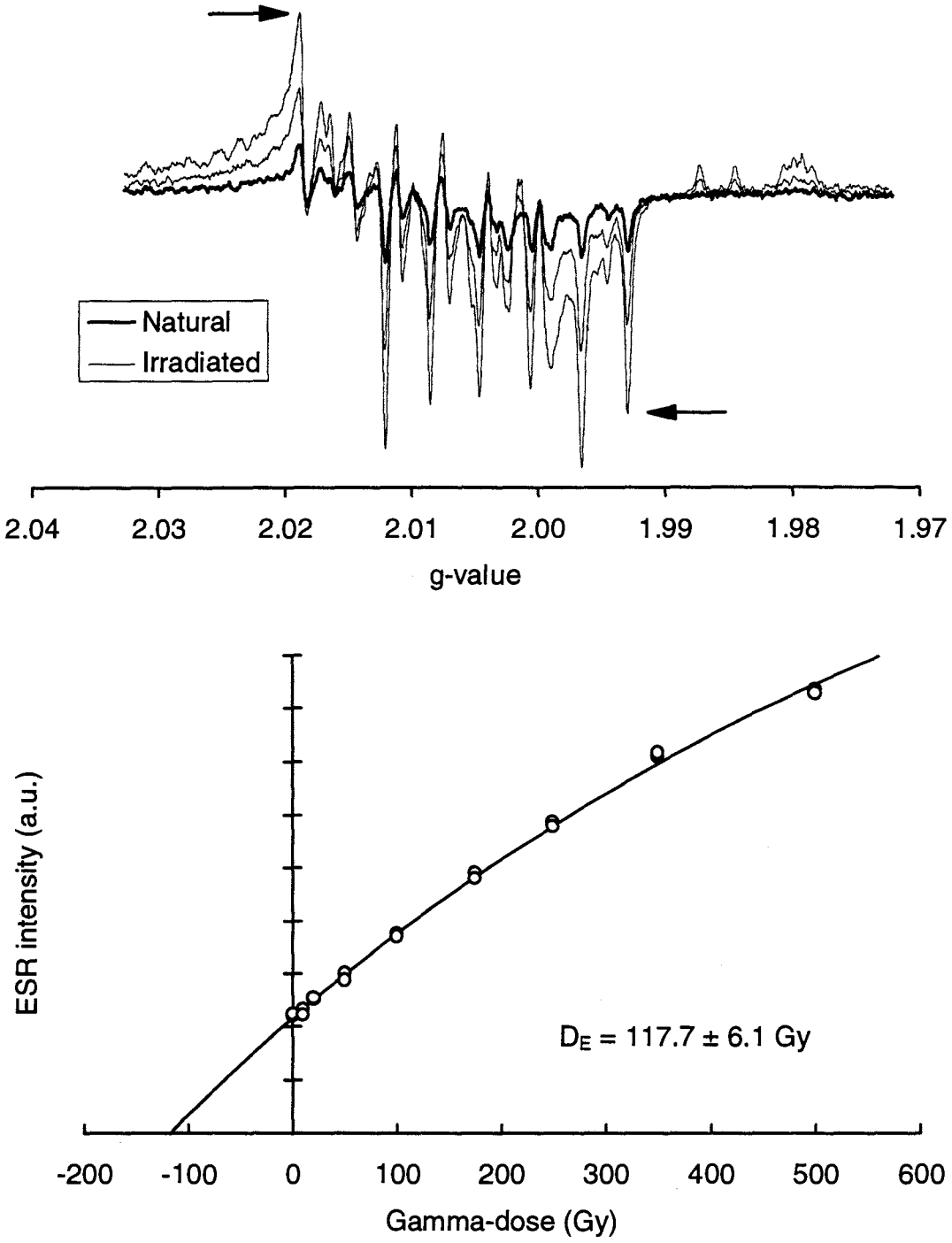

Figure 7.4(a). ESR spectra of the Al signal (Natural, N+175 Gy and N+500 Gy) and dose response curve for sample $Ox_{OD}AC150$. The arrows indicate the method used to estimate the peak-to-peak height intensity. A D_E-value of 117.7 ± 6.1 Gy was estimated from a single saturating exponential fit.

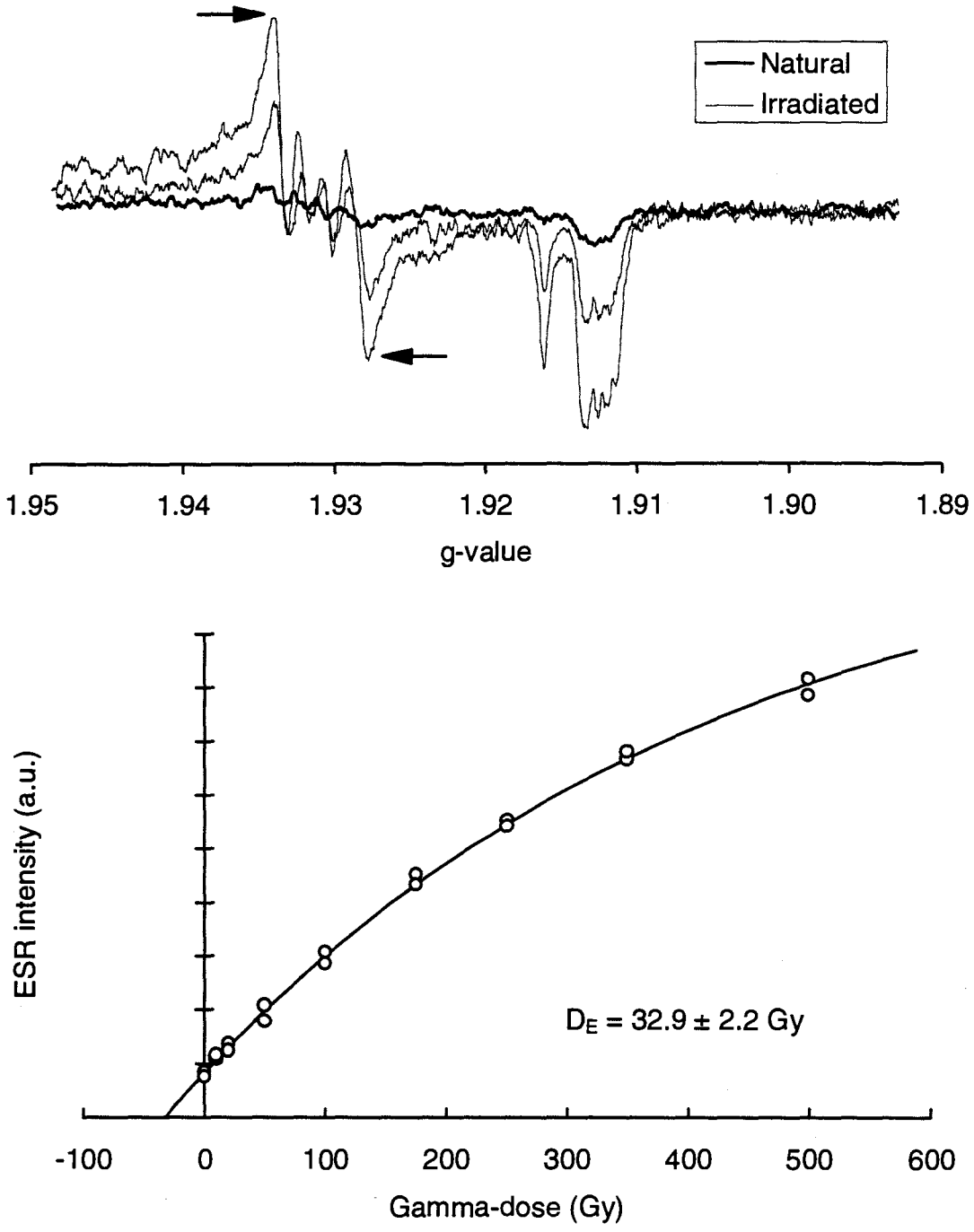

Figure 7.4(b). ESR spectra of the Ti signal (Natural, N+175 Gy and N+500 Gy) and dose response curve for sample Ox_{OD}AC150. The arrows indicate the method used to estimate the peak-to-peak height intensity. A D_E-value of 32.9 ± 2.2 Gy was estimated from a single saturating exponential fit.

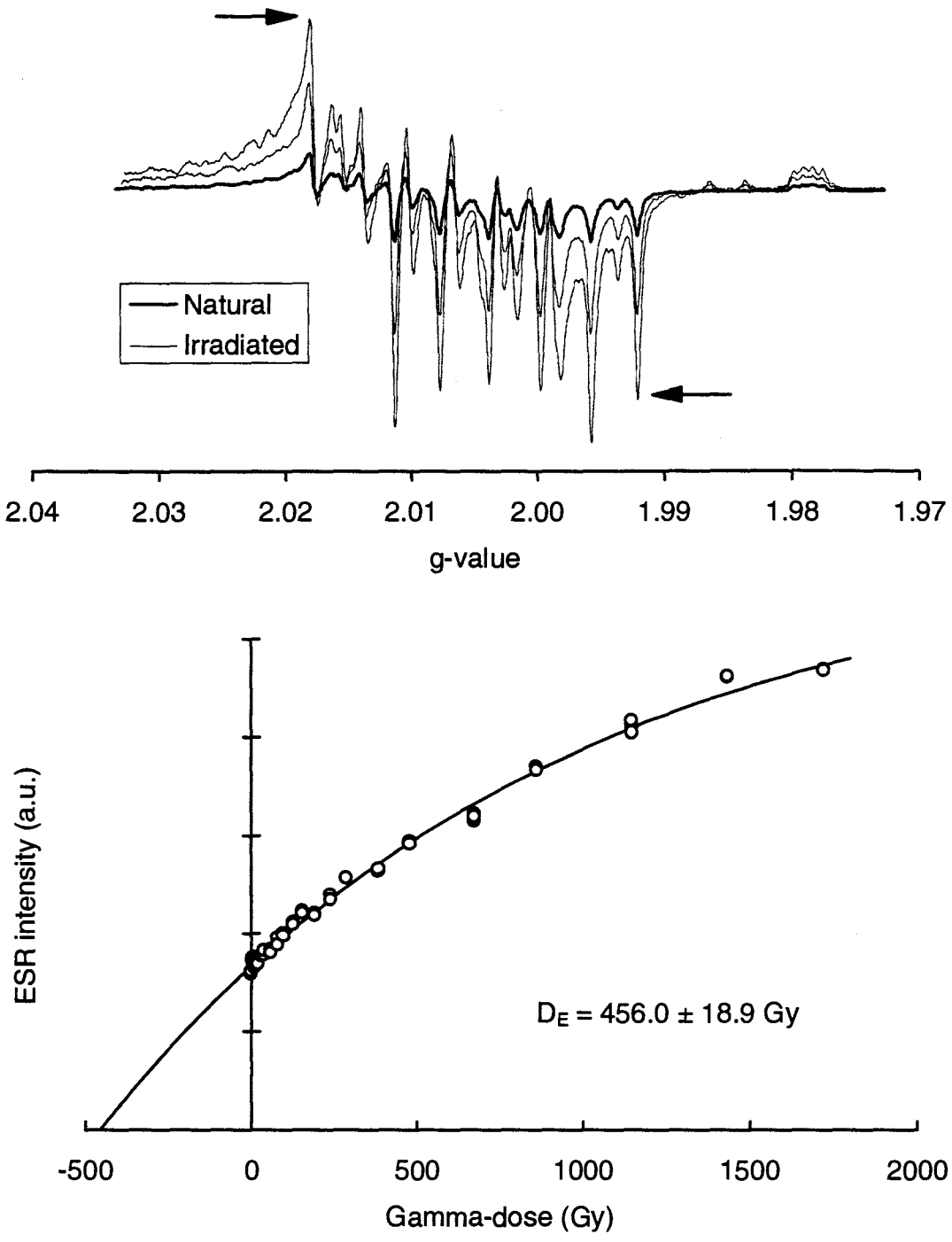

Figure 7.5(a). ESR spectra of the Al signal (Natural, N+288 Gy and N+1720 Gy) and dose response curve for sample Ox_{OD}AC390. The arrows indicate the method used to estimate the peak-to-peak height intensity. A D_E-value of 456.0 ± 18.9 Gy was estimated from a single saturating exponential fit.

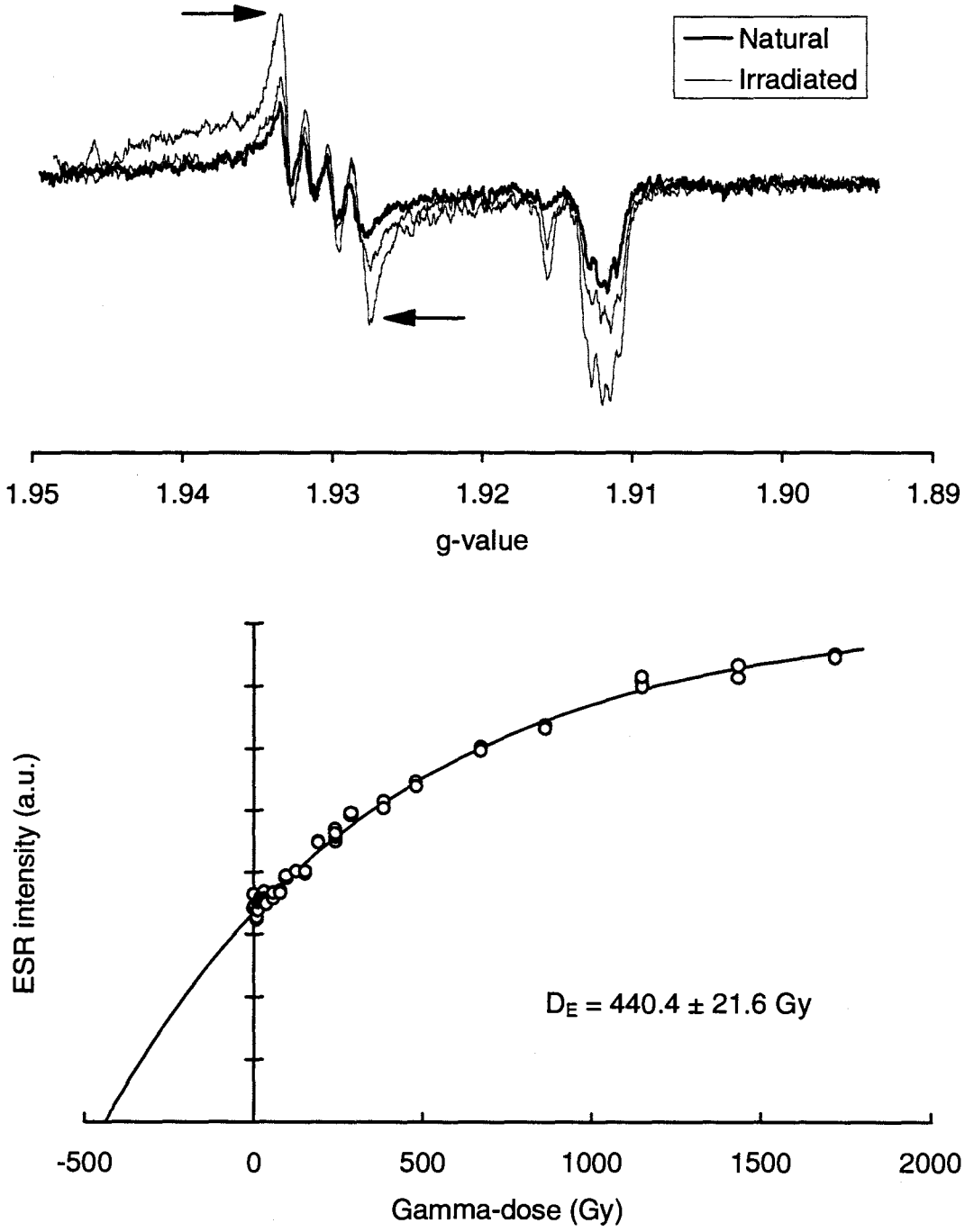

Figure 7.5(b). ESR spectra of the Ti signal (Natural, N+288 Gy and N+1720 Gy) and dose response curve for sample Ox_{OD}AC390. The arrows indicate the method used to estimate the peak-to-peak height intensity. A D_E-value of 440.4 ± 21.6 Gy was estimated from a single saturating exponential fit.

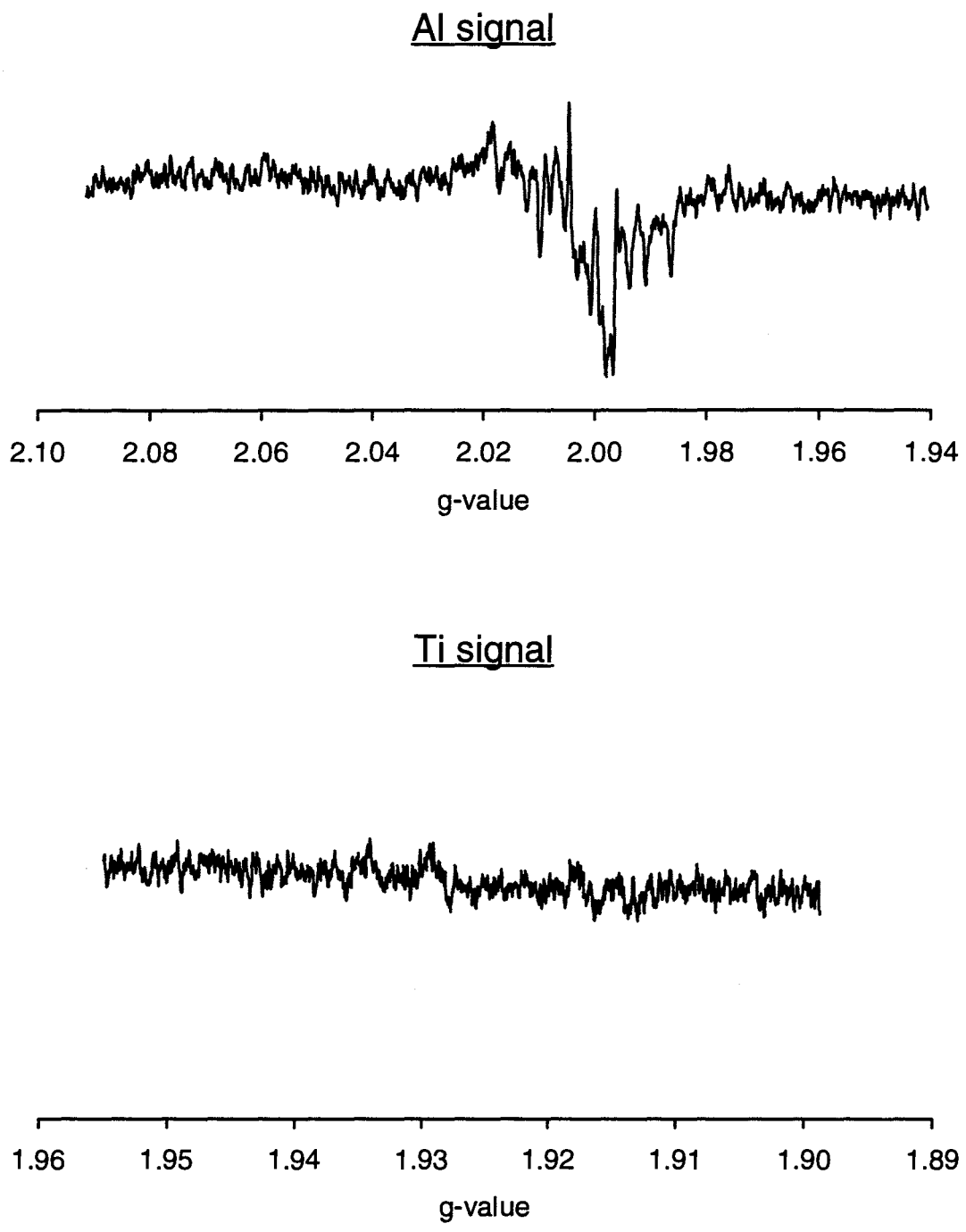

Figure 7.6. ESR spectra of Al and Ti signals for sample Ox_{OD}K166 (natural) from Deaf Adder Gorge, Northern Territory.

Chapter 8 SUMMARY OF RESULTS USING PUBLISHED METHODS

For shell samples from Forster-Tuncurry, the calibrated AMS ^{14}C results for the three cores show a wide range of ages, indicating that the shells consist of a mixture of reworked fossil shells. The AMS ^{14}C dates suggest that the shell hash ages for these cores yield substantial overestimates (≈ 2,000-8,000 years) of the date of sedimentation. Dating of individual shells (or other carbonates) is therefore required to estimate the time of deposition of the enclosing sediment more accurately.

The ESR results for Forster-Tuncurry shells indicate that the D_E-values based on the g=2.0014 signal are smaller than those based on the g=2.0006 signal (X-band, microwave power of 200 mW), with only two exceptions. The dating signal at g=2.0006 (X-band, 200 mW) is probably associated with a rapidly rotating CO_2^- centre (e.g. Barabas *et al.*, 1992a, 1992b). Therefore, D_E-values based on the g=2.0014 signal presumably do not correspond to the CO_2^- centre alone but may be related to other overlapping paramagnetic centres, such as the g=2.0032 and g=2.0020 signals. In spite of this, the AMS ^{14}C dates appear closer to the ESR ages based on the g=2.0014 signal than those based on the g=2.0006 signal. It is likely, however, that both sets of ESR ages are overestimates due to inconstant dose rates caused by reworking of the sediments. Even if sites were chosen where the dose rates had been constant, the question remains as to whether or not the g=2.0014 and g=2.0006 ESR signals are suitable for dating. For example, the ESR dates based on the g=2.0014 signal for Hoedjiespunt 1 at Elands Bay, South Africa, covered a very wide age range and included unexpectedly young ages. This raises doubt about the general validity of using the g=2.0014 signal for dating shells.

For coral samples from Huon Peninsula in Papua New Guinea, the ESR ages based on the g=2.0007 signal, using microwave powers of 5 mW and 200 mW, concur with alpha spectrometric and mass spectrometric uranium-series ages. The use of high or low microwave power has a negligible effect on the dose response and the D_E-values based on

the g=2.0007 signal in coral. This suggests that the g=2.0007 signal in coral should be a reliable signal for dating using either high or low microwave power. For three samples, however, there are substantial differences between the D_E-values obtained by Grün *et al.* (1992) and by this study, despite the fact that portions of the natural and irradiated samples used by Grün *et al.* (1992) were used in this study also. Although there is no direct evidence, these discrepancies may be explained by the presence of a thermally unstable component in the g=2.0007 signal of irradiated aliquots. The g=2.0007 signal may therefore require a preheating treatment after laboratory γ-irradiation.

For the four tooth enamel samples from Tham Khuyen Cave, Vietnam, the contribution of the internal dose rates to the total dose rates is substantial. The ESR ages are therefore obtained using both early and linear uranium-uptake models. The average ESR ages based on these models are 404 ± 51 ka and 534 ± 87 ka, respectively. The difference between these dates is considerable, but it is not possible to determine the most suitable model for correct age estimation without further detailed uranium analyses. The correct age of the Tham Khuyen specimen is most likely to lie between these two estimates and is probably in the range 475 ± 125 ka. This age appears to be supported by faunal studies and a U/Th age of 117 ka from a stratigraphically higher unit at a location near the ESR sampling site.

For quartz samples from Forster-Tuncurry and Allen's Cave, dating signals based on the Al and Ti centres are observed. In every instance, the ESR ages based on these signals are much older than the independent ages, estimated by ^{14}C, OSL and TL methods. Among the ESR estimates, Al signals exhibit much older ages than Ti signals, with one exception. At least at Allen's Cave, the samples are believed to have been well-bleached before burial. The results thus suggest that neither the Al nor Ti signals had been completely zeroed by sunlight exposure and, hence, that the Al and Ti signals in quartz may not be suitable for dating the time of last exposure to sunlight.

Given these preliminary findings on shell, coral, tooth enamel and quartz, several aspects of the ESR dating methods warranted further investigation. For shell, the appropriate form of the dose response function and annealing treatment was investigated for individual shell species (Chapters 9 and 10). Annealing procedures were also examined for corals (Chapter 13) and new light-sensitive ESR signals were sought in quartz sediments (Chapters 11 and 14). In each case, the objective was to make improvements to the reliability of ESR methods used to date terrestrial and marine deposits.

Part III

DEVELOPMENT OF NEW METHODS

Chapter 9 SELECTION OF DOSE RESPONSE FUNCTION FOR SHELL

In this chapter, the mathematical form of the dose response curve is investigated for shell, since this is crucial to the estimation of the accumulated dose by the usual extrapolation method, especially when the D_E is large. Also, to assess the importance of inflexion points as observed by Katzenberger and Willems (1988), a large number of data points were generated. If inflexion points appear in a dose response curve, the ESR method may not be suitable as a dating technique because the form of the extrapolated dose response curve may be unknown or incorrect. The aim of this chapter is to review the mathematical form of the dose response curve and its curve-fitting performance, using a computer. At the same time, observations are made of possible inflexion points in the dose response curve and their effect on D_E-values.

9.1 Materials and methods used

Three modern marine bivalve species — *Anadara trapezia*, *Donax deltoides* and *Katelesia scalarina* — and one modern marine univalve species — *Phalium sinuosum* — were used. The bivalve species are widely distributed around the coast of Australia and are commonly found in Quaternary marine sediments. One marine univalve species was used to check for possible differences in ESR behaviour with the bivalve species. The shells were initially steamed for 20 minutes, opened and washed with water. The dirt parts of the shell edge were removed with a file; this was particularly necessary for *Anadara trapezia*. Also, the outermost keratinous layers were removed using a high-speed engraving tool fitted with sandpaper discs. The shells were then crushed gently and sieved to obtain particles of 64-250 μm diameter. Finally, the separated particles were etched for 10 minutes in 10 % acetic acid, and then washed three times with distilled water. The remaining particles were allowed to dry at room temperature. Fifty aliquots, each weighing 200 mg, were prepared for the each species and serially irradiated with

gamma doses of up to 1350 Gy using a ^{60}Co γ-source at the Division of Plant Industry, CSIRO. ESR signals at g=2.0014 and g=2.0006 were recorded in the same manner as described in section 4.1.1 but using a microwave power of 60 mW for the g=2.0006 signal. The methods used to measure intensities are shown in Figure 4.1. Each intensity measurement was carried out in triplicate, with the sample re-packed into the ESR tube between measurements. For the D_E-value estimation, the 'DOSE' curve-fitting program (Brumby, 1992) was used and two types of fitting function, a single saturating exponential fit and a saturating-exponential-plus-linear fit, were performed. Each aliquot was weighted by the inverse square of its ESR signal intensity or equal weighting was given to all aliquots.

9.2 Results and discussion

The dose response curves for all four species of shell are shown in Figures 9.1, 9.2, 9.3 and 9.4, with curves fitted using a saturating exponential and a saturating-exponential-plus-linear function with each aliquot weighted equally. The data indicate that there are marked differences in the form of the dose response curves for different species of mollusc shell. However, it has not been determined if there are any differences between individual shells of the same species. For *Anadara trapezia*, very similar curves, with similar inflexion points, are observed for both the g=2.0014 and g=2.0006 signals (Figure 9.1). In contrast, the g=2.0006 signal in the other species shows a higher degree of curvature at lower doses and a greater degree of linearity at higher doses. Another finding is that *Phalium sinuosum*, the univalve species, exhibits a high degree of scatter (or inflexions) above 500 Gy dose for the g=2.0014 signal, but this pattern is not observed in the dose response curve for the g=2.0006 signal (Figure 9.4).

For all four species, the saturating-exponential-plus-linear function provides a better fit to the data points than the saturating exponential function. Similar results have been observed for corals (Grün *et al.*, 1992). The requirement of the additional linear function has been explained in terms of electron/hole trap production caused by irradiation (Levy,

1985), which is thought to be a linear process. My results indicate that the linearity is most apparent at larger doses, generally above 400 Gy. A saturating-exponential-plus-linear function may, therefore, only yield significantly different fits to a single saturating exponential function for doses larger than about 400 Gy.

The dose response inflexions observed in this study are small compared to those reported by Katzenberger and Willems (1988). To examine the possible effect of inflexion points on D_E-values, a censored data set of *Donax deltoides* was used to determine D_E-values. For this shell species, the dose response curve based on the g=2.0006 signal exhibits a higher degree of curvature at lower doses than does the g=2.0014 signal (Figure 9.2). To determine the goodness-of-fit of the two dose response functions, curve fitting was attempted with each aliquot weighted equally or by the inverse square of its ESR signal intensity.

Initially, D_E-values were determined for the full data set (i.e. data points from zero added dose to 1350 Gy). The curve-fitting procedure was repeated subsequently, each time removing the data points at the lowest end of the added dose range. The corresponding D_E-values for data point removal in 100 Gy increments are listed in Table 9.1. The D_E-values should be zero, since the shell analysed is modern mollusc. Neither of the curve-fitting functions, however, gives zero D_E-values using either of the signals. Based on the signals at g=2.0014 and g=2.0006, the saturating exponential fit with each aliquot weighted equally yields the largest D_E-values, $\approx$ 14 Gy and 24 Gy, respectively. The degree of overestimation is reduced, however, by weighting each aliquot by the inverse square of its signal intensity: the D_E-values then become $\approx$ 0.04 Gy and 0.15 Gy, respectively. The D_E-values obtained from the saturating-exponential-plus-linear fit, with each aliquot weighted by the inverse square of its intensity, are closest to zero. A weighting of unity for each aliquot does not affect the D_E-values obtained from the saturating-exponential-plus-linear fit to the same extent as for the saturating exponential fit, although a small increase in D_E-value is observed for both ESR signals.

As the minimum dose included in the curve-fitting routine is increased, the differences in the D_E-values become more significant. The results are shown in Figure 9.5. In this figure, the 'minimum dose' corresponds to the smallest dose in the data set used for the D_E-value determination. For example, for a minimum dose of 200 Gy, all data points from 200 Gy to 1350 Gy are used in the D_E-value estimation. An examination of this kind provides an assessment of the accuracy of extrapolating a dose response curve for much older samples. As the form of the dose response curve in such samples can only be described from the dose response region above the level of the 'natural' ESR signal, it is essential that the form of this curve is known *a priori* with some certainty to obtain an accurate D_E-value by extrapolation. The D_E-values obtained from the saturating exponential fit increase progressively for both weighting types for the g=2.0006 signal, and increase up to a minimum dose of 400 Gy for the g=2.0014 signal. In contrast, the D_E-values obtained from the saturating-exponential-plus-linear fit remain closer to zero for both signals. The degree of D_E-value overestimation is, in general, more significant for the dose response curve based on the g=2.0006 signal, which exhibits greater curvature in the low-dose region than the g=2.0014 signal. In the g=2.0006 dose response curve, linearity appears to start at a minimum dose of about 600 Gy. For the dose range above 600 Gy, both fitting functions and weighting types produce similar D_E-values.

9.3 Summary

For all four modern marine shell species examined, the dose response inflexions are very small compared to the results reported by Katzenberger and Willems (1988). For these samples, the saturating-exponential-plus-linear function gives a better fit to the data points than a saturating exponential fit. For both curve-fitting functions, the D_E-values obtained with each aliquot weighted by the inverse square of its signal intensity are closer to the correct D_E-value (in this case, zero) than are the D_E-values obtained using equal weighting. Since similar results are observed for dose response curves based on the signals at g=2.0014 (less curvature) and g=2.0006 (greater curvature), the most reliable fit appears to be obtained using the saturating-exponential-plus-linear function, with each

aliquot weighted by the inverse square of its signal intensity. However, the generality of this observation is not assured and may depend on the degree of curvature and the number of data points. In this study, therefore, both fitting functions, with each aliquot weighted by the inverse square of its signal intensity, were used for D_E-value determinations. The D_E-values deemed most reliable were selected on the basis of the goodness-of-fit of the dose response curves to the data points.

Table 9.1. Estimated D_E-values (Gy) based on the signals at g=2.0014 (microwave power of 2 mW) and g=2.0006 (60 mW) for a modern mollusc of the species *Donax deltoides*.

Dose range (Gy)	D_E-value (Gy) based on g=2.0014 signal				D_E-value (Gy) based on g=2.0006 signal			
	weight = 1		weight = SQR(int.)$^{-1}$		weight = 1		weight = SQR(int.)$^{-1}$	
	SE	SE+L	SE	SE+L	SE	SE+L	SE	SE+L
0 - 1350	13.9 ± 1.6	4.7 ± 1.0	0.037 ± 0.004	0.030 ± 0.003	24.1 ± 2.7	5.2 ± 0.8	0.15 ± 0.01	0.11 ± 0.01
100 - 1350	45.2 ± 3.8	18.3 ± 5.9	34.8 ± 2.0	23.8 ± 3.4	93.7 ± 5.1	27.5 ± 4.6	66.3 ± 3.2	25.5 ± 3.4
200 - 1350	61.4 ± 6.8	12.5 ± 14.2	44.6 ± 4.8	3.6 ± 9.9	139.6 ± 7.5	41.2 ± 12.2	117.5 ± 5.9	50.1 ± 10.6
300 - 1350	78.7 ± 10.4	16.4 ± 30.1	66.6 ± 8.4	12.8 ± 23.4	178.2 ± 11.4	36.9 ± 26.4	159.3 ± 10.4	56.4 ± 26.3
400 - 1350	117.8 ± 19.0	100.1*	122.7 ± 17.5	126.8*	228.6 ± 21.8	1.4×10^{-6}*	201.0 ± 22.2	1.1×10^{-7}*
500 - 1350	65.8 ± 27.6	1.9×10^{-5}*	49.8 ± 21.5	1.8×10^{-6}*	270.3 ± 36.0	161.4*	226.3 ± 37.0	1.7×10^{-4}*
600 - 1350	81.1 ± 44.8	2.5×10^{-6}*	55.2 ± 36.2	1.9×10^{-5}*	349.3 ± 34.6	336.9*	344.3 ± 32.4	340.8*

Notes: 1. Abbreviations: SE = saturating exponential fit; SE+L = saturating-exponential-plus-linear fit.
2. Each aliquot was weighted equally (1) or by the inverse square of its signal intensity (SQR(int.)$^{-1}$).
3. For D_E-values with an asterisk, the 'DOSE' program (Brumby, 1992) failed to estimate uncertainties.

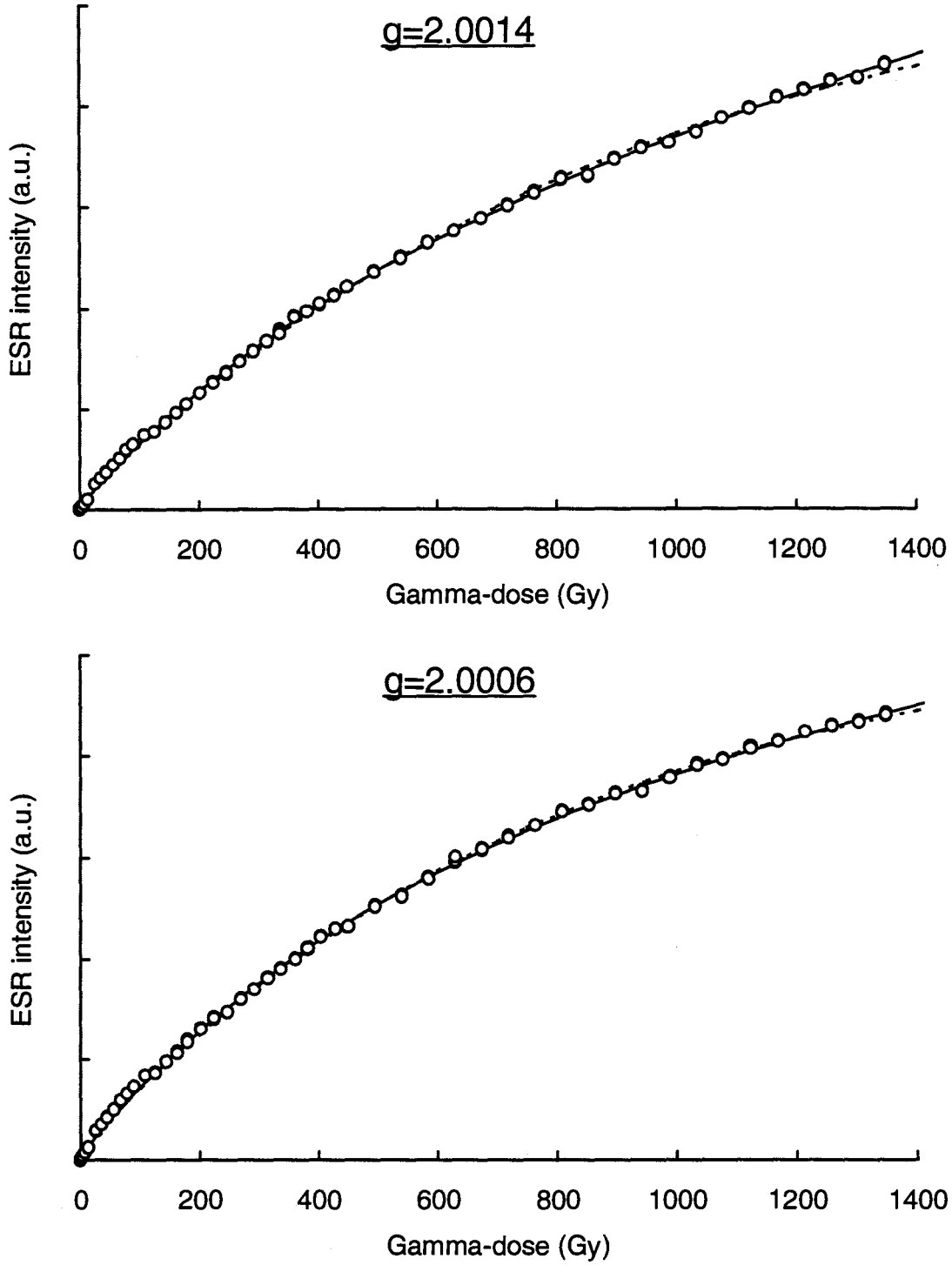

Figure 9.1. Dose response curves based on the signals at g=2.0014 (2 mW) and g=2.0006 (60 mW) for *Anadara trapezia*, a marine bivalve shell. Dashed and solid lines represent saturating exponential and saturating-exponential-plus-linear fits, respectively. For each γ dose, three measurements of ESR intensity were made and all are shown.

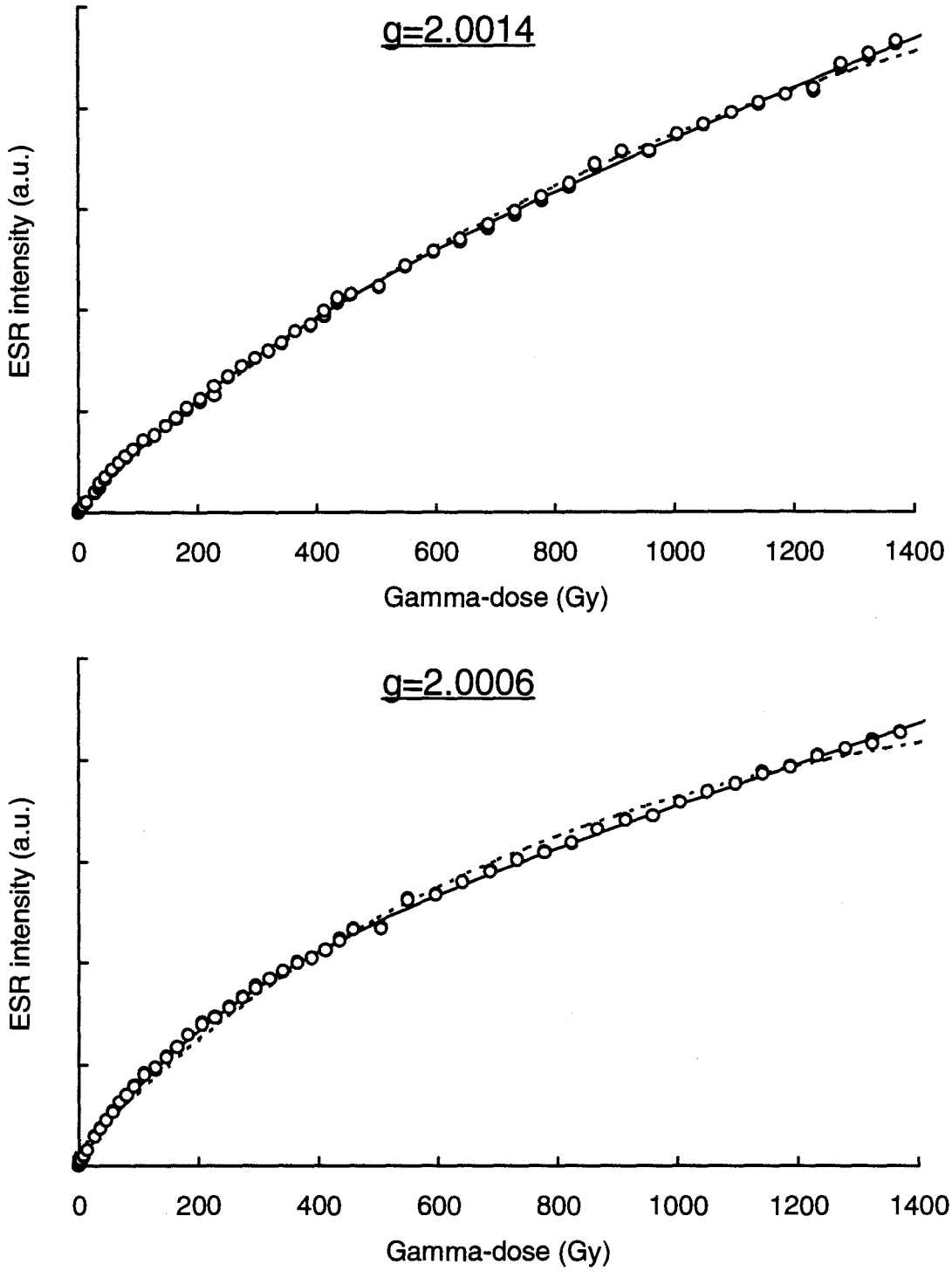

Figure 9.2. Dose response curves based on the signals at g=2.0014 (2 mW) and g=2.0006 (60 mW) for *Donax deltoides*, a marine bivalve shell. Dashed and solid lines represent saturating exponential and saturating-exponential-plus-linear fits, respectively. For each γ dose, three measurements of ESR intensity were made and all are shown.

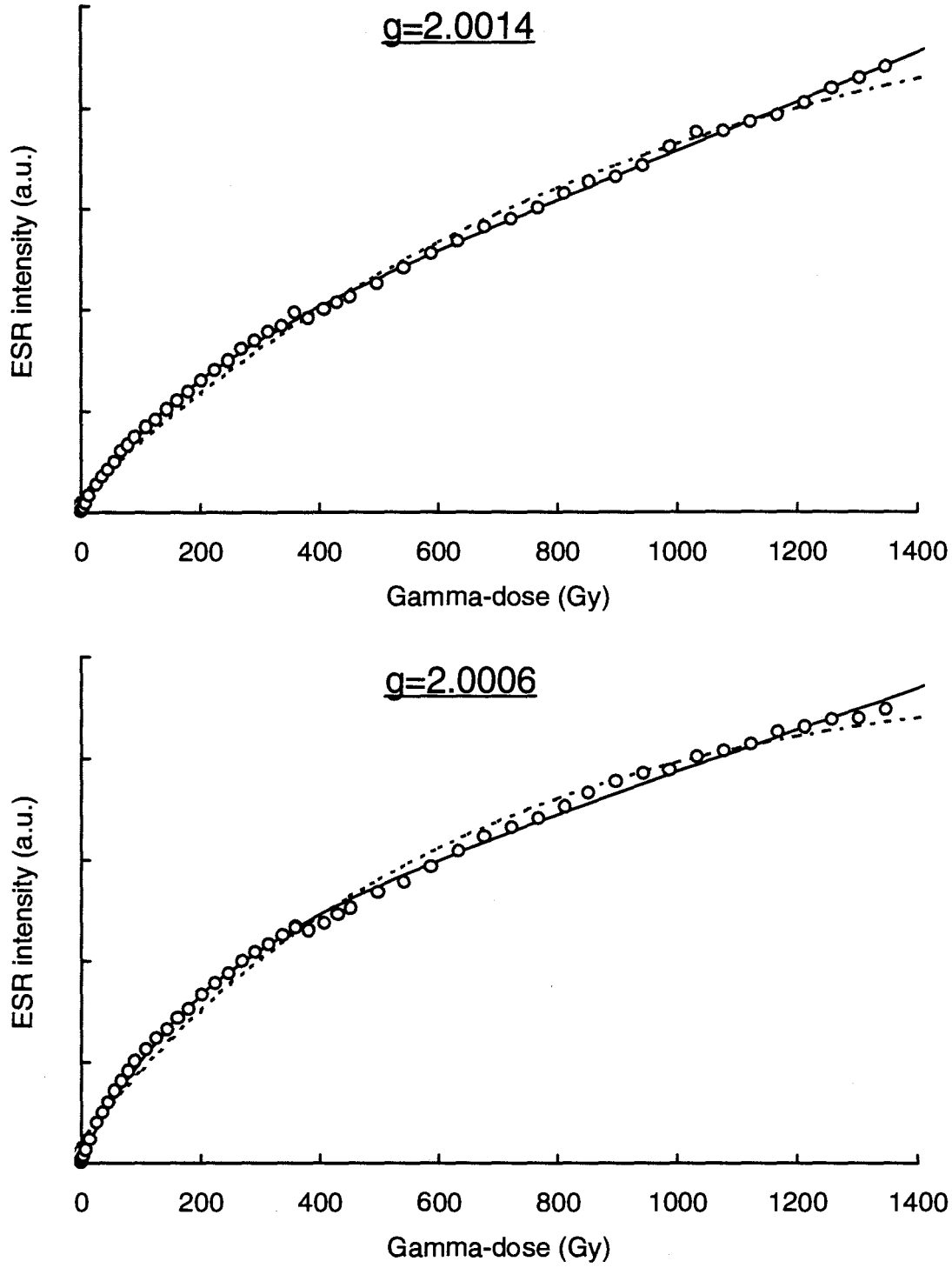

Figure 9.3. Dose response curves based on the signals at g=2.0014 (2 mW) and g=2.0006 (60 mW) for *Katelesia scalarina*, a marine bivalve shell. Dashed and solid lines represent saturating exponential and saturating-exponential-plus-linear fits, respectively. For each γ dose, three measurements of ESR intensity were made and all are shown.

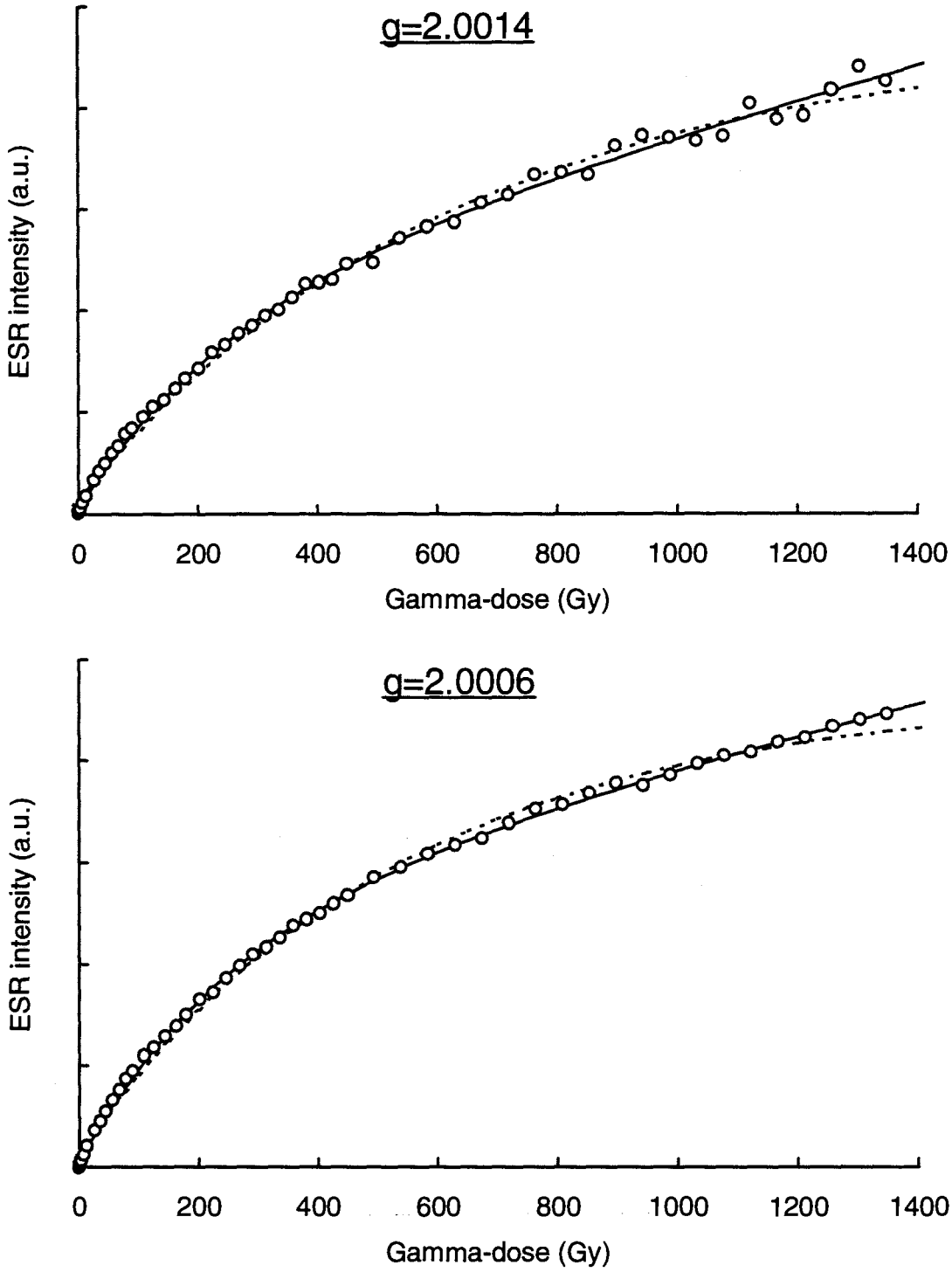

Figure 9.4. Dose response curves based on the signals at g=2.0014 (2 mW) and g=2.0006 (60 mW) for *Phalium sinuosum*, a marine univalve shell. Dashed and solid lines represent saturating exponential and saturating-exponential-plus-linear fits, respectively. For each γ dose, three measurements of ESR intensity were made and all are shown.

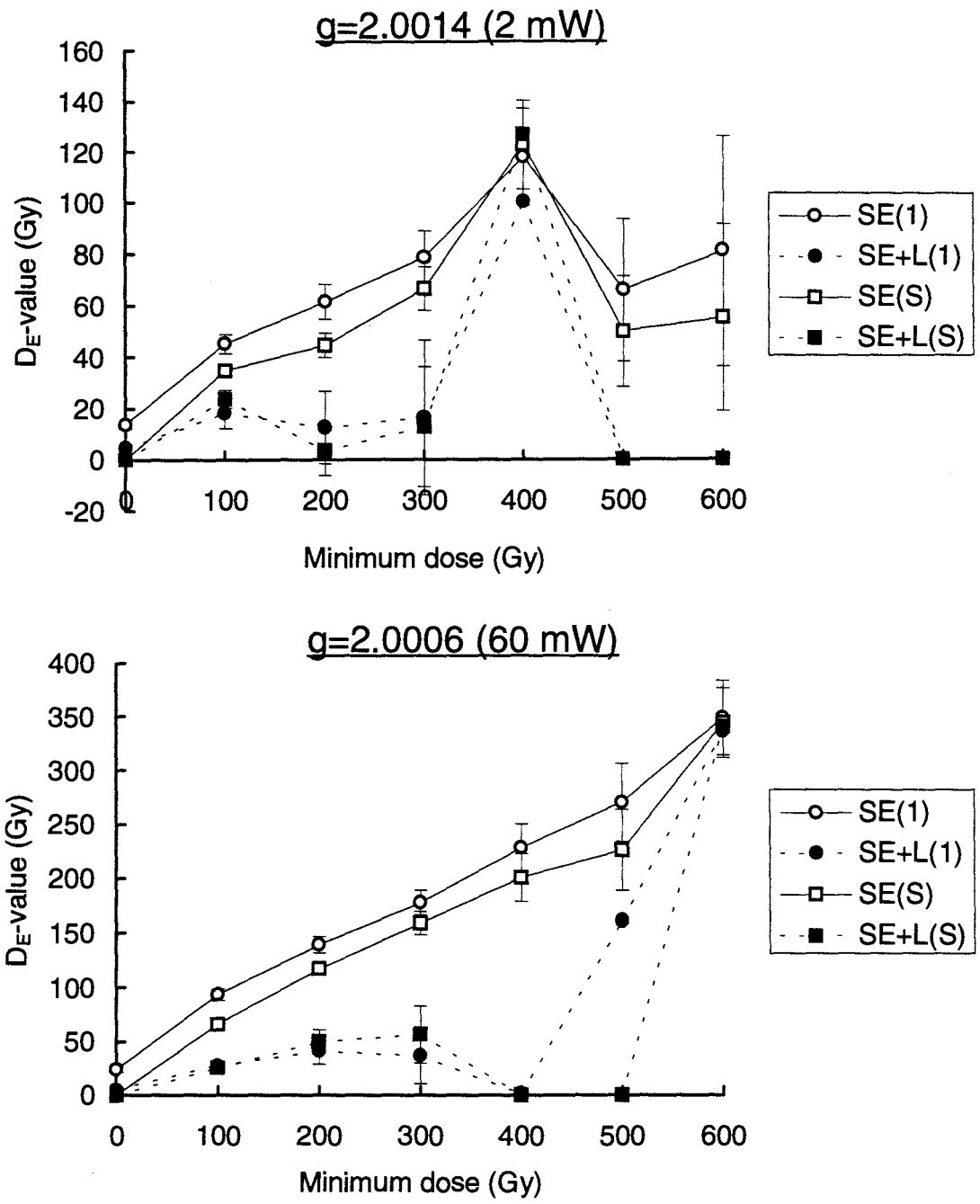

Figure 9.5: Estimated D_E-values ($\pm 1\sigma$ analytical errors), based on the signals at g=2.0014 (microwave power of 2 mW) and g=2.0006 (200 mW), as a function of minimum dose for a modern mollusc of the species *Donax deltoides*. The saturating exponential ('SE') and saturating-exponential-plus-linear ('SE+L') functions of the 'DOSE' program (Brumby, 1992) are used for curve fitting. Each aliquot was weighted equally ('1') or by the inverse square of its ESR signal intensity ('S').

Chapter 10 ANNEALING EXPERIMENTS ON SHELL

Annealing effects on ESR spectra in aragonite and calcite-containing shells were examined using X-band and Q-band spectrometers. For aragonite shells, the changes in signal amplitude at g=2.0058 (X-band and Q-band), g=2.0014 (X-band) and g=2.0006 (X-band: microwave power of 60 mW; Q-band) were monitored using a modern bivalve mollusc. The calcite-containing shells from Elands Bay, South Africa, exhibit markedly different spectra between the natural (unirradiated) and irradiated aliquots. To examine the effects on the spectra of possible thermally unstable components, samples were annealed using various time/temperature combinations and changes in the spectra were monitored.

10.1 Annealing effects on X-band spectra of aragonite shell

Changes in the signal amplitudes and dose response curves have been studied using the signals at g=2.0058, 2.0032, 2.0020 and 2.0014 before, during, and after annealing.

10.1.1 Methods used

To monitor changes in the signal intensities at g=2.0058, 2.0032, 2.0020 and 2.0014, twelve aliquots of a modern bivalve mollusc of species *Anadara trapezia* were prepared in the same manner as described in section 9.1, given 400 Gy of γ-irradiation, and then annealed for periods of up to 24 hours at 145°C in an oven (Lindberg, Model 51849). To examine the effects of annealing on the dose response curves for these signals, 25 aliquots were selected from the group of aliquots employed in Chapter 9, and these were used subsequently for the annealing experiments. The aliquots, given doses in the range 0-1350 Gy, were annealed at 150°C for 14 hours in an oven (Lindberg, Model 51849) prior to ESR measurements.

In a third set of experiments, the simultaneous annealing and γ-irradiation of a sample was planned to monitor changes in the signal amplitude at g=2.0058, 2.0032, 2.0020 and 2.0014. Since it was difficult to anneal and irradiate samples at the same time, an alternative method was employed. One aliquot was given an initial dose of 50 Gy and then annealed at 150°C for 2 hours. After recording the spectra, this dose/anneal/record procedure was repeated a further 11 times, resulting in the sample receiving a total dose of 600 Gy. This procedure is based on the assumption that the thermally unstable component(s) in the signals can be transferred to the stable defects by annealing at 150°C for 2 hours.

X-band spectra were recorded in the same manner as described in section 4.1.1, using microwave powers of 2 mW (g=2.0058, 2.0032, 2.0020 and 2.0014) and 60 mW (g=2.0006).

10.1.2 Results and discussion

Annealing effects on ESR signals

Typical changes in the signal intensities at g=2.0058, 2.0032, 2.0020, 2.0014 (microwave power of 2 mW) and g=2.0006 (microwave power of 60 mW) following annealing at 145°C are shown in Figures 10.1(a)-(c). The intensity of the signal at g=2.0020 decreased rapidly on heating, being almost unmeasurable after 8 hours. The signal intensities at g=2.0014 and 2.0032 decreased also, but the latter signal showed an initial small increase. Only the signal at g=2.0058 increased significantly and remained unchanged after 12 hours annealing. The growing intensity of this signal on heating has been reported previously (e.g. Yokoyama *et al.*, 1983) and suggests a high thermal stability of this signal. The signal at g=2.0032 appeared to strongly overlap other signals, which were not symmetrical against the baseline before annealing. After 24 hours annealing, the g=2.0032 signal became almost symmetrical against the baseline, indicating that the interfering signals may have been removed by annealing (see Figure 10.1(a)).

The signal at g=2.0006, measured using a microwave power of 60 mW, showed an initial small increase on heating at 140°C, 145°C and 150°C, followed by a steady decrease (see Figure 10.1(c)). This behaviour is qualitatively similar to that of the signal at g=2.0032, recorded at 2 mW microwave power. This suggests that either (a) the g=2.0032 signal is not completely saturated at high microwave power (60 mW) and still contributes significantly to the intensity of the g=2.0006 signal, or (b) none of the signal observed at 2 mW corresponds to the g=2.0006 signal. Further studies on these signals using a Q-band spectrometer are discussed in section 10.2.

Annealing effects on dose response curves

Dose response curves based on the signals at g=2.0058, 2.0032, 2.0020 and 2.0014, before and after annealing at 150°C for 14 hours, are shown in Figures 10.2(a) and 10.2(b). Before annealing, the signal intensities at g=2.0020 and g=2.0014 continue to increase up to a dose of 1350 Gy while the g=2.0032 signal appears to saturate at about 1000 Gy. After annealing, the dose response curve based on the g=2.0014 signal did not show significant changes in the curvature, whereas the signal intensities at g=2.0020 decreased significantly for all aliquots. The dose response curves based on the g=2.0058 and g=2.0032 signals indicate the early onset of saturation, at about 400 Gy dose. The mechanism by which the g=2.0058 signal of aragonite grows on heating has not been studied previously, but the similar dose saturation characteristics of the g=2.0058 and g=2.0032 signals implies a possible connection between these signals. Yokoyama *et al.* (1983, 1985a) assumed that a transfer of electrons from the g=2.0006 and g=2.0032 signals occurs in Palaeolithic calcite by heating but no physical model was given.

Growth mechanism and dating prospect of the g=2.0058 signal

Dose response curves based on the signals at g=2.0058, 2.0032, 2.0020 and 2.0014, using the aliquots annealed following 50 Gy of γ-irradiation (a procedure subsequently

repeated eleven times), are shown in Figure 10.3(a). This experiment is assumed to simulate the continuous transfer of the thermally unstable component(s) to the g=2.0058 signal during irradiation. The major difference between Figures 10.2(b) and 10.3(a) is that in Figure 10.3(a) the dose response curve based on the g=2.0032 signal declines after a dose of about 250 Gy. The dose response curves based on the signals at g=2.0032 and 2.0058 are similar to the concentration-time curves A_2 and A_3, respectively, reported by Szabó (1969) and shown in Figure 10.3(b). To explain the growth of the g=2.0058 signal, the following interpretation is introduced. Part of the intensity of the signal at g=2.0032 is due to SO_3^- defects (Barabas, 1992) and the signal at g=2.0058 is due to SO_2^- defects (Barabas, 1992; Miki *et al.*, 1993). The SO_3^- defects are thermally unstable and, when thermally activated, may transfer to SO_2^- sites, thereby giving rise to the intensity of the signal at g=2.0058. Further support for this theory is that the g=2.0058 signal observed in fossil shells does not usually grow by γ-irradiation, being described often as a radiation-insensitive signal (e.g. Radtke *et al.*, 1985). This suggests that the g=2.0058 signal is not formed directly by γ-irradiation at ambient temperatures, and that thermal activation is required for the formation of SO_2^- defects.

According to Katzenberger *et al.* (1989), a component of the anisotropic spectrum due to CO_2^- defects also occurs at about g=2.0032, but this signal may be too broad to contribute to the intensity due to SO_3^- defects. The signal observed at g=2.0032 is of narrow width and shows an initial rise in intensity during heating, which Katzenberger *et al.* (1989) suggested may be related to a CO_2^- enriched outer layer of the shell.

The hypothesis of g=2.0058 signal creation can be expressed as follows:

$$\text{A (diamagnetic)} \xrightarrow[\text{ionising radiation}]{k_1} \text{B } (SO_3^-;\ g=2.0032) \xrightarrow[\text{thermal activation}]{k_2} \text{C } (SO_2^-;\ g=2.0058)$$

Two processes create SO_2^- defects: ionising radiation (from A to B) and thermal activation (from B to C). The first transformation is first-order with respect to the concentration of A (with rate constant k_1) and the second transformation is first-order with respect to the concentration of B (with rate constant k_2). To apply this hypothesis, the ionising radiation (i.e. the natural dose rate) and the thermal activation (temperature) are required to be constant; equations for the growth of B and C with respect to time can then be obtained. The peak-to-peak signal amplitudes at g=2.0058 may correspond directly to the concentration of C, whereas the concentration of B cannot be determined in this way from the g=2.0032 signal because of the interfering signals. The concentration of B can, however, be represented by the increase in amplitude of the g=2.0058 signal after annealing (14 hours at 150°C). The rate of increase in intensity after annealing at 150°C for 14 hours (shown in Figure 10.2(b)) and the signal intensity at g=2.0058 after annealing at 150°C for 2 hours (shown in Figure 10.3(a)) are proportional to the concentrations of B and C, respectively. These data are fitted in Figure 10.4 with the curves based on equations (10.1) and (10.2) below, which correspond to equations (11) and (12), respectively, given by Szabó (1969):

$$\frac{[B]}{[A]_0} = \frac{1}{\kappa - 1}[\exp(-\tau) - \exp(-\kappa\tau)] \qquad (10.1)$$

$$\frac{[C]}{[A]_0} = 1 + \frac{1}{1-\kappa}[\kappa \exp(-\tau) - \exp(-\kappa\tau)] \qquad (10.2)$$

In these equations, dimensionless quantities of τ and κ are defined as $k_1 t$ and k_2/k_1, respectively, where t represents time. The data used in Figure 10.4 are in agreement between the experimental data and Szabó's theory, given the experimental errors.

If this hypothesis of g=2.0058 signal creation is correct, it could be applied to dating studies by determining both τ and κ. The ratios $[B]/[A]_0$ and $[C]/[A]_0$ can be estimated by measuring the amplitude of the g=2.0058 signal in the natural sample before and after annealing, and also in the annealed sample which has received a sufficiently large γ-dose

to reach saturation. Both τ and κ are, then, obtained by solving equations (10.1) and (10.2) simultaneously. For dating purposes, τ (equal to $k_1 t$) is equivalent to information which could be obtained from a dose response curve using the g=2.0058 intensity after annealing. The equation $\tau = D_E a$ can then be introduced from $k_1 = ad$, where a is the radiolytic yield and d is the annual dose, since the accumulated dose, D_E, is equal to dt. It is possible to determine D_E by solving equations (10.1) and (10.2) simultaneously. However, information from a dose response curve should be more satisfactory if the annual dose has varied during the period of sample burial.

From ESR spectra, the ratio of the increase in amplitude of the g=2.0058 signal on annealing (proportional to [B]) to the amplitude of this signal in the natural sample (proportional to [C]) can be obtained. To apply this ratio to the kinetic formulae, equation (10.3) is derived from the equations given by Szabó (1969):

$$\frac{[B]}{[C]} = \frac{k_1[\exp(-k_1 t) - \exp(-k_2 t)]}{k_2[1 - \exp(-k_1 t)] - k_1[1 - \exp(-k_2 t)]} \qquad (10.3)$$

The ratio ([B]/[C]) is expected to be large when the storage temperature is low and/or the annual dose is large, since [B] and [C] are proportional to the annual dose and the storage temperature, respectively. In this equation, if the values of the rate coefficients were known, or could be calibrated, the age of the sample (t) could be estimated. The value of k_1 could be estimated on the basis of the annual dose and the radiolytic yield. However, the temperature-dependent value, k_2, may be specific to particular species (Imai and Shimokawa, 1993), so equation (10.3) is unlikely to be generally suitable for determining the sample age (t). There are alternative ways of using equation (10.3) without encountering these problems. For example, the ratio [B]/[C] provides at least semi-quantitative information on the relation between age, annual dose and storage temperature.

The experimental data shown in Figure 10.4 do not provide any direct evidence that B is associated with the g=2.0032 signal. Nevertheless, this signal is most likely to be involved because: (a) the chemistry of the thermally activated process can then be rationalised (although the fate of the released oxygen atom is not clear); and (b) saturation of the dose response curves for both the unannealed g=2.0032 signal and the annealed g=2.0058 signal occur over a similar range of doses. For further studies, the signal intensities at g=2.0058 and g=2.0032 before and after annealing can be compared by double integrating the signals, to determine whether or not the decrease in intensity of the g=2.0032 signal is equal to the increase in intensity of the g=2.0058 signal. The g=2.0032 signal is, however, superimposed on other signals (e.g. CO_2^-), whose intensities may also change on annealing; the result may therefore not be reliable.

From the above considerations, the g=2.0058 signal can be used for D_E-value estimations provided the samples (including the natural aliquots) are subjected to suitable thermal treatment following γ-irradiation. Annealing experiments have been performed using different temperatures and a thermal treatment of 14 hours at 150°C seems to be appropriate. The dose response curve of the signal at g=2.0058 appears to saturate, however, at relatively low doses (e.g. 400 Gy). This may mean that the signal cannot be applied to very old samples, despite the signal having the benefit of excellent thermal stability.

10.2 Annealing effects on Q-band spectra of aragonite shell

Changes in amplitude of the Q-band ESR signals at g=2.0058, 2.0032 and 2.0006 in aragonite shell were monitored during isothermal annealing at 91-130°C. The kinetics of the decay of the g=2.0032 signal and the growth of the g=2.0058 signal were compared to examine the hypothesis discussed in the preceding section.

10.2.1 Methods used

Modern marine mollusc shell of the species *Katelesia scalarina* was used for these experiments (see also section 9.1). Twenty-five aliquots, each weighing 200 mg, were irradiated with gamma doses of 1327 Gy, using a ^{60}Co γ-source at the Division of Plant Industry, CSIRO, and were then gently preheated at 100°C for 10 minutes in an oven. All aliquots were stored at around -5°C when not in use. For annealing experiments, temperatures of 91, 101, 110, 120 and 130°C were selected, and the aliquots, contained in a 3 mm outside-diameter ESR tube, were plunged into a thermostatically-regulated silicone oil bath for selected periods of time.

Q-band (≈ 35 GHz) spectra were recorded using a Varian 4502 EPR spectrometer at room temperature (≈ 21°C), with a modulation frequency of 100 kHz, a microwave power of 0.6 mW, a modulation amplitude of 0.2 Gpp, a scan range of 100 G, a scan speed of 28 G min^{-1} with a time constant of 1 s.

10.2.2 Results and discussion

Examples of Q-band spectra and changes in the intensities at g=2.0058, 2.0032, 2.0020 and 2.0006 after annealing at 130°C are shown in Figures 10.5 and 10.6, respectively. The Q-band spectra exhibit essentially the same features as reported by Barabas *et al.* (1992a), namely that the signals at g=2.0058, 2.0032, 2.0020 and 2.0006 appear to be isolated from each other. To explain the kinetics of each signal, the experimental data were fitted using various types of equation.

g=2.0058 and g=2.0032 signals

After gentle annealing at 100°C for 10 minutes, the g=2.0058 signal exhibits a rather complicated spectrum, as shown in Figure 10.5. Approximately three signals were

observed at about g=2.0060 which were not detectable by X-band. After stronger annealing, i.e. 22 minutes at 130°C, these signals disappeared and only the g=2.0058 signal remained. The amplitude of the g=2.0058 signal increased with annealing time and the data can be fitted by the first-order equation, $y = b - a \exp(-kt)$.

As discussed in section 10.1.2, the g=2.0032 signal (due to SO_3^- centres) may give rise to the g=2.0058 signal (due to SO_2^- centres). I therefore attempted to fit the g=2.0032 signal decay curve by the sum of two first-order decay equations. In this composite equation, the first-order constant for growth of the g=2.0058 signal was used for one of the two first-order decay constants, while the other decay constant was allowed to vary freely. For all annealing temperatures attempted, the experimental data and fitted equations are in close accord (examples are shown in Figure 10.6). The results consistently support the mechanism for growth of the g=2.0058 signal hypothesised in section 10.1.2. Nevertheless, it should be noted that there are other combinations of parameters which also allow an equally good fit to the data.

Using X-band, an initial increase was observed for the g=2.0032 signal (see Figure 10.1(b)), but this characteristic was not noticed at any temperature using Q-band. This suggests that the g=2.0032 signal in the X-band is interfered with by other signal(s). Since a neighbouring signal at g=2.0020 decreases significantly upon thermal heating (Figures 10.1(b) and 10.6), this could be the main signal which affects the g=2.0032 signal. That is, if the g=2.0020 signal contributes substantially to the amplitude of the signal at g=2.0032, then as the intensity of the g=2.0020 signal decreases with annealing, an apparent increase in the g=2.0032 signal may occur.

g=2.0020 signal

Unlike the signals at g=2.0058, 2.0032 and 2.0006, the g=2.0020 signal in the Q-band was not completely symmetrical and appears to be influenced by the g=2.0006 signal. The thermal decay of this signal, due to an unknown centre, was investigated by fitting first-

order, second-order and third-order kinetic equations, and a logarithmic equation. The best agreement was obtained with the logarithmic equation ($y = b - a \ln(t)$), the rate of decay being inversely proportional to time and the signal due to a single species. This differs from the analysis reported by Grün (1985b), who, using a different sample, suggested that the decay of the g=2.0020 signal in the X-band was first-order but appeared to be second-order because of interfering signals.

g=2.0006 signal

The signal at g=2.0006, due to freely rotating CO_2^- centres, could not be measured in the X-band because of interfering neighbouring signals (e.g. g=2.0032 and g=2.0020 signals). With Q-band, the g=2.0006 signal appears to be isolated from the other signals and is almost symmetrical about the baseline (see Figure 10.5). For each temperature examined, the signal intensity initially increased then decreased with annealing time. The changes in the signal amplitude were satisfactorily fitted to the sum of a first-order growth equation and a first-order decay equation (examples are shown in Figure 10.6). This finding suggests that the g=2.0006 signal includes thermally unstable components and that the use of Q-band does not allow a thermally stable component of the signal to be isolated. It has been reported that the g=2.0006 signal is associated with water molecules (Debuyst *et al.*, 1993) and that thermal annealing of the signal may be linked to the loss of water molecules (Miki and Kai, 1991; Murata *et al.*, 1993). This theory, however, does not explain the growth of the g=2.0006 signal.

With X-band, an initial increase in intensity was observed at g=2.0006 using a microwave power of 60 mW (see Figure 10.1(c)). Barabas *et al.* (1992b) proposed the use of high microwave power to enhance the g=2.0006 signal relative to interfering signals. The Q-band results, showing an initial increase in the g=2.0006 signal, may support Barabas *et al.*'s suggestion but there is no evidence that the use of high microwave power completely eliminates the effect of interfering signals.

10.3 Annealing effects on X-band spectra of calcite-containing shell

10.3.1 Methods used

The aliquots from Elands Bay, South Africa, discussed in Chapter 4 were used subsequently for the analyses described here. All aliquots were annealed for 15 hours at 150°C in an oven (Lindberg, Model 51849) to remove thermally unstable components and give rise to the g=2.0058 signal. The X-band ESR spectra were measured before and after annealing in the same manner as described in section 5.1, but using a microwave power of 2 mW.

10.3.2 Results and discussion

The 'natural' (unirradiated) aliquots of calcite-containing shell exhibit ESR signals at g=2.0058, g=2.0032, g=2.0020, g=2.0006 and g=1.9973; examples are shown in Figure 10.7. After preheating at 150°C for 15 hours, the signal intensities at g=2.0058 in the natural aliquots increased, whereas those at g=2.0032 and g=2.0020 decreased. For sample E14, the signal intensity at g=2.0006 in the natural aliquot appears to be increased by annealing. This may be due to a reduction of the superimposing effect of the g=2.0020 signal on the g=2.0006 signal following annealing. For the other samples examined, signal intensities at g=2.0006 in the natural aliquots decreased only slightly after annealing. The latter result suggests that the g=2.0058 and g=2.0006 signals in the natural aliquots have high thermal stability.

After γ-irradiation, the ESR spectra exhibited more complex signals. The signal at g=2.0006 was overlapped by signals at g=2.0027 and g=2.0020 (see Figure 10.8), thereby preventing the use of the unannealed g=2.0006 signal for D_E-value evaluation. These spectra, however, become closely comparable to those of the natural aliquots

following 15 hours annealing at 150°C. The g=2.0032 and g=2.0020 signals become almost unrecognisable and the g=2.0006 signal appears to be isolated. Since the g=2.0006 signal probably has a high thermal stability, it could be used for dating calcite-containing shells.

10.4 Conclusions

10.4.1 Aragonite shell

The signal at g=2.0058 (X-band and Q-band) was not enhanced by γ-irradiation unless annealed. The amplitude of the signal increased substantially during annealing and appeared to reach a stable level. After annealing at 150°C for 14 hours, the dose response curve reached saturation at a lower dose than before annealing, a result which is also found for the g=2.0032 signal. By applying equations from Szabó (1969) and considering the chemical characteristics of those signals, the mechanism of growth of the g=2.0058 signal could be explained as the result of thermal activation of the g=2.0032 signal. Annealing experiments at various temperatures suggest that the g=2.0058 signal has a high thermal stability and can be used for D_E-value estimation following suitable thermal treatment (such as 150°C for 14 hours).

The amplitude of the g=2.0020 signal (X-band and Q-band) decreased significantly on heating. The thermal decay of this signal was fitted best by a logarithmic equation ($y = b - a \ln(t)$), indicating that the signal is due to a single species.

The signal at g=2.0006 appears to be isolated from other signals using Q-band. The amplitude of the g=2.0006 signal with X-band (microwave power of 60 mW) and Q-band exhibited an initial increase on heating, followed by a decrease. These changes could be fitted by the sum of first-order growth and first-order decay expressions, implying that the signals at g=2.0006 in the X-band (microwave power of 60 mW) and Q-band include

thermally unstable components. The g=2.0006 signal may therefore not be suitable for dating without appropriate thermal treatment.

10.4.2 Calcite-containing shell

After annealing at 150°C for 15 hours, the signal intensities at g=2.0058 increased in the natural and irradiated aliquots, as observed also for the aragonite shell samples. The signal at g=2.0006 (X-band) in the natural aliquot changed little on heating, indicating a high thermal stability. In the irradiated aliquots, the g=2.0006 signal was strongly overlapped by signals at g=2.0020 and g=2.0032. The latter signals were removed by annealing for 15 hours at 150°C. As with aragonite shell, the signals at g=2.0058 and g=2.0006 could be used for D_E-value estimation following suitable preheating treatment (such as 150°C for 15 hours).

10.5 Summary

For both aragonite and calcite-containing shells, an increase in amplitude of the g=2.0058 signal was observed on heating. The growth mechanism of this signal can be explained as the result of the g=2.0032 signal (due to SO_3^- defects) being thermally activated and transformed to give rise to the g=2.0058 signal (due to SO_2^- defects). This theory is based on equations given by Szabó (1969) and the data obtained in the X-band and Q-band, both sets of experimental data being consistent with this hypothesis. Because of its high thermal stability, the g=2.0058 signal can be used for dating bio-carbonate materials, provided a suitable heating treatment is administered after γ-irradiation. A preheating treatment of about 150°C for 15 hours seems to be appropriate. The construction of dose response curves based on this signal indicates that it may be difficult to determine D_E-values greater than $\approx$ 200 Gy because of saturation effects; onset of the latter, however, may vary between samples.

The signal at g=2.0006 in carbonates, attributed to freely rotating CO_2^- centres (e.g. Barabas *et al.*, 1992a), has often been described as the 'dating' signal. However, this signal usually cannot be observed in aragonitic carbonates in the X-band because of interfering signals. With Q-band, the g=2.0006 signal appears to be isolated from other signals and exhibits an almost symmetrical spectrum about the baseline. The signal intensity at g=2.0006 shows an initial increase on heating, which suggests that it contains thermally unstable components.

The annealing behaviour of the g=2.0006 signal using X-band and a high microwave power (60 mW) was comparable to that observed with Q-band: the amplitude of the signal increased and then decreased. This appears to agree with a theory proposed by Barabas *et al.* (1992b) that the intensity of the g=2.0006 signal (X-band) is comparable to that of the g=2.0006 signal (Q-band). These signals, however, cannot be used for dating without suitable preheating treatments because of thermally unstable components in the signals.

For calcite-containing shells, the signal intensity at g=2.0006 (X-band) did not show significant changes on heating at 150°C for 15 hours, thus indicating its high thermal stability. The irradiated aliquots exhibited more complex spectra than the natural aliquots at about g=2.0006, and the g=2.0006 signal could not be measured satisfactorily because of interfering signal(s). These overlapping signals seem to be removed by annealing at 150°C for 15 hours, after which the spectra appear similar to those of the natural aliquots. This result suggests that the signal at g=2.0006 (X-band) in calcite-containing shells can be used for dating if γ-irradiated aliquots are given a thermal treatment of 150°C for 15 hours.

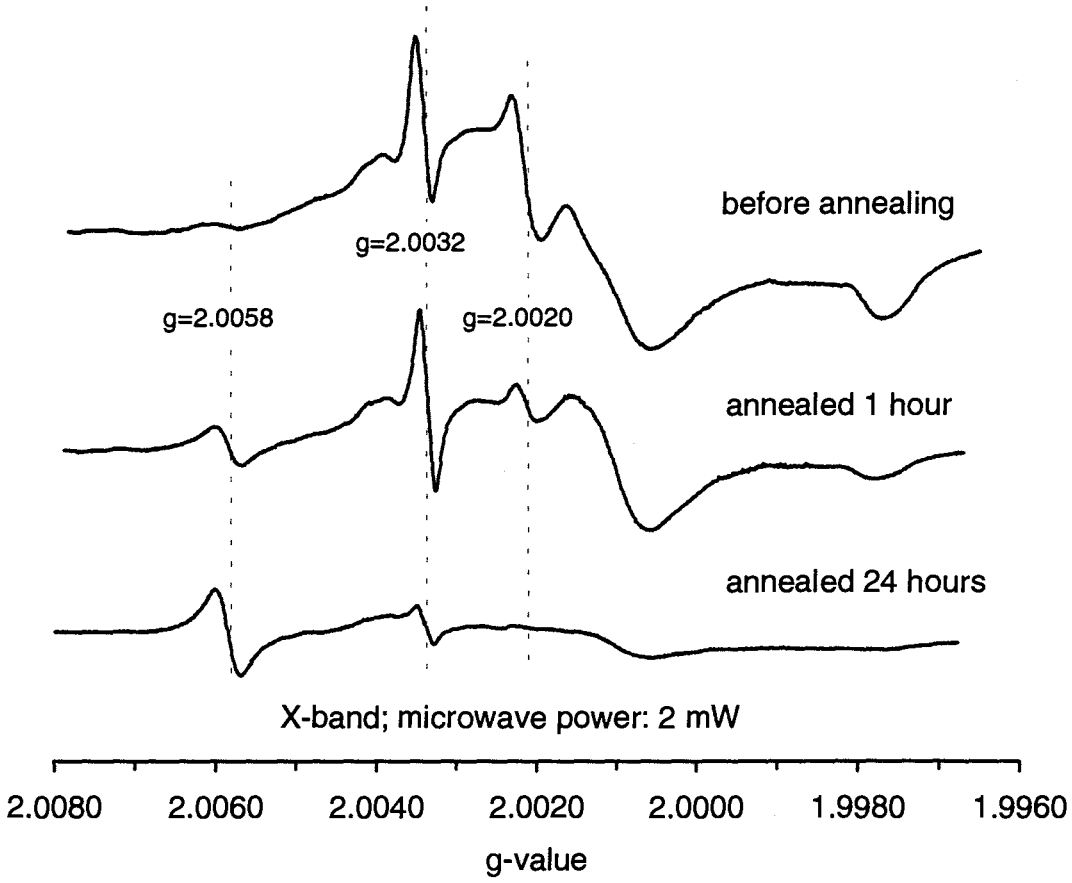

Figure 10.1(a). Changes in ESR spectra of marine bivalve mollusc *Anadara trapezia* as a result of annealing. The sample was given a γ-dose of 400 Gy then annealed at 145°C for the duration indicated.

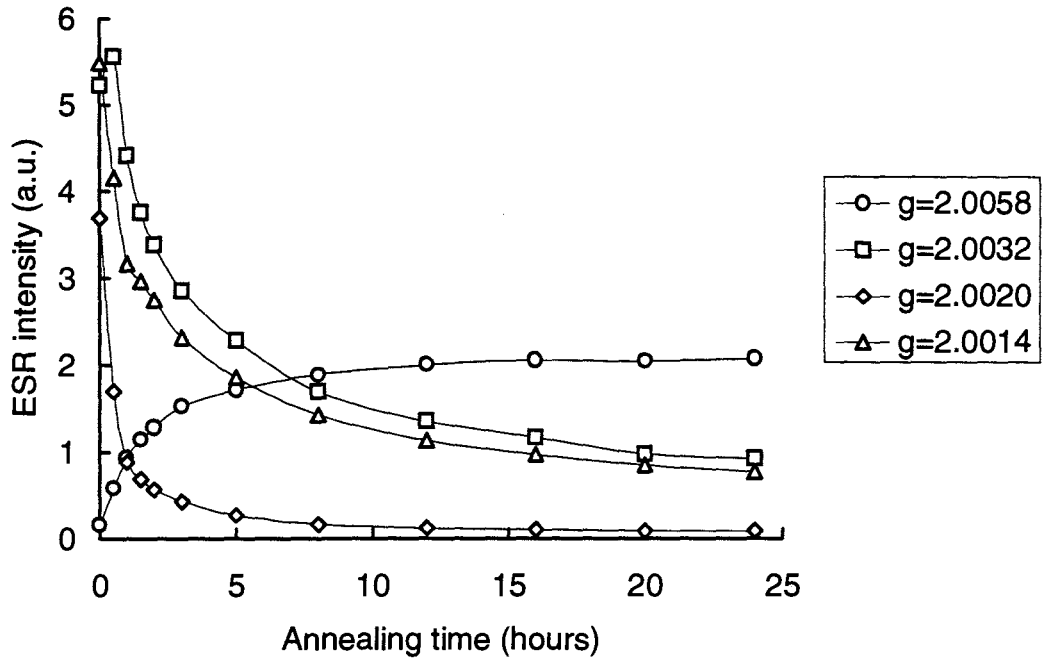

Figure 10.1(b). Build-up and decay of ESR intensities in *Anadara trapezia*, following a γ-dose of 400 Gy and annealing at 145°C. ESR spectra were recorded using a microwave power of 2 mW.

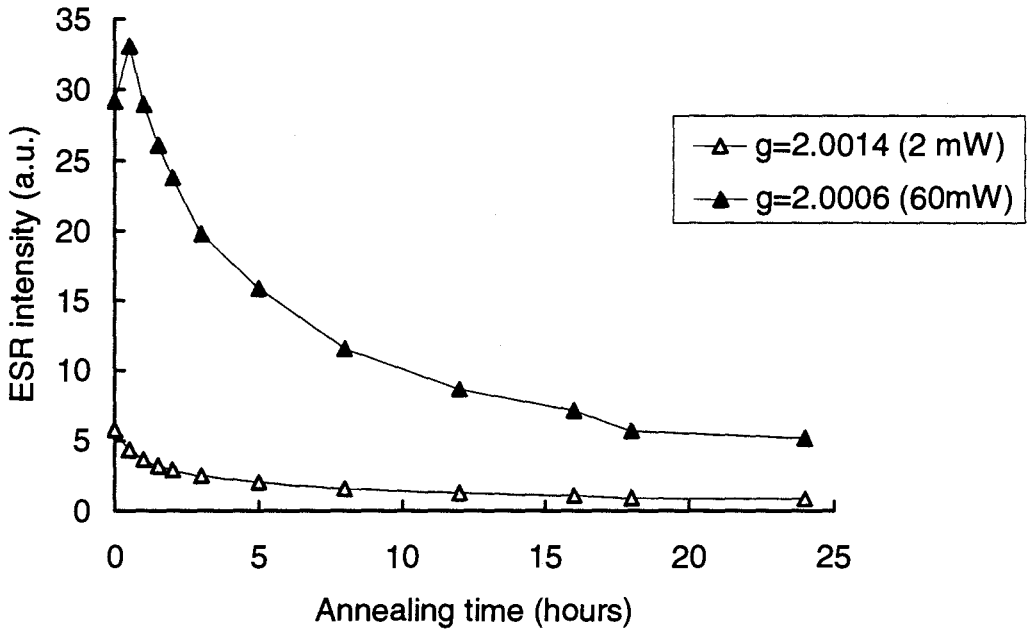

Figure 10.1(c). Build-up and decay of ESR intensities at g=2.0014 (microwave power of 2 mW) and g=2.0006 (microwave power of 60 mW) in *Anadara trapezia*, following 400 Gy of γ-irradiation and annealing at 145°C.

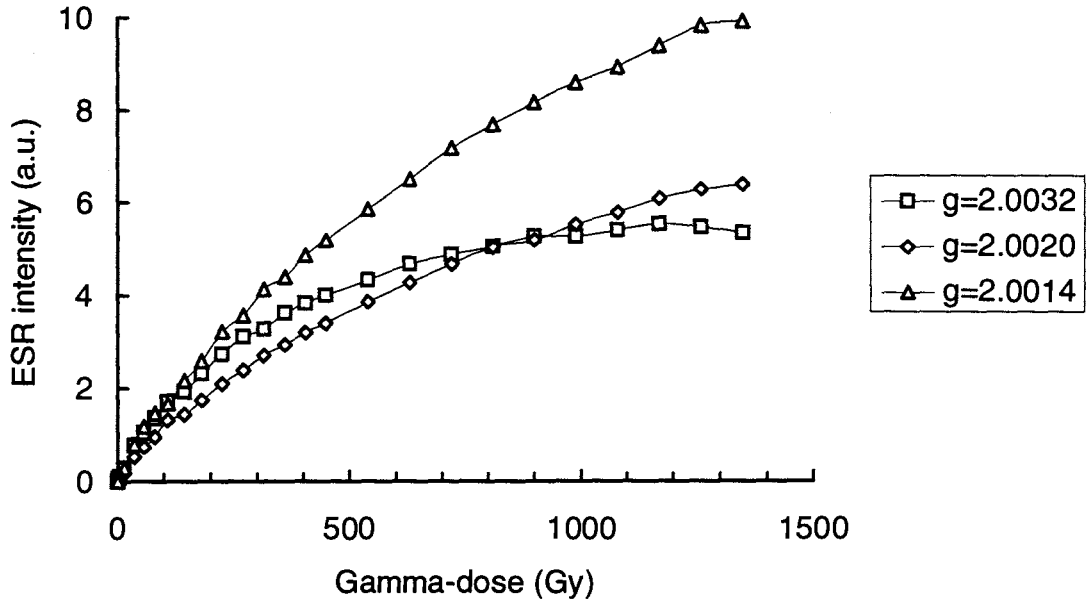

Figure 10.2(a). Dose response curves based on the signals at g=2.0032, 2.0020 and 2.0014 in *Anadara trapezia* before annealing. A microwave power of 2 mW was used.

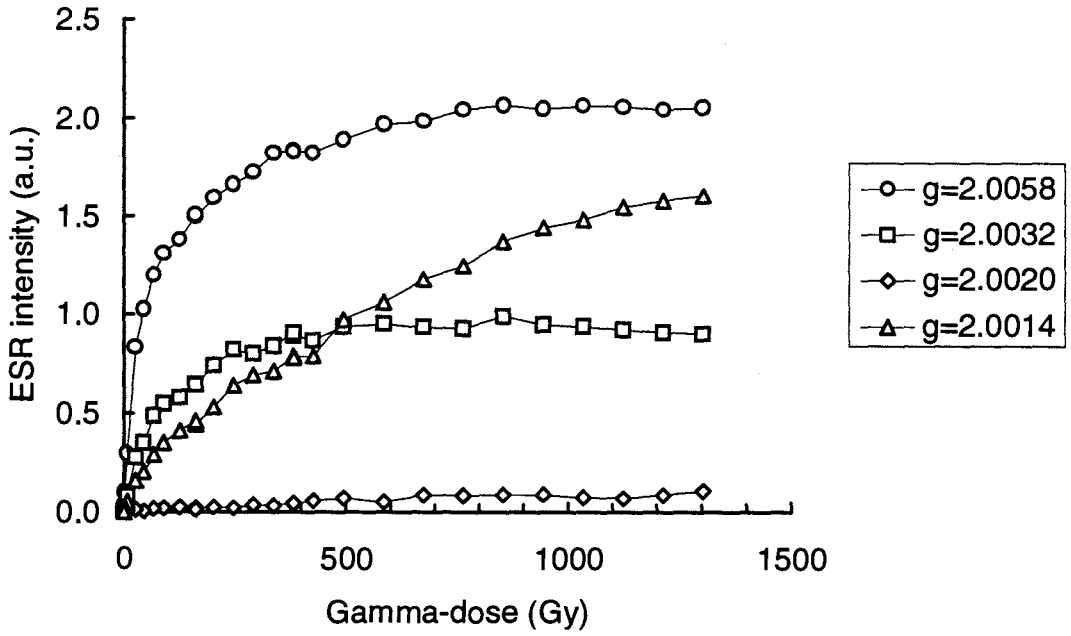

Figure 10.2(b). Dose response curves based on the signals at g=2.0058, 2.0032, 2.0020 and 2.0014 in *Anadara trapezia* after annealing at 150°C for 14 hours. ESR spectra were recorded using a microwave power of 2 mW.

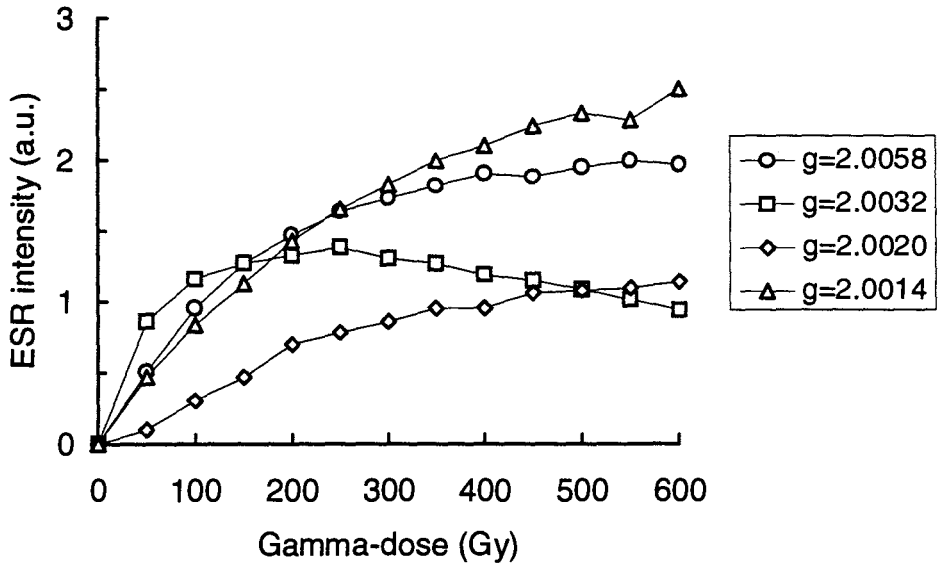

Figure 10.3(a). Dose response curves based on the signals at g=2.0058, 2.0032, 2.0020 and 2.0014 in *Anadara trapezia*. The samples were given a dose of 50 Gy then annealed at 150°C for 2 hours followed by ESR measurements. This procedure was repeated a further 11 times resulting in the sample receiving a total dose of 600 Gy.

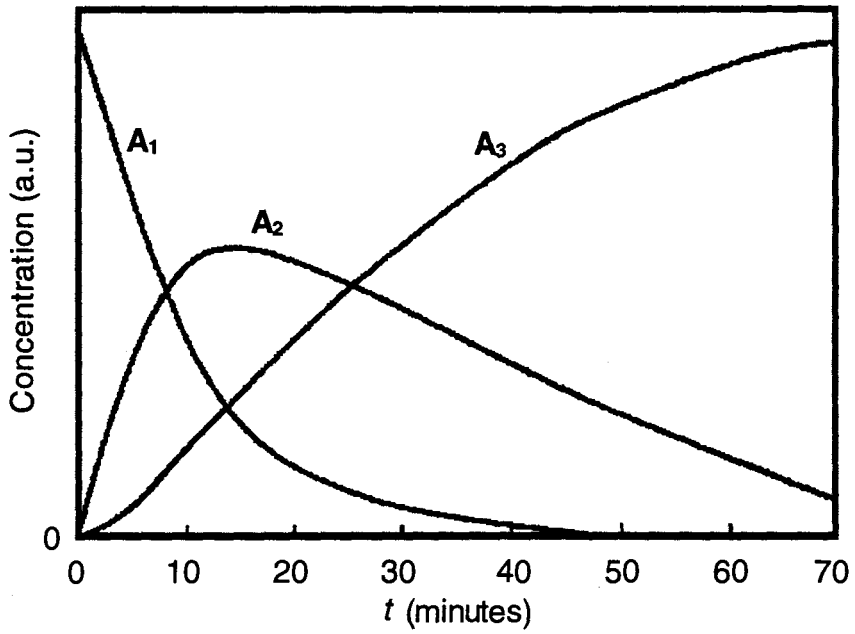

Figure 10.3(b). Concentration-time curves for substances A_1, A_2 and A_3 using equations (10), (11) and (12), respectively, given by Szabó (1969). A_2 and A_3 appear to correspond to the signal intensities at g=2.0032 (SO_3^- centres) and g=2.0058 (SO_2^- centres), respectively, in *Anadara trapezia*.

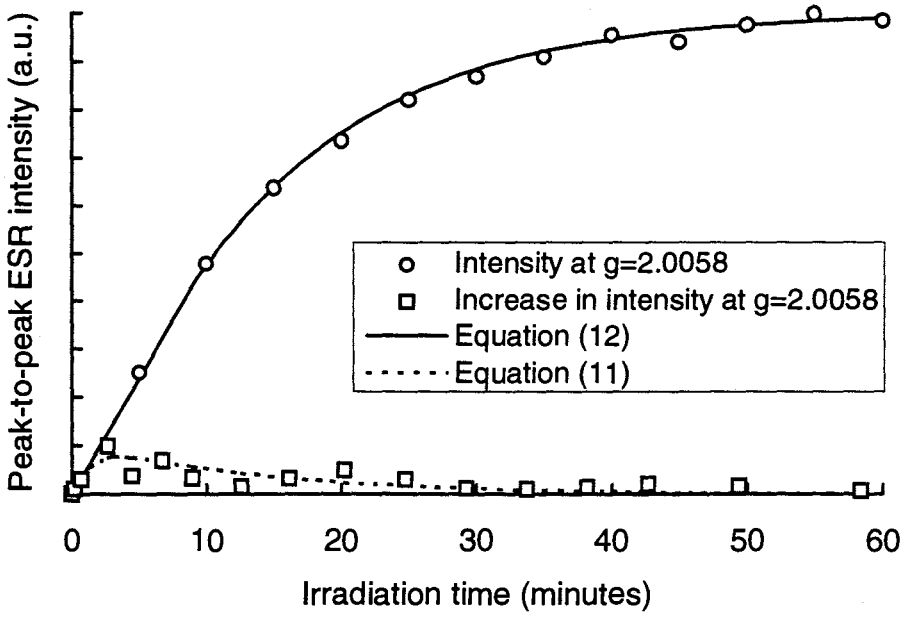

Figure 10.4. Simulation experiments of concentration-time curves for the intensity of the g=2.0058 signal (circles) after consecutive annealing increments of 150°C for 2 hours, and the increase in intensity of the g=2.0058 signal (squares) after annealing at 150°C for one period of 14 hours, versus irradiation time for *Anadara trapezia* shell. The dashed and solid curves were calculated using equations (11) and (12) of Szabó (1969), respectively.

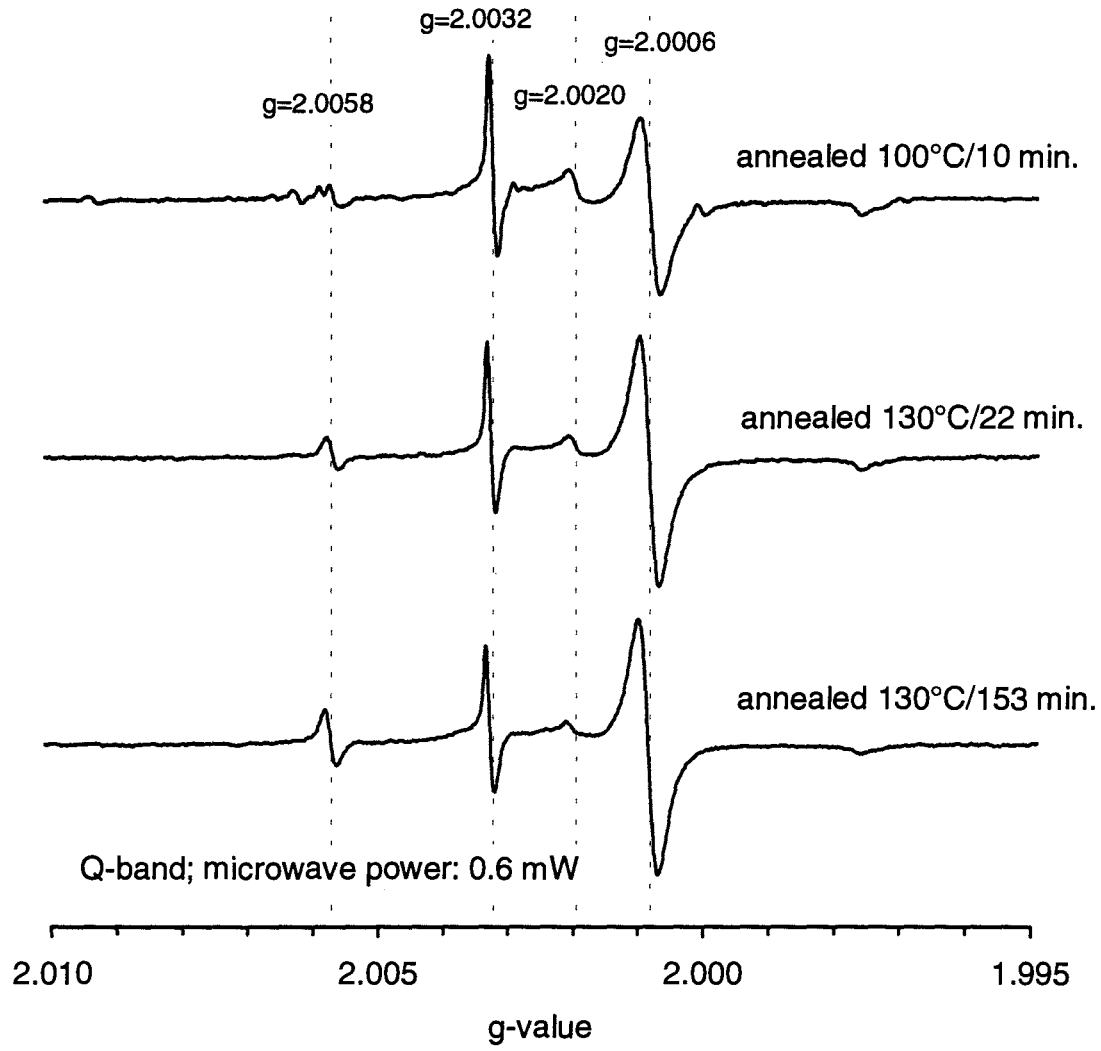

Figure 10.5. Q-band ESR spectra for a sample of modern *Katelesia scalarina* shell after 1327 Gy of γ-irradiation. The sample was initially gently annealed at 100°C for 10 minutes (top), then annealed at 130°C for 22 minutes (middle) and 130°C for 153 minutes (bottom).

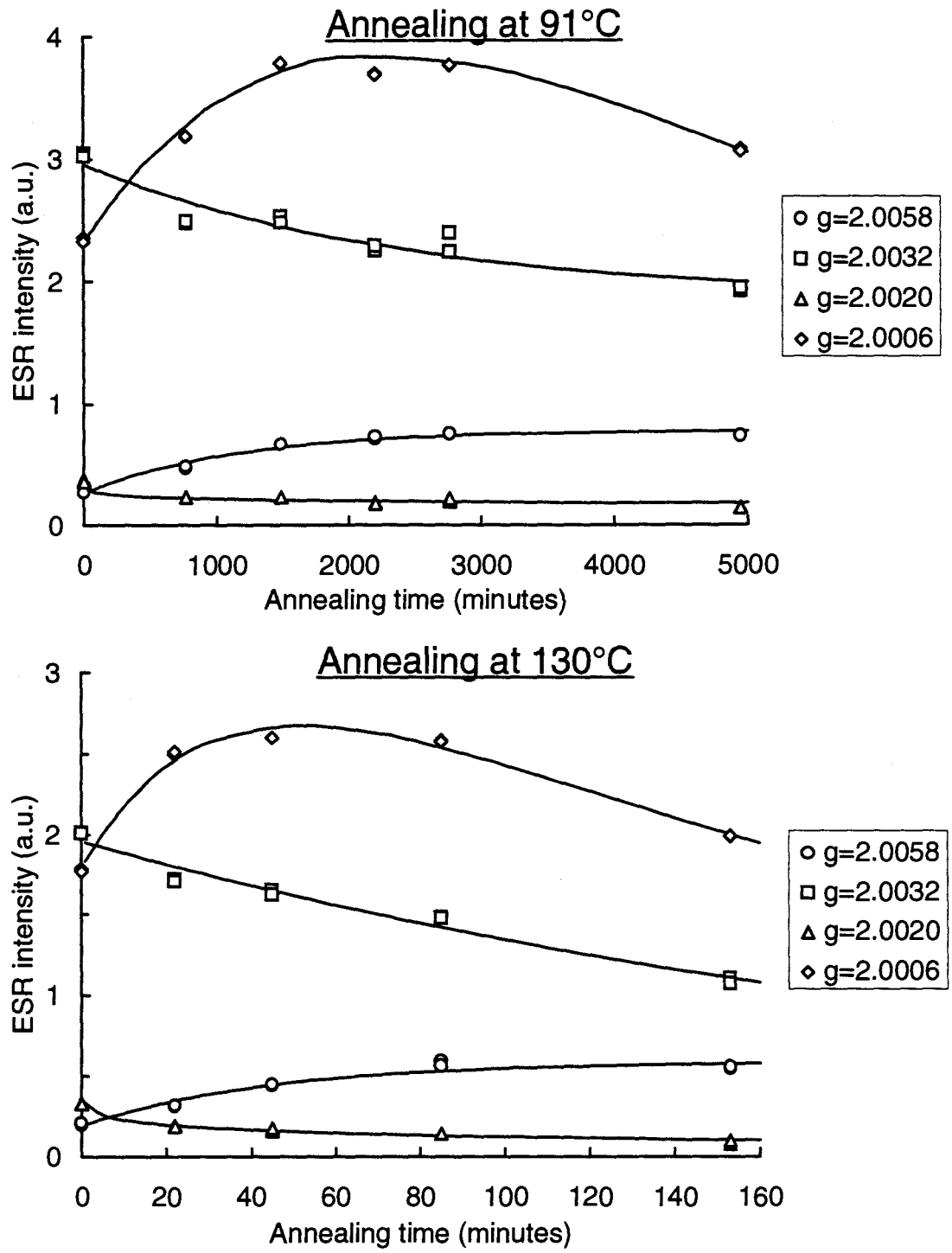

Figure 10.6. Changes in the Q-band intensities at g=2.0058, 2.0032, 2.0020 and 2.0006 after annealing at 91°C and 130°C following 1327 Gy of γ-irradiation. The continuous curves correspond to equations for first-order growth (g=2.0058), the sum of two first-order decays (g=2.0032), logarithmic decay (g=2.0020) and the sum of a first-order growth and a first-order decay equation (g=2.0006).

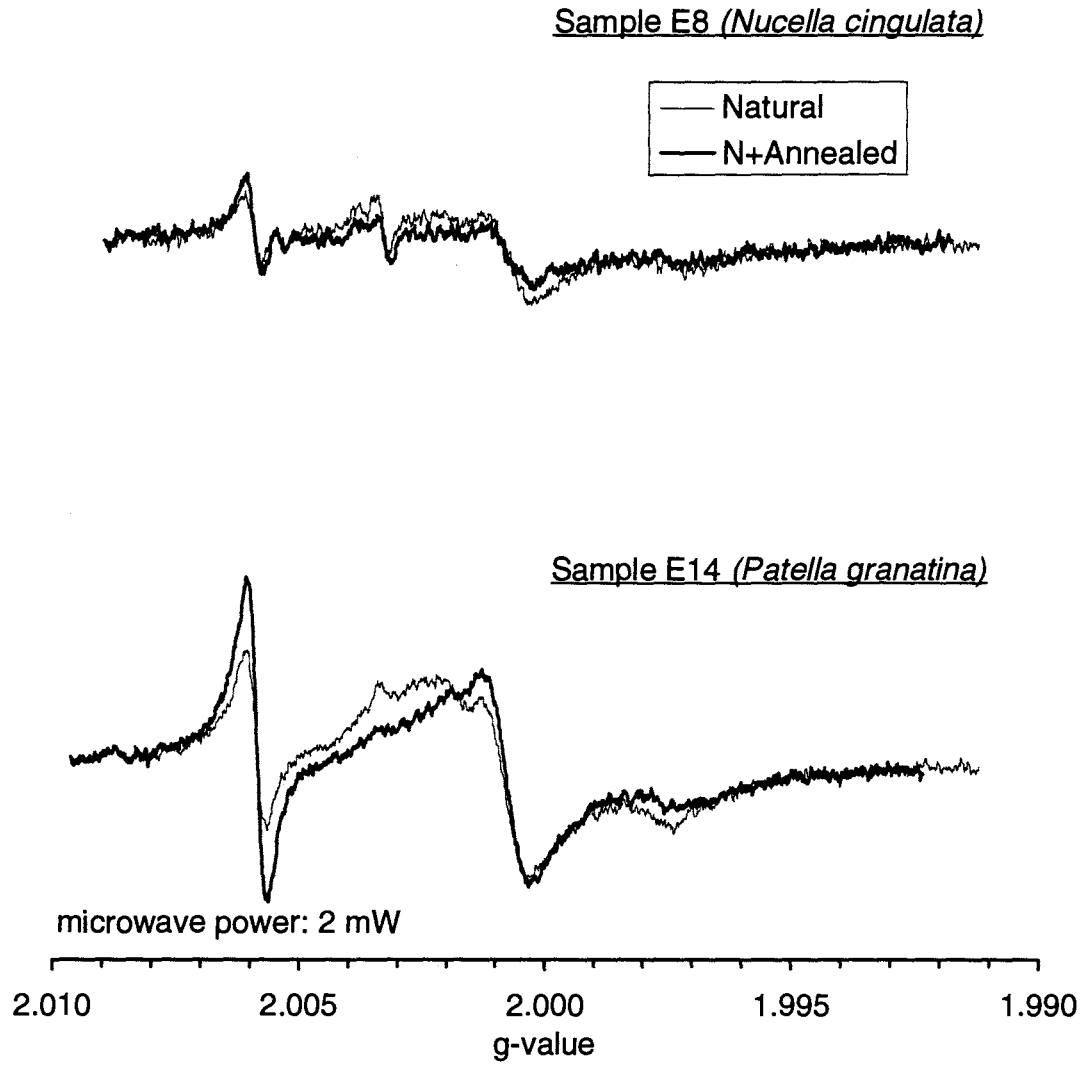

Figure 10.7. ESR spectra of 'natural' (unirradiated) aliquots of calcite-containing shell samples E8 (*Nucella cingulata*) and E14 (*Patella granatina*) from Elands Bay, South Africa. Natural aliquots (fine lines) were subsequently annealed at 150°C for 15 hours (thick lines).

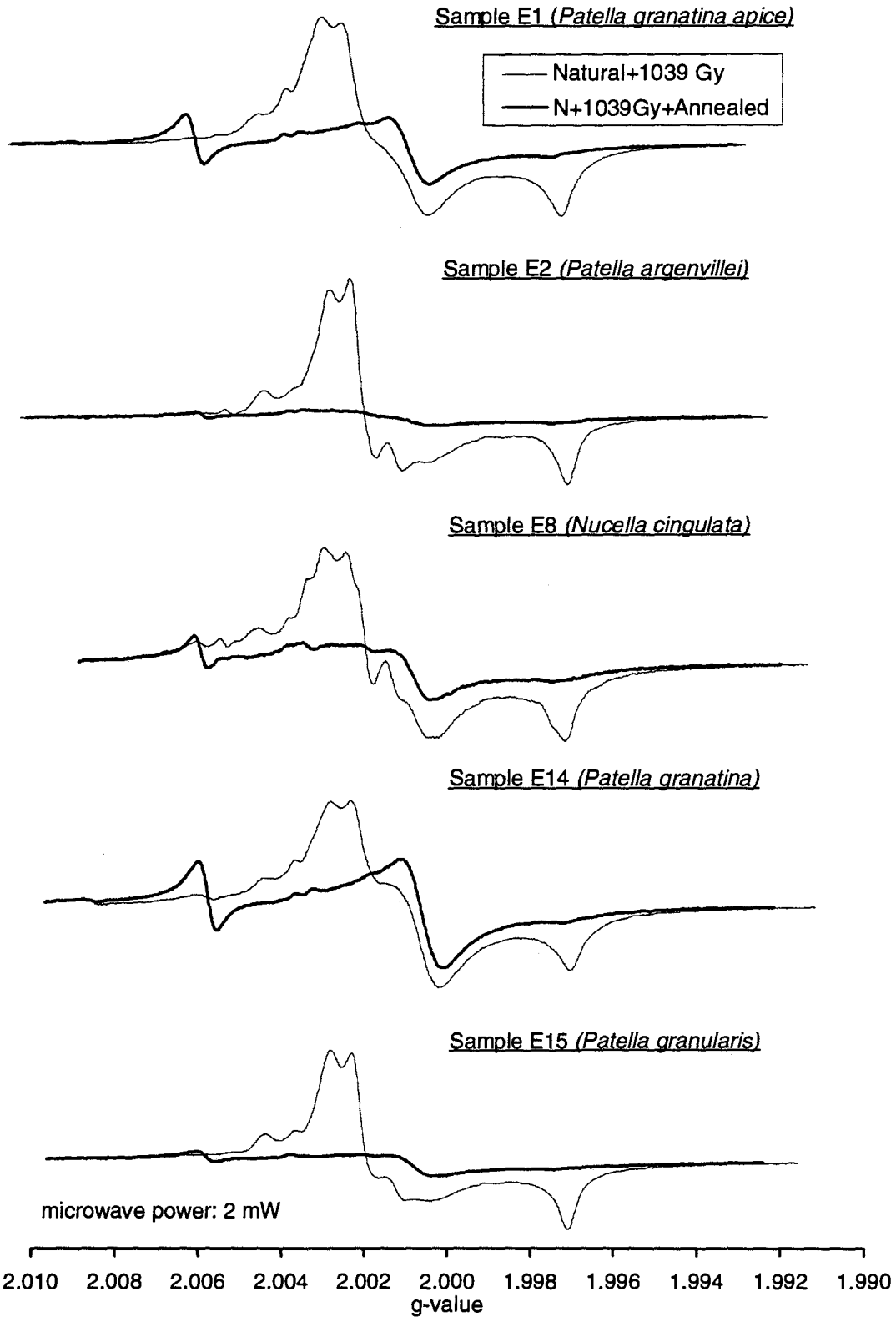

Figure 10.8. ESR spectra for calcite-containing shell samples from Elands Bay, South Africa. The natural samples were given a gamma dose of 1039 Gy (fine lines) and then annealed at 150°C for 15 hours (thick lines).

Chapter 11 SUNLIGHT BLEACHING EXPERIMENTS ON ESR SIGNALS IN QUARTZ

11.1 Forster-Tuncurry and Lake George, New South Wales

As described in section 7.3, the ESR ages of quartz samples Q13 and Q18, based on the Al and Ti signals, were significantly older than their associated TL ages. It was proposed that the discrepancy was caused by incomplete zeroing of the ESR signals by sunlight prior to sediment deposition. To test this proposal, changes in the ESR intensity of the Al and Ti centres due to exposure to sunlight were monitored, and the potential for dating using these ESR signals was investigated.

11.1.1 Methods used

The characteristics of the ESR signals of Al and Ti centres were compared for both natural (Q13-A, Q18-A and LG-A) and thermally annealed samples (Q18-B and LG-B). The latter pair were annealed for 24 hours at 550°C in an oven (Lindberg, Model 51849) and the ESR signals of the Al and Ti centres were then checked to ensure they had been quenched completely. The natural and thermally annealed samples were given a dose of 500 Gy from a ^{60}Co γ-source (dose rate $\approx$ 11 Gy min^{-1}). Fifty aliquots (ten aliquots for each sample), each weighing 200 mg, were placed in quartz tubes (about 40 mm long and 5 mm diameter) with polythene caps. All fifty tubes were placed in an aluminium rack that held the tubes horizontally to maximise sunlight exposure. The maximum vertical depth of sample was about 1.5 mm. The rack was placed on the roof of a building where it was not shaded from the sun. After various periods of exposure (8, 16, 23, 30, 56, 70, 85, 99 and 132 days, including night time), selected tubes were removed from the rack and stored in the dark. The final set of tubes was removed after 132 days of exposure, at which time all the ESR spectra were measured to avoid possible errors arising from long-term instability of the spectrometer.

The ESR measurements were carried out at liquid nitrogen temperature (≈ 77K) with a quartz dewar using an X-band Bruker 200D-SRC spectrometer set to a microwave power of 1 mW, a modulation frequency of 100 kHz and a modulation amplitude of 0.5 Gpp. The ESR spectra of the Al centre were recorded at a scan speed of 0.1 G s^{-1} with a time constant of 500 ms, while the ESR spectra of the Ti centre were measured at a scan speed of 0.05 G s^{-1} with a time constant of 2000 ms.

11.1.2 Results and discussion

The ESR intensities of the Al and Ti centres declined with increasing exposure time, as shown in Figures 11.1 and 11.2, respectively; the absolute ESR intensities of the unbleached aliquots (i.e. zero exposure time) are scaled to 100. The Al and Ti signal intensities of the samples examined here were not saturated by the laboratory γ-irradiation. The intensity of the Al signal dropped significantly during the first 30 days of exposure (to 55-75 % (mean 58 %) of its initial value for all samples except Q18-B) but changed little with further exposure. Only sample Q18-B behaved differently, with the intensity of its Al centre dropping to 25 % of its initial value after 132 days of continuous exposure. As this sample was annealed and irradiated prior to bleaching, whereas Q18-A had been irradiated only before bleaching, the higher proportion of bleachable Al defects in Q18-B must be attributable to the effect of annealing. There may also be an effect resulting from the dose rate used in laboratory (≈ 11 Gy min^{-1}), which is about 10^9 times greater than the natural dose rate (estimated as ≈ 1 mGy $year^{-1}$). However, no such annealing or dose rate effects are observed for the Lake George samples (LG-A and LG-B). The changes in Al intensity in four of the samples are comparable, and indicate that, on average, around 42 % of the initial ESR signal at the Al centre is bleached after 132 days. Similar results were reported by Yokoyama *et al.* (1985b), who found that about 40 % of the total Al centre ESR signal is bleachable; this figure was based on the assumption that, throughout the past 0.5 Ma of sand deposition, the sand grains have always contained the same concentration of unbleachable Al centres at the time of deposition. More recently, Tanaka

et al. (1995) also reported that the Al-centre signal in aeolian quartz sand declined by ≈ 37 % after 20 hours of exposure to ultraviolet light.

The Ti signal in the samples from Lake George (LG-A and LG-B) was not detectable, so only changes in ESR intensities of Ti centres on exposure to sunlight for the marine samples from Forster-Tuncurry (Q13-A, Q18-A and Q18-B) are shown in Figure 11.2. As with the Al signal, the ESR intensity of the annealed and irradiated sample Q18-B has a higher relative concentration of bleachable Ti defects than its N+γ counterpart (Q18-A). In contrast to the Al centre, the Ti-centre intensities of all the Forster-Tuncurry samples dropped, on average, to 5 % of their initial values after 132 days of sunlight exposure; this degree of bleaching far exceeds that observed for the Al centre. Furthermore, there appears to be no Ti bleaching 'residual level' at long exposure times (see Figure 11.2(b)), suggesting that a continued decrease in ESR signal may be achieved with further sunlight exposure.

The results indicate that the ESR intensity of the Ti centre is bleachable and has the potential to be used for ESR dating. There is, however, no clear evidence to explain the discrepancies between the D_E-values based on the Ti signal and those obtained by TL (see section 7.3). In the case of complete signal zeroing, D_E-values based on the Ti-centre ESR intensities should be reliable insofar as Ti-centre thermal stability is concerned (Shimokawa and Imai, 1985; Shimokawa *et al.*, 1988; Imai and Shimokawa, 1989). But it is not clear whether the Ti signal, or even the TL signal (D_E plateau region of 325-500°C for sample Q13 and 300-500°C for sample Q18), is reset completely before the sediment is deposited underwater. The TL signal associated with the 325°C peak in quartz should be reset beneath large depths of water (cf. Rendell *et al.*, 1994), and as this TL peak forms part of the D_E plateau region, the TL age determinations for samples Q13 and Q18 should be accurate. In contrast, the specific wavelengths of light required to reset the ESR signals are not known. Depositional environments of marine sediments are complex, and the effect of sunlight on the Ti and TL signals is apt to be influenced by the spectral absorption and light scattering properties of water and suspended material. As

wavelength transmission varies with water depth (Aitken, 1985; Berger, 1990), it may be possible that the D_E-values obtained from the Ti and TL signals indicate their different sensitivities to the light transmitted to the sea bed, through water of varying depth and turbidity.

Assuming that the Ti signal was bleached completely at the time of deposition, and that only 42 % of the natural intensity of the Al signal was bleached prior to deposition (i.e. 58 % of the natural intensity of the Al signal remains as a 'residual' intensity), then the D_E-values based on the Al signal agree with those obtained using the Ti signal. Yokoyama *et al.* (1985b) applied this 'total bleach' method to ESR and obtained ages in agreement with faunal studies. The total bleach ESR method is based on the assumption that only bleachable Al centres are produced during the period of burial and that the ratio of bleachable to unbleachable Al centres at the moment of sediment deposition can be deduced experimentally by exposing aliquots to sunlight for selected periods of time.

The results in Figure 11.1 do not support this theory, however, showing that the ratio of bleachable to unbleachable Al centres is not uniform (i.e. sample Q18-B indicates a ratio of approximately 3:1, while the others have a ratio of around 2:3). An alternative assumption is that, during the period of sample burial, natural radiation produces Al centres of which about 58 % are unbleachable. In this case, the Al signal would be unsuitable for dating because the unbleachable 'residual' ESR intensity present at the moment of burial will vary from sample to sample (depending on their degree of prior sunlight exposure), and cannot be estimated using modern material.

11.2 Allen's Cave, South Australia

The ESR ages obtained for samples Ox_{OD}AC150 and Ox_{OD}AC390 using the Al and Ti signals were significantly older than the corresponding ^{14}C, OSL and TL ages (described in section 7.3). As in the preceding section, changes in ESR intensity at the Al and Ti

centres as the result of exposure to sunlight were monitored for sample Ox_{OD}AC390, and the potential for dating using these signals was investigated.

11.2.1 Methods used

The same aliquot of sample Ox_{OD}AC390 used for ESR dating in section 7.2.3 was used for these experiments. The aliquot had been subjected to a total dose of 1720 Gy, annealed at 100°C for 24 hours and then at 120°C for 20 hours to remove possible unstable centres. The sample was then exposed to sunlight in the manner described in section 11.1.1. After selected periods of exposure (6, 16, 30 and 52 days, including night time), ESR spectra of the Al and Ti signals were recorded using X-band Bruker ESR 300E spectrometer, under the same conditions as described in section 7.1. The laboratory was illuminated using only wavelengths longer than ≈ 590 nm in order to prevent any laboratory bleaching of light-sensitive ESR signals.

11.2.2 Results and discussion

The relative ESR intensities of the Al and Ti centres decreased with increasing exposure time, as shown in Figure 11.3; the ESR intensities of the unbleached sample are scaled to 100. The intensity of the Al signal decreased to 47 % of its initial value, while the intensity of Ti signal declined to 13 %, after 52 days of exposure. These findings are similar to those reported for the Forster-Tuncurry and Lake George samples, and suggest that the Ti centre is more light-sensitive than the Al centre. The Ti centre may be completely bleached with further exposure, while the Al signal would appear to reach a residual level of around 40-50 % of its initial (near-saturated) intensity. Under field conditions, however, where sediment is intermittently transported then buried, zeroing of these signals is likely to take much longer than the 'continuous exposure' times reported here.

11.3 Newly discovered ESR light-sensitive signals in quartz

During the sunlight bleaching experiments on sample Ox_{OD}AC390, three new light-sensitive ESR signals were discovered. These ESR light-sensitive signals were observed at g=1.9870, 1.9842 and 1.9162, and are illustrated in Figures 11.4(a) and 11.4(b). These signals appear to be bleached completely after 6 days of exposure (including night time) to unfiltered sunlight. These signals remained unchanged during a further 10 days of exposure, while the Al and Ti signals continued to decrease in intensity. At this stage in the investigation, the minimum exposure time required to bleach the signals completely is not known. But it is clear, even with the limited data available, that these newly found signals are considerably more light-sensitive than the Al and Ti signals, and that they offer improved prospects for dating the time of last exposure to sunlight.

It is generally believed that no light-sensitive signals suitable for dating are observable by ESR (Schwarcz, 1994). A reason why these signals have not been noticed by previous researchers could be that these signals are relatively narrow in signal width and low in amplitude, so that the recording conditions ordinarily used to measure the Al or Ti signals do not allow the detection of small changes in these signals. In addition, very dim room illumination is required for sample preparation and ESR measurement; for the sample examined here, dim red illumination (>590 nm) was used for all ESR operations. Such darkroom conditions have never been reported before in ESR dating studies. Further studies on the bleaching and dose response behaviour of these signals are discussed in the following section and in Chapter 14.

11.4 Sunlight bleaching experiments on newly discovered ESR light-sensitive signals in quartz

From the observations reported in section 11.3, a question arises: is there a relation between the light-sensitive ESR signals (g=1.9870, 1.9842 and 1.9162) and the TL and

OSL dating signals? Over the last decade, several researchers have attempted to identify the ESR centres associated with the TL dating peaks (Halliburton *et al.*, 1984; McKeever *et al.*, 1985; Yang and McKeever, 1988, 1990; McKeever, 1991). Two main TL dating peaks have been distinguished in quartz: one is referred to as the rapidly-bleached peak and the other as the slowly-bleached peak. These are observed at 325°C and 375°C, respectively, when the sample is heated at 5 K s^{-1}. The 325°C peak and the OSL signal originate from the same trapped-electron population (Smith *et al.*, 1986; Spooner *et al.*, 1988; Spooner, 1994) and are bleached rapidly (within minutes) and completely by ultraviolet and most visible wavelengths. In contrast, the 375°C peak is bleached only by ultraviolet wavelengths, and a non-zero (unbleachable) residual level is attained, even after several hours of solar illumination (Spooner *et al.*, 1988). In terms of emission spectra, the 325°C and 375°C peaks are centred at 380 nm and 470 nm, respectively (McKeever, 1984; Prescott and Fox, 1990; Scholefield *et al.*, 1994), suggesting that the two TL peaks are involved with different recombination centres.

In this section, sunlight bleaching experiments were performed on the ESR light-sensitive signals at g=1.9870, 1.9842 and 1.9162 in sample Ox_{OD}AC150 to monitor changes in ESR intensity as the result of light exposure. Also, an orange filter, transmitting only wavelengths greater than 510 nm, was used to investigate the influence of wavelength on bleaching behaviour. The 325°C TL peak would be bleached by wavelengths passing through the filter, whereas the 375°C signal is bleached only by the ultraviolet component of unfiltered sunlight. If the ESR signals are related to either of these TL peaks, then similar wavelength-dependent behaviour might be expected.

11.4.1 Methods used

Two aliquots, each weighing 200 mg, of sample Ox_{OD}AC150 were given a dose of 449 Gy from a ^{60}Co source (dose rate ≈ 10.5 Gy min^{-1}) and then annealed for 5 minutes at 220°C in an oven (Varian aerograph, Series 1700). This annealing procedure is used routinely in the optical dating of Australian quartz sediments (see Roberts *et al.*, 1994a).

To monitor changes in ESR intensity, one of the aliquots was placed in a glass dish covered with commercially available kitchen wrap, and then exposed to sunlight. After selected periods of exposure (up to 11 hours), the intensities of the ESR signals at the Al and Ti centres (see Figure 7.1) and the signals at g=1.9870, 1.9842 and 1.9162 were measured. The intensity of the signal at g=1.9162 was measured from the peak (at g=1.9162) to the base line obtained from the region between g=1.908 and g=1.895. For the signals at g=1.9870 and 1.9842, the intensities were measured from the peaks (at g=1.9870 and 1.9842) to the base line obtained from the region between g=1.989 and g=1.980. To investigate the wavelength-dependent characteristics of the light-sensitive ESR signals, another aliquot was exposed to sunlight for 10 hours in a glass dish covered with an orange filter (transmitting only wavelengths greater than 510 nm). After the ESR measurements, the same sample was again exposed to sunlight but, this time, without the filter; thereafter, the ESR measurements were repeated.

ESR measurements were carried out at liquid nitrogen temperature ($\approx$ 77K) with a quartz dewar using an X-band (9.25 GHz) Bruker ESP 300E spectrometer with a microwave power of 1 mW, a modulation frequency of 100 kHz, a modulation amplitude of 0.5 Gpp and time constant of 655 ms. For the Al and Ti centres, a scan speed of 0.3 G s^{-1} was used. A scan speed of 0.03 G s^{-1} was used for the signals at g=1.9870 and 1.9842, while the signal at g=1.9162 was recorded with a scan speed of 0.06 G s^{-1}.

To prevent inadvertent bleaching in the laboratory, ESR measurements were performed at night; the lights installed in the equipment were concealed, except for the necessary indicator lights which were covered with red filter (>590 nm wavelength transmission). The computer screen was also covered with red filter and a dim red display colour was used during the spectral measurements. A lamp wrapped in red filter was used on occasions.

11.4.2 Results and discussion

The relative ESR intensity of the signals at g=1.9870, 1.9842 and 1.9162, together with the intensities of the Al and Ti signals, decrease with increasing exposure time, as shown in Figure 11.5; the absolute ESR intensities of the unbleached aliquots (i.e. zero exposure time) are scaled to 100. The changes in intensity of the signals at g=1.9870, 1.9842 and 1.9162 are almost identical and drop by more than 90 % of their initial intensities after 11 hours of exposure. The intensities of the Al and Ti signals decreased by 29 % and 38 %, respectively, over the same time period. These results suggest that the signals at g=1.9870, 1.9842 and 1.9162 probably relate to the same ESR centre or set of centres, but that they clearly differ from the Al and Ti signals. The exposure time required to bleach completely the signals at g=1.9870, 1.9842 and 1.9162 is of the order of 10-20 hours. There is, however, the possibility that the signal cannot be completely bleached, and that a non-zero residual level is reached, even after prolonged exposure. The rate of signal decline with bleaching time and the level of signal remaining after 11 hours of unfiltered sunlight exposure are comparable to the characteristics of the 375°C TL signal, but are unlike those associated with the 325°C TL and OSL signals.

ESR spectra of the signals at g=1.9870, 1.9842 and 1.9162, and the Al and Ti signals, before and after bleaching with and without the interposed orange filter (>510 nm transmission) are shown in Figures 11.6(a) and 11.6(b). No change in the signal intensities was observed after 10 hours of sunlight exposure with an interposed orange filter. However, after 10 hours exposure without the filter, the signals at g=1.9870, 1.9842 and 1.9162 are almost completely bleached, while the Al and Ti signal intensities decreased to 84 % and 67 % of their initial intensities, respectively. This wavelength-dependent bleaching behaviour further suggests that the signals at g=1.9870, 1.9842 and 1.9162 are not related to the 325°C TL or OSL signals but may be associated with the 375°C TL signal.

11.5 Summary

In the samples of quartz examined, the Al centre was found to be only partially bleached by unfiltered sunlight and to have a similar ratio of bleachable to unbleachable signal in all samples (bar one). The ratio of bleachable to unbleachable Al centres is approximately 2:3 after prolonged sunlight exposure (132 days, including night time, rainy and cloudy days), with the exception of one more bleachable sample (Q18-B). If 42 % of the Al centres produced by natural radiation are bleachable in all quartz samples, it is theoretically possible to obtain correct D_E-values and, hence, ages by the total bleach ESR method.

The Ti signal is almost completely reset by unfiltered sunlight after 132 days of exposure. This period may be sufficient for certain geological deposits (e.g. aeolian sediments) but is too stringent a criterion to be of use for dating sediments exposed only briefly to sunlight prior to deposition (e.g. fluvial or coastal deposits). Ti centres have great thermal stability (Yokoyama *et al.*, 1985c; Shimokawa and Imai, 1985; Falguères *et al.*, 1991), with a mean lifetime of sufficient duration to enable Quaternary sediments to be dated (with the foregoing proviso concerning the depositional environment).

Reported here for the first time are three new light-sensitive ESR signals. These occur at g=1.9870, 1.9842 and 1.9162 at liquid nitrogen temperature (≈ 77K) and are bleached almost completely by 10 hours exposure to unfiltered sunlight. Since these signals are not bleached by sunlight transmitted through an orange filter (>510 nm transmittance), the signals are not associated with the 325°C TL signal, which has been shown to be related to the OSL signal in quartz (Spooner, 1994). The results suggest, however, that the light-sensitive ESR signals may be related to the 375°C TL signal, on the basis of the wavelength-dependence of bleaching, the rate of bleaching by unfiltered sunlight, and the residual level attained after several hours of solar illumination. These latter signals offer the greatest potential for dating solar-reset quartz by ESR; Quaternary dating applications are presented in Chapter 14.

It should be noted that to extend the application of these newly discovered signals to water-lain sediments requires a knowledge of the efficacy of bleaching beneath a cover of water. In this regard, the observations from the filtered sunlight bleaching experiments imply poor prospects for dating if only wavelengths longer than 510 nm are transmitted through the water column. In such instances, sub-aqueous bleaching of the ESR signals would likely be insufficient for dating purposes. Nonetheless, many terrestrial deposits should be amenable to dating using these light-sensitive ESR signals, in the same manner as the 375°C TL signal has received widespread application.

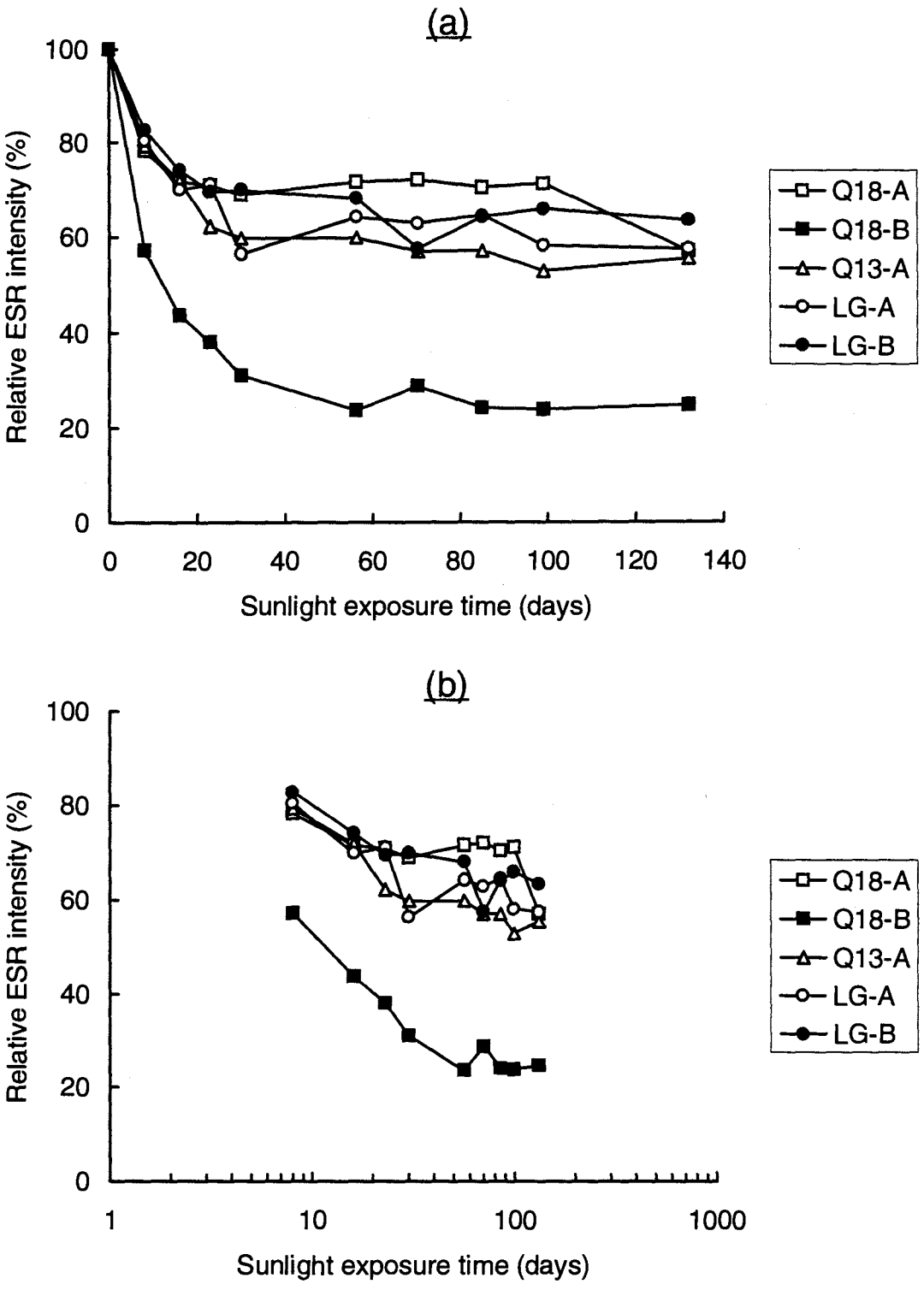

Figure 11.1. Changes in the relative ESR intensity of the Al signal on exposure to sunlight; using (a) linear and (b) logarithmic scales for sunlight exposure time (zero days = 100% ESR intensity).

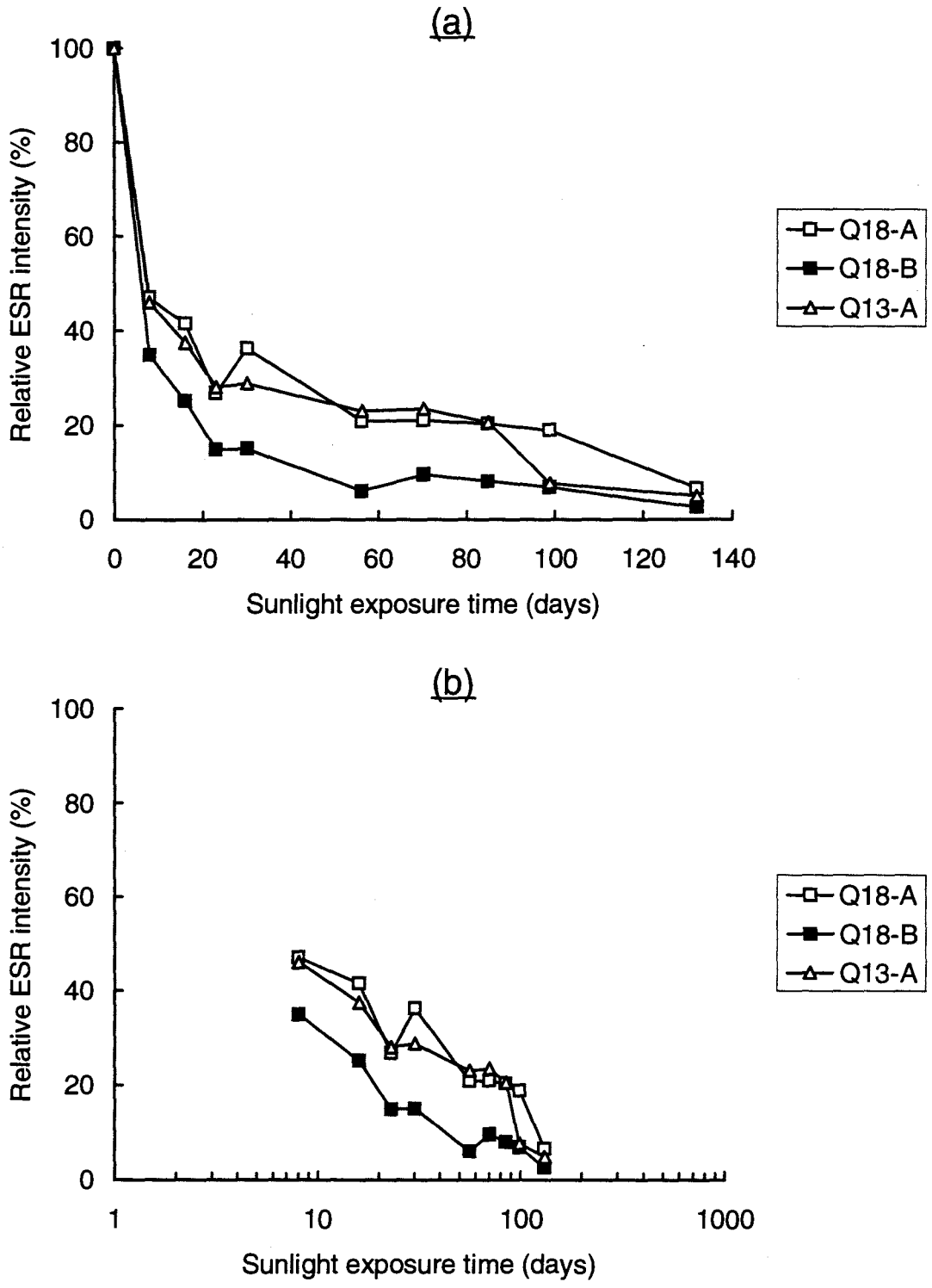

Figure 11.2. Changes in the relative ESR intensity of the Ti signal on exposure to sunlight; using (a) linear and (b) logarithmic scales for sunlight exposure time (zero days = 100% ESR intensity).

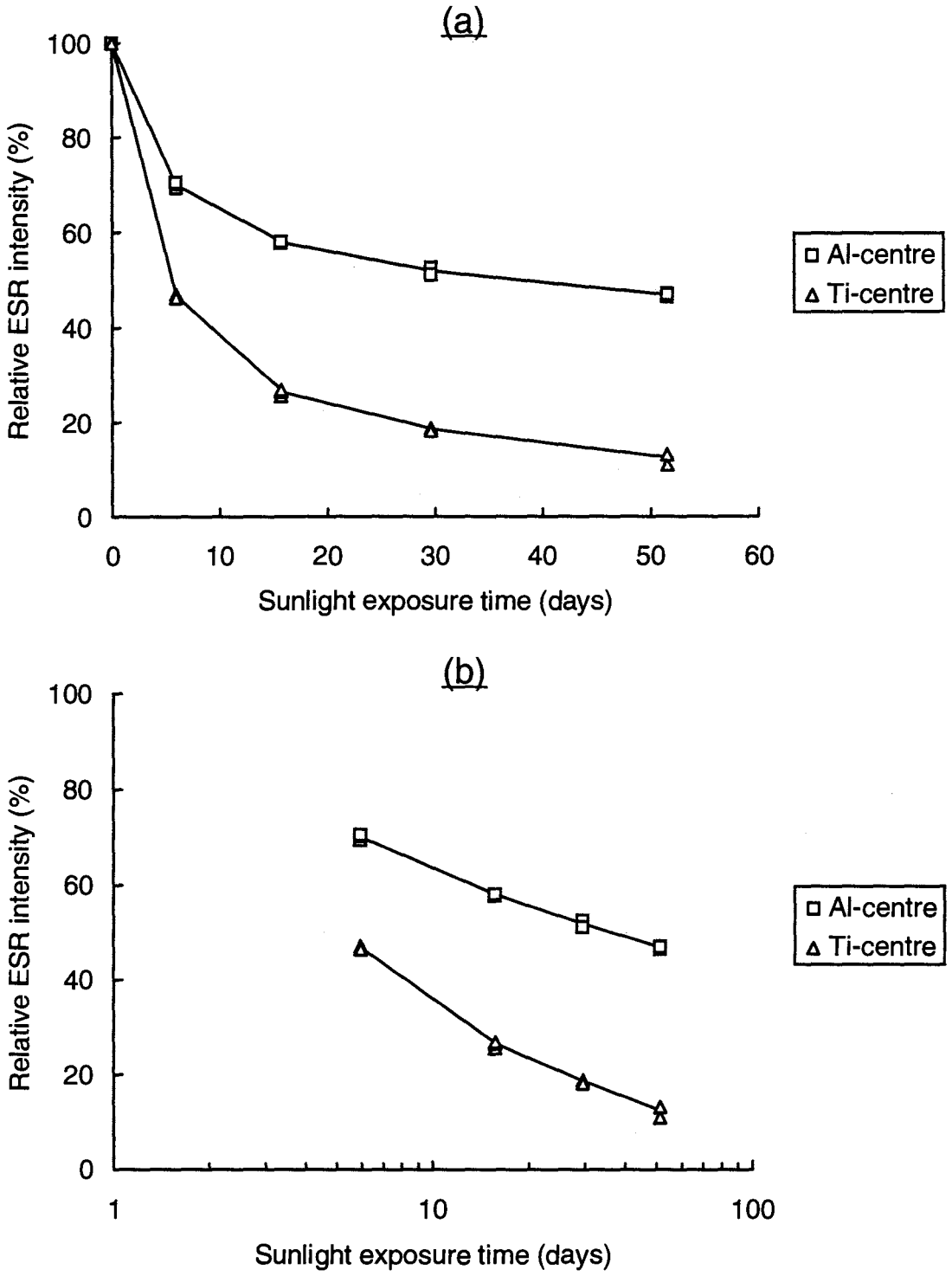

Figure 11.3. Changes in the relative ESR intensity of the Al and Ti signals in sample Ox_{OD}AC390 on exposure to sunlight; using (a) linear and (b) logarithmic scales for sunlight exposure time (zero days = 100% ESR intensity). The 'as collected' (natural) sample had been given a dose of 1720 Gy, followed by annealing at 100°C for 24 hours and then at 120°C for 20 hours.

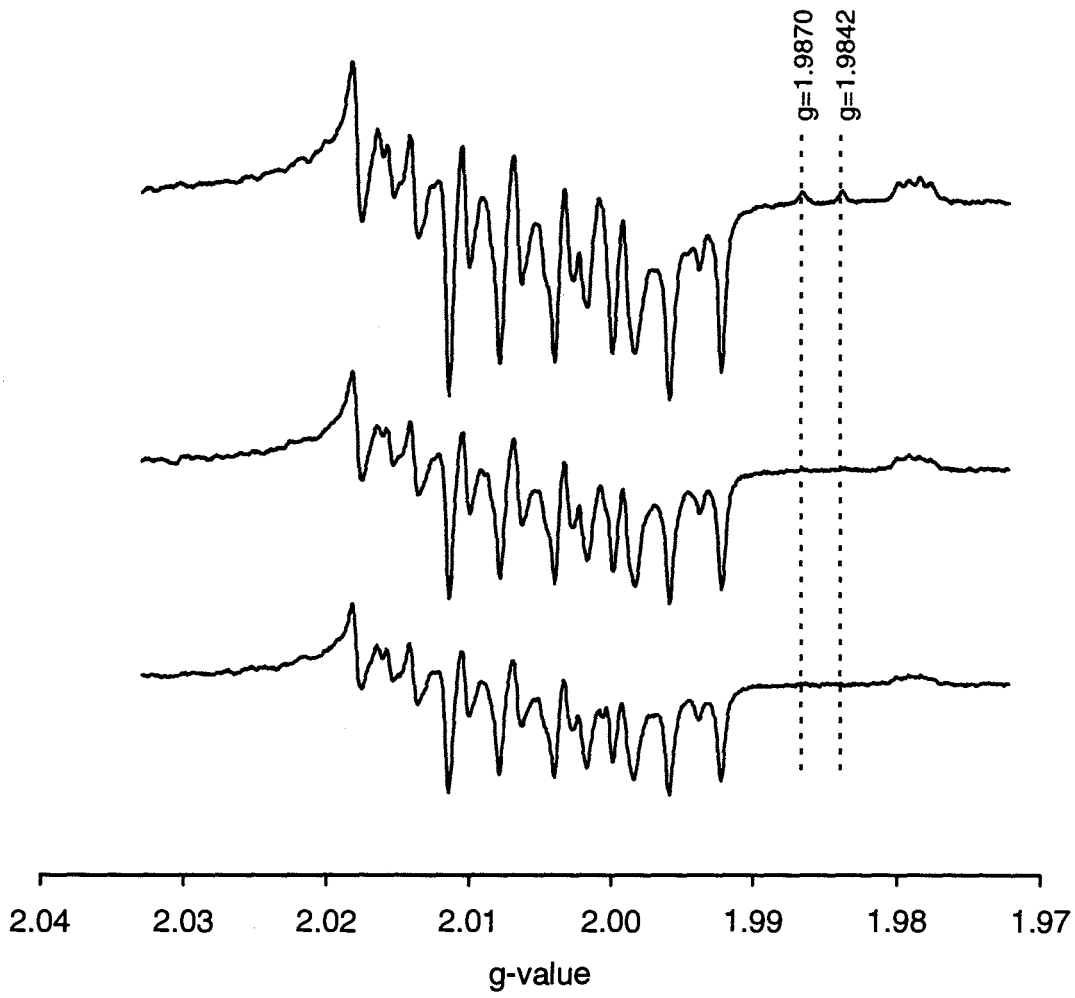

Figure 11.4(a). ESR spectra in the vicinity of the Al signal of Ox_{OD}AC390. The natural sample was given a dose of 1720 Gy, followed by annealing at 100°C for 24 hours and then at 120°C for 20 hours (top). The sample was then exposed to sunlight for 6 days (middle) and 16 days (bottom).

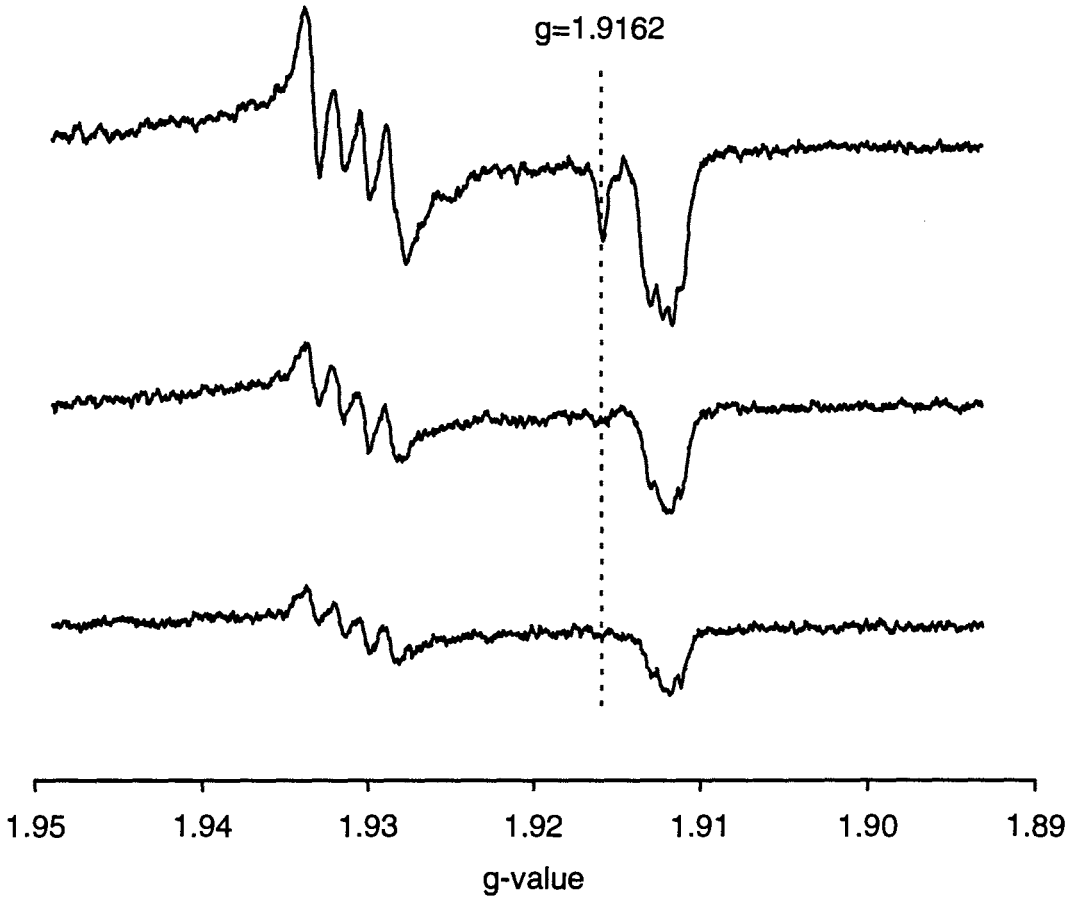

Figure 11.4(b). ESR spectra in the vicinity of the Ti signal of Ox_{OD}AC390. The natural sample was given a dose of 1720 Gy, followed by annealing at 100°C for 24 hours and then at 120°C for 20 hours (top). The sample was then exposed to sunlight for 6 days (middle) and 16 days (bottom).

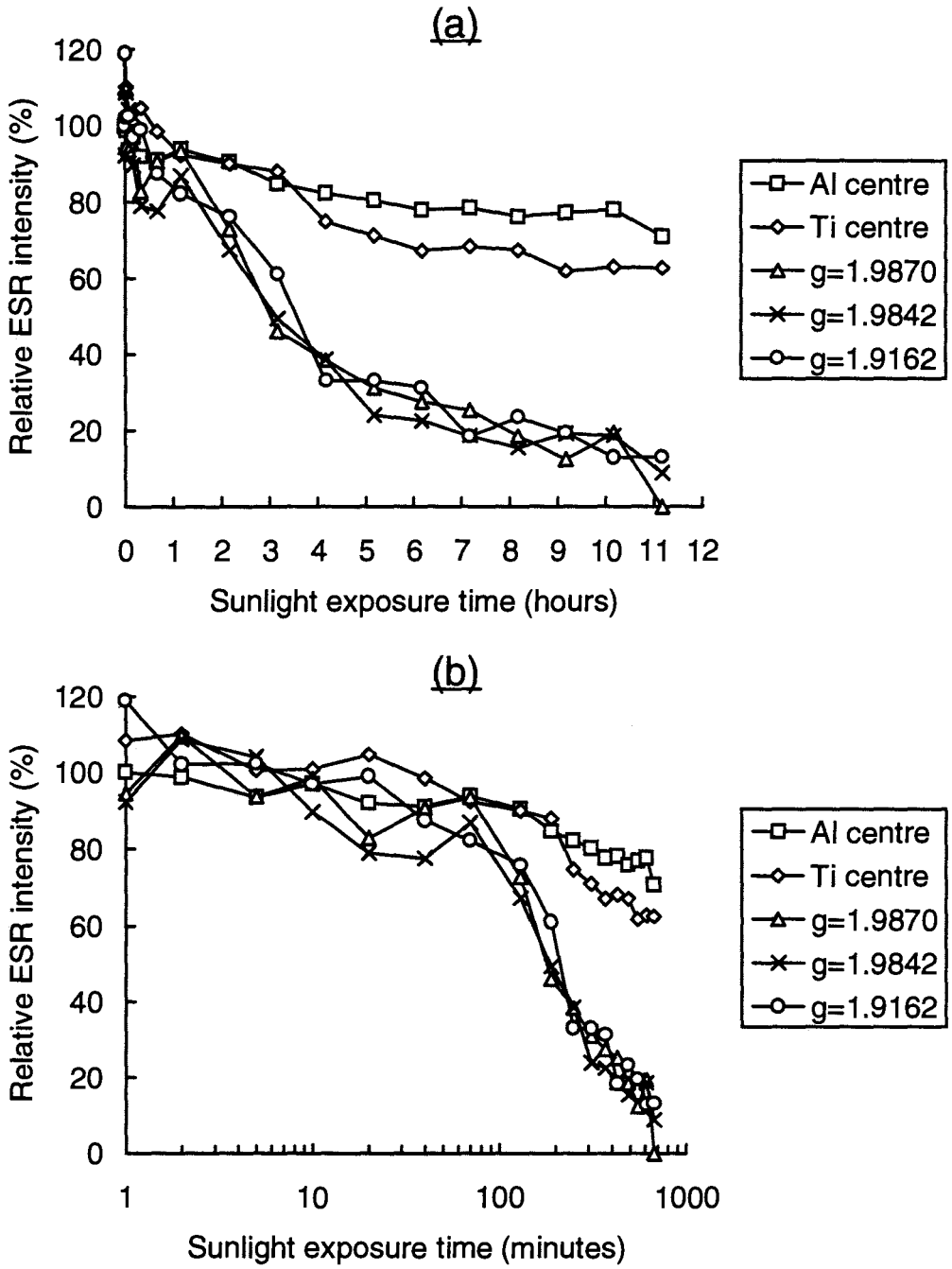

Figure 11.5. Changes in the relative ESR intensity on exposure to sunlight of the Al and Ti signals, and the signals at g=1.9870, 1.9842 and 1.9162 in sample Ox_{OD}AC150; using (a) linear and (b) logarithmic scales for sunlight exposure time (zero minutes = 100% ESR intensity). The 'as collected' (natural) sample had been given a dose of 449 Gy, followed by annealing at 220°C for 5 minutes (as used routinely in the optical dating of Australian quartz; Roberts *et al.*, 1994a).

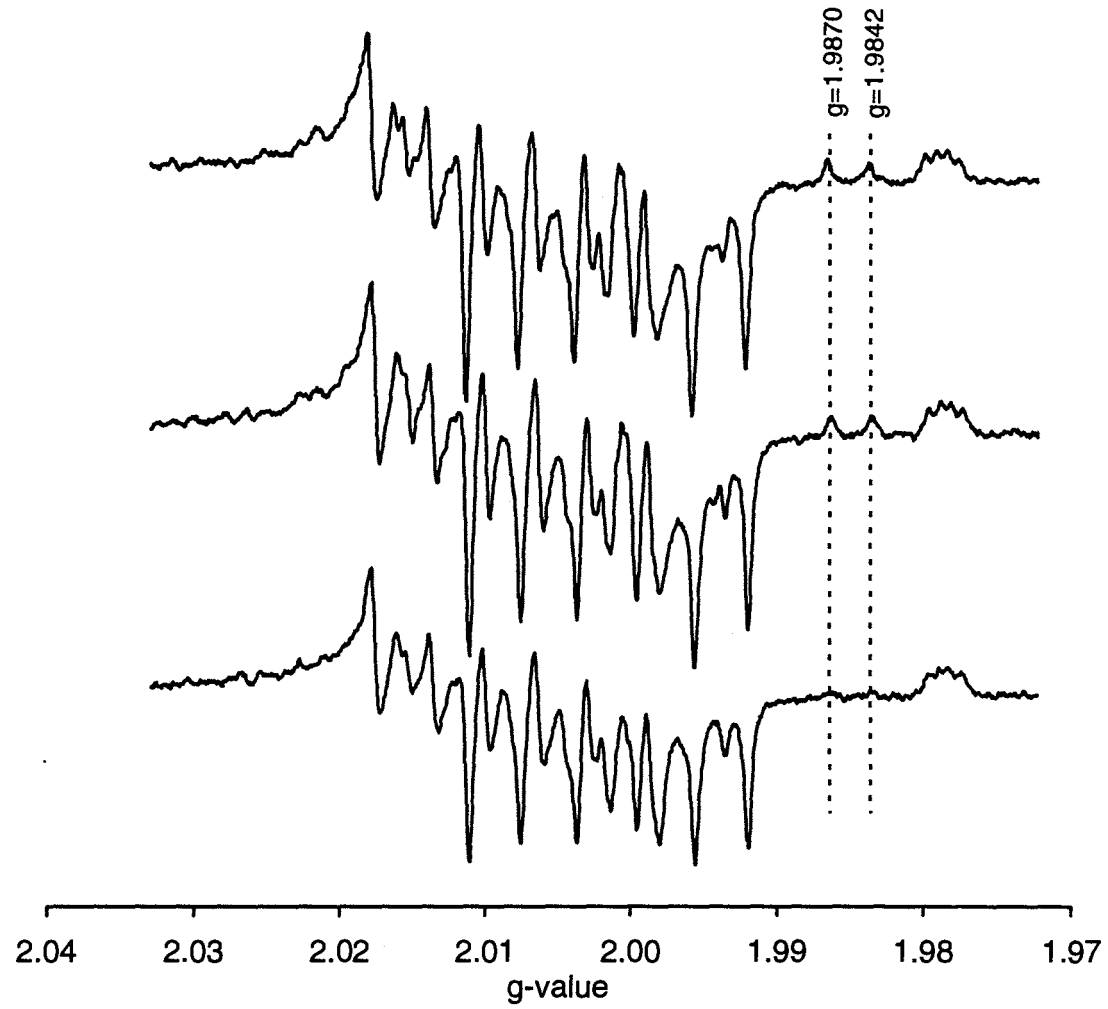

Figure 11.6(a). ESR spectra in the vicinity of the Al signal of Ox_{OD}AC150. The natural sample was given a dose of 449 Gy, followed by annealing at 220°C for 5 minutes (top). The sample was then exposed to sunlight through an orange filter (>510 nm transmission) for 10 hours (middle). The same experiment was performed subsequently without the filter (bottom).

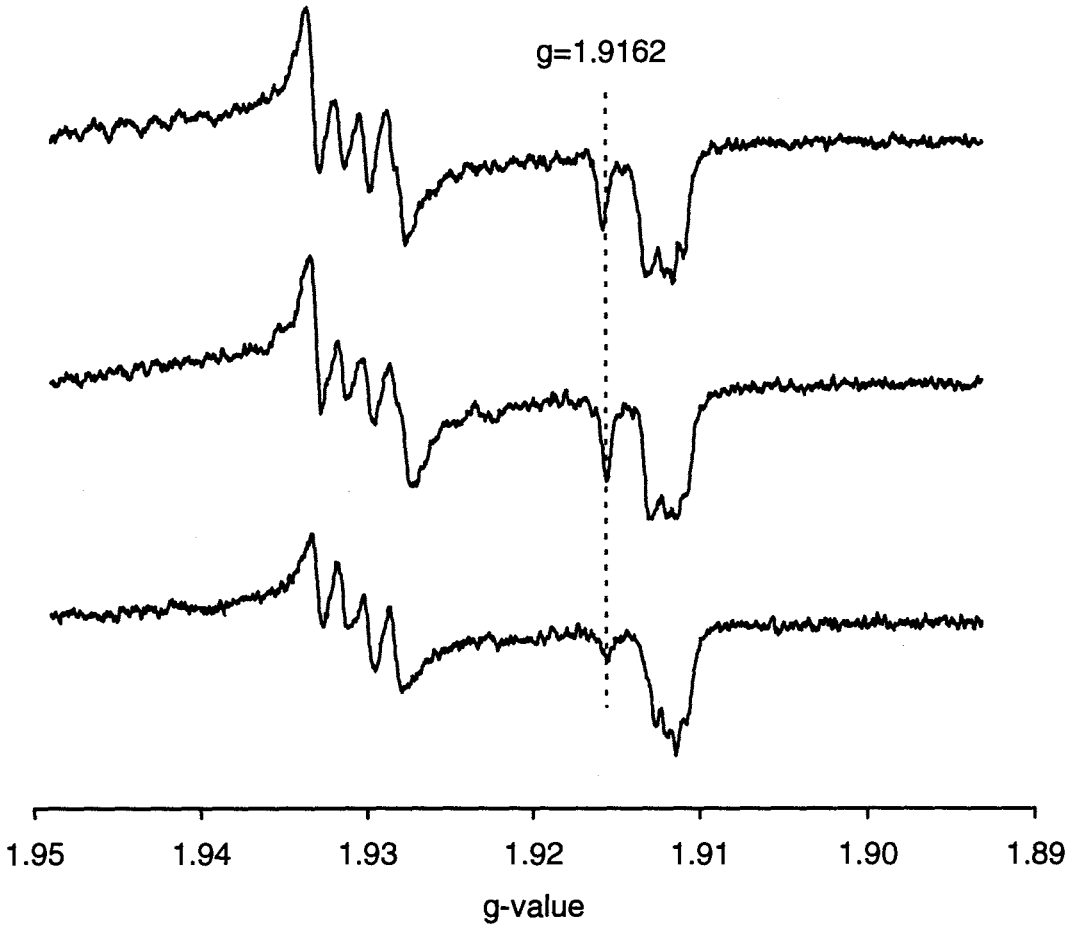

Figure 11.6(b). ESR spectra in the vicinity of the Ti signal of Ox_{OD}AC150. The natural sample was given a dose of 449 Gy, followed by annealing at 220°C for 5 minutes (top). The sample was then exposed to sunlight through an orange filter (>510 nm transmission) for 10 hours (middle). The same experiment was performed subsequently without the filter (bottom).

Part IV

DATING USING NEW METHODS

Chapter 12 SHELL SAMPLES

The X-band signals at g=2.0058 for aragonite and calcite-containing shells, g=2.0014 (aragonite shells) and g=2.0006 (calcite-containing shells), after annealing at 150°C for 14-45 hours, were investigated for dating. Using a Q-band (≈ 35 GHz) spectrometer, D_E-values based on the signal at g=2.0006 were obtained for selected shell samples from Forster-Tuncurry, New South Wales. For the calcite-containing shell samples from Elands Bay, South Africa, D_E-values based on the signal at g=2.0006 (X-band) were obtained after annealing. D_E-values based on the annealed signals at g=2.0058 and g=2.0014 were obtained for shell samples from both Elands Bay and Forster-Tuncurry.

The prospects for dating using the signals at g=2.0014 (aragonite shells, before and after annealing), g=2.0006 (aragonite shells: X-band, microwave power of 200 mW, before annealing), g=2.0006 (aragonite shells: Q-band, before annealing), g=2.0006 (calcite-containing shells: X-band, after annealing) and g=2.0058 (aragonite and calcite-containing shells: after annealing) are discussed in the final two sections of this chapter.

12.1 Forster-Tuncurry, New South Wales

12.1.1 Methods used

The aliquots of aragonite shell from cores FT13-10, FT14-1 and FT/BMR19-3A discussed in Chapter 4 were employed subsequently for the analyses described in this chapter. The signal intensity at g=2.0006 was measured with a Q-band (≈ 35 GHz) Varian 4502 EPR spectrometer at room temperature (≈ 21°C), with a modulation frequency of 100 kHz, a microwave power of 0.6 mW, a modulation amplitude of 0.25 Gpp, a scan range of 100 G, a scan speed of 28 G min^{-1} with a time constant of 1 s. After measurement of the unannealed natural and N+γ ESR signals, all aliquots were then annealed for 14 hours at 150°C in an oven (Lindberg, Model 51849) to give rise to the

signal at g=2.0058 (see Chapter 10). The X-band signal at g=2.0058 was measured in the same manner as described in section 5.1, but using a microwave power of 2 mW. D_E-values and ESR ages based on the signals at g=2.0006 (Q-band, before annealing) and g=2.0058 (X-band, after annealing) were estimated using the procedures described in section 4.1.1.

12.1.2 ESR ages obtained

The D_E-values based on the signals at g=2.0006 (Q-band, before annealing) and g=2.0058 (X-band, after annealing) are compared in Table 12.1 and Figures 12.1(a) and 12.1(b) with the results obtained in Chapter 4. The D_E-values based on the signal at g=2.0014 (X-band, after annealing) were obtained only for samples 13 and 15 since the signal intensities of the other samples were too weak to be measured. Some examples of the ESR spectra and dose response curves are shown in Figures 12.2(a)-(d).

Using a Q-band spectrometer, the signal at g=2.0006 appears to be symmetrical and isolated from the signals at g=2.0032 and g=2.0020. The D_E-values based on the g=2.0006 signal (Q-band) correspond closely (i.e. at the 1σ or 2σ level) with those based on the g=2.0006 signal (X-band, 200 mW), except for samples 17, 21, 22, 27 and 45 (see Figure 12.1(a)). However, D_E-values based on the g=2.0006 signal (Q-band) of only three samples (17, 29 and 44) agree within the 1σ or 2σ error limits with the D_E-values based on the g=2.0014 signal (before annealing); for the other samples, the D_E-values based on the g=2.0014 signal are smaller than those based on the g=2.0006 signal (Q-band), as shown in Figure 12.1. These results suggest that the D_E-values based on the g=2.0006 signal using X-band (microwave power of 200 mW) and Q-band are comparable for the shell samples examined. In contrast, signal intensities at g=2.0014 appear not to correspond to those based on the g=2.0006 signals using X-band (microwave power of 200 mW) and Q-band spectrometers.

After annealing at 150°C for 14 hours, the signal intensities at g=2.0058 in the natural (unirradiated) aliquots increased by between 26% and 294% of the initial intensities, and the signal intensities of the irradiated aliquots increased in proportion to the given doses. The resulting dose response curves appear to be saturated at much smaller doses than those of the g=2.0006 (X-band and Q-band) and g=2.0014 (X-band) signals, and D_E-values based on the g=2.0058 signal are overestimated if all dose points are used in the D_E-value estimations (see Figures 12.2(b) and 12.2(d)). The D_E-values used in the age calculation are, therefore, estimated using a saturating-exponential-plus-linear fit and excluding some of the largest dose points; larger random errors in D_E-values were introduced by using fewer data points. The D_E-values based on the g=2.0058 signal after annealing are generally much greater than those based on the signals at g=2.0014, g=2.0006 (X-band, 200 mW) and g=2.0006 (Q-band) (Figure 12.1(b)). For only three samples (13, 15 and 44) are the D_E-values based on the unannealed g=2.0014 signal in concordance at the 1σ or 2σ level with the D_E-values of the annealed g=2.0058 signal. D_E-values based on the annealed g=2.0058 signal of seven samples (13, 15, 17, 18, 23, 43 and 44) agree at the 1σ or 2σ level with those based on the g=2.0006 signal (X-band, 200 mW), while D_E-values based on the annealed g=2.0058 signal of eight samples (13, 15, 18, 21, 27, 43, 44 and 45) are within the 1σ error limits of D_E-values based on the g=2.0006 signal (Q-band). For samples 13, 15, 18, 43 and 44, D_E-values based on the signals at g=2.0006 (X-band, 200 mW), g=2.0006 (Q-band) and g=2.0058 (X-band, after annealing) are in agreement at the 1σ or 2σ level. D_E-values based on the g=2.0058 signal (X-band, after annealing) could, therefore, provide a useful alternative to those based on the signals at g=2.0006 (X-band, 200 mW) and g=2.0006 (Q-band).

After annealing, the signal intensities at g=2.0014 of natural (unirradiated) aliquots were not measurable for most of the samples. D_E-values based on the annealed g=2.0014 signal were obtained only for the two oldest samples (13 and 15) (see Table 12.1). For these samples, the D_E-values are in accordance at the 1σ level with those based on the signals at g=2.0006 (X-band, 200 mW), g=2.0006 (Q-band) and g=2.0058 (X-band, after annealing), and they are in agreement at the 2σ level with D_E-values based on the

g=2.0014 signal before annealing. This result suggests that annealing at 150°C for 14 hours does not significantly affect the D_E-values based on the g=2.0014 signal.

12.1.3 Comparisons with independent age controls

The age estimates obtained by radiocarbon analyses of bulk shell 'hash', AMS radiocarbon determinations on individual shells, and ESR analyses are given in Table 12.2. ESR ages based on the signals at g=2.0006 (Q-band) and g=2.0058 (X-band, after annealing) are compared with AMS ^{14}C ages in Figure 12.3.

The ESR ages based on the g=2.0006 signal (Q-band) are much greater than the AMS ^{14}C ages, except for samples 17, 23 and 44 which concur at the 1σ level. Similar results are observed for the ESR ages based on the g=2.0058 signal (X-band, after annealing): ESR ages are much greater than the AMS ^{14}C dates, with only samples 23 and 44 in agreement at the 1σ level. The ESR ages based on the g=2.0014 signal (before annealing) are in closer accord with the AMS ^{14}C dates, as noted previously in section 4.1.3 (see Figure 4.4).

It should be noted that these comparisons are based on the assumption that the external dose rates used for the ESR age calculations are appropriate. Most shell samples examined here, however, are *Anadara trapezia* (see Table 4.1), whose original habitat is muddy environments, such as in estuaries. Muds typically exhibit much higher dose rates than sandy sediments (see Table 4.2(b)). There is, therefore, a reasonable likelihood that the ESR ages obtained could be overestimated due to the use of dose rates for the sandy sediments where the samples were collected. The degree of dose rate underestimation will depend on the length of time the shell spent previously buried in muddy deposits, with the degree of age overestimation being potentially greatest for young shell samples. Calibration of ^{14}C ages from past changes in atmospheric ^{14}C production rates does not significantly reduce the ESR-^{14}C age discrepancies; maximum ^{14}C age increases of 3,000-4,000 years are appropriate for the time periods examined here (see Bard *et al.*, 1993).

12.2 Elands Bay, South Africa

12.2.1 Methods used

The aliquots from Elands Bay, South Africa, that were discussed in Chapters 4 and 10 were used subsequently for the analyses described in this chapter. All samples were annealed for 15 hours at 150°C in an oven (Lindberg, Model 51849) to give rise to the signal at g=2.0058. For aragonite shell samples E4, E7 and E11, additional thermal treatments of 150°C for 15 hours (30 hours total) and 150°C for 30 hours (45 hours total) were made prior to ESR measurements to monitor the changes in D_E-values based on the signals at g=2.0058 and g=2.0014. The signal intensities at g=2.0058 (aragonite and calcite-containing shells) and g=2.0006 (calcite-containing shells) were measured after annealing in the same manner as described in section 5.1, but using a microwave power of 2 mW. The signal intensity at g=2.0014 (aragonite shells) was recorded in the same manner as described in section 4.1.1. The D_E-values based on the signals at g=2.0058, g=2.0014 and g=2.0006 were estimated using the same procedures as described in section 4.1.1, and the ESR ages were calculated in the same manner as described in section 4.2.1.

12.2.2 ESR ages obtained

The D_E-values based on the signals at g=2.0058 (aragonite and calcite-containing shells), g=2.0014 (aragonite shells) and g=2.0006 (calcite-dominated shells) after annealing are compared in Table 12.3 with the results obtained in Chapter 4. Additional D_E-values based on the signals at g=2.0058 and g=2.0014 were obtained for aragonite shell samples E4, E7 and E11 after preheating treatments of 30 hours and 45 hours at 150°C. For sample E13, no D_E-value was obtained because both the g=2.0058 and g=2.0006 signals were overlapped by the Mn^{2+} signal. After annealing at 150°C, the signal intensities at

g=2.0014 for samples E4 (45 hours), E9 and E10 (15 hours) were not measurable, so D_E-values for these samples were not obtained. Some examples of ESR spectra and dose response curves are shown in Figures 12.4(a)-(d). The ESR ages obtained are given in Table 12.4 and compared in Figure 12.5.

g=2.0058 signal (aragonite and calcite-containing shells)

For both aragonite and calcite-containing shell samples, the signal intensities at g=2.0058 increased after annealing. The corresponding dose response curves appear to be saturated at much lower doses (as low as about 300 Gy) than the dose response curves of the signals at g=2.0014 (aragonite shells, before and after annealing) and g=2.0006 (calcite-containing shells, after annealing). This observation is similar to that made for the Forster-Tuncurry shell samples, and the D_E-values based on the g=2.0058 signal are similarly overestimated if all dose points are used in the D_E-value estimations (see Figure 12.4(a)). The D_E-values used in the age calculations were, therefore, estimated by excluding some of the highest dose points; larger random errors in D_E-values were introduced by using fewer data points. For samples E9, E10, E11, E12 and E14, the natural and N+γ signal intensities at g=2.0058 after annealing are close to saturation (see Figure 12.4(b)), and the D_E-values obtained are likely to be overestimates.

For all aragonite shell samples (E4, E7, E9, E10, E11 and E12), the D_E-values based on the g=2.0058 signal after annealing are much greater (1.6-12 times) than the D_E-values for the g=2.0014 signal before annealing (see Figure 12.6). The D_E-values based on the annealed g=2.0058 signal are, however, self-consistent at each site: 0.7-7.9 Gy for Borrew Pit Midden, 33-40 Gy for Malkappan Elandas, <170-260 Gy for Hoedjiespunt 1 and 53-65 Gy for Hoedjiespunt 2. Similar self-consistency is observed in the ESR ages, for which the environmental dose rates are, for these samples, dominated by the external dose rates, as described in section 4.2.2. For Borrew Pit Midden, the ESR ages of samples E1, E2 and E3 based on the g=2.0058 signal after annealing (1.0-3.5 ka) are close to the age of sample E4 based on the g=2.0014 signal before annealing ($\approx$ 2.9 ka),

whereas the ESR age of sample E4 based on the annealed g=2.0058 signal is much greater (≈ 12 ka). For Malkappan Elandas, the samples exhibit ESR ages of 66-89 ka based on the annealed g=2.0058 signal, while sample E7 yielded a much younger ESR age of ≈ 39 ka based on the g=2.0014 signal before annealing. For samples from Hoedjiespunt 1, large discrepancies are observed between the ESR ages based on the g=2.0014 signal before annealing and the ages based on the g=2.0058 signal after annealing. The ESR ages of samples E9 and E10 (*Tellina madagascariensis*) range from 17-42 ka (g=2.0014, before annealing) to 146-199 ka (g=2.0058, after annealing), whereas samples E11 and E12 (*Dosinia lupinus*) yield a tighter age range of 57-77 ka (g=2.0014, before annealing) to 106-126 ka (g=2.0058, after annealing). For Hoedjiespunt 2, samples E15 and E16 indicate ESR ages of 117-139 ka, compared to ≈ 298 ka for sample E14, all ages being based on the annealed g=2.0058 signal. A tighter grouping of ages (86-105 ka) is obtained for all three samples using the g=2.0006 signal after annealing.

For samples E4, E7 and E11, there are no significant changes in the D_E-values based on the g=2.0058 signal induced by prolonged annealing at 150°C for 30 hours or 45 hours; the D_E-values for all three annealing times are in agreement at the 1σ level, as shown in Figure 12.7. For sample E11, large D_E-value errors are introduced because the natural signal intensity is close to the saturation level. This result suggests that increasing the period of preheating at 150°C from 15 hours to 45 hours does not affect the D_E-values based on the g=2.0058 signal, thus implying high thermal stability of this signal in the aragonite shell samples examined.

g=2.0014 signal (aragonite shells)

Annealing at 150°C for 15 hours made no significant change to the pre-annealing D_E-values based on the 2.0014 signal for samples E4 (*Argobuccinum argus*) and E7 (*Burnupena papyracea*). In contrast, marked changes are observed in the pre- and post-annealing (150°C for 15 hours) D_E-values based on the g=2.0014 signal for the samples

from Hoedjiespunt 1 (E9, E10, E11 and E12). For samples E9 and E10 (*Tellina madagascariensis*), D_E-values could not be obtained after annealing because the signal intensities at g=2.0014 in the 'natural' (unirradiated) and some low-dose aliquots were indistinguishable from background. This appears to be caused by an overlap of the g=2.0014 and g=2.0032 signals (see Figure 12.4(b)). Samples E11 and E12 (*Dosinia lupinus*) yield different D_E-values ($\approx$ 107 Gy and 84 Gy, respectively) based on the g=2.0014 signal before annealing, but after annealing at 150°C for 15 hours, their D_E-values agree at the 1σ level ($\approx$ 138 Gy and 136 Gy, respectively). The effects of annealing on the D_E-values based on the g=2.0014 signal appear, therefore, to depend on the shell species: *Argobuccinum argus* (E4) and *Burnupena papyracea* (E7) species are unaffected by annealing at 150°C for 15 hours, whereas *Tellina madagascariensis* (E9 and E10) and *Dosinia lupinus* (E11 and E12) species are strongly affected by annealing. Consequently, only certain shell species contain thermally unstable centre(s) associated with the g=2.0014 signal.

After annealing at 150°C for 30 hours and 45 hours, the D_E-values based on the g=2.0014 signal in samples E4 and E7 do not differ significantly from the D_E-values for either the unannealed aliquots or the aliquots annealed at 150°C for 15 hours; for both samples, all D_E-values agree at the 1σ level (see Figure 12.7). In contrast, the D_E-value based on the g=2.0014 signal of sample E11 (*Dosinia lupinus*) increased after the first 15 hour annealing at 150°C, but then remained unchanged after additional annealing of up to 45 hours total. This indicates that the preheating treatment of 150°C for 15 hours may substantially affect the D_E-values based on the g=2.0014 signal only if the signal includes thermally unstable components that cause the unannealed D_E-values to be underestimated. These unstable centre(s), however, seem to be removed by a 15 hour preheating treatment at 150°C.

g=2.0006 signal (calcite-containing shells)

For shell samples of *Choromytilus meridionalis* (E3, E5 and E13), no D_E-values could be obtained because the g=2.0006 signal was overlapped by the Mn^{2+} signal. The mean D_E-values based on the g=2.0006 signal after annealing are systematically smaller than those based on the annealed g=2.0058 signal (Figure 12.6). For Borrew Pit Midden, samples E1 and E2 yield younger ESR ages based on the annealed g=2.0006 signal (≈ 1.8 ka and <1.2 ka, respectively) than the ages based on the annealed g=2.0058 signal (≈ 3.4 ka and 3.5 ka, respectively). At Hoedjiespunt 2, the D_E-value based on the annealed g=2.0006 signal in sample E15 corresponds at the 1σ level to the D_E-value based on the annealed g=2.0058 signal, but samples E14 and E16 yield substantially smaller D_E-values based on the annealed g=2.0006 signal than those based on the annealed g=2.0058 signal.

At each of the Borrew Pit Midden and Malkappan Elandas sites, however, the pair of ESR ages based on the annealed g=2.0006 signal are similar to the ESR age based on the annealed g=2.0014 signal. The annealed g=2.0006 signal ages of samples E1 and E2 are close to the ESR ages of sample E4 (0.0-2.9 ka) based on the g=2.0014 signal before and after annealing. For samples E6 and E8 from Malkappan Elandas, the ESR ages based on the annealed g=2.0006 signal agree, within their 1σ error limits, at ≈ 50 ka. These ages also compare favourably with those of sample E7 based on the g=2.0014 signal before and after annealing (39 ka and 45 ka, respectively). It is concluded that the D_E-values based on the signals at g=2.0014 (aragonite shells) and g=2.0006 (calcite-containing shells) after annealing are in good agreement at each of these two sites, and thus the ESR ages based on these signals after annealing are also comparable.

12.2.3 Comparisons with independent age controls

Different ages are obtained using the ESR signals at g=2.0058 (aragonite and calcite-containing shells) and g=2.0014 (aragonite shells) or g=2.0006 (calcite-containing shells) after annealing at 150° for 15 hours (or longer). For Borrew Pit Midden, ESR ages of 1-

12 ka (g=2.0058, after annealing) and < 2 ka (g=2.0014 and g=2.0006, after annealing) are obtained. From this site, a radiocarbon age of about 900 years B.P. was obtained from bone. It is possible, however, for the shell samples to yield age overestimates for the deposit if the shells had been reworked prior to deposition of the sediment. Also, as the ESR ages have relatively large errors, it is difficult to define with precision ages younger than a few thousand years by the ESR method. For the samples from Malkappan Elandas, the ESR ages obtained are much younger than the last interglacial: 66-89 ka (g=2.0058, after annealing) and 45-53 ka (g=2.0014 and g=2.0006, after annealing). For samples from Hoedjiespunt 1, for which a last interglacial age was also expected, the ESR ages of samples E9 and E10 (*Tellina madagascariensis*) based on the annealed g=2.0058 signal are too old (182-199 ka and 146-161 ka, respectively), indicating the D_E-values are overestimates. In contrast, the ESR ages of samples E11 and E12 (*Dosinia lupinus*) based on the annealed g=2.0058 signal (106-122 ka and 110-126 ka, respectively) are consistent with a last interglacial age, whereas ESR ages based on the annealed g=2.0014 signal are slightly younger (87-98 ka and 89-101 ka, respectively). For Hoedjiespunt 2, the ESR ages of samples E15 and E16 based on the annealed g=2.0058 signal are in close accordance at about 117-139 ka. The ESR age of sample E14 based on this signal (≈ 298 ka) is clearly an overestimate, but the sample age based on the annealed g=2.0006 signal (≈ 105 ka) is comparable with the ages of samples E15 and E16 (86-104 ka). These ages for Hoedjiespunt 2 are similar to those for Hoedjiespunt 1 and suggest site formation at around the time of, and shortly following, the start of the last interglacial.

12.3 Conclusions

For calcite-containing shell samples from Elands Bay, the 'natural' (unirradiated) aliquots exhibit a dating signal at g=2.0006. After γ-irradiation, however, these aliquots have thermally unstable signals which overlap with the g=2.0006 signal. After a 15 hour preheat at 150°C, these thermally unstable signals are removed; the spectra become comparable to those of the natural aliquots, and the g=2.0006 signal appears to be

isolated. D_E-values based on the g=2.0006 signal can, therefore, be obtained for calcite-containing shell samples after annealing at 150°C for 15 hours.

Using a Q-band spectrometer (≈ 35 GHz, microwave power of 0.6 mW), the dating signal at g=2.0006 in aragonite shell samples, a signal usually attributed to a rapidly rotating CO_2^- centre (e.g. Barabas *et al.*, 1992a, 1992b), appears to be isolated from other signals. The D_E-values based on the g=2.0006 signal (Q-band) are in agreement with those based on the g=2.0006 signal (X-band, microwave power of 200 mW), whereas the D_E-values based on the g=2.0014 signal are smaller. This discrepancy seems to be caused by thermally unstable centre(s) in the g=2.0014 signal and implies that the g=2.0014 signal does not correspond to the CO_2^- centre alone. The contribution of thermally unstable centre(s) to this signal varies between different shell species, but these unstable centre(s) can be removed by a 15 hour preheat at 150°C. For the shell samples from Forster-Tuncurry, the ESR ages based on the g=2.0014 signal (without annealing) are a closer match to the AMS ^{14}C dates than the ESR ages based on the signals at g=2.0058 (after annealing at 150°C for 14 hours) and g=2.0006 (X-band and Q-band), which are older than the AMS ^{14}C dates. However, it is possible that the ESR ages for *Anadara trapezia* species shells (i.e. most of the Forster-Tuncurry samples) are likely to be overestimates. For the shell samples from Elands Bay, the ESR ages based on the signals at g=2.0014 (aragonite shells) and g=2.0006 (calcite-containing shells), after a 15 hour anneal at 150°C, are in agreement at each of the sites. The D_E-values based on these signals are also comparable after annealing for 15 hours at 150°C, suggesting that both signals may be related to the same centre (rapidly rotating CO_2^-), at least for the shell species examined.

With careful estimation, D_E-values based on the annealed g=2.0058 signal concur with those based on the signal at g=2.0006 (X-band and Q-band, before annealing) for approximately 50 % of the shell samples from Forster-Tuncurry. In contrast, D_E-values based on the annealed g=2.0058 signal in samples from Elands Bay are invariably greater than those based on the signals at g=2.0014 (aragonite shells, before and after annealing)

and g=2.0006 (calcite-containing shells, after annealing). The ESR ages obtained, therefore, give two age estimates for each site. Since there is no independent absolute chronology available for each site, it is not possible to select between the annealed g=2.0058 signal and the annealed g=2.0014 or g=2.0006 signals for the most suitable dating signal. However, the g=2.0058 signal after annealing yields ESR ages for certain shell species from Hoedjiespunt 1 and 2 of around, and slightly following, the last interglacial, in accord with geological expectations.

Table 12.1. ESR analyses of shell samples from Forster-Tuncurry Shelf, New South Wales.

Core number (Water depth)	Sub-bottom (cm)	Sample number	D_E-value (Gy), before annealing			D_E-value (Gy), after annealing	
			g=2.0014 (2 mW)	g=2.0006 (200 mW)	g=2.0006 (Q-band)	g=2.0058 (2 mW)	g=2.0014 (2 mW)
FT13-10 (43 m)	120-140	13	29.0 ± 2.0	35.4 ± 1.2	38.4 ± 1.8	39.9 ± 7.8	31.5 ± 5.5
		14	7.0 ± 0.4	15.3 ± 0.4	14.9 ± 1.2	36.0 ± 1.7	-
		15	35.5 ± 3.4	46.5 ±11.7	50.9 ± 2.6	43.4 ± 11.5	44.4 ± 4.0
		17	5.9 ± 0.7	9.1 ± 0.3	6.3 ± 0.4	9.9 ± 0.9	-
		18	5.5 ± 0.6	11.8 ± 0.3	11.5 ± 0.4	10.2 ± 1.5	-
FT14-1 (19 m)	435-445	21	3.4 ± 0.2	8.8 ± 0.1	12.7 ± 0.5	14.6 ± 1.9	-
		22	1.7 ± 0.1	4.0 ± 0.1	2.6 ± 0.2	8.1 ± 0.3	-
		23	0.68 ± 0.06	4.1 ± 0.1	3.8 ± 0.1	4.6 ± 0.2	-
		27	2.5 ± 0.1	4.2 ± 0.2	5.5 ± 0.2	5.1 ± 0.2	-
		28	2.0 ± 0.3	5.6 ± 0.1	5.5 ± 0.4	8.4 ± 0.6	-
		29	3.8 ± 0.8	4.2 ± 0.2	5.2 ± 0.3	8.8 ± 0.9	-
FT/BMR19-3A (90 m)	290-300	43	4.6 ± 0.4	7.2 ± 0.3	7.8 ± 0.7	8.3 ± 0.5	-
		44	4.0 ± 0.3	5.8 ± 0.2	5.6 ± 0.8	4.7 ± 0.4	-
		45	4.2 ± 0.4	6.6 ± 0.2	11.3 ± 1.4	9.7 ± 0.6	-

Notes: Annealing was performed at 150°C for 14 hours.
- : Signal too weak to be measured.

Table 12.2. Age estimates by beta-counting radiocarbon, AMS radiocarbon and ESR for shell samples from Forster-Tuncurry Shelf, New South Wales.

Core number (Water depth)	Sub-bottom (cm)	Sample number	Radiocarbon		ESR age (years), before annealing			ESR age (years), after annealing	
			Shell hash age (years B.P.)	AMS age (years B.P.)	g=2.0014 (2 mW)	g=2.0006 (200 mW)	g=2.0006 (Q-band)	g=2.0058 (2 mW)	g=2.0014 (2 mW)
FT13-10 (43 m)	120-140	14	12,690 ± 83 (Beta 45170)	9,280 ± 400	9,600 ± 600 (10,100 ± 600)	20,900 ± 900 (22,000 ± 800)	20,300 ± 1,800 (21,400 ± 1,800)	47,800 ± 3,100 (51,300 ± 2,900)	
		18		9,905 ± 400	11,300 ± 1,300	23,700 ± 1,200	23,300 ± 1,300	20,700 ± 3,100	-
		17		11,390 ± 350	11,400 ± 1,300	17,500 ± 900	12,100 ± 800	18,900 ± 1,800	-
		15		32,800 ± 800	49,400 ± 5,100	64,200 ± 16,400	70,100 ± 4,500	60,100 ± 16,100	61,400 ± 6,000
		13		35,500 ± 1,100	42,200 ± 3,200	51,400 ± 2,500	55,600 ± 3,200	57,700 ± 11,500	45,800 ± 8,200
FT14-1 (19 m)	435-445	28	8,510 ± 93 (Beta 45432)	6,380 ± 450	4,300 ± 600	12,000 ± 600	11,700 ± 900	17,700 ± 1,600	-
		21		7,010 ± 400	7,000 ± 500	18,000 ± 800	25,800 ± 1,600	29,400 ± 4,000	-
		27		7,520 ± 400	5,100 ± 400 (5,400 ± 400)	8,600 ± 600 (9,200 ± 500)	11,300 ± 700 (12,100 ± 700)	10,600 ± 700 (11,300 ± 600)	-
		23		8,365 ± 400	1,300 ± 100 (1,400 ± 100)	7,700 ± 500 (8,300 ± 400)	7,200 ± 500 (7,800 ± 400)	8,700 ± 700 (9,400 ± 700)	-
		22		8,460 ± 400	2,700 ± 200 (2,800 ± 200)	6,300 ± 300 (6,600 ± 300)	4,200 ± 300 (4,400 ± 300)	12,700 ± 800 (13,400 ± 700)	-
		29		9,090 ± 340	8,200 ± 1,800	8,900 ± 700	11,200 ± 900	18,800 ± 2,200	-
FT/BMR19-3A (90 m)	290-300	43	17,640 ± 113 (Beta 45437)	10,400 ±450	11,400 ± 1,100	17,700 ± 1,200	19,200 ± 2,000	20,300 ± 1,600	-
		44		12,390 ± 450	10,000 ± 900	14,600 ± 900	14,000 ± 2,100	11,800 ± 1,200	-
		45	18,420 ± 281 (Beta 45438)	15,570 ± 470	9,800 ± 1,100 (10,500 ± 1,200)	15,200 ± 1,000 (16,400 ± 900)	25,700 ± 3,500 (28,000 ± 3,700)	22,000 ± 1,900 (23,900 ± 1,800)	-

Notes:
1. ESR ages without and with parentheses are based on early and linear uranium-uptake models, respectively.
2. Annealing was performed at 150°C for 14 hours.
3. Radiocarbon shell hash ages are based on isotopic fractionation corrected ^{14}C depletion with respect to 95% of the activity of NBS oxalic acid using the ^{14}C half-life of 5570 years and assuming a $\delta^{13}C$ value of -1 ± 2‰ with respect to PDB. The ages are corrected for an Oceanic Reservoir Apparent Age of -450 ± 35 years (Gillespie and Polach, 1979).

Table 12.3. ESR D_E-values based on the signals at g=2.0014, g=2.0006 and g=2.0058 (X-band, microwave power of 2 mW) for shell samples from Elands Bay, South Africa.

Sample site	Sample number	Shell species	D_E-values (Gy)							
			Before annealing	Annealed for 15 hours			Annealed for 30 hours		Annealed for 45 hours	
			g=2.0014	g=2.0058	g=2.0014	g=2.0006	g=2.0058	g=2.0014	g=2.0058	g=2.0014
Borrew Pit Midden (Elands 1)	E 1	*Patella granatina apices*	-	2.5 ± 0.3	-	1.3 ± 0.1	-	-	-	-
	E 2	*Patella argenvillei*	-	2.3 ± 0.4	-	0.0 ± 0.7	-	-	-	-
	E 3	*Choromytilus meridionalis*	-	0.69 ± 0.04	-	Mn^{2+}	-	-	-	-
	E 4	*Argobuccinum argus*	1.9 ± 0.2	7.9 ± 2.0	0.7 ± 1.2	-	6.7 ± 1.5	0.0 ± 1.6	6.6 ± 0.8	N/S
Malkappan Elandas (Elands 2)	E 5	*Choromytilus meridionalis*	-	33.0 ± 4.4	-	Mn^{2+}	-	-	-	-
	E 6	*Patella granatina*	-	33.2 ± 10.4	-	20.3 ± 2.0	-	-	-	-
	E 7	*Bumupena papyracea*	19.4 ± 1.0	40.2 ± 4.7	22.4 ± 2.9	-	35.5 ± 7.9	24.3 ± 1.9	35.6 ± 5.6	23.3 ± 1.4
	E 8	*Nucella cingulata*	-	34.0 ± 3.7	-	24.3 ± 4.2	-	-	-	-
Hoedjiespunt 1 (Elands 3)	E 9	*Tellina madagascariensis*	21.8 ± 9.7	260.5 ± 27.9*	N/S	-	-	-	-	-
	E10	*Tellina madagascariensis*	56.8 ± 3.0	225.6 ± 33.0*	N/S	-	-	-	-	-
	E11	*Dosinia lupinus*	106.5 ± 12.9	171.8 ± 22.9*	138.0 ± 7.3	-	121.2 ± 34.6*	126.7 ± 4.4	183.2 ± 46.2*	137.4 ± 7.6
	E12	*Dosinia lupinus*	84.3 ± 5.0	171.5 ± 21.3*	135.7 ± 9.9	-	-	-	-	-
Hoedjiespunt 2 (Elands 4)	E13	*Choromytilus meridionalis*	-	Mn^{2+}	-	Mn^{2+}	-	-	-	-
	E14	*Patella granatina*	-	147.0 ± 16.1*	-	50.5 ± 2.2	-	-	-	-
	E15	*Patella granularis*	-	53.2 ± 6.4	-	47.1 ± 2.3	-	-	-	-
	E16	*Patella argenvillei*	-	65.4 ± 8.6	-	40.0 ± 3.4	-	-	-	-

Notes: 1. Abbreviations: Mn^{2+} = signal overlapped by Mn^{2+} signal; N/S = no signal observed.
2. Annealing temperature is 150°C.
3. The D_E-values marked with an asterisk are considered to be overestimates because the natural signal intensities are close to saturation.

Table 12.4. ESR ages based on the signals at g=2.0014, g=2.0058 and g=2.0006 for shell samples from Elands Bay, South Africa.

Sample site	Sample number	Shell species	ESR ages (ka)							
			Before annealing	Annealed for 15 hours			Annealed for 30 hours		Annealed for 45 hours	
			g=2.0014	g=2.0058	g=2.0014	g=2.0006	g=2.0058	g=2.0014	g=2.0058	g=2.0014
Borrew Pit Midden (Elands 1)	E 1	*Patella granatina apices*	-	3.4 ± 0.5	-	1.8 ± 0.2	-	-	-	-
	E 2	*Patella argenvillei*	-	3.5 ± 0.7	-	0.0 ± 1.2	-	-	-	-
	E 3	*Choromytilus meridionalis*	-	1.0 ± 0.1	-	Mn^{2+}	-	-	-	-
	E 4	*Argobuccinum argus*	2.9 ± 0.3	11.7 ± 3.0	1.0 ± 1.8	-	10.0 ± 2.4	0.0 ± 2.4	9.8 ± 1.4	N/S
Malkappan Elandas (Elands 2)	E 5	*Choromytilus meridionalis*	-	88.8 ± 13.3	-	Mn^{2+}	-	-	-	-
	E 6	*Patella granatina*	-	86.6 ± 28.0	-	53.2 ± 6.6	-	-	-	-
	E 7	*Burnupena papyracea*	38.9 ± 3.1	78.9 ± 10.4	44.6 ± 6.3	-	70.0 ± 16.1	48.3 ± 4.7	70.1 ± 11.9	46.5 ± 4.0
	E 8	*Nucella cingulata*	-	66.2 ± 8.4	-	47.7 ± 8.8	-	-	-	-
Hoedjiespunt 1 (Elands 3)	E 9	*Tellina madagascariensis*	16.6 ± 7.5 (17.3 ± 7.8)	182.4 ± 23.9* (199.2 ± 25.1)*	N/S	-	-	-	-	-
	E10	*Tellina madagascariensis*	39.2 ± 3.2 (41.6 ± 3.3)	145.8 ± 23.9* (160.7 ± 25.4)*	N/S	-	-	-	-	-
	E11	*Dosinia lupinus*	68.2 ± 9.9 (76.5 ± 10.5)	106.3 ± 16.7* (121.5 ± 18.0)*	86.8 ± 8.4 (98.4 ± 8.2)	-	77.0 ± 22.8* (86.8 ± 25.4)*	80.2 ± 7.0 (90.6 ± 6.6)	112.8 ± 30.0* (129.1±33.6)*	86.5 ± 8.5 (98.0 ± 8.3)
	E12	*Dosinia lupinus*	56.9 ± 5.6 (63.7 ± 5.6)	109.9 ± 16.6* (126.4 ± 17.8)*	88.6 ± 9.8 (100.9 ± 9.9)	-	-	-	-	-
Hoedjiespunt 2 (Elands 4)	E13	*Choromytilus meridionalis*	-	Mn^{2+}	-	Mn^{2+}	-	-	-	-
	E14	*Patella granatina*	-	298.2 ± 37.9*	-	105.2 ± 8.1	-	-	-	-
	E15	*Patella granularis*	-	116.8 ± 15.9	-	103.8 ± 8.0	-	-	-	-
	E16	*Patella argenvillei*	-	139.2 ± 20.6	-	86.0 ± 9.4	-	-	-	-

Notes:
1. Abbreviations: Mn^{2+} = signal overlapped by Mn^{2+} signal; N/S = no signal observed.
2. Annealing temperature is 150°C.
3. ESR ages without and with parentheses are based on early and linear uranium-uptake models, respectively.
4. ESR ages marked with an asterisk are considered to be overestimates because the natural signal intensities are close to saturation.

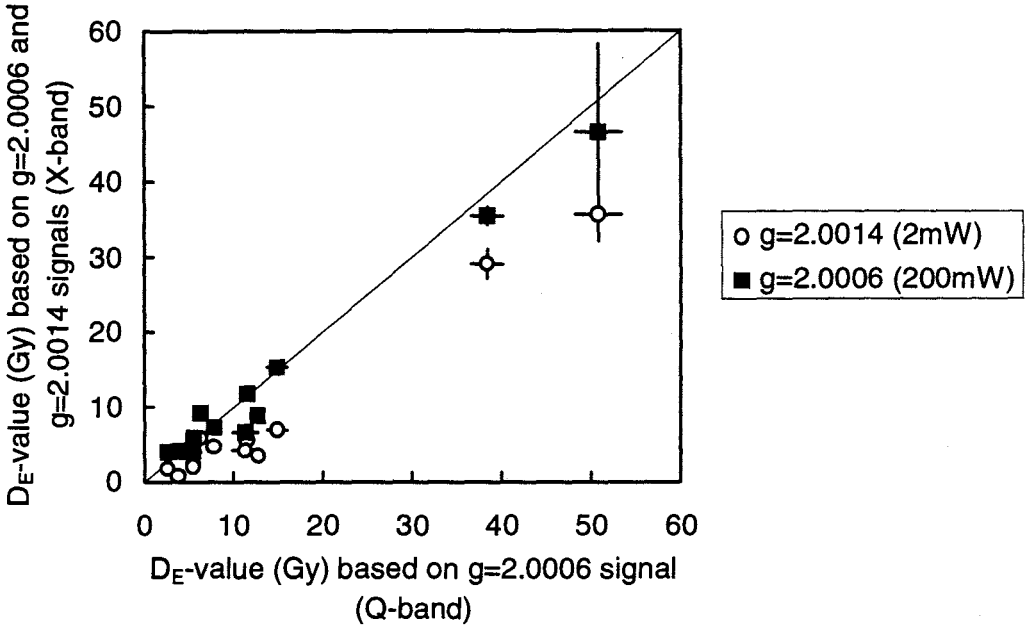

Figure 12.1(a). D_E-values based on the g=2.0006 signal (Q-band) versus those based on the unannealed g=2.0014 (X-band, 2 mW) and g=2.0006 (X-band, 200 mW) signals for shell samples from Forster-Tuncurry Shelf, New South Wales.

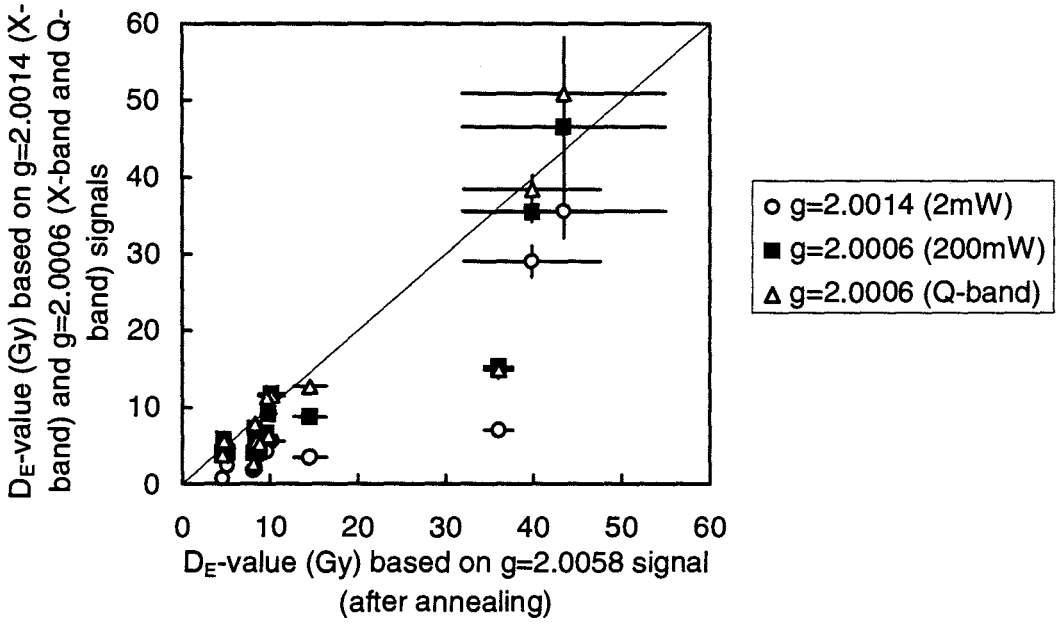

Figure 12.1(b). D_E-values based on the signal at g=2.0058 (X-band, 2 mW after annealing) versus those based on the unannealed signals at g=2.0014 (X-band, 2 mW), g=2.0006 (X-band, 200 mW) and g=2.0006 (Q-band) for shell samples from Forster-Tuncurry Shelf, New South Wales.

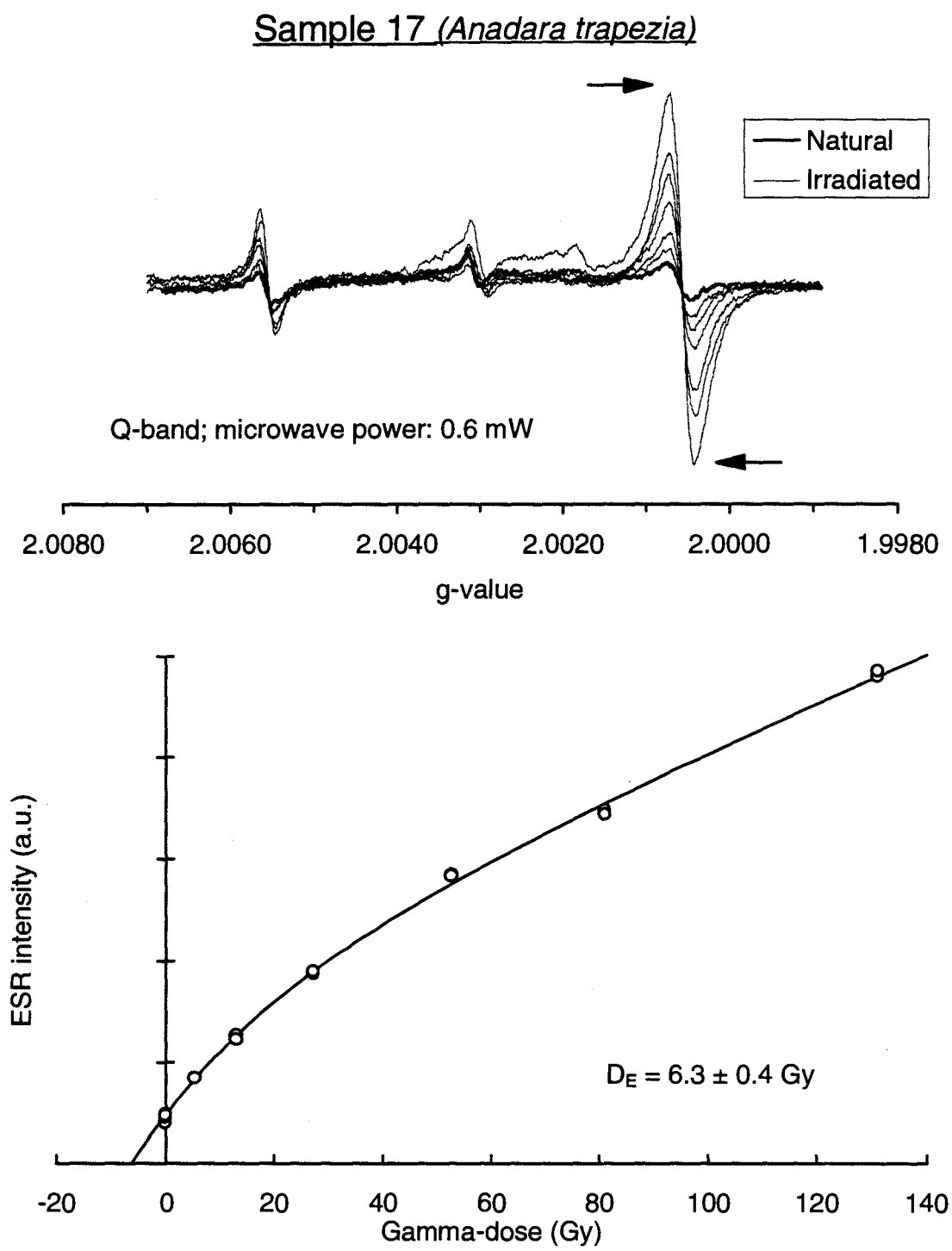

Figure 12.2(a). ESR spectra and dose response curve based on the signal at g=2.0006 (Q-band, microwave power of 0.6 mW) for shell sample 17 (*Anadara trapezia*) from Forster-Tuncurry, New South Wales. The arrows indicate the method used to estimate the peak-to-peak signal height intensity. A D_E-value of 6.3 ± 0.4 Gy was estimated from a saturating-exponential-plus-linear fit.

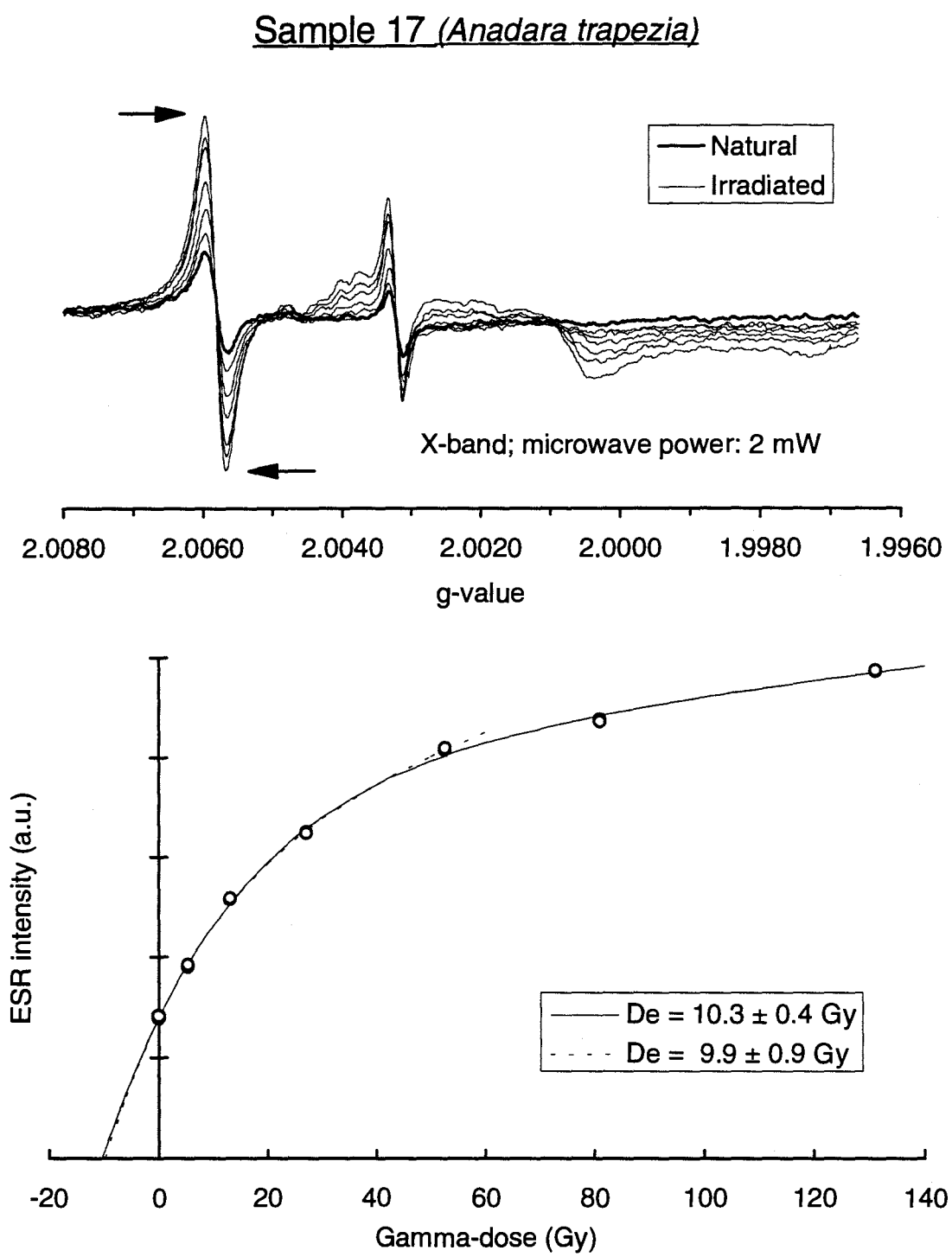

Figure 12.2(b). ESR spectra and dose response curves based on the signal at g=2.0058 (X-band, microwave power of 2 mW) for shell sample 17 (*Anadara trapezia*) from Forster-Tuncurry, New South Wales. The arrows indicate the method used to estimate the peak-to-peak signal height intensity. D_E-values of 10.3 ± 0.4 Gy (solid line) and 9.9 ± 0.9 Gy (dashed line) are estimated from saturating-exponential-plus-linear fits to all dose points and to the first five points, respectively.

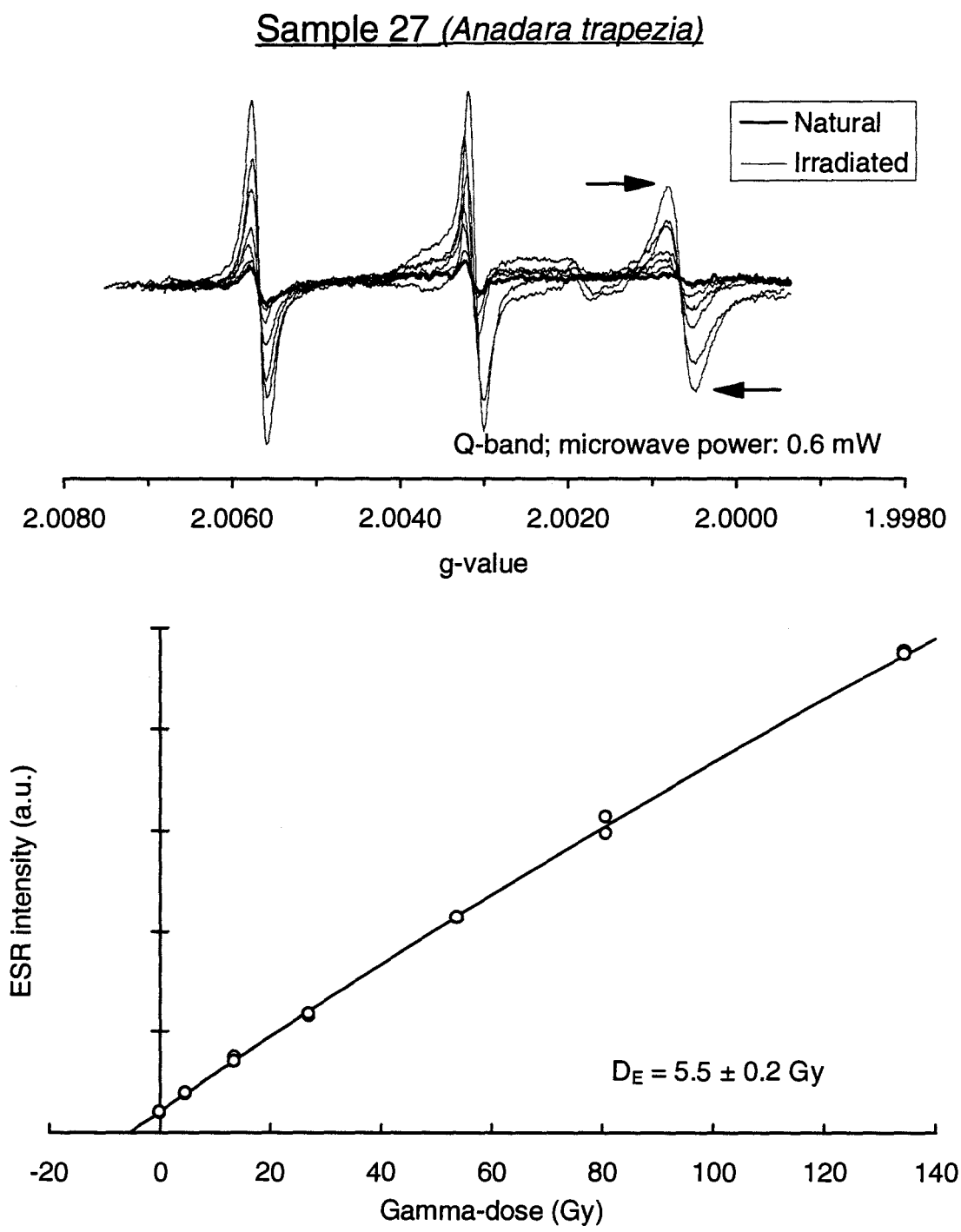

Figure 12.2(c). ESR spectra and dose response curve based on the signal at g=2.0006 (Q-band, microwave power of 0.6 mW) for shell sample 27 (*Anadara trapezia*) from Forster-Tuncurry, New South Wales. The arrows indicate the method used to estimate the peak-to-peak signal height intensity. A D_E-value of 5.5 ± 0.2 Gy was estimated from a saturating exponential fit.

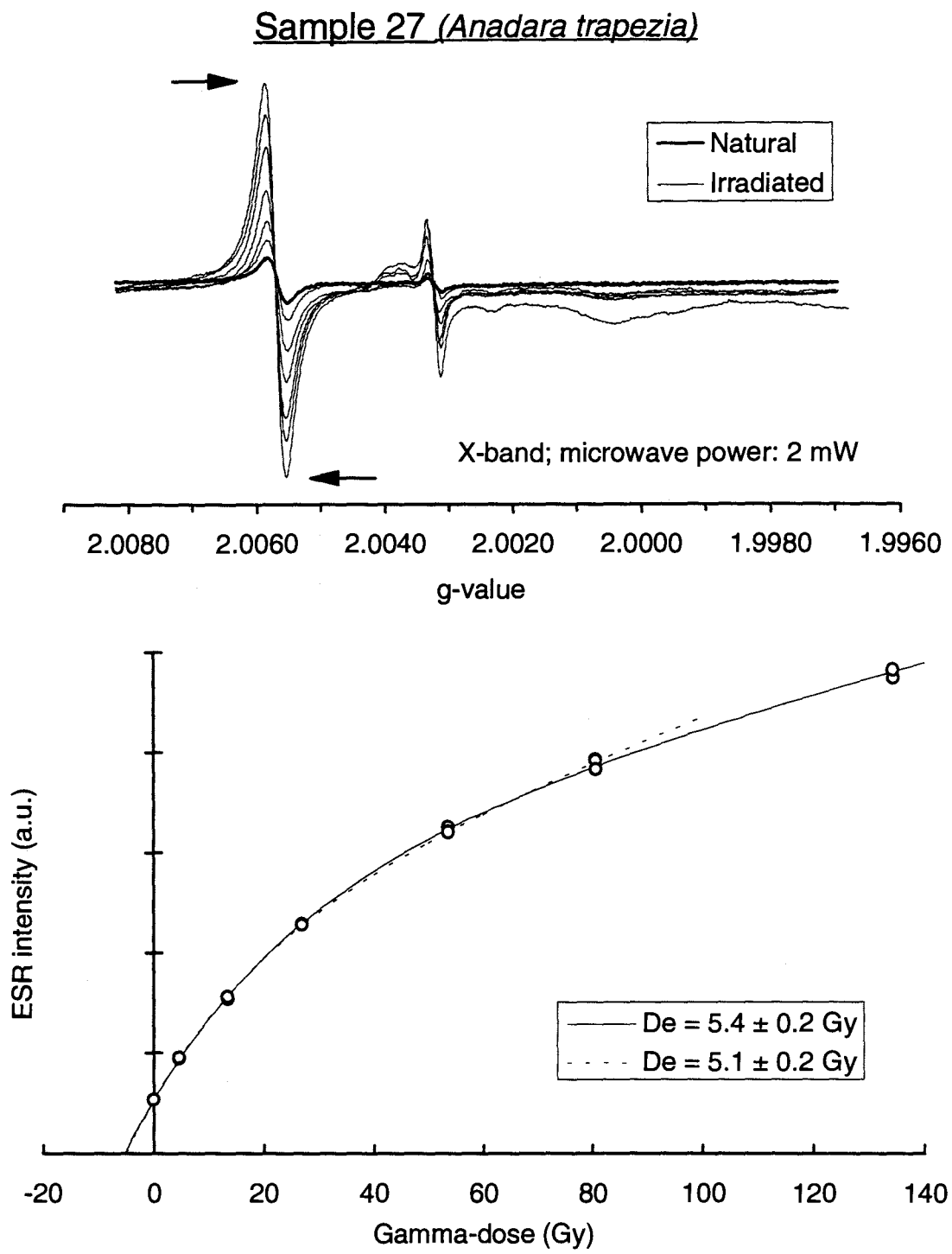

Figure 12.2(d). ESR spectra and dose response curves based on the signal at g=2.0058 (X-band, microwave power of 2 mW) for shell sample 27 (*Anadara trapezia*) from Forster-Tuncurry, New South Wales. The arrows indicate the method used to estimate the peak-to-peak signal height intensity. D_E-values of 5.4 ± 0.2 Gy (solid line) and 5.1 ± 0.2 Gy (dashed line) were estimated from saturating-exponential-plus-linear fits to all dose points and to the first six points, respectively.

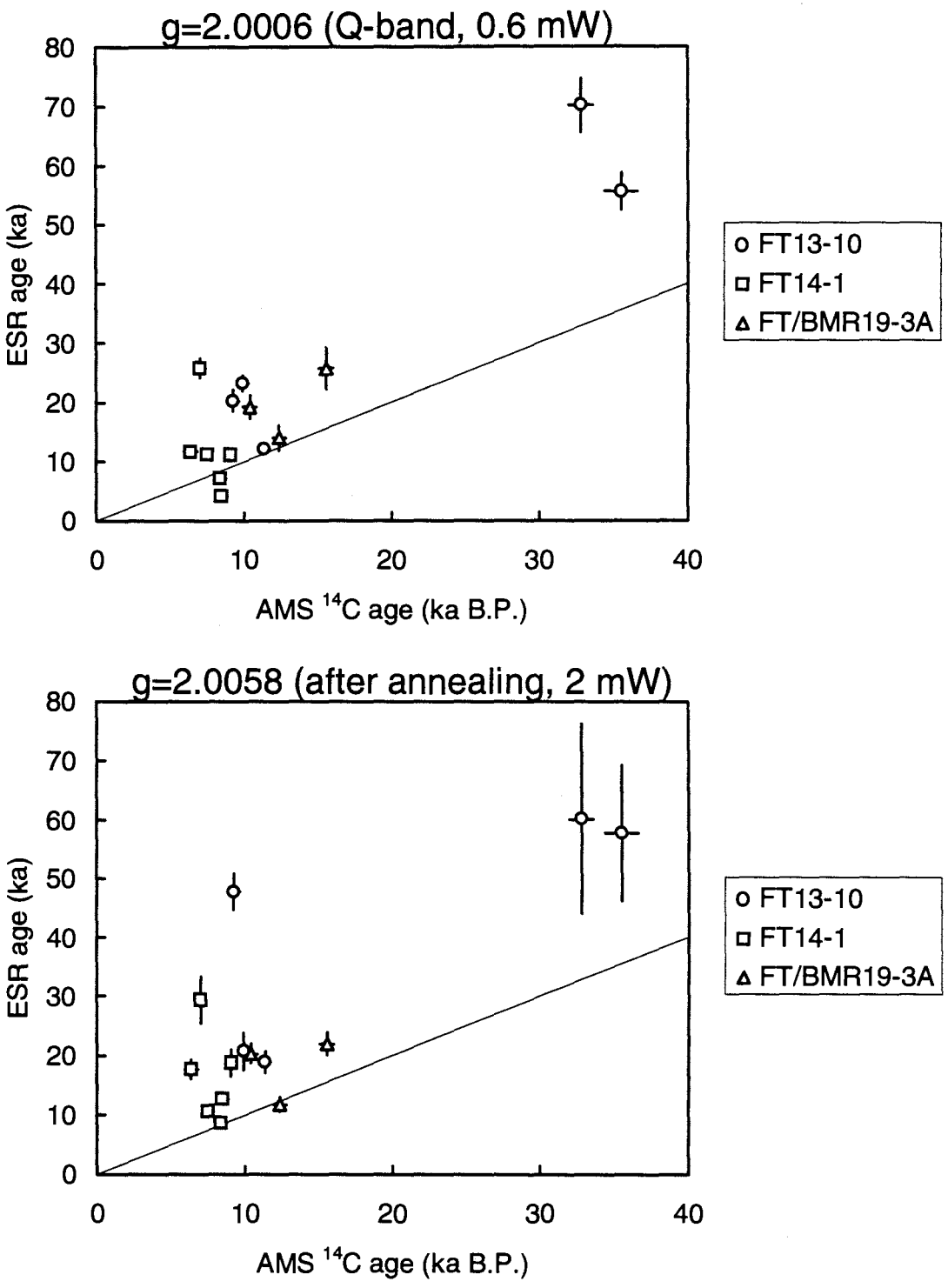

Figure 12.3. Plots of AMS ^{14}C age versus ESR age based on the signals at g=2.0006 (Q-band, microwave power of 0.6 mW) and g=2.0058 (X-band, microwave power of 2 mW, after annealing at 150°C for 14 hours) for shell samples from Forster-Tuncurry Shelf, New South Wales. The ESR ages are calculated based on an early uranium-uptake model.

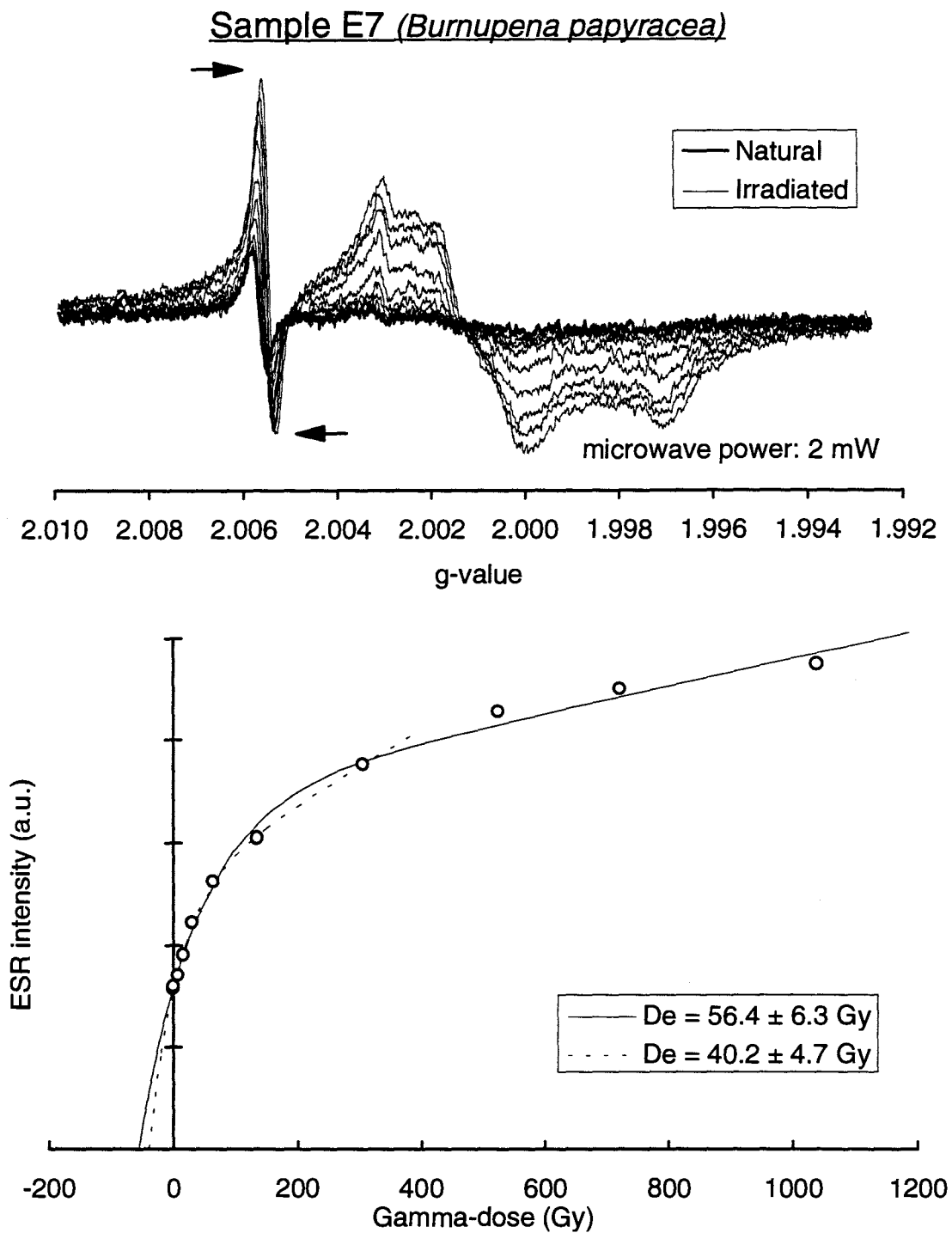

Figure 12.4(a). ESR spectra and dose response curves for shell sample E7 (*Burnupena papyracea*) from Elands Bay, South Africa, after annealing at 150°C for 15 hours. The arrows indicate the method used to estimate the peak-to-peak height intensity at g=2.0058. D_E-values of 56.4 ± 6.3 Gy (solid line) and 40.2 ± 4.7 Gy (dashed line) are obtained from saturating-exponential-plus-linear fits to all dose points and to the first seven points, respectively.

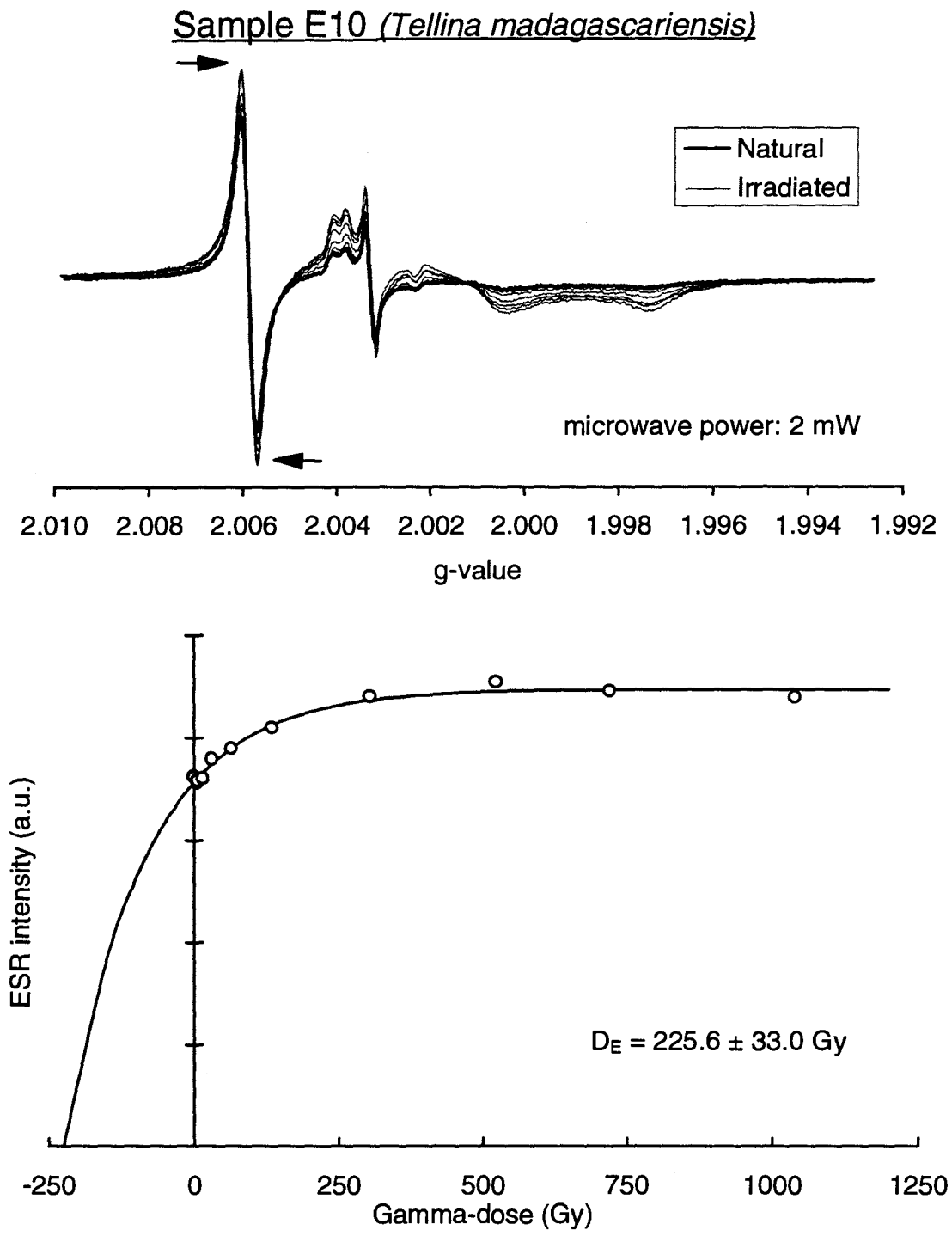

Figure 12.4(b). ESR spectra and dose response curve for shell sample E10 (*Tellina madagascariensis*) from Elands Bay, South Africa, after annealing at 150°C for 15 hours. The arrows indicate the method used to estimate the peak-to-peak height intensity at g=2.0058. A D_E-value of 225.6 ± 33.0 Gy is obtained from a saturating exponential fit.

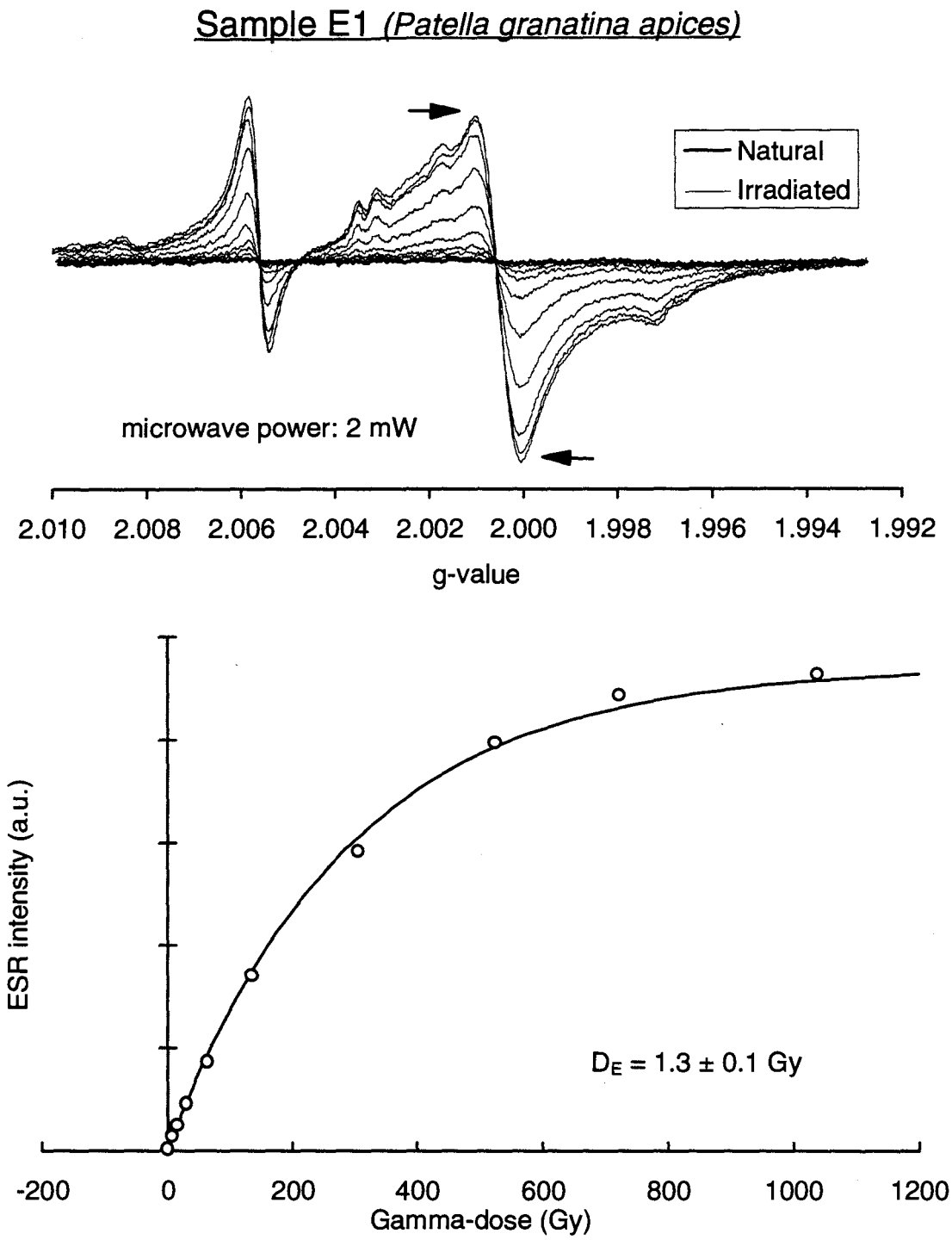

Figure 12.4(c). ESR spectra and dose response curve for shell sample E1 (*Patella granatina apices*) from Elands Bay, South Africa, after annealing at 150°C for 15 hours. The arrows indicate the method used to estimate the peak-to-peak height intensity at g=2.0006. A D_E-value of 1.3 ± 0.1 Gy is obtained from a saturating exponential fit.

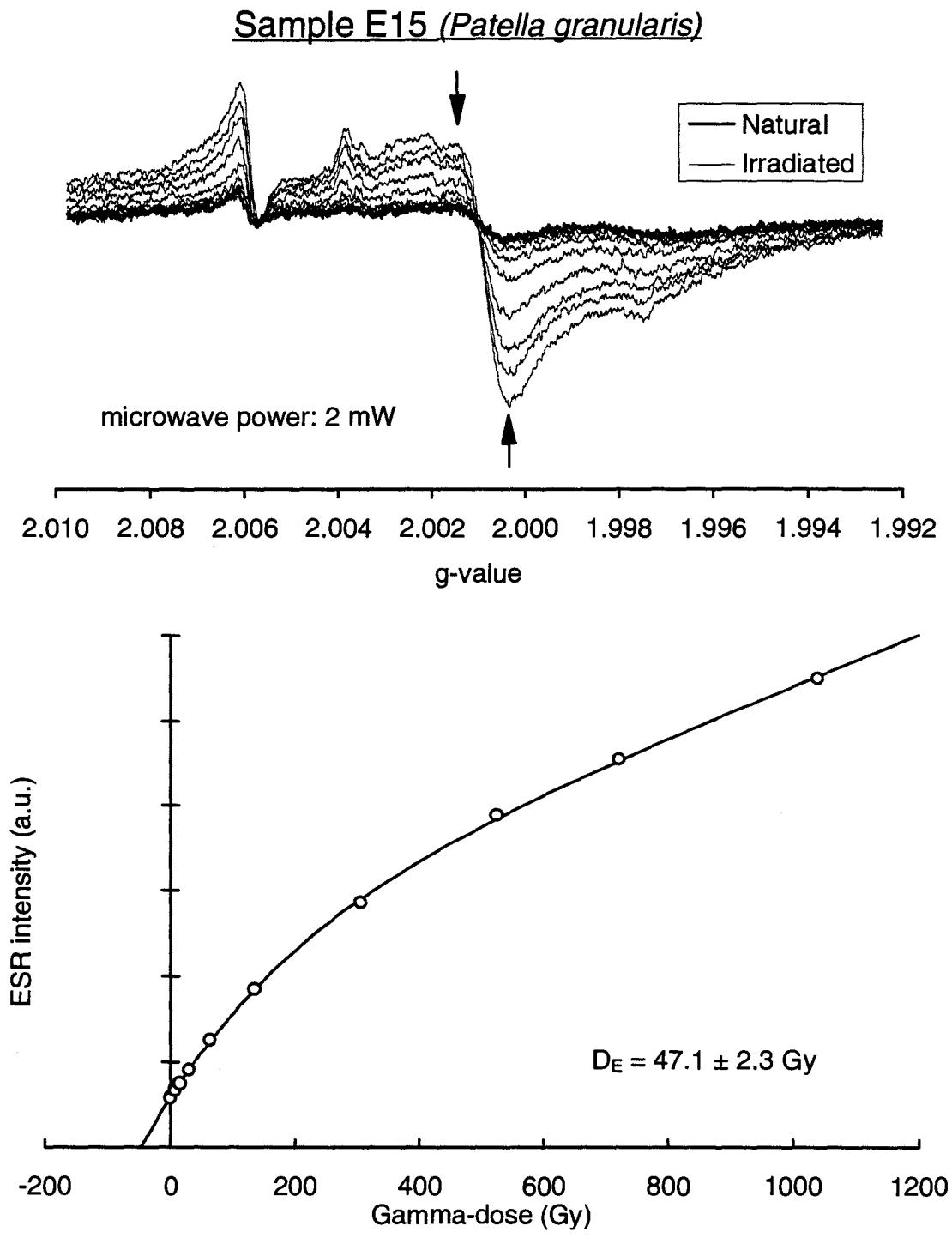

Figure 12.4(d). ESR spectra and dose response curve for shell sample E15 (*Patella granularis*) from Elands Bay, South Africa, after annealing at 150°C for 15 hours. The arrows indicate the method used to estimate the peak-to-peak height intensity at g=2.0006. A D_E-value of 47.1 ± 2.3 Gy is obtained from a saturating-exponential-plus-linear fit.

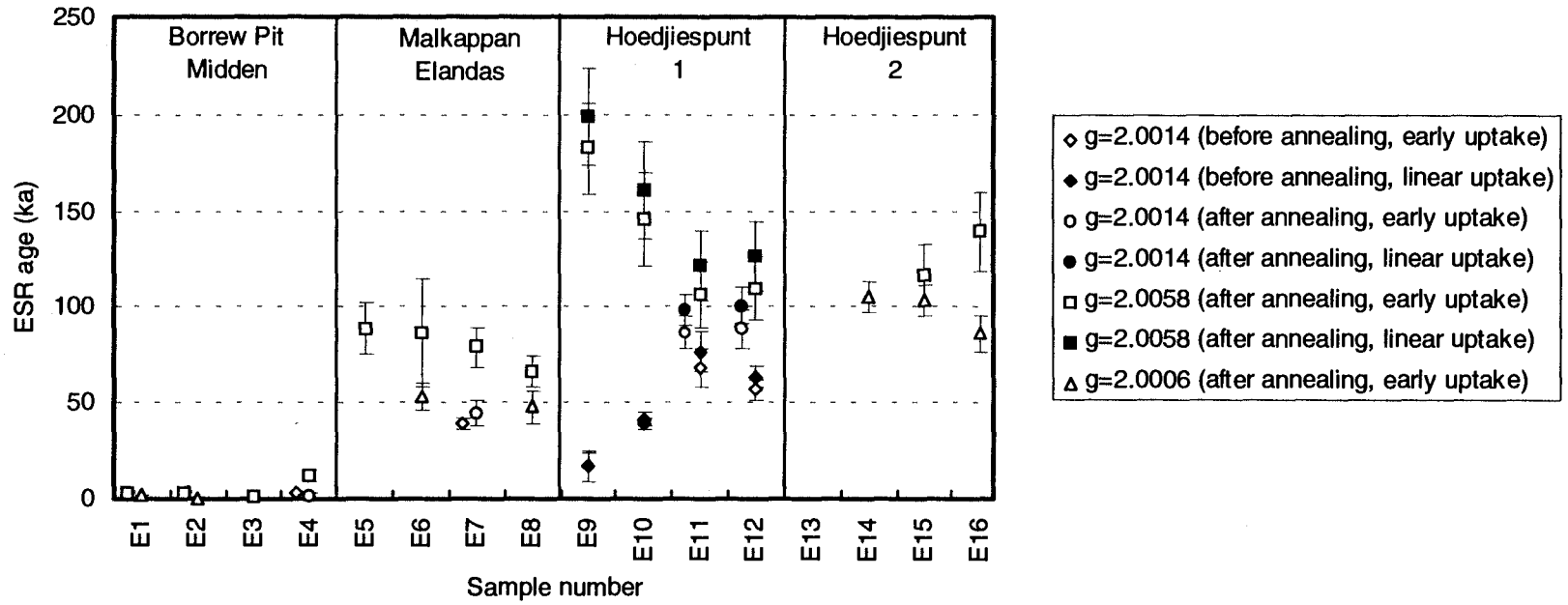

Figure 12.5. ESR dates based on the signals at g=2.0014 (before and after annealing), g=2.0058 and g=2.0006 (after annealing) for shell samples from Elands Bay, South Africa. Annealing was carried out at 150°C for 15 hours. Open and solid symbols represent the ESR ages based on early and linear uranium-uptake models, respectively.

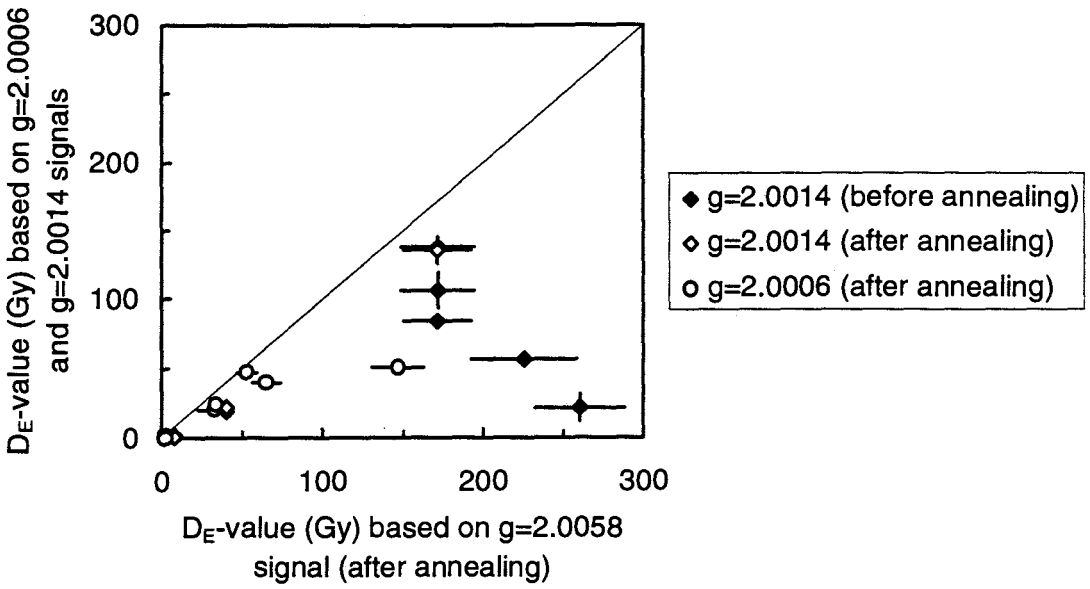

Figure 12.6. D_E-values based on the g=2.0058 signal (after annealing) versus D_E-values based on the signals at g=2.0014 (before annealing), g=2.0014 and g=2.0006 (after annealing) for shell samples from Elands Bay, South Africa. Annealing was carried out at 150° for 15 hours.

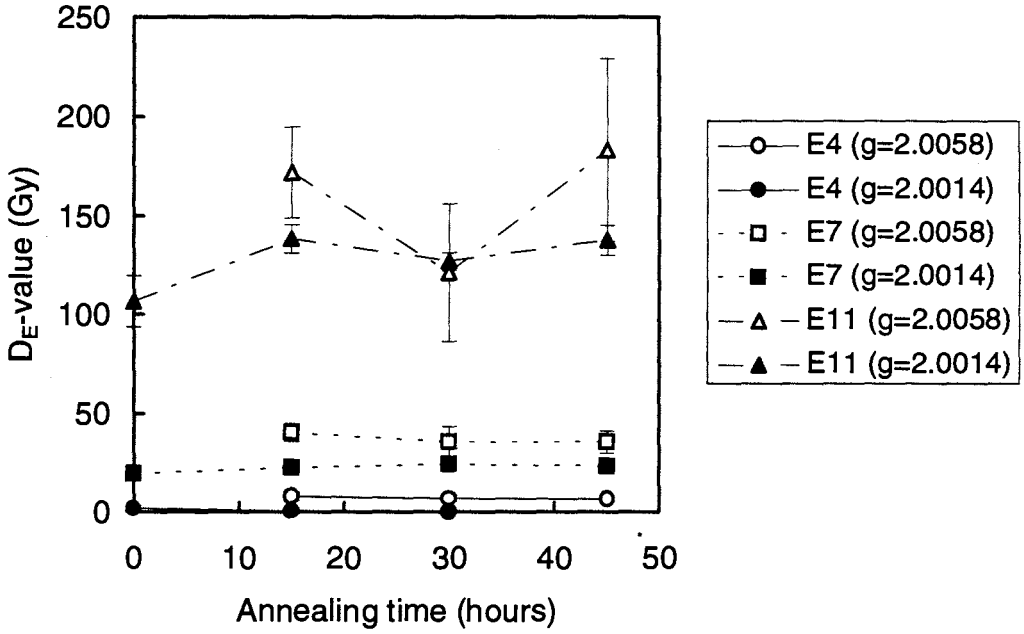

Figure 12.7. D_E-values, based on the signals at g=2.0058 (open symbols) and g=2.0014 (solid symbols), versus annealing time for aragonite shell samples E4 (*Argobuccinum argus*), E7 (*Burnupena papyracea*) and E11 (*Dosinia lupinus*) from Elands Bay, South Africa. Annealing was carried out at 150°C.

Chapter 13 CORAL SAMPLES

Coral samples from Huon Peninsula, Papua New Guinea, were examined using methods not previously attempted, to investigate the advantages of using a Q-band spectrometer and a preheating treatment. For samples 669, 670 and 671, ESR spectra were recorded with a Q-band (≈ 35 GHz) spectrometer to obtain D_E-values based on the signal at g=2.0007. The coral samples were then annealed to remove the thermally unstable component of the signal at g=2.0007, and to transfer unpaired electrons to the signal at g=2.0058. After annealing, ESR measurements of the signals at g=2.0007 and g=2.0058 were performed for all samples. The prospects for dating using the signals at g=2.0007 (Q-band, before annealing), g=2.0007 (X-band, before and after annealing) and g=2.0058 (after annealing) are discussed in the final section of this chapter.

13.1 Methods used

For each sample, the same thirteen aliquots discussed in Chapter 5 were used subsequently for the analyses described in this chapter. The signal intensity at g=2.0007 for samples 669, 670 and 671 was measured with a Q-band (≈ 35 GHz) Varian 4502 EPR spectrometer at room temperature (≈ 21°C), with a modulation frequency of 100 kHz, a microwave power of 0.6 mW, a modulation amplitude of 0.25 Gpp, a scan range of 100 G, a scan speed of 28 G min^{-1} with a time constant of 1 s. All samples were then annealed for 14 hours at 150°C in an oven (Lindberg, Model 51849) to give rise to the signal at g=2.0058 (see Chapter 10). The signals at g=2.0058 and g=2.0007 were measured in the same manner as described in section 5.1 but using a microwave power of 2 mW. The D_E-values based on the signals at g=2.0007 (Q-band, before annealing), g=2.0007 (X-band, after annealing) and g=2.0058 (X-band, after annealing) were estimated using the methods described in section 4.1.1.

13.2 ESR ages obtained

ESR results based on the signals at g=2.0007 (Q-band, before annealing), g=2.0007 (X-band, after annealing) and g=2.0058 (X-band, after annealing) were compared with the results obtained using published methods (see Chapter 5). Table 13.1(a) gives the D_E-value comparisons (see also Figures 13.1(a) and 13.1(b)), while Table 13.1(b) lists the ESR age comparisons (see also Figures 13.2(a) and 13.2(b)). For samples 665, 667 and 669, ESR spectra and dose response curves based on the signal at g=2.0058 are shown in Figures 13.3(a), 13.3(b) and 13.3(c), respectively. Q-band spectra and dose response curves based on the signal at g=2.0007 in samples 669, 670 and 671 are shown in Figures 13.3(d), 13.3(e) and 13.3(f), respectively.

Using a Q-band spectrometer, the signal at g=2.0007 appears to be symmetrical and isolated from the signal at g=2.0020. The D_E-value uncertainties obtained for samples 669, 670 and 671 using a Q-band spectrometer are larger than those obtained using the X-band spectrometer because the cavity of a Q-band spectrometer is much smaller ($\approx$ 9 mm length) than for the X-band ($\approx$ 5 cm). Inaccurate re-positioning of an ESR tube in the Q-band spectrometer is, therefore, more likely to result in poorer tube-to-tube reproducibility. By careful tuning of the spectrometer and re-positioning of the ESR tube, the D_E-values (and ESR ages) based on the signal at g=2.0007, using both X-band (microwave powers of 5 mW and 200 mW) and Q-band, are in agreement at the 1σ level (samples 670 and 671) or 2σ level (sample 669). This suggests that the observed signal intensities at g=2.0007 are comparable for coral samples examined by X-band (microwave powers of 5 mW and 200 mW) and Q-band spectrometers.

The effects of annealing were also examined. After annealing, signal intensities at g=2.0058 in the natural (unirradiated) aliquots decreased by about 7-28 % of the initial intensities, whereas the signals in the irradiated aliquots increased in proportion to the given doses. It appears that the annealed dose response curves of all coral samples saturate at doses above $\approx$ 300 Gy, and D_E-values may be overestimated if the higher dose

points are included in the D_E-value estimations (see Table 13.1(a)). The D_E-values used in the age calculations were therefore estimated using only the first eight dose points (up to 313 Gy added dose) and a saturating-exponential-plus-linear fit; larger errors in D_E-values were introduced by using fewer data points. With only one exception (sample 663; microwave power of 2 mW), the D_E-values obtained using the first eight points are in agreement at the 1σ level with the D_E-values obtained using X-band microwave powers of 5 mW and 200 mW (without annealing prior to spectra measurement). The corresponding ESR ages agree within the 1σ error limits (Table 13.1(b)).

To observe the effect of annealing on the D_E-values based on the signal at g=2.0007 (X-band), the intensity of this signal was measured before and after annealing. With two exceptions (samples 663 and 669), the D_E-values obtained before and after annealing agree at the 1σ level (for samples 662, 664, 666, 668 and 670) or 2σ level (for samples 665, 667 and 671). It is concluded, therefore, that the heating treatment of 14 hours at 150°C does not substantially affect the D_E-values based on the signal at g=2.0007. The ESR ages based on this signal before and after annealing are also in good agreement at the 1σ level (see Table 13.1(b)).

13.3 Comparisons with independent age controls

The age estimates obtained by alpha spectrometric and mass spectrometric uranium-series methods, geological expectations, and the ESR methods employed in this study and by Grün *et al.* (1992) are compared in Table 13.2. The $^{230}Th/^{234}U$ ages in parentheses are not considered for age comparisons since these samples are regarded as yielding unreliable data (see Table 13.2).

The ESR ages based on the Q-band signal at g=2.0007 and the X-band signals at g=2.0058 and g=2.0007 (after annealing) in samples 670 and 671 (terrace II) compare favourably with the ages of ≈ 41-44 ka and ≈ 50-53 ka, respectively, estimated by alpha spectrometric and mass spectrometric uranium-series methods. These dates are much

older than the geological estimate of 29 ka but other alpha spectrometric U-series ages (Omura *et al.*, 1994) indicate that the geological estimate may be too young. The ESR ages of samples 664 and possibly 666 (terrace IIIb) agree with the geological estimate of about 40 ka, whereas the ESR ages of sample 665 agree more closely with the U-series ages of 53-56 ka. ESR ages of samples 668 and 669 (terrace IIIa) concur with the geological estimate (44-53 ka), whereas sample 667 yielded much larger ESR ages than either the U-series ages (49-58 ka) or the geological estimate. The ESR ages of samples 662 and 663 (terrace IV) are in close agreement with the geological and U-series age estimates (69-73 ka).

The ESR ages are plotted against the U-series ages in Figures 13.2(a) and 13.2(b). The g=2.0058 signal ages appear to systematically overestimate the U-series ages, although the wide error limits on the ESR age determinations mask any definite trend (Figure 13.2(a)). Certainly, the g=2.0007 signal ages show no such pattern (Figure 13.2(b)).

13.4 Conclusions

Using a Q-band spectrometer, the signal at g=2.0007 appears to be isolated from the other signals, as reported by Barabas *et al.* (1992a). With careful tuning and re-positioning of the ESR tube, D_E-values based on the signal at g=2.0007 (Q-band) agree with those obtained using an X-band spectrometer (at microwave powers of 5 mW and 200 mW). This suggests that the signal intensities at g=2.0007 in coral samples are comparable using both X-band and Q-band spectrometers.

Annealing at 150°C for 14 hours does not significantly affect the D_E-values based on the signal at g=2.0007 in corals. The D_E-values obtained after annealing are similar to those based on the annealed g=2.0058 signal and agree at the 1 σ level, with only one exception. This supports the findings described in Chapter 10 that, after annealing at 150°C for 14 hours, the signal at g=2.0058 has potential for dating of coral. It also could be suitable for dating other carbonate materials (e.g. mollusc shell) that do not possess a clear g=2.0007

signal. A preheating treatment may therefore be used for corals prior to ESR measurements; signals at both g=2.0007 and g=2.0058 are suitable for dating after annealing (150°C for 14 hours). As the preheating treatment employed was, however, proposed originally for the signal at g=2.0058 (see Chapter 10), further investigation of the g=2.0007 signal is warranted to examine a wider range of annealing temperatures and times.

For samples from terrace II and IIIb, only minor differences are observed in the ESR ages obtained using the annealed and unannealed signals at g=2.0007 and g=2.0058. In both cases, the ESR ages are much greater than the geological estimates but the ESR ages are supported by alpha spectrometric and mass spectrometric U-series dates, suggesting that the geological evaluation is incorrect. At the other sites, ESR ages based on the signals at g=2.0007 and g=2.0058 after annealing (150°C for 14 hours) concur with alpha spectrometric and mass spectrometric U-series ages and with geological estimates. Since annealing does not affect the D_E-values (and ESR ages) significantly, published methods (without any thermal pretreatment) may be as reliable as the annealing procedures described in this study.

Finally, since a higher microwave power improves the signal-to-noise ratio (Barabas *et al.*, 1992a), it may be more practical to use a higher microwave power for ESR measurements of the signal at g=2.0007, particularly for younger samples. The D_E-value obtained appears to be insensitive to microwave power (see Table 13.1(a)), so the most favourable signal-to-noise ratio should be exploited to minimise the analytical errors.

Table 13.1(a). ESR analyses of corals from Huon Peninsula, Papua New Guinea (after Grün *et al.*, 1992; Chappell *et al.*, 1994a, 1994b and Omura *et al.*, 1994).

Lab. no.	Reef	Field no. (Lab. no.)	D_E-values[1] (Gy)						
			Grün *et al.* (1992)	This study					
				g=2.0007 (before annealing)			after annealing[2]		
			g=2.0007 (5 mW)	X-band		Q-band (0.6 mW)	g=2.0058 (2 mW)		g=2.0007 (2 mW)
				5 mW	200 mW		(all points)	(8 points)[3]	
670	terrace II (29 ka)	KWA I1 (KK-08)	31.5 ± 2.8	30.8 ± 2.0	28.1 ± 0.9	26.9 ± 2.9	33.7 ± 1.7	30.5 ± 1.8	31.2 ± 1.5
671		KWA N1 (AO344)	31.7 ± 2.5	32.1 ± 1.4	30.8 ± 1.4	34.8 ± 3.1	37.8 ± 2.5	31.0 ± 2.3	27.6 ± 1.3
666	terrace IIIb (40 ka)	KWA J1 (KK-10)	37.6 ± 2.3	34.3 ± 2.8	-	-	55.8 ± 4.4	33.4 ± 9.8	29.6 ± 3.4
664		KAN C2 (KK-11)	23.7 ± 2.0	23.6 ± 1.3	-	-	34.8 ± 3.4	31.3 ± 7.3	25.8 ± 1.3
665		KWA K1 (AO347)	31.5 ± 2.7	40.8 ± 1.7	-	-	49.8 ± 3.4	38.0 ± 5.1	32.8 ± 2.7
669	terrace IIIa (44 - 53 ka)	KAN D4 (AO345)	40.5 ± 4.4	44.3 ± 1.2	39.4 ± 1.5	32.3 ± 4.0	50.5 ± 3.6	40.8 ± 3.1	31.9 ± 2.5
667		KWA Q1 (AO346)	37.3 ± 4.0	45.4 ± 2.5	-	-	52.7 ± 2.9	49.3 ± 6.6	51.1 ± 2.9
668		KAN D5 (AO360)	41.7 ± 4.4	43.2 ± 1.7	-	-	52.2 ± 1.9	38.3 ± 6.7	42.9 ± 3.1
663	terrace IV (70 ka)	SIAL E1 (AO369)	50.1 ± 5.4	60.4 ± 2.0	-	-	67.4 ± 4.2	48.3 ± 2.0	51.8 ± 2.2
662		FRT F1 (AO349)	48.7 ± 4.1	50.6 ± 3.2	-	-	61.3 ± 4.9	52.1 ± 7.6	54.3 ± 3.3

Notes:
1. D_E-values were estimated by a saturating-exponential-plus-linear fit. Each aliquot was weighted by the inverse square of its ESR signal intensity using the 'DOSE' program (Brumby, 1992).
2. Samples were annealed for 14 hours at 150°C.
3. First 8 points (aliquots with 0 - 313 Gy added dose) were used for the D_E-value estimations.

Table 13.1(b). ESR ages of corals from Huon Peninsula, Papua New Guinea (after Grün *et al.*, 1992; Chappell *et al.*, 1994a, 1994b and Omura *et al.*, 1994).

Lab. no.	Reef	Field no. (Lab. no.)	U (ppm)	ext. D (μGy a^{-1})	ESR age (years)					
					Grün *et al.* (1992)	This study				
						g=2.0007 (before annealing)			after annealing[1]	
					g=2.0007 (5 mW)	X-band		Q-band	g=2.0058 (2 mW) (8 points)[2]	g=2.0007 (2 mW)
						5 mW	200 mW	(0.6 mW)		
670	terrace II (29 ka)	KWA I1 (KK-08)	3.12	140 ± 30	49,000 ± 5,400	48,200 ± 4,300	44,800 ± 3,200	43,000 ± 5,500	47,700 ± 4,200	48,600 ± 3,900
671		KWA N1 (AO344)	2.64	140 ± 30	54,400 ± 5,600	55,000 ± 4,300	53,200 ± 4,300	58,000 ± 6,500	53,000 ± 5,300	48,900 ± 4,100
666	terrace IIIb (40 ka)	KWA J1 (KK-10)	3.12	140 ± 30	56,200 ± 4,900	52,300 ± 5,300	-	-	51,300 ±15,300	46,700 ± 6,100
664		KAN C2 (KK-11)	3.16	140 ± 30	38,900 ± 4,200	38,800 ± 3,300	-	-	48,400 ±11,700	41,600 ± 3,400
665		KWA K1 (AO347)	2.93	140 ± 30	50,900 ± 5,500	62,100 ± 4,600	-	-	58,800 ± 8,700	52,500 ± 5,400
669	terrace IIIa (44 - 53 ka)	KAN D4 (AO345)	3.81	140 ± 30	52,600 ± 6,500	56,300 ± 3,600	51,500 ± 3,600	44,000 ± 6,100	52,900 ± 5,100	43,800 ± 4,300
667		KWA Q1 (AO346)	3.17	140 ± 30	55,300 ± 6,900	64,200 ± 5,200	-	-	68,300 ±10,000	70,300 ± 5,700
668		KAN D5 (AO360)	3.68	140 ± 30	54,900 ± 6,600	56,400 ± 4,000	-	-	51,500 ± 9,600	56,100 ± 5,200
663	terrace IV (70 ka)	SIAL E1 (AO369)	2.70	140 ± 30	68,000 ± 8,400	78,300 ± 5,200	-	-	66,200 ± 4,900	69,700 ± 5,200
662		FRT F1 (AO349)	3.26	140 ± 30	74,600 ± 7,800	76,800 ± 6,800	-	-	78,500 ±12,400	81,000 ± 7,000

Notes:
1. Samples were annealed for 14 hours at 150°C.
2. First 8 points (aliquots with 0 - 313 Gy added dose) were used for the D_E-value estimations.
3. Abbreviation: ext. D = external dose rate. This consists only of the assumed cosmic ray dose rate of 140 ± 30 μGy a^{-1} which corresponds to a depth of about 3 ± 2 m below the ground surface (after Prescott and Hutton, 1988).
4. An initial $^{234}U/^{238}U$ ratio of 1.14 ± 0.01 was assumed. Modern sea water has a mean value of 1.144 ± 0.002 (Chen *et al.*, 1986).
5. An alpha efficiency value (k) of 0.05 ± 0.01 was used, following Grün *et al.* (1992).

Table 13.2. Age estimates for corals from Huon Peninsula, Papua New Guinea (after Grün *et al.*, 1992; Chappell *et al.*, 1994a, 1994b and Omura *et al.*, 1994).

Lab. no.	Reef	Field no. (Lab no.)	Alpha spectrometric U-series age	Mass spectrometric U-series age	ESR age (years)					
					Grün *et al.* (1992)	This study				
						g=2.0007 (before annealing)			after annealing[1]	
					g=2.0007 (5 mW)	X-band 5 mW	X-band 200 mW	Q-band (0.6 mW)	g=2.0058 (2 mW) (8 points)	g=2.0007 (2 mW)
-	terrace IIc	BOBO U21 (KS-15)	33,400 ± 600	-	-	-	-	-	-	-
-	terrace IIa	KANZ U14	34,800 ± 130	-	-	-	-	-	-	-
-		BOBO U10	37,800 ± 250	-	-	-	-	-	-	-
-		KANZ U9 (AO403)	41,800 ± 600	-	-	-	-	-	-	-
670	terrace II	KWA I1 (KK-08)	44,000 ± 1,400	41,120 ± 500	49,000 ± 5,400	48,200 ± 4,300	44,800 ± 3,200	43,000 ± 5,500	47,700 ± 4,200	48,600 ± 3,900
671	(29 ka)	KWA N1 (AO344)	50,500 ± 1,300	52,860 ± 440	54,400 ± 5,600	55,500 ± 4,300	53,200 ± 4,300	58,000 ± 6,500	53,000 ± 5,300	48,900 ± 4,100
666	terrace IIIb (40 ka)	KWA J1 (KK-10)	(38,200 ± 1,100)[a,b]	-	56,200 ± 4,900	52,300 ± 5,300	-	-	51,300 ± 15,300	46,700 ± 6,100
-		KANZ 34 (KS-12)	44,500 ± 700	-	-	-	-	-	-	-
664		KAN C2 (KK-11)	(46,400 ± 1,600)[b]	-	38,900 ± 4,200	38,800 ± 3,300	-	-	48,400 ±11,700	41,600 ± 3,400
665		KWA K1 (AO347)	56,000 ± 1,500	53,160 ± 430	50,900 ± 5,500	62,100 ± 4,600	-	-	58,800 ± 8,700	52,500 ± 5,400
669	terrace IIIa (44 - 53 ka)	KAN D4 (AO345)	(42,300 ± 1,100)[a]	-	52,600 ± 6,500	56,300 ± 3,600	51,500 ± 3,600	44,000 ± 6,100	52,900 ± 5,100	43,800 ± 4,300
-		KAN D4 (AO359)	(42,800 ± 1,100)[a]	-	-	-	-	-	-	-
667		KWA Q1 (AO346)	57,500 ± 1,500	48,970 ± 1,590	55,300 ± 6,900	64,200 ± 5,200			68,300 ±10,000	70,300 ± 5,700
668		KAN D5 (AO360)	(57,800 ± 1,400)[b]	(46,360 ± 710)[b]	54,900 ± 6,600	56,400 ± 4,000	-	-	51,500 ± 9,600	56,100 ± 5,200
-		KAN D5 (KK-09)	(61,600 ± 2,000)[b]	-	-	-	-	-	-	-
-	terrace $IIIa_l$	KANZ 33 (KS-17)	45,800 ± 700	-	-	-	-	-	-	-
-	terrace $IIIa_m$	KANZ 4 (KS-16)	51,200 ± 800	-	-	-	-	-	-	-
-	terrace $IIIa_u$	KANZ 3 (KS-11)	51,800 ± 800	-	-	-	-	-	-	-
-	terrace $IIIa_{u+}$	KANZ 1	61,000 ± 550	-	-	-	-	-	-	-
663	terrace IV (70 ka)	SIAL E1 (AO369)	(65,800 ± 1,800)[b]	(59,120 ± 1,290)[b]	68,000 ± 8,400	78,300 ± 5,200	-	-	66,200 ± 4,900	69,700 ± 5,200
662		FRT F1 (AO349)	72,800 ± 2,200	69,130 ± 730	74,600 ± 7,800	76,800 ± 6,800	-	-	78,500 ±12,400	81,000 ± 7,000

Notes:
1. Samples were annealed for 14 hours at 150°C.
2. $^{230}Th/^{234}U$ ages in parentheses are considered to be unreliable since those samples do not meet the following criteria:
   (a) The uranium concentration should be the same as in present-day counterparts (2 to 4 ppm).
   (b) The initial $^{234}U/^{238}U$ activity ratio, $(^{234}U/^{238}U)_0$, should be consistent with that in modern sea water, 1.13 to 1.16 (mean = 1.144 ± 0.002; Chen *et al.*, 1986).
   (c) The sample should be free (i.e. contain < 0.02 ppm) of initial ^{230}Th incorporated at its living stage, and/or secondary ^{230}Th, introduced by contamination during diagenesis.

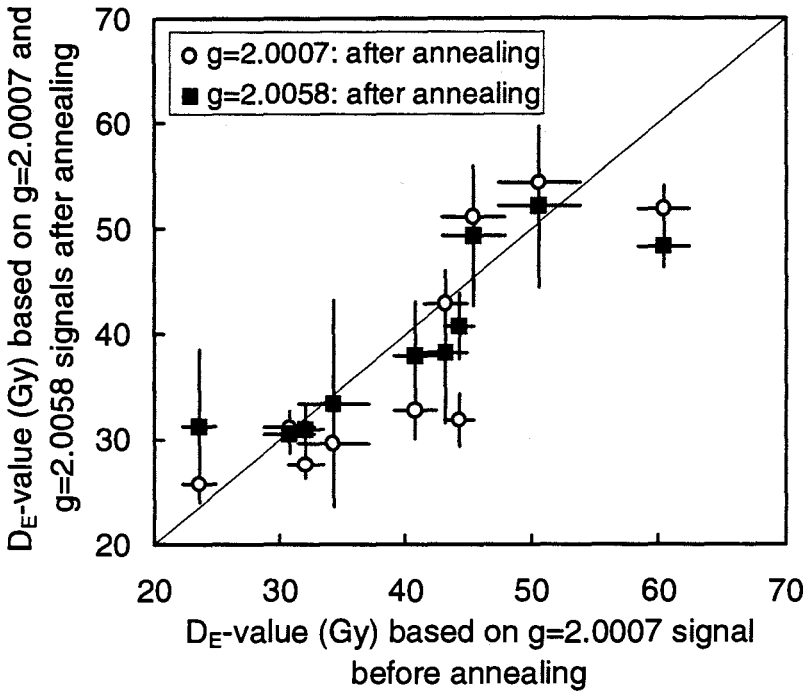

Figure 13.1(a). D_E-values based on g=2.0007 signal (before annealing) versus D_E-values based on g=2.0007 and g=2.0058 signals after annealing at 150°C for 14 hours.

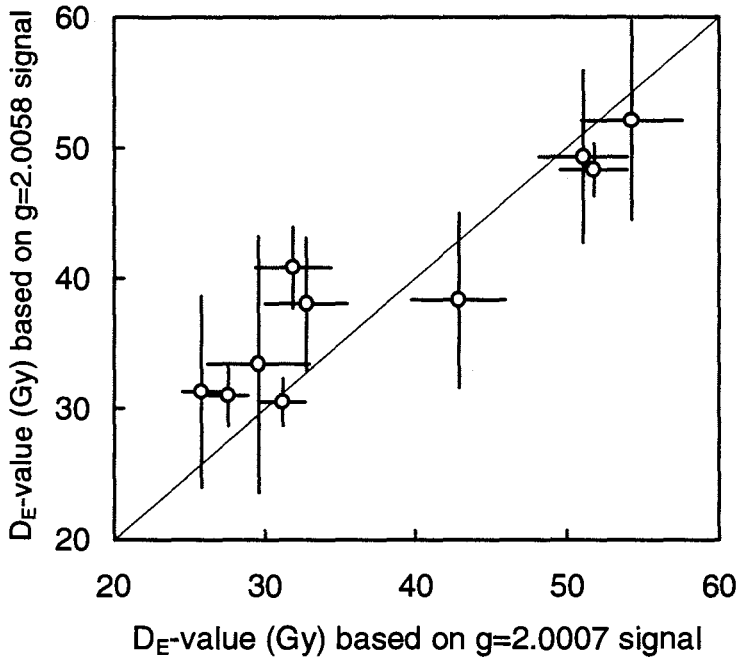

Figure 13.1(b). D_E-values based on g=2.0007 signal versus D_E-values based on g=2.0058 signal (both after annealing at 150°C for 14 hours).

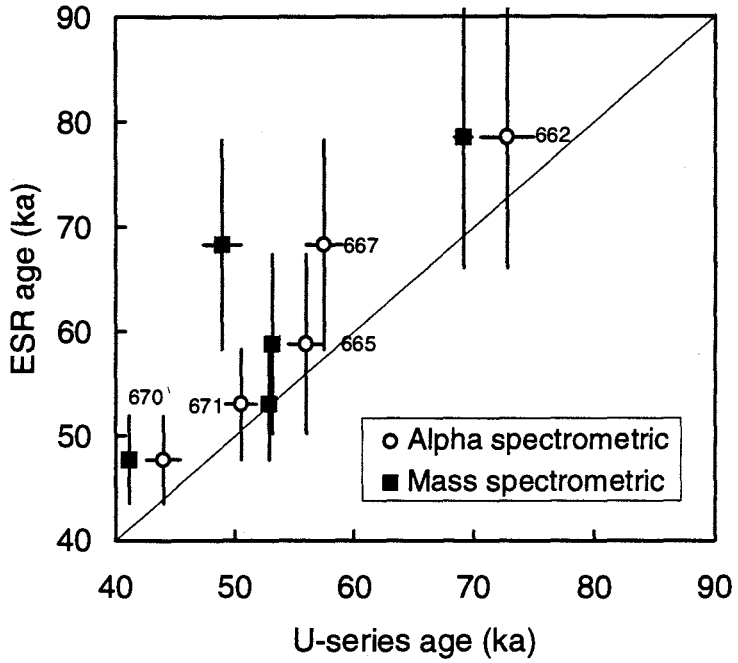

Figure 13.2(a). ESR ages, based on the signal at g=2.0058 after annealing (150°C for 14 hours), versus alpha spectrometric (circles) and mass spectrometric (squares) U-series ages.

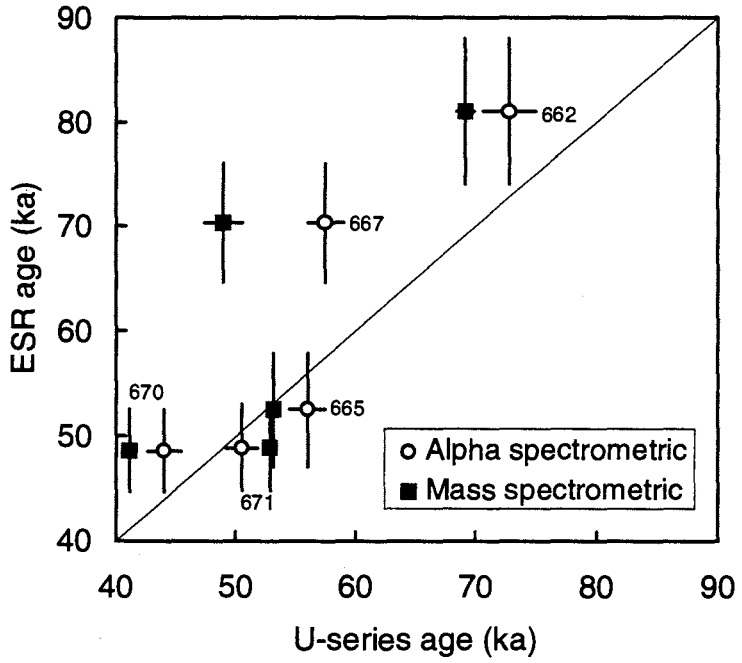

Figure 13.2(b). ESR ages, based on the signal at g=2.0007 after annealing (150°C for 14 hours), versus alpha spectrometric (circles) and mass spectrometric (squares) U-series ages.

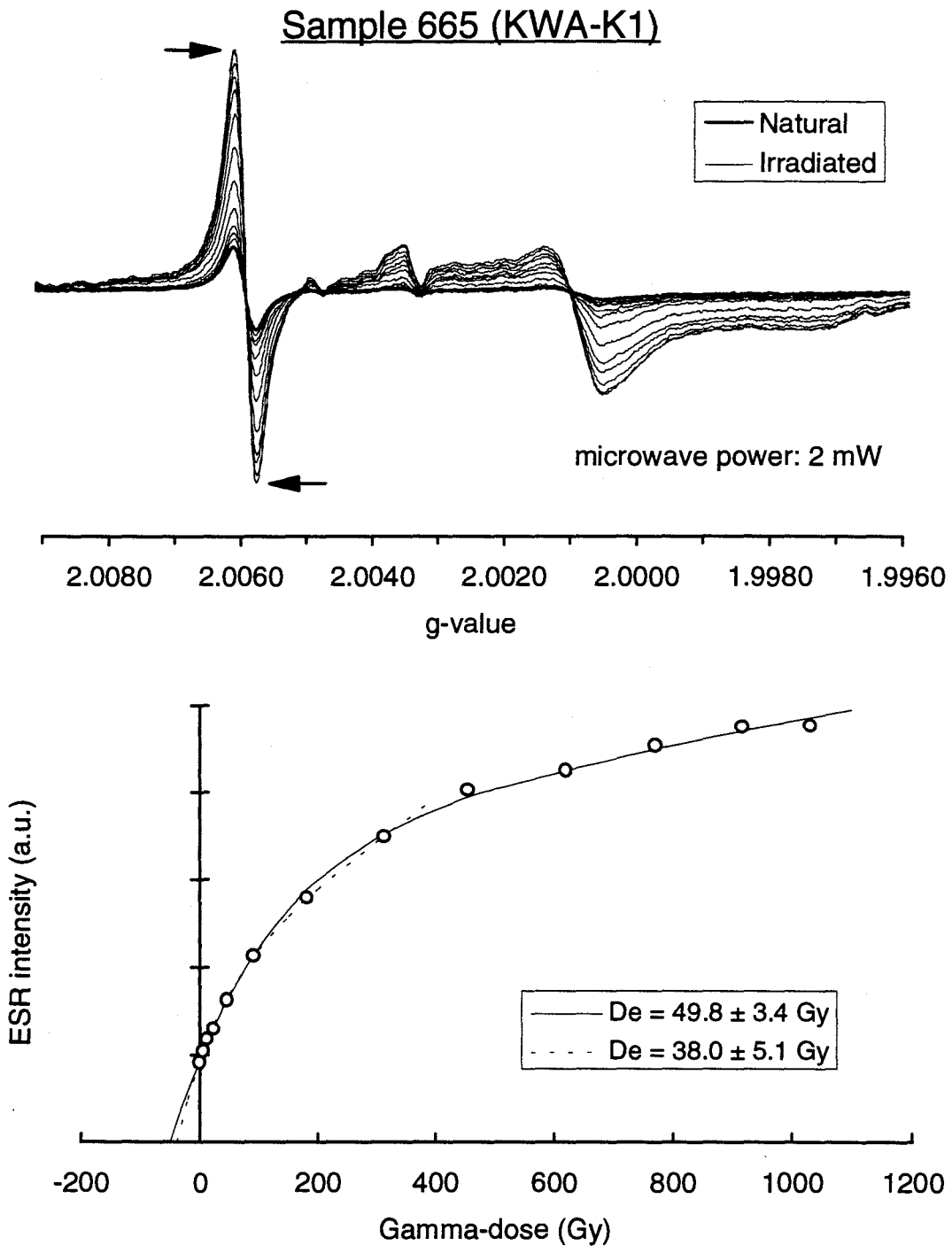

Figure 13.3(a). ESR spectra and dose response curves for coral sample 665 (KWA-K1) after annealing (14 hours at 150°C). The arrows indicate the method used to estimate the peak-to-peak height intensity at g=2.0058. D_E-values of 49.8 ± 3.4 Gy (solid line) and 38.0 ± 5.1 Gy (dashed line) were obtained from a saturating-exponential-plus-linear fit using all the points and the first eight points, respectively.

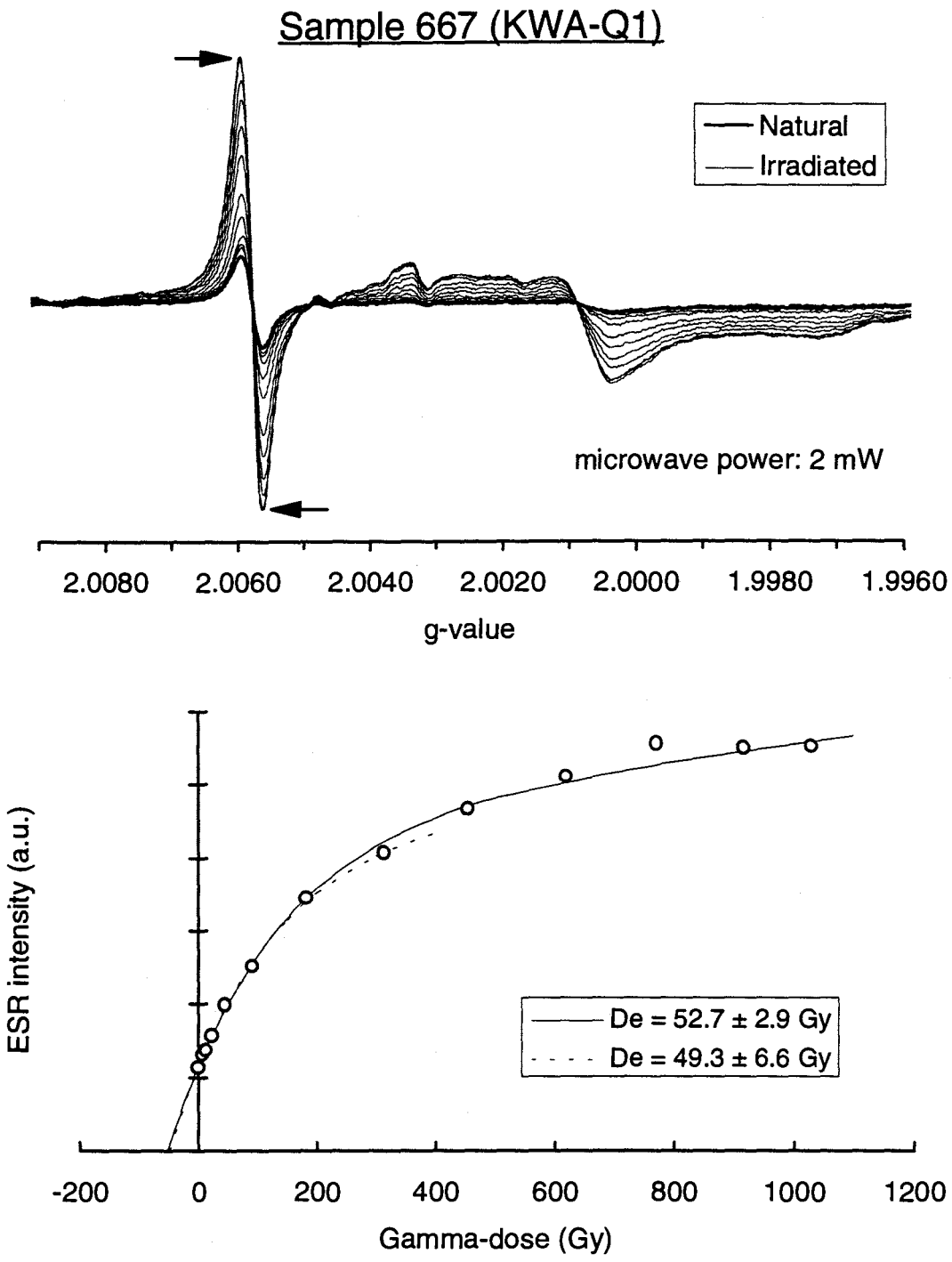

Figure 13.3(b). ESR spectra and dose response curves for coral sample 667 (KWA-Q1) after annealing (14 hours at 150°C). The arrows indicate the method used to estimate the peak-to-peak height intensity at g=2.0058. D_E-values of 52.7 ± 2.9 Gy (solid line) and 49.3 ± 6.6 Gy (dashed line) were obtained from a saturating-exponential-plus-linear fit using all the points and the first eight points, respectively.

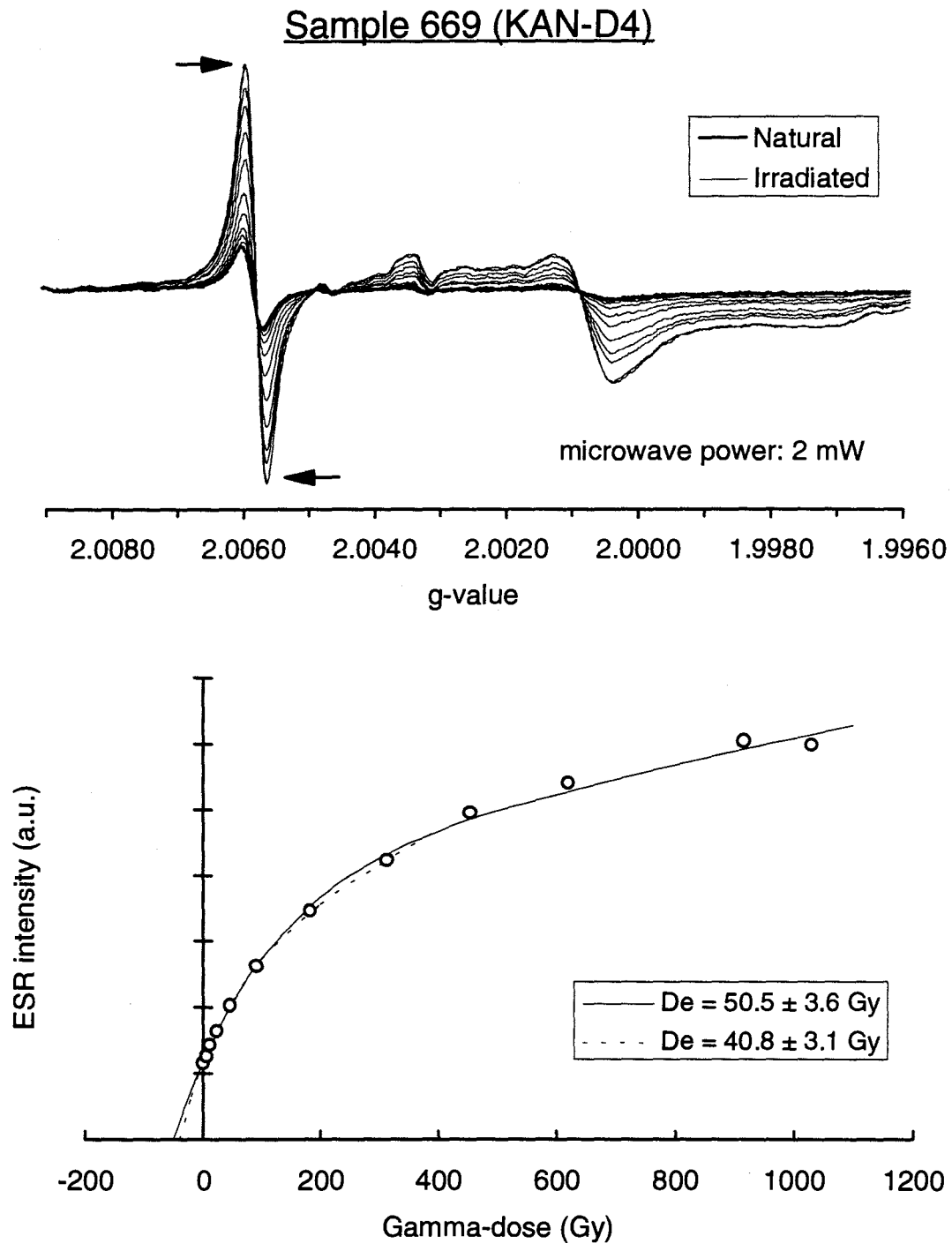

Figure 13.3(c). ESR spectra and dose response curves for coral sample 669 (KAN-D4) after annealing (14 hours at 150°C). The arrows indicate the method used to estimate the peak-to-peak height intensity at g=2.0058. D_E-values of 50.5 ± 3.6 Gy (solid line) and 40.8 ± 3.1 Gy (dashed line) were obtained from a saturating-exponential-plus-linear fit using all the points and the first eight points, respectively.

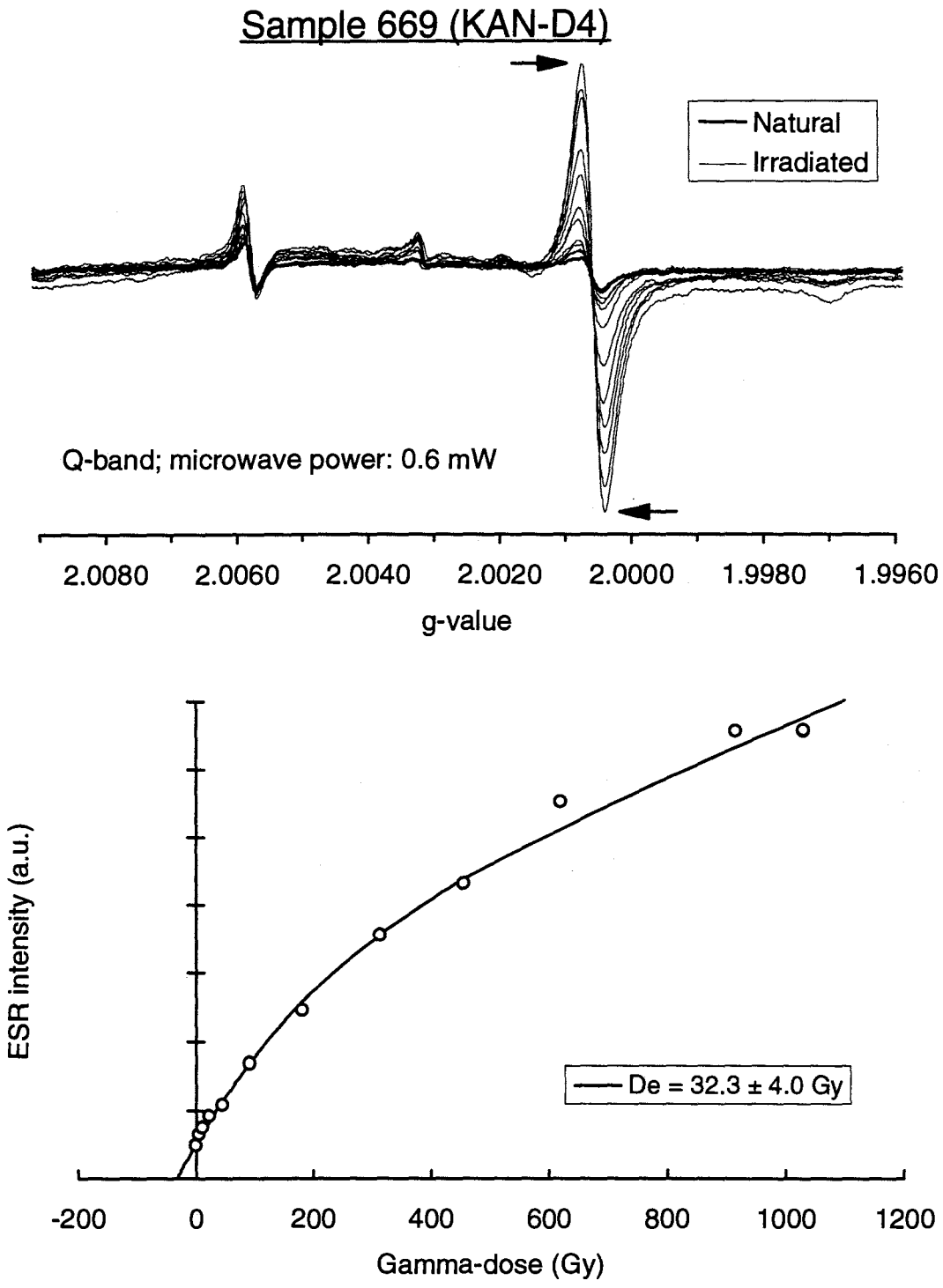

Figure 13.3(d). ESR spectra and dose response curve for coral sample 669 (KAN-D4) using a Q-band spectrometer. The arrows indicate the method used to estimate the peak-to-peak height intensity at g=2.0007. A D_E-value of 32.3 ± 4.0 Gy was obtained from a saturating-exponential-plus-linear fit.

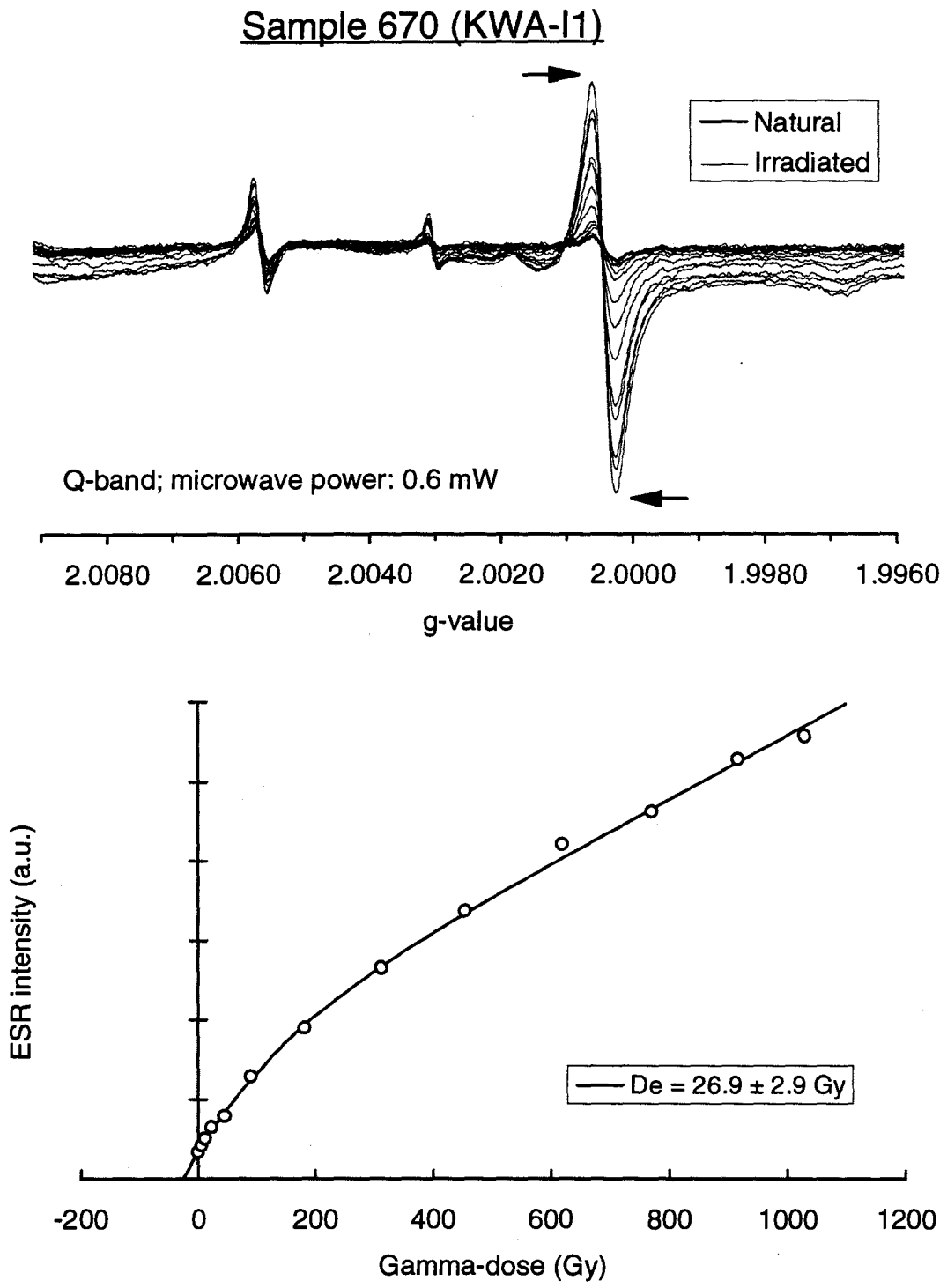

Figure 13.3(e). ESR spectra and dose response curve for coral sample 670 (KWA-I1) using a Q-band spectrometer. The arrows indicate the method used to estimate the peak-to-peak height intensity at g=2.0007. A D_E-value of 26.9 ± 2.9 Gy was obtained from a saturating-exponential-plus-linear fit.

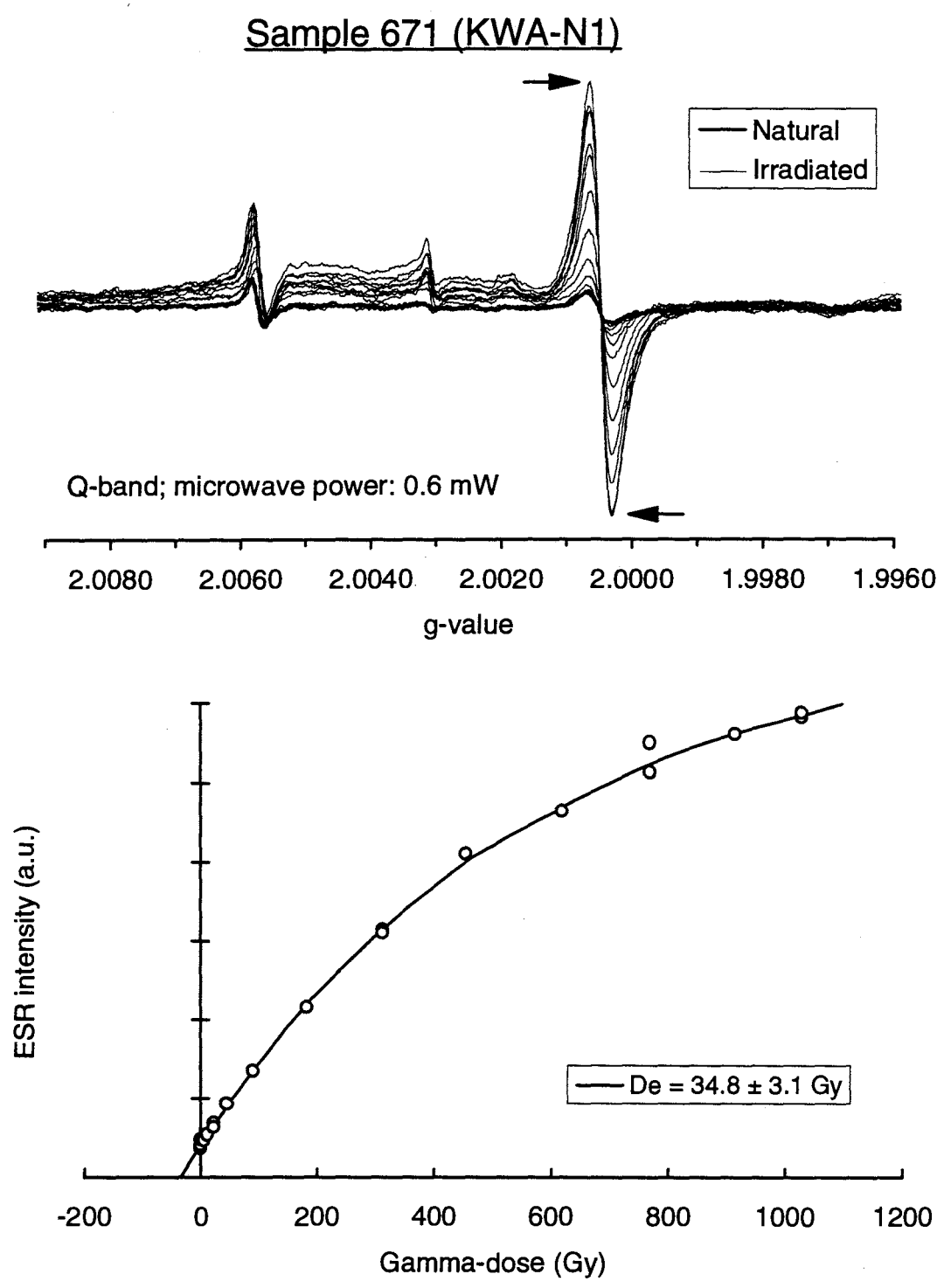

Figure 13.3(f). ESR spectra and dose response curve for coral sample 671 (KWA-N1) using a Q-band spectrometer. The arrows indicate the method used to estimate the peak-to-peak height intensity at g=2.0007. A D_E-value of 34.8 ± 3.1 Gy was obtained from a saturating-exponential-plus-linear fit.

Chapter 14 ESR DATING OF QUARTZ SAMPLES FROM ALLEN'S CAVE, SOUTH AUSTRALIA

ESR ages of samples $Ox_{OD}AC390$ and $Ox_{OD}AC150$ were obtained using the newly discovered ESR light-sensitive signals (see sections 11.3 and 11.4). For sample $Ox_{OD}AC150$, ESR ages were estimated using the signals at g=1.9870, 1.9842 and 1.9162. An ESR age for sample $Ox_{OD}AC390$ was obtained using the signal at g=1.9162, recorded during the work described in Chapter 7.

14.1 Methods used

For sample $Ox_{OD}AC150$, ten 200 mg aliquots of 'natural' quartz were prepared and then subjected to a selection of gamma doses (0, 10, 20, 50, 100, 175, 250, 350 and 500 Gy) using a ^{60}Co source (dose rate $\approx$ 10.5 Gy min^{-1}). To examine the ESR signal saturation level, one aliquot was exposed to an especially large dose (3970 Gy) but this aliquot was not used for D_E-value evaluations. To investigate the effect of preheating the aliquots prior to ESR spectra measurement, ESR spectra were recorded before and after the preheating treatment (holding the aliquots at a temperature of 220°C for 5 minutes, as used in optical dating of this sample (Roberts *et al.*, 1994a)).

ESR spectra were measured at liquid nitrogen temperature ($\approx$ 77K) with a quartz dewar using an X-band (9.25 GHz) Bruker ESP 300E spectrometer, a microwave power of 1 mW and a modulation frequency of 100 kHz. ESR spectra of the Al and Ti centres were recorded in the same manner, and under the same conditions, as described in section 7.1. ESR spectra of the g=1.9870 and 1.9842 signals were recorded with a modulation amplitude of 2.26 Gpp, a time constant of 5243 ms and a scan speed of 2.68 G min^{-1}, while the spectra of the g=1.9162 signal were recorded with a modulation amplitude of 1.60 Gpp, a time constant of 2621 ms and a scan speed of 5.36 G min^{-1}. The intensities of the signals were measured in the manner presented in section 11.4.1 and the D_E-values

were determined using the procedures described in section 4.1.1. All ESR measurements were made under dim red lighting conditions (see section 11.4.1) and the environmental dose rate assessments are described in section 7.1.

14.2 ESR ages obtained

ESR results for samples $Ox_{OD}AC390$ and $Ox_{OD}AC150$ are given in Table 14.1(a) and Table 14.1(b), respectively. ESR spectra and dose response curves for sample $Ox_{OD}AC390$ (at g=1.9162) and $Ox_{OD}AC150$ (at g=1.9870, 1.9842 and 1.9162) are shown in Figures 14.1 and 14.2(a)-(c), respectively. For sample $Ox_{OD}AC390$, it was not possible to obtain ESR ages based on the signals at g=1.9870 and 1.9842 because the signal-to-noise ratio was too low under the measurement conditions used.

For both samples, the D_E-values based on the light-sensitive signals are much smaller than the values obtained using the Al and Ti centres. In terms of D_E-values, light-sensitive signals < Ti signal < Al signal. This ranking (though with the sign reversed) accords with the light sensitivities of these signals as shown by the sunlight bleaching experiments described in Chapter 11. The D_E-values given by the light-sensitive signals for sample $Ox_{OD}AC150$ are in agreement at the 2σ level, whereas neither the Al nor Ti signal appear to have been bleached as completely before sample burial (Table 14.1(b)). The same is true for sample $Ox_{OD}AC390$: the light-sensitive signal at g=1.9162 is bleached to a much greater extent than either the Al or Ti signals (Table 14.1(a)).

Some changes in the D_E-value for sample $Ox_{OD}AC150$ are observed after preheating for 5 minutes at 220°C, the procedure most commonly used in optical (OSL) dating of quartz (Smith *et al.*, 1986; Roberts *et al.*, 1994a). After preheating, the D_E-values based on the signals at g=1.9870 and 1.9842 became smaller (by $\approx$ 15 % and 19 %, respectively), whereas the Al and Ti centre signals and the g=1.9162 signal gave D_E-values that increased by $\approx$ 13 %, 42 % and 29 %, respectively. The preheat-induced D_E-value increases occurred because the signal intensities of all aliquots, including the natural

(unirradiated) aliquots, increased after preheating (see Figures 14.2(c) and 14.3). In contrast, the preheat-induced D_E-value decreases resulted from an increase in intensity of the irradiated aliquots only (see Figure 14.2(b)). These results imply that the Al, Ti and g=1.9162 signals encompass thermally unstable components in both the natural and irradiated aliquots, whereas such components at g=1.9870 and 1.9842 are produced only during laboratory irradiation. The results observed for the signals at g=1.9870, 1.9842 and 1.9162 should, however, be investigated further since the changes apparently induced by preheating are relatively small.

Dose response curves based on the Al and Ti centres and the signals at g=1.9870, 1.9842 and 1.9162 (including the aliquots given a dose of 3970 Gy) are shown in Figures 14.4(a) and 14.4(b). For the signals at g=1.9870, 1.9842 and 1.9162, saturation occurs at about 1000 Gy. The Ti signal appears to saturate at around 2000 Gy and the Al signal saturation level is in excess of 4000 Gy. After preheating, the signal intensity in the aliquots given a dose of 3970 Gy increased by $\approx$ 11 % at the Ti centre and by $\approx$ 59 % at g=1.9162. In contrast, little change was observed at g=1.9870 and g=1.9842 after preheating the N+3970 Gy aliquots. This result suggests that the signals at g=1.9870 and g=1.9842 may be due to the same type(s) of defect but that a different defect may be responsible for the signal at g=1.9162. The fact that all three signals have similar light sensitivities and saturation levels would appear, however, to imply a less exclusive relation between the source defects of these signals.

14.3 Comparisons with independent age controls

The estimated ESR ages of samples Ox_{OD}AC390 and Ox_{OD}AC150 are compared with ^{14}C, TL and OSL ages in Table 14.2(a) and Table 14.2(b), respectively. The ages of sample Ox_{OD}AC150 obtained by ^{14}C, OSL and TL methods are in good agreement at 9-11 ka. For this sample, the signals at g=1.9870, 1.9842 and 1.9162 yield mean ESR ages of 10-13 ka, both before and after preheating, in close accordance with the independent age estimates (see Figure 14.5). The ESR ages based on the Ti signal and particularly the Al

signal are considerably greater, due presumably to incomplete zeroing of these signals at the time of sample deposition. A similar result is obtained for Ox_{OD}AC390: close correspondence between the OSL age determination and the ESR age for the unpreheated g=1.9162 signal, but gross age overestimation by both the Ti and Al signals.

The preheating treatment causes a minor change in the ESR ages based on the signals at g=1.9870, 1.9842 and 1.9162. It is not clear, therefore, whether the applied preheat, or preheating in general, is appropriate for these signals. The closest agreement with the independent age estimates appears to be with the preheated g=1.9870 and g=1.9842 ESR ages, and the unpreheated g=1.9162 signal age (Figure 14.5). The latter ESR age increases by ≈ 29 % upon preheating. If this percentage adjustment is made to the unpreheated g=1.9162 ESR age for Ox_{OD}AC390, then the corresponding preheated age would be ≈ 41 ka, bringing the ESR age determination into closer accordance with the OSL age estimate (≈ 38 ka) for this sample. However, no firm conclusions about the necessity for preheating can be drawn from these data, as the changes in mean age due to preheating are of the same magnitude as the 1σ age uncertainties. Furthermore, since the trapped-electron population involved in ESR dating may be related to only a subset of the trapped-electron population used in luminescence dating, the need to preheat ESR aliquots prior to spectra measurement should be investigated further. Suffice to say here that the preheating treatment does not affect the main conclusion of this quartz study: that the newly discovered light-sensitive ESR signals offer enormous potential for dating sub-aerially deposited sediments.

14.4 Conclusions

Three new light-sensitive ESR signals (at g=1.9870, 1.9842 and 1.9162) are reported in this study, and the ages obtained from their D_E-values are consistent with independent age estimates (^{14}C, TL and OSL). At this stage, it is not clear if the quartz samples need to be annealed after laboratory irradiation and before spectra measurement; the ages obtained with and without annealing are in close agreement with the independent age controls.

A further finding of this study is the different dose saturation characteristics of the light-sensitive ESR and luminescence signals. Dose response curves based on the light-sensitive ESR signals in samples $Ox_{OD}AC390$ and $Ox_{OD}AC150$ are compared with the OSL dose response characteristics in Figure 14.6. For both samples, D_0 values (the characteristic saturation doses) based on ESR are much greater than those indicated by OSL: ≈ 2.5 times for the signals at g=1.9870 and 1.9842 (before and after preheating), and ≈ 2.2 and 4.6 times for the signal at g=1.9162 before and after preheating, respectively. These comparisons suggest that the light-sensitive ESR signals, particularly the g=1.9162 signal after the preheating treatment, should enable dating of quartz sediments as young as Holocene in age to deposits as old as 1-2 Ma (given an environmental dose rate of 0.5-1 Gy ka^{-1}, typical of many Australian sandy deposits). This is a considerably greater age range than can be covered by either TL or OSL, whose signal intensities are saturated at much lower doses.

There is one further implication of the different dose response characteristics of the luminescence and light-sensitive ESR signals. If the latter relate to the same trapped-electron population as the 375°C TL signal, then the lower D_0 values of the luminescence signals imply a limitation in the number of available recombination centres. The data collected in this study permit only a weak inference to be drawn on this subject, and more detailed investigations are warranted.

Table 14.1(a). ESR results for sample $Ox_{OD}AC390$ from Allen's Cave, South Australia.

Sample code	ESR signal	Dose rate (Gy ka^{-1})	D_E-value (Gy)	Age (ka)
$Ox_{OD}AC390$	Al	1.67± 0.09	456.0 ± 18.9	273.1 ± 18.6
	Ti		440.4 ± 21.6	263.7 ± 19.2
	g=1.9162		53.9 ± 7.9	32.3 ± 5.0

Note: No preheating was performed.

Table 14.1(b). ESR results for sample $Ox_{OD}AC150$ from Allen's Cave, South Australia.

Sample code	ESR signal	Dose rate (Gy ka^{-1})	Before preheating		After preheating	
			D_E (Gy)	Age (ka)	D_E (Gy)	Age (ka)
$Ox_{OD}AC150$	Al	2.32 ± 0.09	117.7 ± 6.1	50.7 ± 3.3	133.3 ± 11.1	57.5 ± 5.3
	Ti		32.9 ± 2.2	14.2 ± 1.1	46.6 ± 2.6	20.1 ± 1.4
	g=1.9870		28.6 ± 1.3	12.3 ± 0.7	24.3 ± 1.8	10.5 ± 0.9
	g=1.9842		30.8 ± 2.7	13.3 ± 1.3	25.0 ± 1.8	10.8 ± 0.9
	g=1.9162		22.7 ± 1.2	9.8 ± 0.6	29.2 ± 1.9	12.6 ± 1.0

Note: Preheating treatment involved holding aliquots at 220°C for 5 min.

Table 14.2(a). ESR and optical dates for sample $Ox_{OD}AC390$ from Allen's Cave, South Australia.

Sample code	Dating method		Dose rate (Gy ka^{-1})	D_E-value (Gy)	Age (ka)
$Ox_{OD}AC390$	OSL		1.67 ± 0.09	66.6 ± 2.3	38.2 ± 3.1
	ESR	Al signal		456.0 ± 18.9	273.1 ± 18.6
		Ti signal		440.4 ± 21.6	263.7 ± 19.2
		g=1.9162		53.9 ± 7.9	32.3 ± 5.0

Notes: 1. OSL and dose rate data from Roberts *et al.* (1994a, 1996).
2. No preheating was performed on ESR samples.
3. OSL aliquots were preheated for 5 min at 220°C.

Table 14.2(b). ESR, ^{14}C, OSL and TL dates for sample $Ox_{OD}AC150$ from Allen's Cave, South Australia.

Sample code	Dating method		Dose rate (Gy ka^{-1})	D_E-value (Gy)	Age (ka)
$Ox_{OD}AC150$	^{14}C		2.32 ± 0.09	-----	9.65 ± 0.65 (8.70 ± 0.30 B.P.; ANU-8077)
					$10.2 \pm \begin{matrix}0.6\\0.3\end{matrix}$ (9.27 ± 0.14 B.P.; ANU-6850)
					10.5 ± 0.5 (9.53 ± 0.19 B.P.; ANU-6849)
	OSL			23.5 ± 0.6	9.7 ± 0.6
	TL			25.9 ± 1.4	10.7 ± 0.9
	ESR	Al signal		117.7 ± 6.1 (133.3 ± 11.1)	50.7 ± 3.3 (57.5 ± 5.3)
		Ti signal		32.9 ± 2.2 (46.6 ± 2.6)	14.2 ± 1.1 (20.1 ± 1.4)
		g=1.9870		28.6 ± 1.3 (24.3 ± 1.8)	12.3 ± 0.7 (10.5 ± 0.9)
		g=1.9842		30.8 ± 2.7 (25.0 ± 1.8)	13.3 ± 1.3 (10.8 ± 0.9)
		g=1.9162		22.7 ± 1.2 (29.2 ± 1.9)	9.8 ± 0.6 (12.6 ± 1.0)

Notes: 1. ^{14}C, OSL, TL and dose rate data from Roberts *et al.* (1994a, 1996).
2. OSL and ESR (in parentheses) aliquots were preheated for 5 min at 220°C.
3. TL age is determined from the 265 - 380°C plateau region.
4. ^{14}C ages are calibrated according to Stuiver and Reimer (1993). The conventional ages are given in parentheses, with the laboratory code.

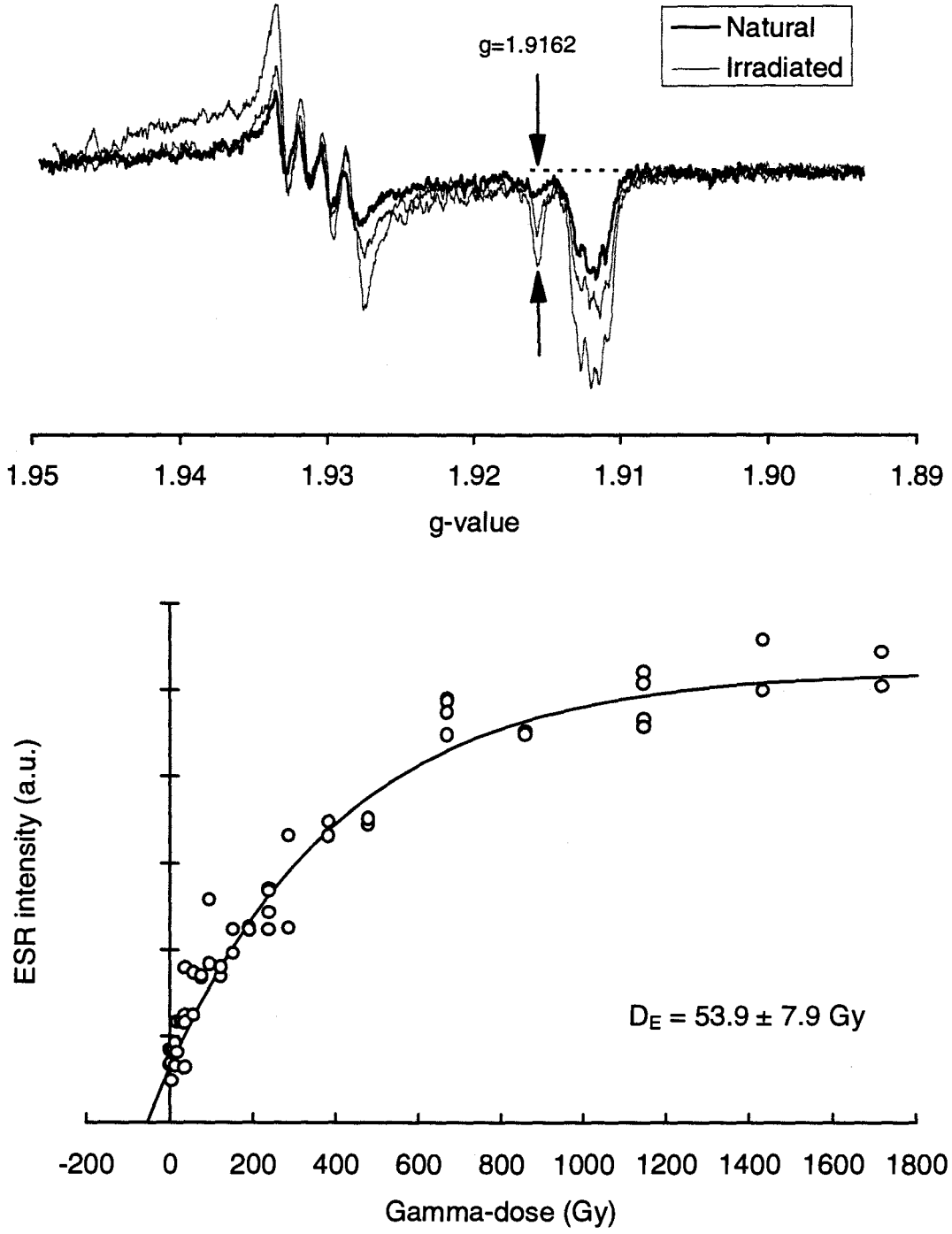

Figure 14.1. ESR spectra based on the signal at g=1.9162 (Natural, N+288 Gy and N+1720 Gy) and dose response curve for sample Ox_{OD}AC390. The arrows indicate the method used to estimate the signal intensity. A D_E-value of 53.9 ± 7.9 Gy was estimated from a single saturating exponential fit.

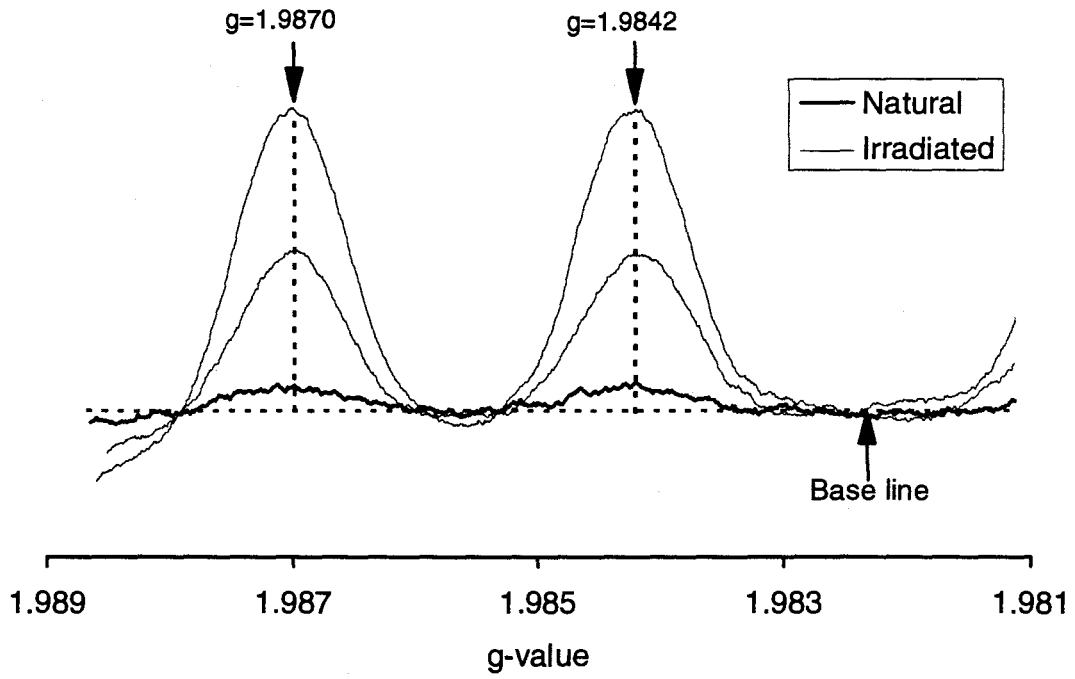

Figure 14.2(a). ESR spectra based on the signals at g=1.9870 and 1.9842 (Natural, N+175 Gy and N+500 Gy) for sample Ox_{OD}AC150. The arrows indicate the method used to estimate the signal intensities.

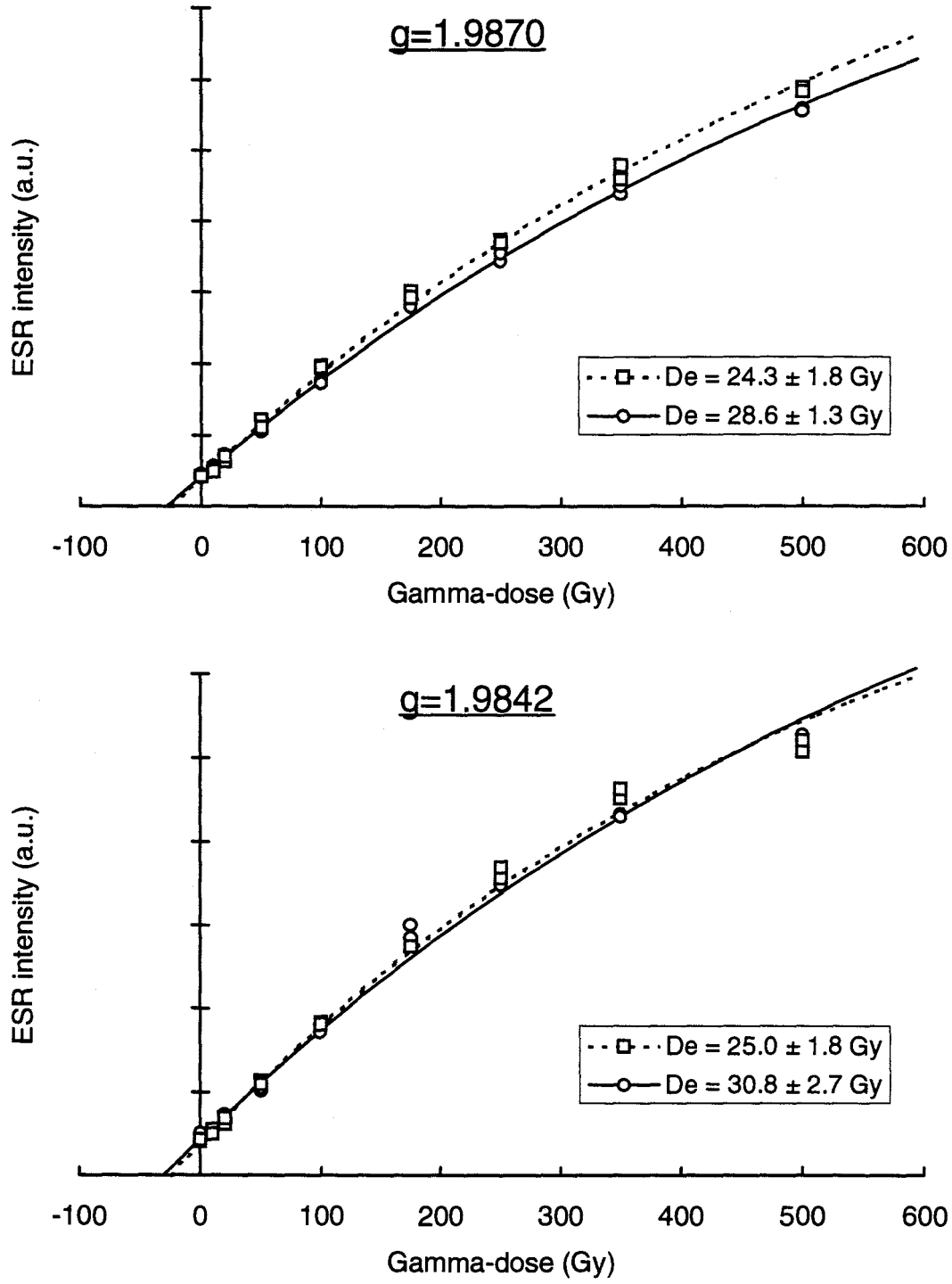

Figure 14.2(b). Dose response curves for sample $Ox_{OD}AC150$ based on the signals at g=1.9870 and g=1.9842. Data points are fitted by a single saturating exponential function. Solid and dashed lines represent the best-fit curves before and after preheating (220°C for 5 min), respectively.

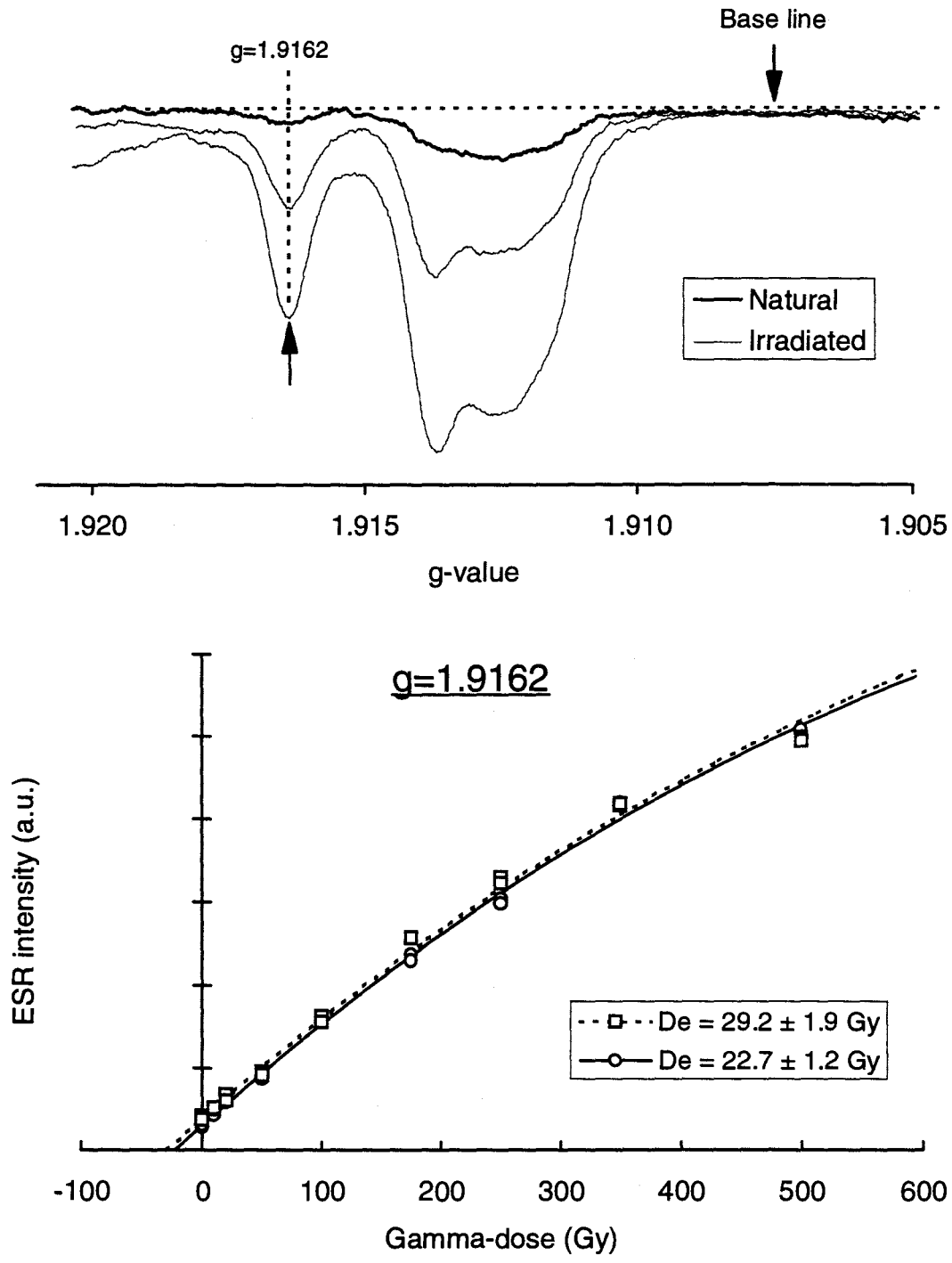

Figure 14.2(c). ESR spectra based on the signal at g=1.9162 (Natural, N+175 Gy and N+500 Gy) and dose response curves for sample $Ox_{OD}AC150$. The arrows indicate the method used to estimate the signal intensity. Data points are fitted by a single saturating exponential function. Solid and dashed lines represent the best-fit curves before and after preheating (220°C for 5 min), respectively.

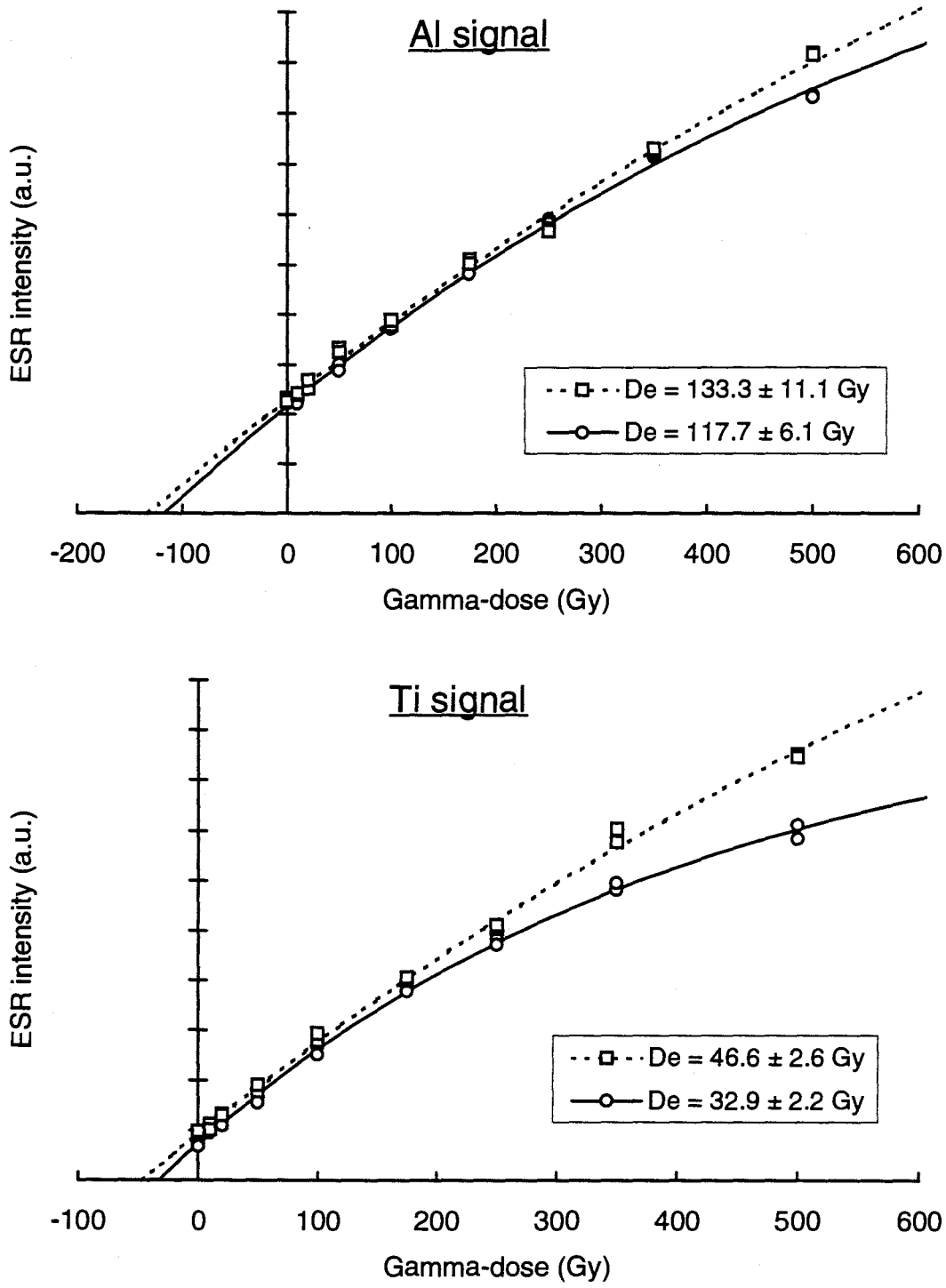

Figure 14.3. Dose response curves for sample Ox_{OD}AC150 based on the Al and Ti signals. Solid and dashed lines represent single saturating exponential fits before and after preheating (220°C for 5 min), respectively.

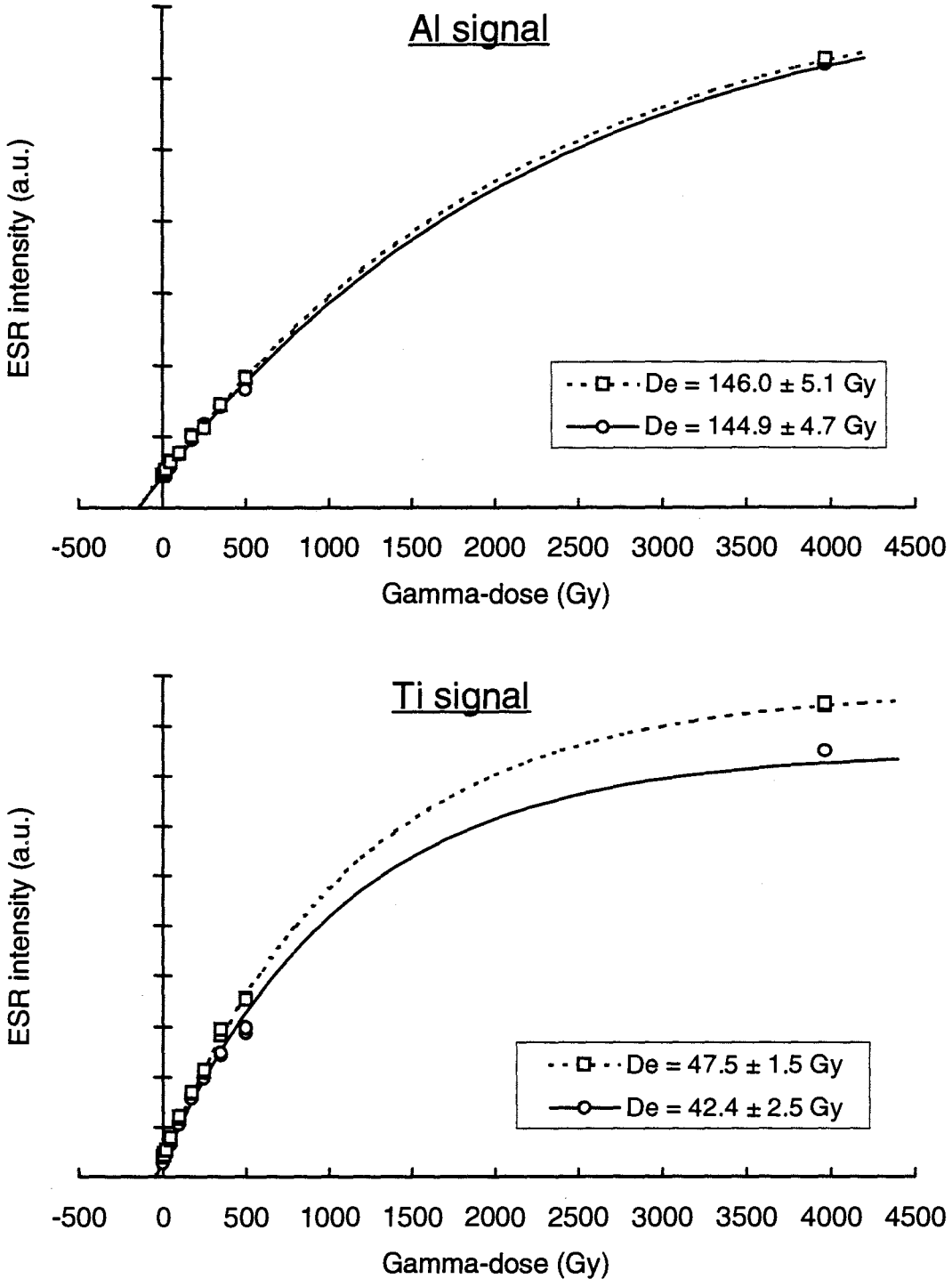

Figure 14.4(a). Dose response curves for sample Ox_{OD}AC150 based on the Al and Ti signals. Solid and dashed lines represent single saturating exponential fits before and after preheating (220°C for 5 min), respectively.

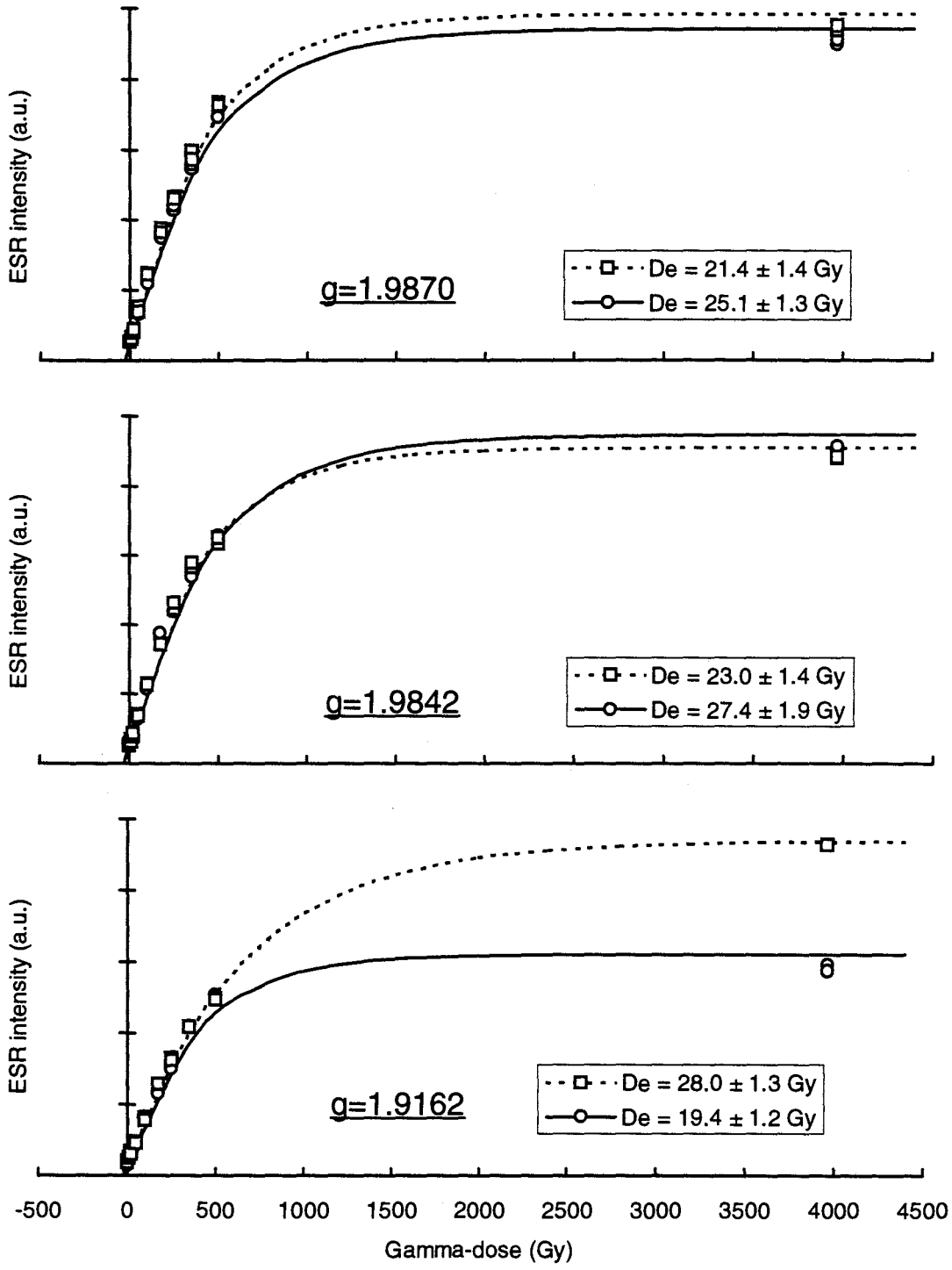

Figure 14.4(b). Dose response curves for sample $Ox_{OD}AC150$ based on the signals at g=1.9870, 1.9842 and 1.9162. Solid and dashed lines represent single saturating exponential fits before and after preheating (220°C for 5 min), respectively.

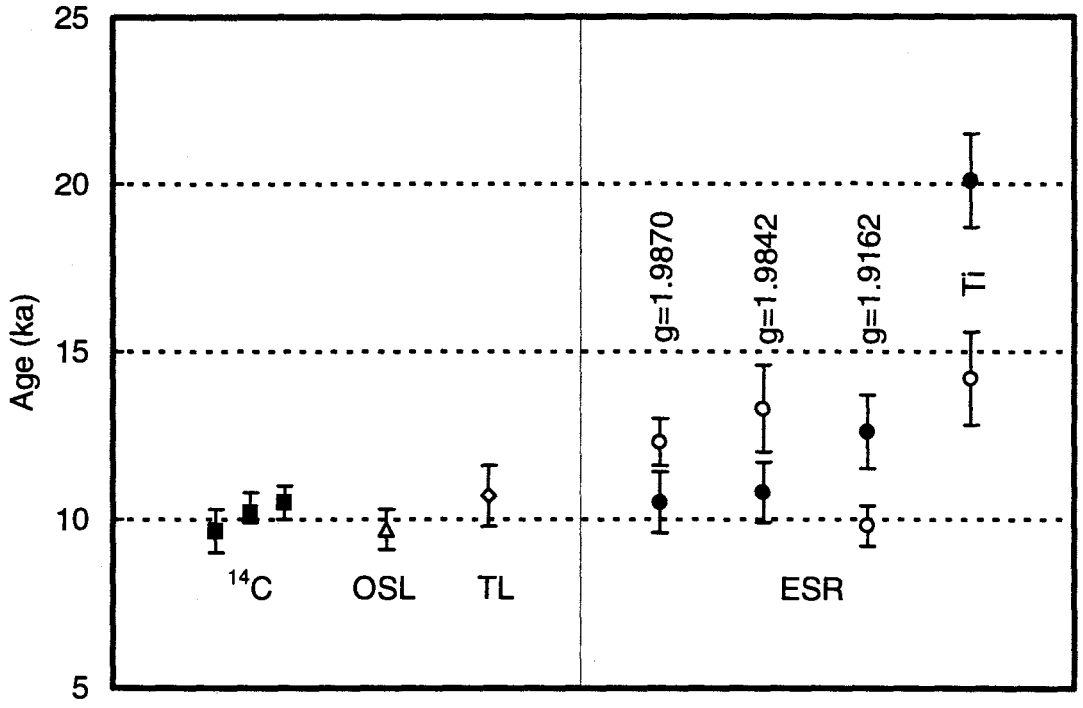

Figure 14.5. Ages estimated by ^{14}C, OSL, TL and ESR methods for sample Ox_{OD}AC150. ^{14}C ages are calibrated according to Stuiver and Reimer (1993) and the TL age is determined from the 265-380°C plateau region. OSL and ESR (solid circles) samples were preheated for 5 min at 220°C, while ESR samples shown by open circles were not preheated prior to spectra measurement.

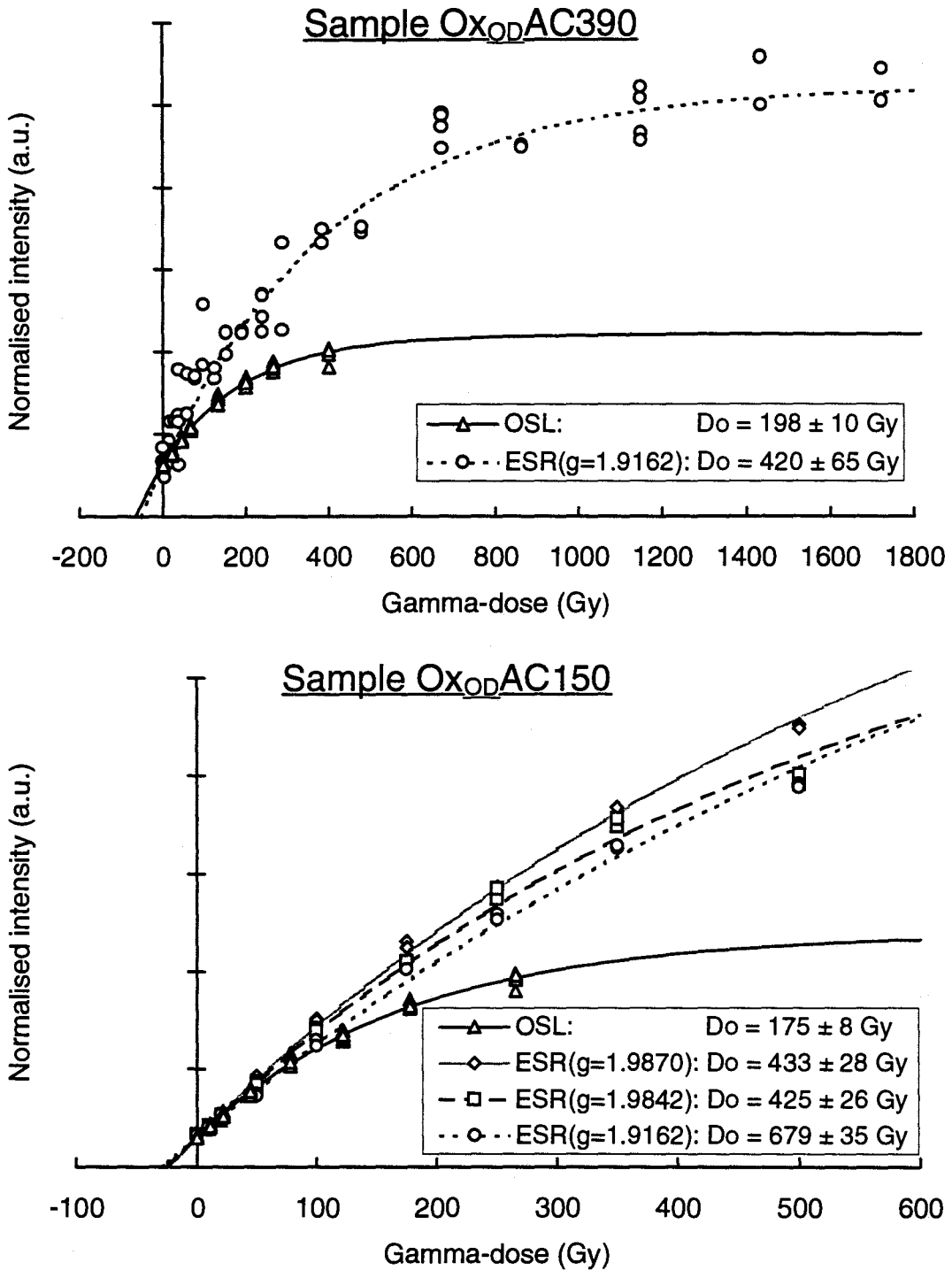

Figure 14.6. ESR and OSL dose response curves for samples $Ox_{OD}AC390$ and $Ox_{OD}AC150$. Signal intensities are normalised to the intensity of the natural (unirradiated) aliquot. ESR ($Ox_{OD}AC150$) and OSL samples were preheated for 5 min at 220°C. The ESR D_0 values (characteristic saturation doses) for sample $Ox_{OD}AC150$ are estimated from the dose response curves that include the 3970 Gy data points.

Chapter 15 SUMMARY OF RESULTS AND IMPLICATIONS FOR FUTURE WORK

15.1 Summary

15.1.1 Shells (aragonite and calcite-containing shells)

The AMS ^{14}C dates for the shell samples from Forster-Tuncurry, New South Wales, indicate that the shells consist of a mixture of reworked fossil shells. From the AMS ^{14}C dates on individual shells, shell 'hash' ^{14}C ages appear to be substantial overestimates by about 2,000-8,000 years. The use of shell hash samples for dating may thus be inappropriate for high-energy coastal deposits, such as occur on the southeastern Australian shelf. The dating of individual shells (or other marine carbonates) is therefore indispensable for obtaining more accurate age estimates for periods of coastal sedimentation. The routine use of the AMS ^{14}C method, however, is not practical at this time because of its expense for a large number of samples and because the working limit of ^{14}C dating is 30,000-40,000 years.

As an alternative method, with prospects for dating the past 0.5 Ma or more, ESR dating of marine shells (aragonite and calcite-containing) was investigated in this study using both X-band and Q-band spectrometers. For aragonite shells, D_E-values were obtained based on the signals at g=2.0058 (X-band, after annealing), g=2.0014 (X-band, before and after annealing) and g=2.0006 (X-band, microwave power of 200 mW; Q-band). For the shell samples which contained substantial amounts of calcite (44-100% by mass), the signals at g=2.0058 (X-band, after annealing) and g=2.0006 (X-band, after annealing) were used for the D_E-value estimations.

For the aragonite shell samples from Forster-Tuncurry, the D_E-values based on the g=2.0006 signal (Q-band) are in agreement with those based on the g=2.0006 signal (X-

band, microwave power of 200 mW). This implies that these signals are probably due to the freely rotating CO_2^- centre (e.g. Barabas *et al.*, 1992a, 1992b). In contrast, the unannealed g=2.0014 signal yields generally smaller D_E-values than those based on the g=2.0006 signals (X-band, 200 mW; Q-band). If the g=2.0006 signals produce the correct D_E-values, then the D_E-values based on the unannealed g=2.0014 signal are underestimates. Similar results are also obtained for some aragonite shell species from Elands Bay, South Africa. The g=2.0014 signal may therefore be affected by a thermally unstable component. The magnitude of the latter appears to vary between different shell species, but seems to be removed by annealing at 150°C for 14 hours. After annealing, the D_E-values based on the g=2.0014 signal in aragonite shells concur with those based on the g=2.0006 signal in calcite-containing shells collected from the same sampling sites. Consequently, D_E-values based on the signals at g=2.0006 (X-band, 200 mW, aragonite shells), g=2.0006 (Q-band, aragonite shells), g=2.0006 (X-band, calcite-containing shells) and g=2.0014 (X-band, aragonite shells) are comparable after annealing at 150°C for 14-15 hours.

D_E-values based on the g=2.0058 signal, which Barabas (1992) attributed to freely rotating SO_2^- radical anions, are often greater after annealing at 150°C for 14-15 hours than the D_E-values based on the annealed signals at g=2.0006 (X-band, 200 mW; Q-band, aragonite shells), g=2.0006 (X-band, calcite-containing shells) and g=2.0014 (X-band, aragonite shells). Overestimation of D_E-values based on the annealed g=2.0058 signal has been observed previously (e.g. Skinner, 1983), and these results could represent another example. It should be noted, however, that the ESR ages based on the annealed g=2.0058 signal are self-consistent for the shell samples at each of the sites at Elands Bay. This is true also for the ESR ages based on the signals at g=2.0006 (X-band, calcite-containing shells) and g=2.0014 (aragonite shells). The g=2.0058 signal has a very high thermal stability (Yokoyama *et al.*, 1983) and this signal in foraminifera increases steadily with age up to around 700 ka (Siegele and Mangini, 1985). Consequently, it is not possible to distinguish which signal yields the correct ages for these shell samples without independent age control.

It is concluded that the ESR signals at g=2.0058 (X-band, aragonite and calcite-containing shells), g=2.0014 (X-band, aragonite shells), g=2.0006 (X-band, 200 mW, aragonite shells), g=2.0006 (X-band, calcite-containing shells) and g=2.0006 (Q-band, aragonite shells) appear to be suitable for dating after annealing at 150°C for 14-15 hours. However, it should be noted that the g=2.0058 signal often yields greater D_E-values than are obtained using the other signals. The use of a Q-band spectrometer presents some difficulties for dating: a Q-band spectrometer is often not commercially available and requires extremely careful tuning and re-positioning of the ESR tube. For X-band measurements, since a higher microwave power improves the signal-to-noise ratio, it may be advisable to use a higher microwave power to measure the intensity of the g=2.0006 signal, particularly for younger samples; a microwave power of 200 mW appears to be suitable. Finally, it may be difficult to accurately evaluate the environmental dose rates if the shell samples have experienced variable dose rates throughout their period of burial (e.g. reworked shells). This can be particularly significant for younger samples.

15.1.2 Coral

The ESR ages based on the signals at g=2.0058 and g=2.0007 in coral were obtained using X-band and Q-band spectrometers. In the X-band, D_E-values were based on the g=2.0058 signal after annealing at 150°C for 14 hours. D_E-values based on the g=2.0007 signal were acquired using X-band (microwave powers of 5 mW and 200 mW) and Q-band, and D_E-values based on the g=2.0007 signal (X-band, 2 mW) were also obtained after annealing.

Similar results to the shell samples were obtained: D_E-values based on the g=2.0007 signal using X-band (5 mW and 200 mW) and Q-band are in agreement. In addition, annealing at 150°C for 14 hours does not affect significantly the D_E-values based on the g=2.0007 signal (X-band, 2 mW). D_E-values based on the g=2.0007 signal using X-band thus appear to be comparable at high and low microwave powers, and for both X-band

and Q-band. Also, the absence of any major effect from annealing implies that the g=2.0007 signal has an insignificant thermally unstable component.

Unlike the shell samples, most of the D_E-values based on the annealed g=2.0058 signal correspond favourably with those based on the g=2.0007 signal using X-band and Q-band. This suggests that the annealed g=2.0058 signal in coral, as also in shell, has potential use for dating. Since the g=2.0058 signal is widely observed in other carbonate materials, there may be a possibility of using this signal for dating after annealing.

The coral samples examined in this study do not indicate the conspicuous presence of a thermally unstable component, but this may not be true for corals from other sites. Since the g=2.0007 signal is affected negligibly by annealing, it is advisable to anneal samples prior to ESR measurement. Then, both the g=2.0058 and g=2.0007 signals can be used for dating. As for the shell samples, it may be more practical to use a higher microwave power (e.g. 200 mW) for measurement of the g=2.0007 signal to improve the signal-to-noise ratio, particularly in younger samples.

15.1.3 Quartz

Dating of quartz has great potential in Quaternary geology and archaeology because quartz grains are widely distributed and found in almost every depositional environment, including deep sea sediments, marine and coastal deposits, terrestrial landforms and archaeological sites. In previous studies, five different dating signals (OHC, E', Ge, Al and Ti) have been investigated. However, ESR dating of sedimentary quartz grains has still not been established as yielding reliable ages. OHC centre (g=2.011), E' centre (g=2.0001) and Ge centre (g=1.997) signals are observed at room temperature, and Al and Ti centres are detected at liquid nitrogen temperature ($\approx$ 77K).

All quartz samples examined in this study were collected from Australian sites and, surprisingly, exhibited no dating signals at room temperature. The ESR signals due to Al

and Ti centres were detected at liquid nitrogen temperature (≈ 77K). It is uncertain whether or not this peculiarity is unique to Australian quartz. The Al and Ti signals were investigated for their dating prospects, in which the signal resetting mechanism is bleaching by sunlight, as used successfully in TL and OSL dating. This approach gives the elapsed time since the constituent quartz grains of a deposit were last exposed to sunlight.

ESR ages based on the Al and Ti signals were obtained for marine sediments from Forster-Tuncurry, New South Wales, and wind-blown sediments from Allen's Cave, South Australia. At both sites, the ESR dates obtained are much older than the independently established ages, estimated by ^{14}C, OSL and TL. Among the ESR estimates, the Al signals appear to produce older ages than the Ti signals. This outcome can be understood from the results of sunlight bleaching experiments. The latter indicate that the Ti signal is more light-sensitive than the Al signal, and bleached almost completely by 132 days of continuous exposure to sunlight (including night time). Nevertheless, the time required for zeroing of the Ti signal appears to be too long to enable this signal to be of practical use for dating marine or wind-blown sediments; the Ti signal is unlikely to be reset completely by sunlight in the natural environment prior to sediment deposition and burial.

During the sunlight bleaching experiments on sample Ox_{OD}AC390, three new light-sensitive ESR signals were discovered at liquid nitrogen temperature (≈ 77K) under the dim red (> 590 nm) laboratory illumination conditions used for OSL and TL dating. These signals were observed at g=1.9870, 1.9842 and 1.9162 and have not been reported previously. Unlike the Al and Ti signals, these signals appear to be more light-sensitive and bleached almost completely after 11 hours exposure to unfiltered sunlight. The intensities of these signals are not reduced, however, by bleaching with only those wavelengths transmitted through an orange filter (> 510 nm wavelength transmission). From these observations, it is concluded that the light-sensitive ESR signals share close affinities with the characteristics of the 375°C TL signal, but are unlike those associated with the 325°C TL and OSL signals.

Ranked in terms of D_E-values, light-sensitive signals < Ti signal < Al signal. This ranking (though with the sign reversed) corresponds to the light sensitivities of these signals in samples Ox_{OD}AC390 and Ox_{OD}AC150 from Allen's Cave. After preheating at 220°C for 5 minutes, a procedure commonly used in the OSL dating of quartz, different responses in the D_E-values based on the light-sensitive, Al, and Ti signals were observed. After preheating, the intensity of the aliquots given a dose of 3970 Gy increased by ≈ 11 % and 59 % at the Ti and g=1.9162 signals, respectively. In contrast, little change was observed at the Al, g=1.9870 or g=1.9842 signals after preheating the N+3970 Gy aliquots. This result suggests that the signals at g=1.9870 and g=1.9842 may be due to the same type(s) of defect, whereas a different defect may be responsible for the signal at g=1.9162. However, as all three light-sensitive signals have similar light sensitivities and dose saturation levels, a less exclusive relation may exist between the source defects of these signals.

The preheating treatment causes only minor changes in the ESR ages based on the signals at g=1.9870, 1.9842 and 1.9162. For sample Ox_{OD}AC150, the independent age estimates agree most closely with the preheated g=1.9870 and g=1.9842 ESR ages, and with the unpreheated g=1.9162 ESR age. It is not clear, however, whether preheating is appropriate for these signals. The need to preheat ESR aliquots prior to spectra measurement should be investigated further for quartz, since the light-sensitive ESR signals used for dating may be only partly related to the luminescence signals used in TL and OSL dating.

For samples Ox_{OD}AC390 and Ox_{OD}AC150, the D_0 values (the characteristic saturation doses) based on the light-sensitive ESR signals greatly exceed those indicated by OSL: ≈ 2.5 times for the signals at g=1.9870 and 1.9842 (both before and after preheating), and ≈ 2.2 and 4.6 times for the signal at g=1.9162 before and after preheating, respectively. This result suggests that these signals should enable the dating of quartz sediments as young as Holocene in age to deposits as old as 1-2 Ma (given an environmental dose rate

of 0.5-1 Gy ka^{-1}, typical of many Australian sandy deposits). This is a considerably greater age range than can be covered by either TL or OSL, whose signal intensities are saturated at much lower doses. If the 375°C TL signal and the light-sensitive ESR signals are indeed related, then the greater D_0 values of the latter imply that saturation of the TL signal is due to a limitation in the number of available recombination centres, rather than available electron traps.

15.2 Implications for future work

In Chapter 10, the annealing kinetics of ESR signals due to paramagnetic centres were investigated using the marine bivalve shell *Katelysia scalarina*. In this study, it has been found that the g=2.0006 signal (Q-band), often described as the 'dating signal' for carbonates (e.g. Barabas *et al.*, 1992a, 1992b), has thermally unstable components. This casts serious doubt on the practice of using this signal for dating. However, it is not known whether this observation also applies to different shell species or to other carbonate materials used for ESR dating. For example, some shell species and coral samples yield D_E-values based on this signal that are not significantly affected by annealing at 150°C for 14-15 hours. Subsequent studies of the g=2.0006 signal (Q-band) should therefore be carried out on different carbonate materials, such as calcite and coral.

For the shell and coral samples examined, the g=2.0058 signal after annealing at 150°C for 14-15 hours was used for D_E-value estimations. Because this signal appears to saturate at relatively low doses (< 300 Gy), the D_E-values are often greatly overestimated if data points up to ≈ 1000 Gy are used. This implies that a single saturating exponential fit or a saturating-exponential-plus-linear fit is not applicable across the full dose range for this signal. It is unclear whether or not the saturated signal is due to a limited number of SO_3^- defects at g=2.0032, which on heating give rise to the SO_2^- defects at g=2.0058. A simple solution to avoid overestimation of D_E-values is to fit only unsaturated data points by a single saturating exponential or a saturating-exponential-plus-linear function.

A different curve-fit function may be needed, however, for the g=2.0058 signal to obtain correct D_E-values using all data points, and this possibility deserves further research.

For the *Anadara trapezia* shells from Forster-Tuncurry, it is possible that the ESR ages are considerably overestimated because of an inappropriate environmental dose rate evaluation. *Anadara trapezia* shells were initially buried in a muddy, estuarine sediment and were then transported and finally deposited in sandy sediments. The analytical data indicate that estuarine sediment (≈ 50 % mud) exhibits much higher dose rates than sandy sediments. Therefore, the total dose rates will be underestimated if the dose rates for sandy sediments are applied for the entire duration of shell burial. This error may be significant, particularly for younger samples. The degree of age overestimation will depend on the length of time that the shell samples were buried initially in a muddy sediment, compared to the length of time that the shells were buried subsequently in sandy sediments. Dating of marine shells by ESR may, therefore, not be reliable for young samples that have been buried in a different substrate to their common living habitat.

Three new light-sensitive ESR signals in quartz samples are reported here for the first time. The sunlight bleaching experiments on these signals suggest a possible relation to the 375°C TL signal but not to the 325°C TL or OSL signals. However, this connection is still ambiguous in several respects and further details are required. Dating of several samples (preferably using the same aliquots) should be carried out by ESR, OSL and TL. Also, further sunlight bleaching experiments using a wider range of optical filters may give more conclusive data on the wavelength dependence of the light-sensitive ESR signals.

In this study, the light-sensitive ESR signals are recorded at liquid nitrogen temperature (≈ 77K) using X-band. Since Q-band spectra typically give better signal resolution, it is possible that any ESR signals related to the 325°C TL signal (i.e. the OSL signal) may be observable using a Q-band spectrometer. Also, spectra measurements at lower temperatures (e.g. helium temperature: ≥ 0 K) may reveal new light-sensitive signals. TL

and OSL signals have not yet been unequivocally linked with particular ESR centres, but experiments such as these offer the prospect of examining the origins of TL and OSL signals in quartz. In addition, the greater age range dating potential of the light-sensitive ESR signals could be applied directly to geological deposits whose ages lie beyond the limit of luminescence methods and which lack materials suitable for other >1 Ma dating techniques (e.g. K-Ar, Ar-Ar, fission-track).

15.3 Conclusions

The specific objectives stated at the outset of this study were: 1) to test published ESR dating methods; 2) to examine the suitability of dose response functions in shell; 3) to investigate annealing effects on the accumulated dose in shell and coral; 4) to seek new light-sensitive ESR signals in quartz; and 5) to develop new ESR dating methods for shell, coral and quartz. These objectives have been met in this study, though with differing degrees of success in terms of developing reliable dating protocols for the various materials examined.

The following conclusions are drawn from the present study:

1) ^{14}C dating problems in marine geology

AMS ^{14}C dates for individual shells from Forster-Tuncurry, New South Wales, indicate that the shells consist of a mixture of reworked fossil shells. As a result, shell 'hash' ^{14}C ages are substantial overestimates of the time of last reworking of the shell deposit. ^{14}C dating of shell hash is confirmed to be ill-suited to high-energy environmental deposits, and shells (or other carbonates) should be dated individually in such circumstances.

2) ESR signals and dating methods for shell

Annealing experiments on shell suggest that the g=2.0006 signal (Q-band) of aragonite in the mollusc *Katelysia scalarina* and the g=2.0014 signal for this and other aragonite shell species have thermally unstable components. The thermally unstable components, however, appear to be removed by annealing at 150°C for 14-15 hours. For both aragonite and calcite-containing shell samples, D_E-values based on the ESR signals at g=2.0006 (X-band, 200 mW, aragonite shells), g=2.0006 (Q-band, aragonite shells), g=2.0006 (X-band, calcite-containing shells) and g=2.0014 (X-band, aragonite shells) appear to be comparable after annealing at 150°C for 14-15 hours. In contrast, D_E-values based on the annealed g=2.0058 signal are often much greater. At this stage, it is not possible to determine which, if any, signal yields the correct age.

3) ESR signals and dating methods for coral

For the coral samples, D_E-values based on the g=2.0007 signal using X-band (5 mW and 200 mW) and Q-band appear to be comparable. The D_E-values based on the g=2.0007 signal are not affected significantly by annealing at 150°C for 14 hours, and the D_E-values based on the annealed g=2.0058 signal concur with those based on the g=2.0007 signal. The ESR ages based on the g=2.0007 (before and after annealing) and g=2.0058 (after annealing) signals are in agreement with the independent age controls, obtained by alpha spectrometric and mass spectrometric uranium-series methods. The g=2.0007 signal and the annealed g=2.0058 signal in coral appear, therefore, to be suitable for dating.

4) New light-sensitive ESR signals in quartz and their dating potential

The most important result of this study is the discovery of three new light-sensitive ESR signals in quartz. These signals are observed at g=1.9870, 1.9842 and 1.9162 at liquid nitrogen temperature (≈ 77K) with an X-band spectrometer, and under dim red (> 590 nm) laboratory illumination. The bleaching behaviour of these signals is comparable to the

bleaching response of the 375°C TL signal, but is unlike that of the 325°C TL and OSL signals. The ESR ages based on these signals are in close agreement with ages estimated by ^{14}C, OSL and TL. There is also the potential with these ESR signals for dating quartz sediments from Holocene to 2 Ma in age, a far larger age range than can be covered by either TL or OSL.

As the above conclusions indicate, this thesis makes several significant contributions to the development of reliable ESR dating methods. A number of concerns have been raised about published methods for shell, in particular, while new light-sensitive signals in quartz have been reported to broaden the range of ESR dating applications. Given the restricted number of samples examined, however, further investigations are necessary to confirm that the ESR methods developed here can be applied routinely to obtain accurate, absolute dates for Quaternary marine and terrestrial deposits.

References

Aitken, M.J. (1985). *Thermoluminescence Dating*. Academic Press, London.

Aitken, M.J. (1990). *Science-based Dating in Archaeology*. Longman, London.

Ashby, J.R., Ku, T.L. and Minch, J.A. (1987). Uranium-series ages of corals from the upper Pleistocene Mulege terrace, Baja California Sur, Mexico. *Geology*, **15**, 139-141.

Bao, T.V. and Kha, L.T. (1966). Report on paleontological and paleoanthropological research at Tham Khuyen, Binh Gia District (Lang Son Province). Documents of the Institute of Archaeology, Hanoi [in Vietnamese].

Barabas, M. (1992). The nature of the paramagnetic centres at g=2.0057 and g=2.0031 in marine carbonates. *Nuclear Tracks and Radiation Measurements*, **20**, 453-464.

Barabas, M., Bach, A., Mudelsee, M. and Mangini, A. (1992a). General properties of the paramagnetic centre at g=2.0006 in carbonates. *Quaternary Science Reviews*, **11**, 165-171.

Barabas, M., Mudelsee, M., Walther, R. and Mangini, A. (1992b). Dose-response and thermal behaviour of the ESR signal at g=2.0006 in carbonates. *Quaternary Science Reviews*, **11**, 173-179.

Bard, E., Arnold, M., Fairbanks, R.G. and Hamelin, B. (1993). ^{230}Th-^{234}U and ^{14}C ages obtained by mass spectrometry on corals. *Radiocarbon*, **35**, 191-199.

Berger, G.W. (1990). Effectiveness of natural zeroing of the thermoluminescence in sediment. *Journal of Geophysical Research*, **95**, 12,375-12,397.

Berger, W.H. and Heath, G.R. (1968). Vertical mixing in pelagic sediments. *Journal of Marine Research*, **26**, 134-143.

Bowler, J.M., Hope, G.S., Jennings, J.N., Singh, G. and Walker, D. (1976). Late Quaternary climates of Australia and New Guinea. *Quaternary Research*, **6**, 359-394.

Brumby, S. (1992). Regression analysis of ESR/TL dose-response data. *Nuclear Tracks and Radiation Measurements*, **20**, 595-599.

Bryant, E., Roy, P.S. and Thom, B.G. (1988). Australia - an unstable platform for tide-gauge measurements of changing sea level: a discussion. *Journal of Geology*, **96**, 635-640.

Buhay, W. Schwarcz, H.P., and Grün, R. (1988). ESR dating of fault gouge: the effect of grain size. *Quaternary Science Reviews*, **7**, 515-522.

Carney, R.S. (1981). Bioturbation and biodeposition. *In*: Boucot, A.J. (ed), *Principles of Benthic Marine Paleoecology*, pp. 843-845. Academic Press, New York.

Cevc, P., Schara, M. and Ravnik, C. (1972). Electron paramagnetic resonance of irradiated tooth enamel. *Radiation Research*, **51**, 581-589.

Chapman, D.M., Geary, M., Roy, P.S. and Thom, B.G. (1982). *Coastal Evolution and Coastal Erosion in New South Wales*. Sydney, Coastal Council of New South Wales, pp. 341.

Chappell, J. (1990). New terrace transact survey data: age/sea-level implications. Presentation at: *International Workshop on Quaternary Sea-level Change*, 15-21 March, 1990. Kikai, Japan.

Chappell, J. and Polach, H. (1991). Post-glacial sea-level rise from a coral record at Huon Peninsula, Papua New Guinea, *Nature*, **349**, 147-149.

Chappell, J., Omura, A., McCulloch, M., Esat, T., Ota, Y. and Pandolfi, J. (1994a). Evised late Quaternary sea levels between 70 and 30 ka from coral terraces at Huon Peninsula. *In*: Ota, Yoko (ed), *Study on coral reef terraces of the Huon Peninsula, Papua New Guinea, Establishment of Quaternary See Level and Tectonic History*. A preliminary report on project 04041048, Monbusho International Research Program, Tokyo.

Chappell, J., Ota, Y. and Berryman, K. (1994b). Holocene and late Pleistocene coseismic uplift of the Huon Peninsula, Papua New Guinea. *In*: Ota, Yoko (ed), *Study on coral reef terraces of the Huon Peninsula, Papua New Guinea, Establishment of Quaternary See Level and Tectonic History.* A preliminary report on project 04041048, Monbusho International Research Program, Tokyo.

Chappell, J. and Shackelton, N.J. (1986). Oxygen isotopes and sea level. *Nature*, **324**, 137-140.

Chen, J.H., Edwards, R.L. and Wasserburg, G.J. (1986). ^{238}U, ^{234}U and ^{232}Th in seawater. *Earth and Planetary Science Letters*, **80**, 241-251.

Churchill, D.M., Galloway, R.W. and Singh, G. (1978). Closed lakes and the palaeoclimatic record. *In*: Pittock, A.B., Frakes, L.A., Jenssen, D., Peterson, J.A. and Zillman, J.W. (eds), *Climatic change and variability - a southern perspective*, pp. 97-108, Cambridge University Press, Cambridge.

Ciochon, R., Long, V.T., Vos, J. de, Grün, R., Gonzalez, L., Younge, C., Larick, R., Taylor, L., Yoshida, H. and Reagan, M. (1996). First dated Middle Pleistocene co-occurrence of *Gigantopithecus* and *Home erectus* and a new extinct species of Gibbon from Tham Khuyen Cave, Vietnam. *Proceedings of the National Academy of Sciences of the United States of America*, in press.

Cuong, N.L. (1984). Paläontologische Untersuchungen in Vietnam. ZFAZ. Archäol. 18: 247 - 251.

Cuong, N.L. (1985). Fossile Menschenfunde aus Nordvietnam. *In*: Herrmann, J. and Ullrich, H. (eds), Menschwerdung - biotischer und gesellschaftlicher Entwicklungsprozess, pp. 96 - 102. Berlin, Akademieverlag.

Debuyst, R., Dejehet, F. and Idrissi, S. (1993). Paramagnetic centres in g-irradiated synthetic monohydrocalcite. *Applied Radiation and Isotopes*, **44**, 293-297.

De Canniere, P., Debuyst, R., Defehet, F., Apers, D. and Grün, R. (1986). ESR dating : a study of ^{210}Po-coated geological and synthetic samples. *Nuclear Tracks*, **11**, 211-220.

Dott, R.H., Jr. (1983). 1982 SEPM presidential address: Episodic sedimentation - how normal is average? How rare is rare? Does it matter? *Journal of Sedimentary Petrology*, **53**, 5-23.

Duchesne, J., Depireux, J. and van der Kaa, J.M. (1961). Origin of free radicals in carbonaceous rocks. *Geochemica et Cosmochemica Acta*, **23**, 209-218.

Falguères, C., Yokoyama, Y. and Miallier, D. (1991). Stability of some quartz centres in quartz. *Nuclear Tracks and Radiation Measurements*, **18**, 155-161.

Gilinskaya, L.G., Shcherbakova, M.Y. and Zanin, Y.N. (1971). Carbon in the structure of apatite according to electron paramagnetic resonance data. *Soviet Physics-Crystallography*, **15**, 1016-1019.

Gillespie, R. and Polach, H.A. (1979). The suitability of marine shells for radiocarbon dating of Australian prehistory. *In*: Berger, R. and Suess H. (eds), *Proceedings Ninth International Conference on Radiocarbon Dating*, pp. 404-421. University of California Press.

Grün, R. (1985a). Beiträge zur ESR-Datierung. *Sonderveröffentlichungen des Geologischen Instituts der Universität zu Köln*, **59**, 1-157.

Grün, R. (1985b). ESR-dating without determination of annual dose: a first application on dating mollusc shells. *In*: Ikeya, M. and Miki, T. (eds), *ESR Dating and Dosimetry*, pp. 115-123. IONICS, Tokyo.

Grün, R. (1986). Beta dose attenuation in thin layers. *Ancient TL*, **4**, 1-8.

Grün, R. (1989). Electron spin resonance (ESR) dating. *Quaternary International*, **1**, 65-109.

Grün, R. and Brumby, S. (1994). The assessment of errors in the past radiation doses extrapolated from ESR/TL dose response data. *Radiation Measurements*, **23**, 307-316.

Grün, R., Schwarcz, H. P. and Zymela, S. (1987). ESR dating of tooth enamel. *Canadian Journal of Earth Sciences*, **24**, 1022-1037.

Grün, R. and Stringer, C.B. (1991). ESR dating and the evolution of modern humans. Archaeometry, **33**, 153-199.

Grün, R., Radtke, U. and Omura, A. (1992). ESR and U-series analyses on corals from Huon Peninsula, New Guinea. *Quaternary Science Reviews*, **11**, 197-202.

Guinasso, N.L. and Schink, D.R. (1975). Quantitative estimate of biological mixing rates in abyssal sediments. *Journal of Geophysical Research*, **80**, 3032-3043.

Gupta, S.K. and Polach, H.A. (1985). *Radiocarbon Dating Practices at ANU*. Radiocarbon Laboratory, Research School of Pacific Studies, ANU, Canberra.

Halliburton, L.E., Jani, M.G. and Bossoli, R.B. (1984). Electron spin resonance and optical studies of oxygen vacancy centers in quartz. *Nuclear Instruments and Methods in Physics Research B1*, 192-197.

Henning, G.J. and Grün, R. (1983). ESR dating in Quaternary geology. *Quaternary Science Reviews*, **2**, 157-238.

Huang, P., Liang, R., Jin, S., Peng, Z. and Rutter, N.W. (1989). Study on accumulated dose in littoral shells of Argentina. *Applied Radiation and Isotopes*, **40**, 1119-1122.

Huh, C.-A. and Kadko, D.C. (1992). Marine sediments and sedimentation processes. *In*: Ivanovich, M. and Harmon, R.S. (eds), *Uranium-series Disequilibrium: Applications to Earth, Marine, and Environmental Sciences*, pp. 460-486. Clarendon Press, Oxford.

Huntley, D.J., Godfrey-Smith D.I. and Thewalt, M.L.W. (1985). Optical dating of sediments. *Nature*, **313**, 105-107.

Huntley, D.J., Hutton, J.T. and Prescott, J.R. (1993). The stranded beach-dune sequence of south-east Australia: A test of thermoluminescence dating, 0-800 ka. *Quaternary Science Reviews*, **12**, 1-20

Huong, H.N., Tung, N.D. and Du, H.V. (1975). Lithic and pollen analysis of the sediments of Tham Khuyen Cave. *Neue Archäol*, Entdeck, 36-39 [in Vietnamese].

Hütt, G., Molodkov, A., Kessel, H. and Raukas, A. (1985). ESR dating of subfossil Holocene shells in Estonia. *Nuclear Tracks and Radiation Measurements*, **10**, 891-898.

Ikeya, M. (1975). Dating a stalactite by electron paramagnetic resonance, *Nature*, **255**, 48-50.

Ikeya, M. (1981). Paramagnetic alanine molecular radicals in fossil shells and bones. *Naturwissenschaften*, **67**,474.

Ikeya, M. (1982). A model of linear uranium accumulation for ESR age of Heidelberg (Mauer) and Tautavel bones. *Japanese Journal of Applied Physics*, **21**, L690-L692.

Ikeya, M. and Ohmura, K. (1981). Dating of fossil shells with electron spin resonance. *Journal of Geology*, **89**, 247-251.

Ikeya, M. and Ohmura, K. (1983). Comparison of ESR ages of corals at marine terraces with ^{14}C and $^{230}Th/^{234}U$ ages. *Earth and Planetary Science Letters*, **65**, 34-38.

Imai, N. and Shimokawa, K. (1989). ESR dating of the tephra "Crystal Ash" distributed in Shinshu, Central Japan. *Applied Radiation and Isotopes*, **40**, 1177-1180.

Imai, N. and Shimokawa, K. (1993). ESR ages trace elements in fossil mollusk shell. *Applied Radiation and Isotopes*, **44**, 161-165.

Ivanovich, M. and Harmon, R.S. (1982). *Uranium series disequilibrium: applications to environmental problems*. Clarendon Press, Oxford.

Ivanovich, M. and Harmon, R.S. (1992). *Uranium-series disequilibrium: applications to earth, marine, and environmental science* (2nd ed.). Clarendon Press, Oxford.

Jones, A., Blackwell, B.A. and Schwarcz, H.P. (1993). Annealing and etching of corals for ESR dating. *Applied Radiation and Isotopes*, **44**, 153-156.

Kai, A. and Ikeya, M. (1989). ESR study of fossil shells in sediments at Hamana Lake. *Applied Radiation and Isotopes*, **40**, 1139-1142.

Kai, A. and Miki, T. (1992). Electron spin resonance of sulphite radicals in irradiated calcite and aragonite. *Radiation Physics and Chemistry*, **40**, 469-476.

Katzenberger, O. and Willems, N. (1988). Interferences encountered in the determination of AD of mollusc samples. *Quaternary Science Reviews*, **7**, 485-489.

Katzenberger, O., Debuyst, R., De Cannière, P., Defehet, F., Apers, D. and Barabas, M. (1989). Temperature experiments on mollusc samples: an approach to ESR signal identification. *Applied Radiation and Isotopes*, **40**, 1113-1118.

Kaufman, A., Broecker, W.S., Ku, T.L. and Thurber, D.L. (1971). The status of U-series methods of mollusk dating. *Geochemica et Cosmochimica Acta*, **35**, 1155-1189.

Kilburn, R. and Rippey, E. (1982). Sea shells of southern Africa. Macmillan South Africa (Publishers) (Pty) Ltd, Johannesburg.

Levy, P. W. (1985). Overview of nuclear radiation damage processes: phenomenological features of radiation damage in crystals and glasses. *SPIE*, **541**, 2-24.

McDermott, F., Grün, R., Stringer, C.B. and Hawkesworth, C.J. (1993). Mass-spectrometric U-series dates for Israeli Neanderthal/early modern hominid sites. Nature, **363**, 252-255.

McKeever, S.W.S. (1984). Thermoluminescence in quartz. *Radiation Protection and Dosimetry*, **8**, 81-98.

McKeever, S.W.S. (1991). Mechanisms of thermoluminescence production: some problems and a few answers? *Nuclear Tracks and Radiation Measurements*, **18**, 5-12.

McKeever, S.W.S., Chen, C.Y. and Halliburton, L.E. (1985). Point defects and the pre-dose effect in natural quartz. *Nuclear Tracks*, **10**, 489-495.

Miki, T. and Kai, A. (1991). Thermal annealing of radicals in aragonitic $CaCO_3$ and $CaPO_4{\cdot}2H_2O$. *Japanese Journal of Applied Physics*, **30**, 404-410.

Miki, T., Kai, A. and Murata, T. (1993). Radiation-induced radicals in sulfite-doped $CaCO_3$. *Applied Radiation and Isotopes*, **44**, 315-319.

Miller, D.E., Yates, R.J., Parkington, J.E. and Vogel, J.C. (1993). Radiocarbon-dated evidence relating to a mid-Holocene relative high sea-level on the south-western Cape coast, South Africa. *South African Journal of Science*, **89**, 35-44.

Molodkov, A. and Hütt, G. (1985). ESR dating of subfossil shells: Some refinements. *In*: Ikeya, M. and Miki, T. (eds), *ESR dating and Dosimetry*, pp. 145-155. IONICS, Tokyo.

Muhs, D.R. and Kennedy, G.L. (1985). An evaluation of uranium-series dating of fossil echinoids from southern California Pleistocene marine terraces. *Marine Geology*, **69**, 187-193.

Murata, T., Kai, A. and Miki, T. (1993). Hydration effects on CO_2^- radicals in calcium carbonates and hydroxyapatite. *Applied Radiation and Isotopes*. **44**, 305-309.

Murray, A.S., Marten, R., Johnston, A. and Martin, P. (1987). Analysis for naturally occurring radionuclides at environmental concentrations by gamma spectrometry. *Journal of Radioanalytical and Nuclear Chemistry (Articles)*, **115**, 263-288.

Ninagawa, K., Yamamoto, I., Yamashita, Y., Wada, T., Sakai, H. and Fujii, S. (1985). Comparison of ESR for fossil calcite shells. *In*: Ikeya, M. and Miki, T. (eds), *ESR Dating and Dosimetry*, pp. 105-114. IONICS, Tokyo.

Nielsen and Roy (1982). Age contamination of radiocarbon dates on shell hash from coastal sand deposits: SE Australian examples. *Proceedings of the 5th Australian Conference on Coastal and Ocean Engineering*, 177-182.

Odom, A.L. and Rink, W.J. (1988). National accumulation of Schottky-Frenkel defects: Implications for a quartz geochronometer. *Geology*, **17**, 55-58.

Omura, A., Emerson, W.K. and Ku, T.-L. (1979). Uranium-series ages of echinoids and corals from the upper Pleistocene Magdalena terrace, Baja California Sur, Mexico. *Nautilus*, **94**, 184-189.

Omura, A., Chappell, J.M.A., Bloom, A..L., Pillans, B., McCulloch, M., Esat, T., Sasaki, K. and Kawada, Y. (1994). Alpha-spectrometric $^{230}Th/^{234}U$ dating of Pleistocene corals. *In*: Ota, Yoko (ed), *Study on coral reef terraces of the Huon Peninsula, Papua New Guinea, Establishment of Quaternary See Level and Tectonic History*. A preliminary report on project 04041048, Monbusho International Research Program, Tokyo.

Peng, Z., Jin, S., Liang, R., Huang, P., Quan, Y. and Ikeya, M. (1989). Study on comparison of ESR dating of coral and shells with $^{230}Th/^{234}U$ and ^{14}C methods. *Applied Radiation and Isotopes*, **40**, 1127-1131.

Prescott, J.R. and Fox, P.J. (1990). Dating quartz sediments using the 325°C TL peak: new spectral data. *Ancient TL*, **8**, 23-35.

Prescott, J.R. and Hutton, J.T. (1988). Cosmic ray and gamma ray dosimetry for TL and ESR. *Nuclear Tracks and Radiation Measurements*, **14**, 223-227.

Prescott, J.R. and Hutton, J.T. (1994). Cosmic ray contributions to dose rates for luminescence and ESR dating: large depths and long-term time variations. *Radiation Measurements*, **23**, 497-500.

Radtke, U. and Grün, R. (1988). ESR dating of corals. *Quaternary Science Reviews*, **7**, 465-470.

Radtke, U., Mangini, A. and Grün, R. (1985). ESR dating of marine fossil shells. *Radiation Measurements*, **10**, 879-884.

Radtke, U., Mangini, A. and Hausmann, R. (1987). Paleosea-level and discrimination of the last and the penultimate interglacial of fossiliferous deposits by absolute dating methods (Th/U, ESR) and geomorphological investigations: Illustrated from marine terraces in Chile. *Berliner Geographische Studien*, **25**, 313-342.

Radtke, U., Grün, R. and Schwarcz, H.P. (1988). Electron spin resonance dating of the Pleistocene coral reef tract of Barbados (W.I.). *Quaternary Research*, **29**, 197-215.

Rendell, H.M., Webster, S.E. and Sheffer, N.L. (1994). Underwater bleaching of signals from sediment grains: new experimental data. *Quaternary Geochronology*, **13**, 433-435.

Roberts, R.G., Spooner, N.A. and Questiaux, D.G. (1994a). Palaeodose underestimates caused by extended-duration preheats in the optical dating of quartz. *Radiation Measurements*, **23**, 647-653.

Roberts, R.G., Jones, R., Spooner, N.A., Head, M.J., Murray, A.S. and Smith, M.A. (1994b). The human colonisation of Australia: optical dates of 53,000 and 60,000 years bracket human arrival at Deaf Adder Gorge, Northern Territory. *Quaternary Geochronology*, **13**, 575-583.

Roberts, R.G., Spooner, N.A., Jones, R., Cane, S., Olley, J.M., Murray, A.S. and Head, M.J. (1996). Preliminary luminescence dates for archaeological sediments on the Nullarbor Plain, South Australia. *Australian Archaeology*, **42**, 7-16.

Roy, P.S. (1991). Shell hash dating and mixing models for palimpsest marine sediments. *Radiocarbon*, **33**, 283-289.

Roy, P.S. and Crawford, E.A. (1977). Significance of sediment dstribution in major coastal rivers, northern N.S.W. *Third Australian Conference on Coastal and Ocean Engineering, Melbourne - Proceedings*, pp. 177-184.

Roy, P.S. and Thom, B.G. (1981). Late Quaternary marine deposition in New South Wales and Southern Queensland - an evolutionary model. *Journal Geological Society of Australia*, **28**, 471-489.

Roy, P.S. and Thom, B.G. (1991). Cainozoic Shelf Sedimentation Model for the Tasman Sea Margin of Southeastern Australia. *In*: Williams, M.A.J., De Deckker, P. and Kershaw, A.P. (eds), *The Cainozoic in Australia: a re-appraisal of the Evidence*, Geological Society of Australia, Special Publication No. 18, 119-136. Australia.

Roy, P.S., Zhuang, W-Y., Birch, G.F. and Cowell, P.J. (1992). Quaternary geology and placer mineral potential of the Forster-Tuncurry Shelf, Southeast Australia. Geological Survey Report: GS 1992/201, Geological Survey of New South Wales, Department of Mineral Resources, Sydney.

Scholefield, R.B., Prescott, J.R., Franklin, A.D. and Fox, P.J. (1994). Observations on some thermoluminescence emission centres in geological quartz. *Radiation Measurements*, **23**, 409-412.

Schwarcz, H.P. (1985). ESR studies of tooth enamel. *Nuclear Tracks*, **10**, 865-867.

Schwarcz, H.P. (1994). Current challenges to ESR dating. *Quaternary Geochronology*, **13**, 601-105.

Schwartz, J.H., Long, V.T., Cuong, N.L., Kha, L.T. and Tattersall, I (1994). A diverse hominoid fauna from the late middle Pleistocene breccia cave of Tham Khuyen, Socialist Republic of Vietnam. *Anthropological Papers of The American Museum of Natural History*, **73**.

Shackleton, N.J. (1987). Oxygen isotopes, ice volume and sea level. *Quaternary Science Reviews*, **6**, 183-100.

Shepherd, S.A. and Thomas, I.M. (1989). Marine invertebrates of southern Australia Part II. South Australian Government Printing Division, Adelaide.

Shimokawa, K. and Imai, N. (1985). ESR dating of quartz in tuff and tephra. *In*: Ikeya, M. and Miki, T. (eds), *ESR Dating and Dosimetry*, pp. 181-186, IONICS, Tokyo.

Shimokawa, K., Imai, N. and Moriyama, A. (1988). ESR dating of volcanic and baked rock. *Quaternary Science Reviews*, **7**, 529-532.

Siegele, R. and Mangini, A. (1985). Progress of ESR studies on $CaCO_3$ of deep sea sediments. *Nuclear Tracks and Radiation Measurements*, **10**, 937-943.

Singh, G., Kershaw, A.P. and Clark, R. (1981a). Quaternary vegetation and fire history in Australia. *In*: Gill, A.M., Groves, R.A. and Noble, I.R. (eds), *Fire and Australian biota*, Australian Academy of Science, Canberra.

Singh, G., Opdyke, N.D. and Bowler, J.M. (1981b). Late Cainozoic stratigraphy, palaeomagnetic chronology and vegetational history from Lake George, N.S.W. *Journal of the Geological Society of Australia*, **28**, 435-452.

Singhvi, A.K., Sharma, Y.P. and Agrawal D.P. (1982). Thermoluminescence dating of sand dunes in Rajasthan, India. *Nature*, **295**, 313-315.

Skinner, A.F. (1983). Overestimate of stalagmitic ESR dates due to laboratory heating. *Nature*, **304**, 152-154.

Skinner, A.F. (1985). Comparison of ESR and $^{230}Th/^{234}U$ ages in fossil aragonitic corals. *In*: Ikeya, M. and Miki, T. (eds), *ESR Dating and Dosimetry*, pp. 135-138. IONICS, Tokyo.

Skinner, A.F. (1986). Dating shells and corals by using the ESR signal in aragonite. *Symposium on Archaeometry '84, Washington, D.C., 14-18 May 1984*, Proceedings, pp. 477-480.

Skinner, A.F. (1988). ESR dating of marine aragonite by electron spin resonance. *Quaternary Science Reviews*, **7**, 461-464.

Smith, B.W., Aitken, M.J., Rhodes, E.J., Robinson, P.D. and Geldard, D.M. (1986). Optical dating: methodological aspects. *Radiation Protection Dosimetry*, **17**, 229-233.

Spooner, N.A. (1994). On the optical dating signal from quartz. *Radiation Measurements*, **23**, 593-600.

Spooner, N.A., Prescott, J.R. and Hutton, J.T. (1988). The effect of illumination wavelength on the bleaching of the thermoluminescence (TL) of quartz. *Quaternary Science Reviews*, **7**, 325-329.

Stuiver, M. and Reimer, P.J. (1993). Extended ^{14}C data base and revised CALIB 3.0 ^{14}C age calibration program. *Radiocarbon*, **35**, 215-230.

Szabo, B.J. and Vedder, J.G. (1971). Uranium-series dating of some Pleistocene marine deposits in southern California. *Earth and Planetary Science Letters*, **11**, 283-290.

Szabó, Z.G. (1969). Kinetic characterization of complex reaction systems. *In*: Bamford, C.H. and Tipper, C.F.H. (eds), *Comprehensive Chemical Kinetics*, pp. 1-80, Elsevier Publishing Company, London.

Tanaka, K., Machette, M.N., Crone, A.J. and Bowman, J.R. (1995). ESR dating of aeolian sand near Tennant Creek, Northern Territory, Australia. *Quaternary Geochronology*, **14**, 385-393.

Tanaka, T., Sawada, S. and Ito, T. (1985). ESR dating of late Pleistocene near-shore and terrace sands in Southern Kanto, Japan. *In*: Ikeya, M. and Miki, T. (eds), *ESR Dating and Dosimetry*, pp. 275-280, IONICS, Tokyo.

Templer, R.H. (1986). The localized transition model of anomalous fading. *Radiation Protection and Dosimetry*, **17**, 493-497.

Thom, B.G. (1983). Transgressive and regressive stratigraphies of coastal sand barriers in southeastern Australia. *Marine Geology*, **56**, 17-158.

Thom, B.G., Bowman, G.M., Gillespie, R., Temple, R. and Barbetti, M. (1981). *Radiocarbon Dating of Holocene Beach Ridge Sequences in Southeast Australia.* Department of Geography, University of New South Wales, Duntroon. Monograph 11, 36.

Thom, B.G., Polach, H. and Bowman, G. (1978). Holocene Age Structure of Coastal Sand Barriers in NSW, Australia. Department of Geography, University of New South Wales, Duntroon. Unpublished report, 86.

Thom, B.G. and Roy, P.S. (1985). Relative sea levels and coastal sedimentation in Southeast Australia in the Holocene. *Journal of Sedimentary Petrology*, **55**, 257-264.

Tsuji, Y., Sakuramoto, Y., Iwasaki, E., Ishiguchi, M. and Ohmura, K. (1985). Ages of pelecypod shells of the last interglacial Shimosueyoshi stage by ESR. *In*: Ikeya, M. and Miki, T. (eds), *ESR Dating and Dosimetry*, pp. 87-92. IONICS, Tokyo.

Walbran, P.D., Henderson, R.A., Jull, A.J.T. and Head, M.J. (1989). Evidence from sediment of long-term *Acanthaster planci* predating on corals of the Great Barrier Reef. *Science*, **245**, 847-850.

Wells, F.E. (1984). A guide to the common molluscs of south-western Australian estuaries. Western Australian Museum, Perth.

Wintle, A. and Huntley, D.J. (1979). Thermoluminescence dating of a deep-sea ocean core. *Nature*, **279**, 710-712.

Yang, X.H. and McKeever, S.W.S. (1988). Characterization of the pre-dose effect using ESR and TL. *Nuclear Tracks and Radiation Measurements*, **14**, 75-79.

Yang, X.H. and McKeever, S.W.S. (1990). The pre-dose effect in crystalline quartz. *Journal of Physics D: Aplied Physics*, **23**, 237-244.

Yates, R.J., Miller, D.E., Manhire, A.H., Parkington, J.E. and Vogel, J.C. (1986). A late mid-Holocene high sea-level: a preliminary report on geo-archaeology at Elands Bay, western Cape Province, South Africa. *South African Journal of Science*, **82**, 164-165.

Yokoyama, Y., Bibron, R., Leger, C. and Quaegebeur, J.P. (1985a). ESR dating of paleolithic calcite: fundamental studies. *Nuclear Tracks*, **10**, 929-936.

Yokoyama, Y., Falgueres C. and Quaegebeur, J.P. (1985b). ESR dating of quartz from Quaternary sediments: first attempt. *Nuclear Tracks and Radiation Measurements*, **10**, 921-928.

Yokoyama, Y., Falgueres C. and Quaegebeur, J.P. (1985c). ESR dating of sediment baked by lava flows: comparison of paleo-doses for Al and Ti centres. *In*: Ikeya, M. and Miki, T. (eds), *ESR Dating and Dosimetry*, pp. 197-204. IONICS, Tokyo.

Yokoyama, Y., Quaegebeur, J.P., Bibron, R. and Leger, C. (1983). ESR dating of Paleolithic calcite: thermal annealing experiment and trapped electron lifetime. *Council of Europe Journal, PACT*, **9**, 371-379.

Zimmerman, D.W. (1971). Thermoluminescence dating using fine grains from pottery. *Archaeometry*, **13**, 29-52.

APPENDIX
(Publications)

A.1 Brumby, S. and Yoshida, H. (1994a). ESR dating of mollusc shell: investigations with modern shell of four species. *Quaternary Geochronology*, **13**, 157-162.

A.2 Brumby, S. and Yoshida, H. (1994b). An investigation of the effect of sunlight on the ESR spectra of quartz centres: implications for dating. *Quaternary Geochronology*, **13**, 615-618.

A.3 Brumby, S. and Yoshida, H. (1995). The annealing kinetics of ESR signals due to paramagnetic centres in mollusc shell. *Radiation Measurements*, **24**, 255-263.

Pergamon

Quaternary Geochronology (Quaternary Science Reviews), Vol. 13, pp. 157–162. 1994.

0277–3791/94 $26.00

0277–3791(94)E0025–6

ESR DATING OF MOLLUSC SHELL: INVESTIGATIONS WITH MODERN SHELL OF FOUR SPECIES

Steven Brumby and Hiroyuki Yoshida

Research School of Chemistry, Australian National University, Canberra, ACT 0200, Australia

The dose response curves for shells of four species of marine mollusc have been studied, using chiefly the g = 2.0014 (2 mW microwave power) and g = 2.0006 (60 mW power) ESR signals. The curves show variable inflexion points and conform only approximately to saturating exponentials with linear components. Annealing experiments suggest the possibility of using the ESR signal at g = 2.0058, after suitable heat treatment, for the estimation of accumulated doses.

INTRODUCTION

Although there have been a number of contributions in the literature devoted to the topic of dating mollusc shell by ESR, confusion still persists. In estimating the accumulated dose (D_E), which signal should be measured, and how?

Molodkov and Hütt (1985) and Hütt *et al.* (1985) identified five lines in the ESR spectra of aragonitic mollusc shell, all of which gave different D_E-values. They considered that D_E-values based on the g = 2.0020 signal (see Fig. 1, top) were reasonable. However Radtke *et al.* (1985) considered that the g = 2.0020 signal had insufficient thermal stability to be a satisfactory dating signal. Furthermore, the amplitude of the signal at g = 2.0007, as usually measured, was influenced by the signal at g = 2.0020, and therefore was also unsuitable for dating. They advocated measuring the amplitude of a g = 2.0014 signal in such a way as to approximately eliminate the effect of the g = 2.0020 signal. Also in 1985, Tsuji *et al.* used a signal at g = 2.0010 for dating and Ninagawa *et al.* dated calcite shells using an ESR signal at g = 2.0044.

Four years later, none of these proposals had won general acceptance. Several groups of workers (Kai and Ikeya, 1989; Huang *et al.*, 1989; Peng *et al.*, 1989) continued to use the signal at g = 2.0006–2.0010, whereas Grün (1989) advised the g = 2.0014 signal. A problem encountered when using the g = 2.0014 signal was that the dose–response curves sometimes showed inflexion points, making extrapolation to determine the D_E hazardous (Katzenberger and Willems, 1988). Katzenberger *et al.* (1989) argued that the g = 2.0014 signal was unsuitable for dating because it consisted of at least three overlapping ESR features. Barabas *et al.* (1992) advocated measuring the amplitude of the g = 2.0006 signal at 'high' microwave power (> 20 mW) with a modulation amplitude of 0.1 mT, but emphasized limitations on the applicability of this method.

We describe here our investigations using for the most part modern shells of four marine mollusc species, aimed at developing a reliable and general methodology for D_E determination.

EXPERIMENTAL

Living molluscs of three marine bivalve species—*Anadara trapezia, Katelesia scalarina* and *Donax deltoides*—and one marine univalve species—*Phalium sinuosum*—were steamed for 20 mins. The shells were separated and washed with water. The outer keratinous layers were removed using a high speed engraving tool fitted with sandpaper discs. In the case of *Anadara trapesia* a preliminary treatment with a file was needed. The shells were crushed and sieved to give particles of 64–250 μm, etched for 10 min in 10% acetic acid, washed three times with distilled water, then allowed to dry at room temperature.

A ^{60}Co source was used for γ-irradiation. 200 mg aliquots were used for ESR, the spectra being recorded digitally using

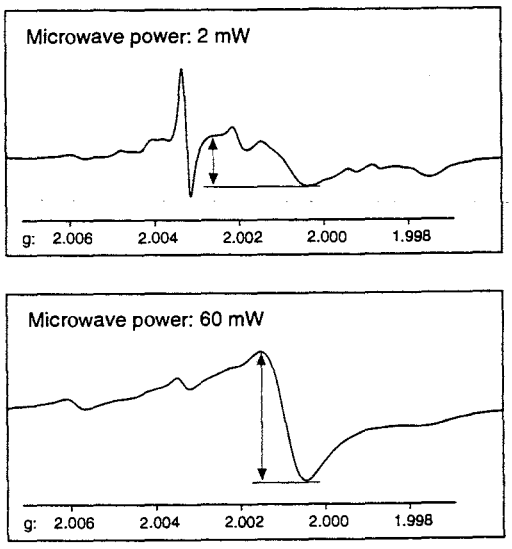

FIG. 1. ESR spectra of modern *Anadara trapesia* shell after γ-irradiation, showing how intensities (amplitudes) were measured.

a Jeol JES-PE spectrometer interfaced to an IBM AT computer.

DOSE–RESPONSE CURVES FOR UN-ANNEALED SHELL

ESR spectra were recorded using microwave powers of 2 mW and 60 mW. For the 2 mW spectra, the intensities of the signal at g = 2.0014 were measured using the method which has been shown diagrammatically a number of times (e.g. Radtke *et al.*, 1985; Katzenberger and Grün, 1985; Katzenberger and Willems, 1988; Grün, 1989) and is shown again in Fig. 1. For the 60 mW spectra the ESR intensities were measured as the peak-to-peak amplitudes of the (first derivative) signal at g = 2.0006, as described by Barabas *et al.* (1992) and as shown in Fig. 1.

Our initial aim was to investigate the mathematical form of the dose–response curve, since this is crucial to the estimation of accumulated doses by the usual back-extrapolation method, especially when the D_E-values are large. To properly assess the importance of inflexion points, as observed by Katzenberger and Willems (1988), we considered it essential to acquire a reasonably large number of data points: accordingly we used 50 aliquots of each species of shell, with applied γ doses spanning the range 0–1500 Gy. Each intensity measurement was made in triplicate, with the sample re-packed into the ESR tube between measurements. The data were analyzed using the program DOSE, which has been described elsewhere (Brumby, 1992).

For all four species of shell, the dose–response curves conformed most closely to the sum of saturating exponentials. Thus, they conformed to the general type described by Katzenberger and Willems (1988); however, the inflexions were less pronounced in our experiments. Over the restricted dose range of 0–400 Gy, the curves showed one or two inflexion points, as illustrated in Fig. 2. The curves shown in Fig. 2 were plotted using data from the

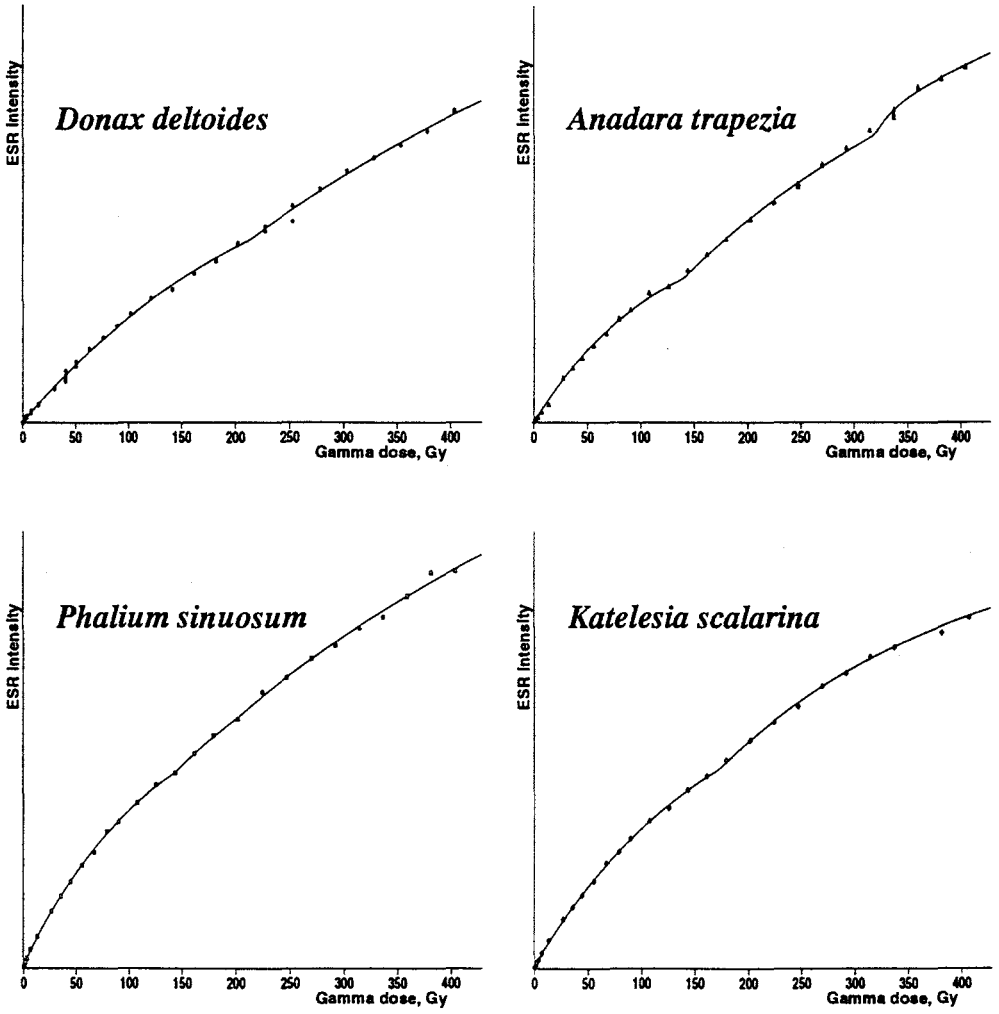

FIG. 2. Dose–response curves of modern shells fitted to the sums of saturating exponentials. *Donax deltoides*—inflexion point at 213 Gy; *Anadara trapesia*—inflexion points at 140 and 320 Gy *Phallium sinuosum*—inflexion points at 144 and 202 Gy *Katelesia scalarina*—inflexion point at 173 Gy.

TABLE 1. Estimated D_E-values (Gy) of modern shells using two types of fitting function, based on intensities determined from ESR spectra recorded using microwave powers of 2 and 60 mW

	Saturating exponential function		Saturating exponential plus linear function	
Shell species	2 mW	60 mW	2 mW	60 mW
Donax deltoides	15.4 ± 1.7	25.5 ± 2.8	5.1 ± 1.1	5.3 ± 0.9
Anadara trapezia	12.5 ± 1.3	12.9 ± 1.2	5.8 ± 0.9	8.3 ± 1.3
Phalium sinuosum	20.3 ± 4.5	17.1 ± 3.3	7.2 ± 3.0	5.8 ± 1.3
Katelesia scalarina	29.6 ± 5.8	29.3 ± 5.4	3.4 ± 1.5	6.2 ± 2.1

spectra recorded using 2 mW microwave power, but very similar curves, with similar inflexion points, were obtained using the 60 mW spectra.

These experiments indicate that there are significant differences between the dose–response curves of different species of mollusc shell. Unfortunately, we have not determined whether there are significant differences between different individuals of the same species.

How serious are these inflexion points when estimating D_E-values? We estimated D_E-values for all four species by fitting the data to a single saturating exponential function, and also to a function consisting of the sum of a saturating exponential and a straight line. The results are shown in Table 1. Bearing in mind that the true D_E-values are zero, two conclusions follow from the table. Firstly, a saturating exponential with linear component is a superior fitting function than a saturating exponential alone. Secondly, it does not seem to make a significant difference whether one uses ESR intensities based on 2 mW or 60 mW spectra.

The D_E-values shown in Table 1 do not necessarily give a direct indication of the error which one would be likely to find when estimating an accumulated dose by extrapolation. It is difficult to generalize about this, because much depends on the lengths of the extrapolated and interpolated portions of the dose response curve, the position of inflection points, and so on. Two examples based on our measurements with *Donax deltoides* will be given. For a sample exposed to a radiation dose of 101 Gy, nine aliquots with additional doses equally spaced in the range 0–812 Gy were used to provide dose response data. The D_E-values found, which would of course be 101 Gy in the absence of extrapolation errors, were (136 ± 4) Gy when a single saturating exponential function was used and (124 ± 7) Gy when a saturating exponential plus linear function was used. When the initial dose was 202 Gy and nine aliquots with additional doses equally spaced in the range 0–1316 Gy were used, the D_E-values found were (260 ± 11) Gy and (217 ± 19) Gy for saturating exponential functions and saturating exponential plus linear functions, respectively. Clearly, in this type of work it is advantageous to use saturating exponential plus linear functions for extrapolation, but even then errors of about 25% are quite possible.

ANNEALING EXPERIMENTS

When mollusc shell was heated following γ-irradiation, typically the ESR intensities developed as shown in Fig. 3. The intensities of the signals at g = 2.0014 and 2.0020 (measured using 2 mW microwave power) decreased. The signal at g = 2.0033 showed initially a small increase, followed by a decrease. The signal at g = 2.0058 increased. For the signal at g = 2.0006 (measured using 60 mW microwave power) there was an initial small increase on heating at 140, 145 or 150°C, followed by a decrease. Since this behaviour was qualitatively similar to the behaviour of the g = 2.0033 signal recorded at 2 mW power, it seems possible that the g = 2.0033 signal, although broadened by the effects of saturation, still contributes significant intensity to the signal measured at 60 mW.

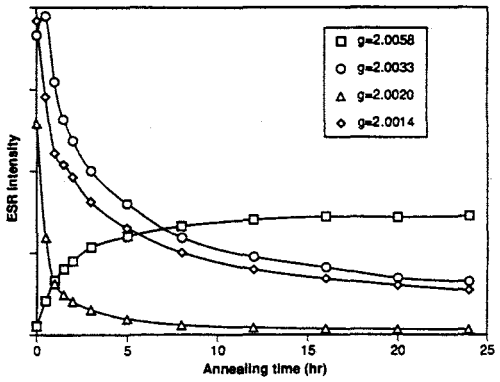

FIG. 3. Build-up and decay at 145°C of ESR intensities (from spectra recorded using 2 mW microwave power) of *Anadara trapezia*, following a γ-dose of 400 Gy.

We have arrived at the following plausible, but admittedly unproven, interpretation of events. Part of the intensity of the signal at g = 2.0033 is due to SO_3^- defects (Barabas, 1992). By a process requiring thermal activation, these defects give rise to SO_2^- defects, with an ESR signal at g = 2.0058 (Barabas, 1992; Miki *et al.*, 1993). As expected on the basis that thermal activation is a requirement for their formation, these SO_2^- defects are not formed directly on γ-irradiation at ambient temperatures. However, ancient shells show significant signals at g = 2.0058, indicating that the processes which occur in a few hours at elevated temperatures also proceed over long periods at ambient temperatures. Once formed, the defects with g = 2.0058 have great thermal stability, as other workers have noted (Yokoyama *et al.*, 1983).

A feature of the highly anisotropic spectrum of CO_2^- also occurs at ca. g = 2.0033 (Katzenberger *et al.*, 1989), but is probably too broad to contribute much to the intensity as measured. There appears to be a narrower, approximately isotropic, component in the g = 2.0033 signal, which shows an initial rise in intensity on heating, and good thermal stability on prolonged heating. It is possible that this signal may be due to an organic constituent of the shell, as suggested by Katzenberger *et al.* (1989).

Our hypothesis may be expressed in the following way:

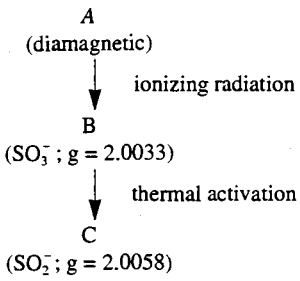

Suppose that the first of these transformations is first order with respect to the concentration of A (with rate constant k_1), which clearly requires that the flux of ionizing radiation (i.e. the annual dose) be constant, and that the second transformation is first order with respect to the concentration of B (with rate constant k_2), requiring that the temperature be constant. In this situation, kinetic analysis yields equations for the build-up of B and C with respect to time which have been given, for example, by Szabó (1969). Accordingly, we γ-irradiated five aliquots of modern *Katelesia scalarina* shell for different times using a dose rate of ca. 0.1 Gy/min, while maintaining the temperature at 150°C using an oil bath. The concentration of C could be monitored directly by measuring the peak-to-peak amplitudes of the ESR signal at g = 2.0058. The concentration of B could not similarly be determined from the g = 2.0033 signal because of the interfering signals; furthermore we wished to maintain the same proportionality to concentration. Therefore the concentration of B was monitored on the basis of the increase in amplitude of the g = 2.0058 signal on annealing for 14 hr at 150°C. The signal amplitudes, considered proportional to the concentrations of B and C, are plotted in Fig. 4, in which the continuous curves were plotted using Eqns (1) and (2), corresponding to the Eqns (11) and (12) given by Szabó (1969).

$$\frac{[B]}{[A]_0} = \frac{1}{\kappa - 1}[\exp(-\tau) - \exp(-\kappa\tau)] \qquad (1)$$

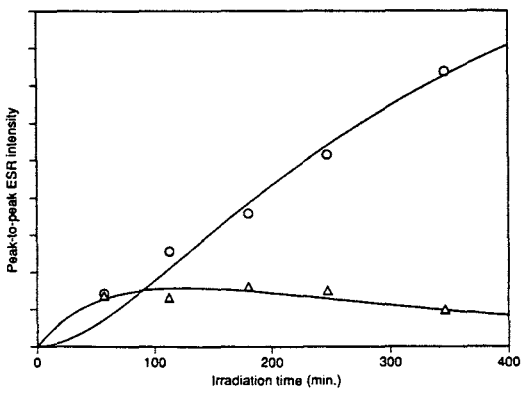

FIG. 4. Intensity of the g = 2.0058 signal (circles) and increase in intensity of the g = 2.0058 signal on prolonged annealing (triangles) versus irradiation time for *Katelesia scalarina* shell, maintained at 150°C during irradiation. The continuous curves were calculated using Eqns (11) and (12) given by Szabó (1969).

$$\frac{[C]}{[A]_0} = 1 + \frac{1}{1 - \kappa}[\kappa \exp(-\tau) - \exp(-\kappa\tau)]. \qquad (2)$$

In these equations, the dimensionless quantities τ and κ are defined as $k_1 t$, where t denotes time, and k_2/k_1, respectively. The agreement between experiment and theory is probably satisfactory in view of the experimental errors involved, but further experiments are needed using different dose rates and temperatures.

It is interesting to consider how this hypothesis, if correct, could be exploited in dating studies. If one measures the amplitude of the g = 2.0058 signal for the natural sample before and after annealing, and also for the annealed sample which has received a sufficiently large γ-dose to cause saturation, then one has the information needed to estimate the ratios $[B]/[A]_0$ and $[C]/[A]_0$. By solving Eqns (1) and (2) simultaneously, using numerical methods, it is possible to determine both τ and κ. From a dating perspective, the important information extracted is τ, equal to $k_1 t$, but this is equivalent to information which could be obtained from a dose response plot, with the response being the g = 2.0058 amplitude after annealing. The argument goes as follows: it may be shown that $k_1 = ad$, where a is the radiolytic yield and d the annual dose; since the accumulated dose, D_E, is equal to dt, one arrives at the relationship $\tau = D_E a$. In practice, determining D_E from a dose response plot is probably a more satisfactory procedure than solving (1) and (2) simultaneously. This is especially true when one suspects that the annual dose may have fluctuated during the life of the sample.

How then can the kinetic equations be used? To provide insight into the thermal and radiation history of the sample, the ratio of the increase in amplitude of the g = 2.0058 signal on annealing (proportional to $[B]$) to the amplitude of this signal in the natural sample (proportional to $[C]$) may be informative. This ratio tends to be large when the storage temperature is low and/or the annual dose is large, and *vice versa*: the precise behaviour, from the equations given by Szabó (1969), is given by Eqn. (3):

$$\frac{[B]}{[C]} = \frac{k_1[\exp(-k_1 t) - \exp(-k_2 t)]}{k_2[1 - \exp(-k_1 t)] - k_1[1 - \exp(-k_2 t)]}. \qquad (3)$$

Of course, if the values of the rate coefficients were known, or could be calibrated, this equation would provide a means by which one could estimate the age of a sample, t. While k_1 may possibly be estimated on the basis of the annual dose and the radiolytic yield, k_2 is certainly temperature dependent, and is probably also strongly species-dependent. There is even evidence that k_2 may vary dramatically within the same individual (Imai and Shimokawa, 1993). Because of these problems, Eqn. (3) may not generally be useful for actually determining the age, t. But there are other ways in which the equation can be used. The ratio $[B]/[C]$ provides at least semi-quantitative information concerning the interplay between age, annual dose and storage temperature. This can be especially useful when comparing samples for which one or more of these parameters can be assumed to be invariant.

Our experiments do not provide any direct evidence that

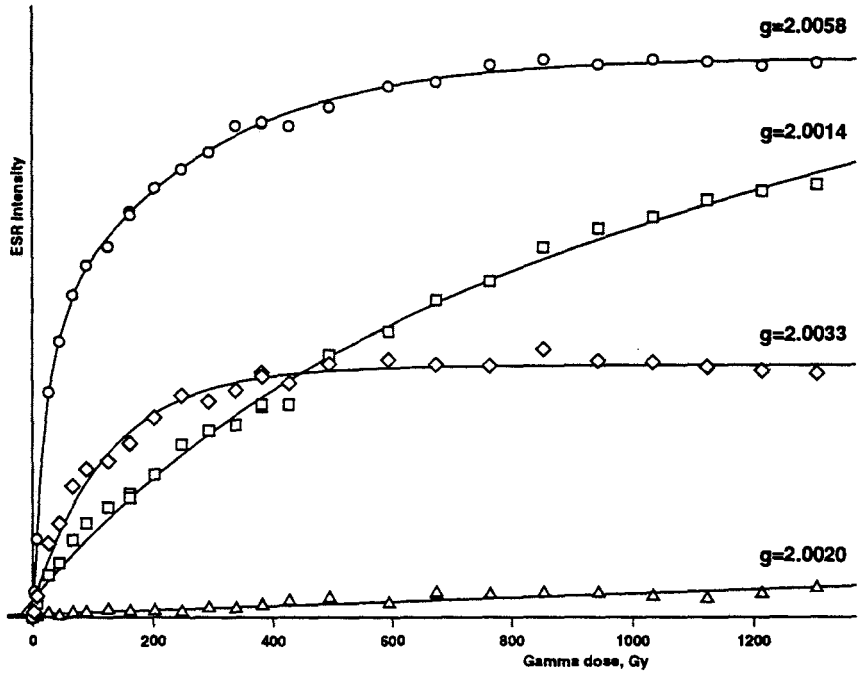

FIG. 5. Dose–response curves based on the intensities of various ESR signals (recorded using 2 mW microwave power) of *Anadara trapezia*, with aliquots annealed for 14 hr at 150°C after γ-irradiation.

species B is correctly associated with the g = 2.0033 signal. We consider that this signal is involved because (a) the chemistry of the thermally activated process may then be rationalized (although the fate of the released oxygen atom is not clear) and; (b) when the dose–response curves for the unannealed g = 2.0033 signal and the g = 2.0058 signal after prolonged annealing are compared, both curves saturate over a similar range of dose. To find further evidence, it might appear that one only has to doubly integrate the g = 2.0058 and g = 2.0033 signals before and after annealing, with a view to determining whether the decrease in intensity of the g = 2.0033 signal is equal to the increase in intensity of the g = 2.0058 signal. We have attempted to do this, but there are severe difficulties. One difficulty is the need to use extremely low microwave powers to avoid saturation effects which might be different for the two types of centre. An even greater difficulty is the fact that the g = 2.0033 signal is superimposed on other signals, the intensities of which also change on annealing. Our measurements seem to be consistent with the proposition that B is associated with the g = 2.0033 signal, but are not conclusive.

We consider that the signal at g = 2.0058 can be used for D_E estimation, provided that the samples are suitably annealed following γ-irradiation. Fourteen hours at 150°C seems to be a suitable post-irradiation treatment. It is necessary to anneal the natural sample as well as irradiated samples. Dose–response curves obtained following thermal treatment in this way are shown in Fig. 5. The only limitation on the use of the g = 2.0058 signal seems to be that, for the samples we have studied, the signal saturates at relatively low doses. This makes the method unsuitable for extremely old samples, which is particularly unfortunate in view of the fact that it is precisely for these very old samples that one would have hoped to benefit most from the excellent thermal stability of the g = 2.0058 signal. A similar method of D_E estimation has been recommended for palaeolithic calcite samples (Yokoyama *et al.*, 1985).

If one follows this procedure, it is advisable to record the spectrum of the natural sample before annealing. The ratio of the increase in intensity of the g = 2.0058 signal on annealing to its initial intensity seems to be potentially highly informative. This ratio is influenced by the annual dose, the storage temperature and species of mollusc and the age.

There are indications in the literature that for some species of shell the g = 2.0058 signal may be directly γ-sensitive, contrary to what we have found. For these species, presumably k_2 is relatively large at ambient temperatures. Using a single *Mya oonogai* shell, Imai and Shimokawa (1993) found that the g = 2.0058 signal was γ-sensitive in some parts of the shell and not in other parts. This may help explain the observed variations in intensity of g = 2.0058 and g = 2.0033 signals, and their correlation with uranium distribution. There is evidence that the properties of the g = 2.0058 signal in corals may similarly be variable (Walther *et al.*, 1992).

CONCLUSIONS

(1) When the g = 2.0014 signal is used for dating,

inflexions in the dose–response curve may give rise to errors in estimated D_E-values. These errors can be minimized if the curves are fitted to the sum of a saturating exponential and a straight line, but may still be significant. It remains to be seen whether the thermal stabilities of component signals are sufficient to avoid underestimating D_E-values.

(2) We do not find any convincing advantage in using the g = 2.0006 signal measured at high microwave power. This technique can only partially suppress the unwanted signals, as shown by the lack of symmetry in the spectra. The signal intensity initially increases on heating, which is another reason why the use of high microwave powers should possibly be viewed with suspicion.

(3) The ESR signal at g = 2.0058 seems to have good potential for dating. However, all aliquots must be subjected to a post-irradiation heat treatment, typically 14 hr at 150°C. It may be difficult to determine D_E-values greater than about 200 Gy because of saturation, but this would presumably depend on the sample. The ratio of the increase in intensity of the signal at g = 2.0058 on annealing to its initial intensity in the natural sample may contain useful information concerning the inter-related effects of age, storage temperature and annual dose.

REFERENCES

Barabas, M. (1992). The nature of the paramagnetic centres at g = 2.0057 and g = 2.0031 in marine carbonates. *Nuclear Tracks and Radiation Measurements*, **20**, 453–464.

Barabas, M., Mudelsee, M., Walther, R. and Mangini, A. (1992). Dose–response and thermal behaviour of the ESR signal at g = 2.0006 in carbonates. *Quaternary Science Reviews*, **11**, 173–179.

Brumby, S. (1992). Regression analysis of ESR/TL dose-response data. *Nuclear Tracks and Radiation Measurements*, **20**, 595–599.

Grün, R. (1989). Electron spin resonance (ESR) dating. *Quaternary International*, **1**, 65–109.

Huang, P., Liang, R., Jin, S., Peng, Z. and Rutter, N.W. (1989). Study on accumulated dose in littoral shells of Argentina. *Applied Radiation and Isotopes*, **40**, 1119–1122.

Hütt, G., Molodkov, A., Kessel, H. and Raukas, A. (1985). ESR dating of subfossil Holocene shells in Estonia. *Nuclear Tracks and Radiation Measurements*, **10**, 891–898.

Imai, M. and Shimokawa, K. (1993). ESR ages and trace elements in a fossil mollusc shell. *Applied Radiation and Isotopes*, **44**, 161–165.

Kai, A. and Ikeya, M. (1989). ESR study of fossil shells in sediments at Hamana Lake. *Applied Radiation and Isotopes*, **40**, 1139–1142.

Katzenberger, O. and Grün, R. (1985). ESR dating of circumarctic molluscs. *Nuclear Tracks and Radiation Measurements*, **10**, 885–890.

Katzenberger, O. and Willems, N. (1988). Interferences encountered in the determination of AD of mollusc samples. *Quaternary Science Reviews*, **7**, 485–489.

Katzenberger, O., Debuyst, R., De Cannière, P., Dejehet, F., Apers, D. and Barabas, M. (1989). Temperature experiments on mollusc samples: an approach to ESR signal identification. *Applied Radiation and Isotopes*, **40**, 1113–1118.

Miki, T., Kai, A. and Murata, T. (1993). Radiation-induced radicals in sulfite-doped $CaCO_3$. *Applied Radiation and Isotopes*, **44**, 315–319.

Molodkov, A. and Hütt, G. (1985). ESR dating of subfossil shells: Some refinements. *In*: Ikeya, M. and Miki, T. (eds), *ESR Dating and Dosimetry*, pp. 145–155. IONICS.

Ninagawa, K., Yamamoto, I., Yamashita, Y., Wada, T., Sakai, H. and Fujii, S. (1985). Comparison of ESR for fossil calcite shells. *In*: Ikeya, M. and Miki, T. (eds), *ESR Dating and Dosimetry*, pp. 105–114. IONICS.

Peng, Z., Jin, S., Liang, R., Huang, P., Quan, Y. and Ikeya, M. (1989). Study on comparison of ESR dating of coral and shells with $^{230}Th/^{234}U$ and ^{14}C methods. *Applied Radiation and Isotopes*, **40**, 1127–1131.

Radtke, U., Mangini, A. and Grün, R. (1985). ESR dating of marine fossil shells. *Nuclear Tracks and Radiation Measurements*, **10**, 879–884.

Szabó, Z.G. (1969). Kinetic characterization of complex reaction systems. *In*: Bamford, C.H. and Tipper, C.F.H. (eds), *Chemical Kinetics*, pp. 17–20. Elsevier.

Tsuji, Y., Sakuramoto, Y., Iwasaki, E., Ishiguchi, M. and Ohmura, K. (1985). Ages of pelecypod shells of the last interglacial Shimosueyoshi stage by ESR. *In*: Ikeya, M. and Miki, T. (eds), *ESR Dating and Dosimetry*, pp. 87–92. IONICS.

Walther, R., Barabas, M., and Mangini, A. (1992). Basic ESR studies on recent corals. *Quaternary Science Reviews*, **11**, 191–196.

Yokoyama, Y., Quaegebeur, J.P., Bibron, R. and Leger, C. (1983). ESR dating of Paleolithic calcite: thermal annealing experiment and trapped electron lifetime. *PACT*, **9**, 371–379.

Yokoyama, Y., Bibron, R., Leger, C. and Quaegebeur, J.P. (1985). ESR dating of palaeolithic calcite; fundamental studies. *Nuclear Tracks and Radiation Measurements*, **10**, 929–936.

Pergamon

Quaternary Geochronology (Quaternary Science Reviews), Vol. 13, pp. 615–618, 1994.

0277-3791/94 $26.00

0277-3791(94)E0068-L

AN INVESTIGATION OF THE EFFECT OF SUNLIGHT ON THE ESR SPECTRA OF QUARTZ CENTRES: IMPLICATIONS FOR DATING

S. Brumby and H. Yoshida
Research School of Chemistry, Australian National University, Canberra, ACT 0200, Australia

The behaviour of ESR signals due to titanium and aluminium centres in quartz sand on exposure to sunlight has been investigated. Samples of sand were recovered from cores taken off the coast of southeast Australia, at Forster-Tuncurry, and at an inland lake, Lake George. Naturally irradiated samples, and also samples which were annealed and then artificially irradiated with gamma rays, were used. The ESR signal due to titanium centres shows promise for dating the last exposure to sunlight of quartz grains.

INTRODUCTION

During the past few years a recurring question has been: can the ESR method be used to date quartz grains in sediments? In other words: does sunlight quench the ESR signals of quartz, as it is known to quench the thermoluminescence? Tanaka *et al.* (1985) directed their attention to the ESR signal due to germanium centres, as may be judged from the reported *g*-value of 1.997. They found that the intensity of the signal decreased to zero after 7 hr of exposure to sunlight. Accordingly, they used ESR to estimate the ages of near-shore and terrace sands. On the basis of an assumed dose rate, good agreement was found with fission track ages. Yokoyama *et al.* (1985a) studied the ESR spectra due to aluminium centres. Their aim was to estimate the ages of samples of quartz sand collected from hominid sites at Arago cave and Terra Amata. The 'zero age' intensities were estimated from material collected at the surface nearby, and were both approximately 60% of the intensities of the samples from the hominid sites. The estimated ages were in agreement with faunal studies. Buhay *et al.* (1988) studied the change in intensity of ESR signals due to Ge, Al, Ti and OH centres in quartz on exposure to UV light and to sunlight. The Ge signals were totally bleached within 10–20 hr, whereas the other signals were little affected within the exposure times investigated. Jin *et al.* (1993) studied the effect of radiation in the visible–UV region on the ESR intensity due to the E′ centre. For quartz grains from loess, there was an *increase* in intensity on exposure, whereas for quartz grains from fault there was no measurable change.

Evidently the E′ centre does not show promise for dating sedimentary quartz, but for the other centres one is concerned not only with the question of bleachability but also with thermal stability. Yokoyama *et al.* (1985b) compared the thermal stabilities of Al, Ti and Ge centres in quartz by isochronal annealing experiments. The order of increasing stability was Al, Ge, Ti, although the differences were not large. In similar experiments, Shimokawa and Imai (1985) found Ti centres to be markedly more stable than Al centres. When they compared the ages determined using Al and Ti ESR signals with ages determined by TL and fission track, they were able to rationalise the results on the basis of the greater thermal stability of the Ti centres. Later comparing the stabilities of Ge, OH and Al centres, Shimokawa and Imai (1987) found the order of increasing stability to be Al, Ge, OH. This provided an explanation for their observation that the ESR age based on the Al signal was in agreement with the TL age, whereas the ESR ages based on the Ge and OH signals agreed with the fission track age. Falguères *et al.* (1991) found the order of increasing thermal stability to be Ge, Al, Ti. Toyoda and Ikeya (1991), using quartz grains separated from granite, found that the Al centres showed *greater* stability than the Ti centres, the reverse of the situation found in previous studies.

We have used samples of quartz sand from a coastal marine environment, and from a lake sediment. In common with many naturally occurring samples of quartz, our samples showed no E′ or OH defect centres detectable by ESR, and weak or unobservable Ge centres. Our primary aim was to determine the ways in which the ESR intensities due to Al and Ti centres developed over a prolonged period of exposure to sunlight.

EXPERIMENTAL

Details of the five samples of quartz studied are given in Table 1. Particles in the size range 75–250 μm were used, and aliquots weighed 200 mg.

Ten aliquots of each sample were placed in quartz tubes (about 40 × 5 mm) with polythene caps. All 50 tubes were placed in a custom-built rack in which the tubes were fixed horizontally, so that the maximum vertical depth of sample was ca. 1.5 mm. The rack was placed in a position where it was not shaded from the

TABLE 1. The samples

Provenance	Depositional environment	Depth	Sample	Treatment*
Forster-Tuncurry, NSW, Australia	Pleistocene barrier	Water depth: 23.5 m Sub-bottom: 190–195 cm	Q13-A	A
		Water depth: 38.3 m Sub-bottom: 120–125 cm	Q18-A Q18-B	A B
Lake George, NSW, Australia	Lake sediment	Water depth: 0 m Sub-bottom: 300 cm	LG-A LG-B	A B

*A — Sample treated with 10% HCl, 10% HF, washed with water and dried. B — After the same pre-treatment, the sample was annealed for 24 hr at 550°C, then exposed to a γ-dose of 500 Gy.

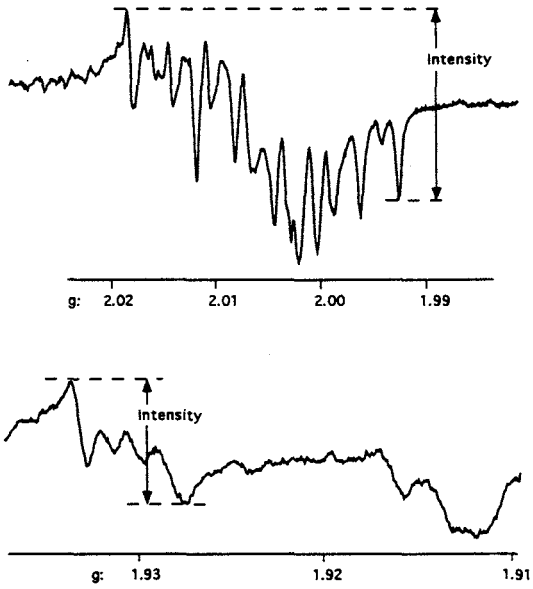

FIG. 1. The methods used to estimate the intensities of the ESR signals due to aluminium centres (above) and titanium centres (below).

sun. After suitable periods of exposure, selected tubes were removed from the rack and stored in the dark. After 132 days the last tubes were removed, and all the ESR spectra were then recorded, while maintaining the samples at the boiling point of liquid nitrogen. The experiment was conducted in this way to avoid possible errors arising from long-term instability of the spectrometer. The ways intensities were measured are shown in Fig. 1.

TL measurements were made by D.M. Price (University of Wollongong).

RESULTS

The ESR intensities measured for the aliquots not exposed to sunlight varied over a wide range, but in Figs 2 and 3 the intensities have been scaled so that all these initial intensities are 100. Figure 2 shows how the relative intensities of the aluminium signal developed with exposure time. The sample Q18-B behaved anomalously, and the intensity of its Al signal fell after 132 days to 25% of its initial value. This sample had been annealed to remove its ESR signals entirely, and then subjected to a 500 Gy dose of γ-rays from a ^{60}Co source: evidently under these conditions a higher proportion of bleachable Al defects

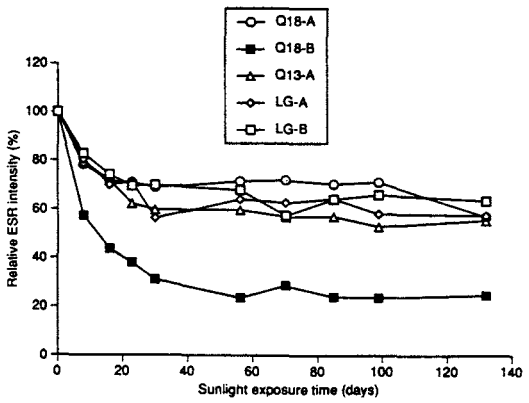

FIG. 2. The change in the relative ESR intensity of the aluminium signal on exposure to sunlight.

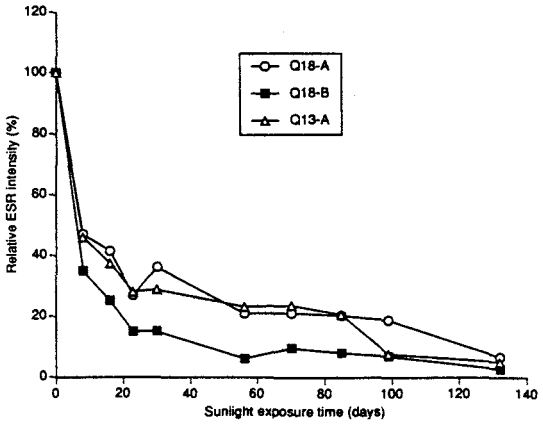

FIG. 3. The change in the relative ESR intensity of the titanium signal on exposure to sunlight.

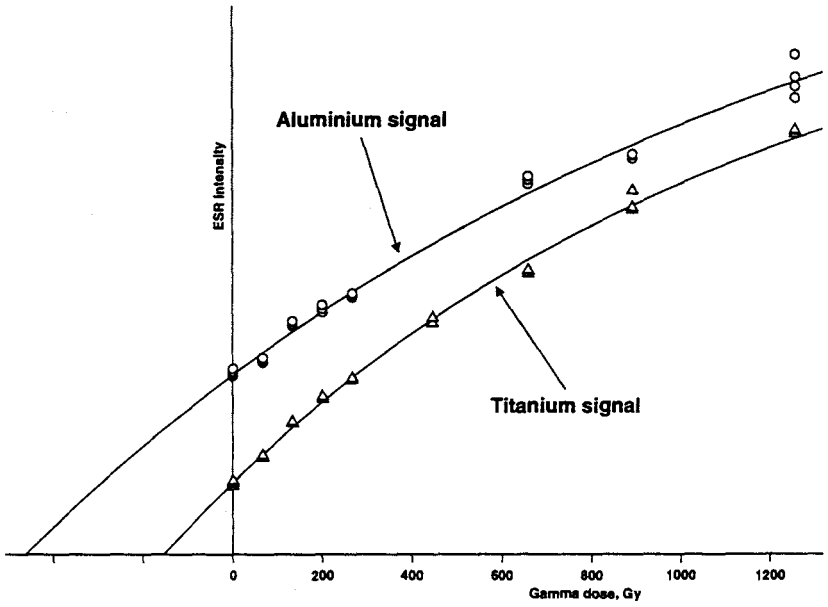

FIG. 4. Dose–response curves for sample Q18-A, based on both aluminium and titanium signals.

were produced than during natural irradiation. For the other four samples the intensities fell on average to 58% of their initial values after 132 days. It is interesting to note that Yokoyama *et al.* (1985a) concluded that unbleachable Al centres had about 60% of the total Al centre intensity; however, this figure was based on the assumption that recently deposited sand and sand at the time it was deposited up to about 0.5 Ma ago both contained the same concentration of unbleachable Al centres.

Figure 3 shows the development of the relative intensities due to titanium centres on exposure to sunlight for the marine samples. After 132 days the intensities fell on average to 5% of their initial values. Unfortunately, our lake sediment samples showed no detectable titanium signals.

For the sample Q18-B, which was annealed and then artificially irradiated, there is little doubt, based on experiments by Buhay *et al.* (1988), that D_E-values estimated using the Al and Ti signals in the ESR spectra would both agree with the applied dose of 500 Gy. For the natural sediment sample Q18-A, the dose–response curves are shown in Fig. 4, and D_E-values estimated by ESR and TL for both the marine samples are reported in Table 2. As expected on the basis of the sunlight bleaching experiments, the D_E-values based on the Al signal are larger than those based on the Ti signal.

Under suitable circumstances, there are compelling reasons to trust the D_E-values based on extrapolation of ESR intensities due to Ti centres. These signals are completely, or nearly completely, reset by sunlight of sufficient intensity and duration. furthermore, there is considerable evidence in the literature (referred to in the introduction above) that Ti centres have excellent thermal stability. At this stage it is not clear how effectively the Ti signal is reset when sediments are deposited from water — clearly the likely turbidity and depth need to be considered. Incomplete resetting of the Ti signal at sedimentation is one of several possible explanations for the discrepancies between the equivalent doses estimated by ESR using the Ti centre and by TL (Table 2). Another possibility is that,

TABLE 2. Equivalent doses estimated by different methods

	Equivalent dose (Gy)		
Sample	ESR — Al signal	ESR — Ti signal	TL
Q13-A	1099±249	298±46	130.9±17.2
Q18-A	462±31	154±5	55.4±7.3

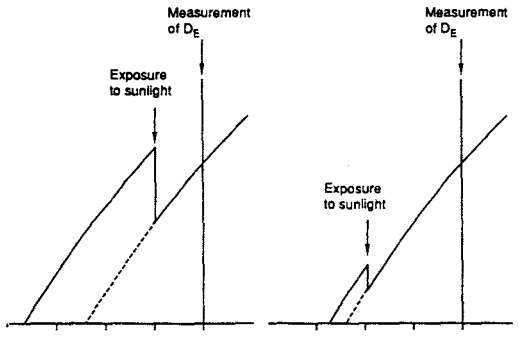

FIG. 5. Build-up of the aluminium centres with respect to time. Two possible histories which both result in the same concentration of aluminium centres at the time of measurement.

because of mixing and reworking of these sediments, the two methods were actually dating different events, involving different periods of exposure to sunlight. Yet another possibility is that the thermoluminescence did not have the required thermal stability under the storage conditions of the sediments.

Can the aluminium signal be used for dating? If one extrapolates the Al dose–response curve to an intensity of 58% of the natural intensity, one obtains D_E-values in reasonably good agreement with those based on the Ti signal. This was the underlying principle used by Yokoyama *et al.* (1985a), which also gave reasonable results. But it is difficult to find a convincing justification for either procedure, and it may be fortuitous that the results seem plausible. The methods require that, following sedimentation, only bleachable Al centres are produced (otherwise the intensity of the unbleachable component at the time of sedimentation could not be estimated from the present day material). But this is not consistent with our observation that the ratio of bleachable to unbleachable Al centres was similar among the samples studied (with one exception). An alternative interpretation is that natural ionizing radiation produces Al centres of which about 58% are unbleachable. If this is correct, the Al centre probably is not suitable for use in dating. This is made clear in Fig. 5, which shows that exposure to sunlight at two different times, and both accompanied by the same relative decrease in intensity of the ESR signal due to aluminium centres, cannot be distinguished.

A plausible, but unproven, variation on the above proposal is that aluminium centres approach thermodynamic equilibrium in the dark, with a bleachable/unbleachable ratio of approximately 2/3 at equilibrium. In this event also, there does not seem to be any straightforward way in which the ESR signal due to aluminium centres can be used for dating.

Of course, if one could assume that the aluminium centres were saturated before sedimentation, then dating the event using the aluminium centre ESR signal would be a possibility, but this assumption cannot usually be made.

CONCLUSION

For dating the last exposure of quartz grains to sunlight by ESR, the aluminium signal is probably not useful, because it is not completely reset by sunlight. The titanium signal, on the other hand, is almost completely reset by sunlight of sufficient duration and intensity. Considering also its excellent thermal stability, the titanium signal seems to have good potential for dating.

REFERENCES

Buhay, W.M., Schwarcz, H.P. and Grün, R. (1988). ESR dating of fault gouge: The effect of grain size. *Quaternary Science Reviews*, **7**, 515–522.

Falguères, C., Yokoyama, Y. and Miallier, D. (1991). Stability of some quartz centres in quartz. *Nuclear Tracks and Radiation Measurements*, **18**, 155–161.

Jin, S.-Z., Deng, Z. and Huang, P.-H. (1993). A comparative study on optical effects of E′ center in quartz grains from loess and fault. *Applied Radiation and Isotopes*, **44**, 175–178.

Shimokawa, K. and Imai, N. (1985). ESR dating of quartz in tuff and tephra. *In*: Ikeya, M. and Miki, T. (eds), *ESR Dating and Dosimetery*, pp. 181–186. IONICS, Tokyo.

Shimokawa, K. and Imai, N. (1987). Simultaneous determination of alteration and eruption ages of volcanic rocks by electron spin resonance. *Geochimica et Cosmochimica Acta*, **51**, 115–119.

Tanaka, T., Sawada, S. and Ito, T. (1985). ESR dating of late Pleistocene near-shore and terrace sands in Southern Kanto, Japan. *In*: Ikeya, M. and Miki, T. (eds), *ESR Dating and Dosimetry*, pp. 275–280. IONICS, Tokyo.

Toyoda, S. and Ikeya, M. (1991). Thermal stabilities of paramagnetic defect and impurity centers in quartz: Basis for ESR dating of thermal history. *Geochemical Journal*, **25**, 437–445.

Yokoyama, Y., Falguères, C. and Quaegebeur, J.P. (1985a). ESR dating of quartz from quaternary sediments: first attempt. *Nuclear Tracks and Radiation Measurements*, **10**, 921–928.

Yokoyama, Y., Falguères, C. and Quaegebeur, J.P. (1985b). ESR dating of sediment baked by lava flows: comparison of paleo-doses for Al and Ti centers. *In*: Ikeya, M. and Miki, T. (eds), *ESR Dating and Dosimetry*, pp. 197–204. IONICS, Tokyo.

Pergamon

Radiation Measurements, Vol. 24, No. 3, pp. 255–263, 1995

1350-4487/95 $9.50 + .00

1350–4487(94)00117–0

THE ANNEALING KINETICS OF ESR SIGNALS DUE TO PARAMAGNETIC CENTRES IN MOLLUSC SHELL

STEVEN BRUMBY and HIROYUKI YOSHIDA
Research School of Chemistry, Australian National University, Canberra, ACT 0200, Australia

(*Received* 14 *March* 1994; *revised* 2 *June* 1994; *revised* 26 *October* 1994; *in final form* 8 *December* 1994)

Abstract—After γ-irradiation of modern shell, the changes in amplitude of the ESR signals at $g = 2.0058$, 2.0032, 2.0020 and 2.0006 (from spectra recorded at X- and Q-band) were monitored during isothermal annealing at 91–130°C. The amplitude of the $g = 2.0020$ signal shows a logarithmic dependence on time, suggesting that the decay may occur by the diffusion together of pairs of defects. The kinetics of the decay of the $g = 2.0032$ signal and of the increase of the $g = 2.0058$ signal seem to be consistent with an earlier suggestion that these processes may be interrelated. The $g = 2.0006$ signal (at Q-band) shows a complex evolution with time.

INTRODUCTION

When estimating ages by luminescence (TL or OSL) or electron spin resonance (ESR) methods it is crucially important to have a plausible estimate of the mean lifetime of the species of trapped electron or hole used in the method. Such an estimate is possible on the basis of measurements at elevated temperatures provided it can be shown that (a) the thermal quenching of the species has 1st-order kinetics, and (b) the Arrhenius equation provides a satisfactory means of extrapolating to the probable storage temperature of the sample. A number of lifetimes estimated in this way were tabulated by Hennig and Grün (1983). Other examples have been given by Grün and de Canniére (1984), Grün (1985), Wintle (1977), Strickertsson (1985) and others.

Assumption (a) is equivalent to assuming that the lifetime of the paramagnetic centre is a constant, independent of the concentration of centres or their spatial distribution. The validity of the assumption can be checked by examining the time dependence of the response (e.g. signal amplitude), or, in the case of TL, by establishing that the glow curve has the appropriate shape (Randall and Wilkins, 1945). Unfortunately, it is often not clear whether these tests have been rigorously applied. Assumption (b) is more difficult, and perhaps impossible, to justify. While it may be possible to demonstrate that the Arrhenium equation is closely obeyed within the temperature range investigated experimentally, a huge extrapolation to the storage temperature is needed. It seems quite likely that a distinct quenching mechanism—an obvious example is quantum mechanical tunnelling—may dominate at the relatively low temperature of storage. The observation of anomalous fading in TL gives serious cause for concern on this account. Possibly any lifetime extrapolated using the Arrhenius equation should be regarded as a minimum value.

Of course, even if the Arrhenius equation were precisely obeyed, extrapolation errors would be considerable, and have been estimated at about a factor of three (Grün, 1989). Reports have appeared in which the extrapolated lifetime was underestimated (Radtke and Grün, 1988) or overestimated (Barabas *et al.*, 1988).

We report here on our ESR studies using a sample of shell from a modern bivalve—*Katelysia scalarina*—exposed to γ-rays in the laboratory. Using both X-band and Q-band spectra, the kinetics of intensity changes of signals at $g = 2.0058$, 2.0032, 2.0020 and 2.0006 have been analysed. Caution is advised in applying these findings to naturally irradiated samples, where spin-transfer and relaxation processes may have occurred to a great extent during storage.

EXPERIMENTAL

The preparation of the *Katelesia scalarina* mollusc shell has been described previously (Brumby and Yoshida, 1994). Material from a number of individual shells was combined, and no assessment was made of variations between individuals of the same species. Thirty aliquots each weighing 200 mg were used. These were given a γ-dose of 1327 Gy using a ^{60}Co source, after which they were placed in an oven at 100°C for 10 min. All aliquots were stored at approx. −5°C when not in use. Preliminary experiments were conducted to determine suitable annealing temperatures and times. The temperatures selected were 91, 101, 110, 120 and 130°C. Then each

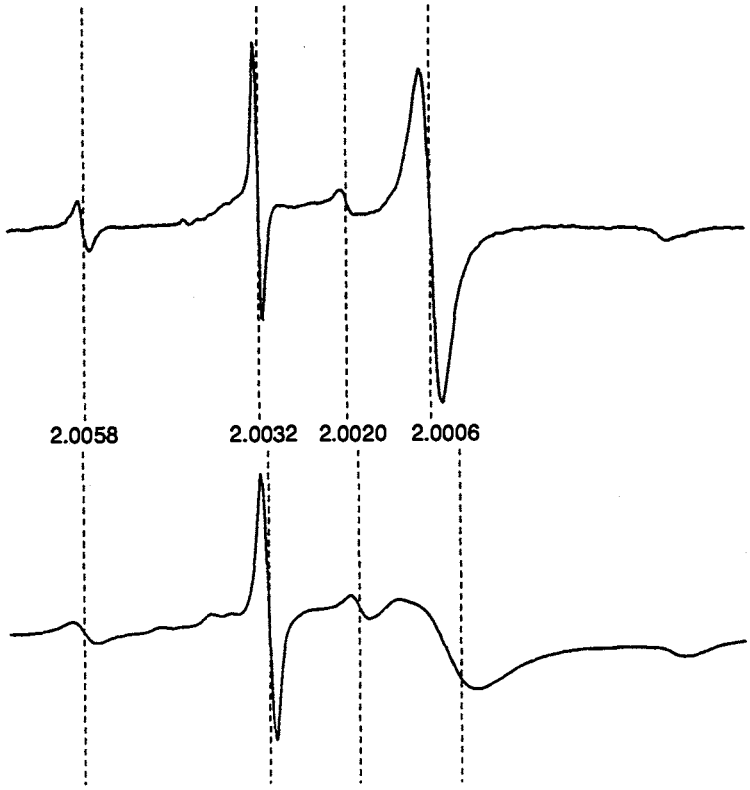

Fig. 1. First derivative ESR spectra at Q-band (above) and X-band (below) of a sample of modern *Katelesia scalarina* shell after γ-irradiation, showing the *g*-values of some features.

aliquot to be annealed, contained in a 3 mm outside diameter ESR tube, was immersed in a thermostatically regulated silicone oil bath for a suitable time. ESR spectra were recorded digitally with the samples at room temperature. Q-band spectra were recorded using a Varian 4502 EPR spectrometer, with a microwave power of 0.6 mW and a modulation amplitude of 0.2 gauss. X-band measurements were made using a Bruker 200D-SRC EPR spectrometer, with a microwave power of 1 mW and modulation amplitude of 0.5 gauss. Typical Q- and X-band spectra are shown in Fig. 1. We compared our Q-band spectrum with the spectrum reported by Barabas *et al.* (1992a) and found that the spectra show essentially the same features, with the possible exception of a minor feature slightly upfield from the $g = 2.0032$ signal in the spectrum of Barabas and co-workers that is not evident in our spectrum.

The $g = 2.0020$ signal

Although this aragonite signal has been observed and studied by several groups (e.g. Katzenberger *et al.*, 1989) the identity of the species that gives rise to it remains a mystery. According to Katzenberger *et al.* (1989) the contour of the signal conforms to the powder spectrum of an axial species with $g_\perp = 2.0020$ and $g_\parallel = 2.0017$, and our observations at Q-band (Fig. 1) seem to be qualitatively consistent with this interpretation.

The amplitude of the signal (measured at both Q- and X-band) is plotted against annealing time at 110°C in Fig. 2. The data at this and other temperatures were fitted to the following functional forms (y and t denote amplitude and time, respectively, and a, b, k are adjustable parameters):

1st-order kinetics: $y = a\exp(-kt)$;

2nd-order kinetics: $y = (a + kt)^{-1}$;

3rd-order kinetics: $y = (a + bt)^{-0.5}$;

logarithmic $y = b - a\ln(t)$.

At all five temperatures investigated, the Q-band amplitudes were in the best agreement with the logarithmic equation*. For the X-band data the 3rd-order and logarithmic equations were about equally satisfactory, in view of the experimental uncertainties. However the Q-band results are

*By this, we mean that the sum of the squares of the residuals (chi-square) was a minimum for this functional form: for the first residual, since ln(0) is not defined, ln(1) was substituted. Of course, even better fits could be obtained using the equation $y = b - a\ln(c + t)$, where c corresponds to the equivalent time of pre-annealing. Then the ln(0) problem is avoided. However, for the present purpose we wished to compare two parameter equations.

probably to be preferred because the amplitudes appear to be less influenced by overlapping signals. Furthermore, it is not easy to provide a plausible justification for why the 3rd-order kinetic equation might be applicable: the obvious explanation that defects diffuse together to form trimers is clearly unacceptable, since the probability of such events would be extremely remote, and certainly less than the probability of dimer formation, which would lead, with at least 25% probability (Fischer and Paul, 1987), to annihilation of the unpaired spin.

The above analysis assumes that the $g = 2.0020$ signal is due to a single species. If there were two species with the same g-value but with different kinetic stabilities then the decay curve could be fitted to the sum of two 1st-order terms. However, there does not seem to be any reason to believe that this situation applies.

We conclude that, at least for our sample, the appropriate equation is a logarithmic one. Using a different sample and a different method of analysis, Grün (1985) considered that the decay of the $g = 2.0020$ signal at X-band was essential 1st-order, but appeared to be 2nd-order because of interfering signals.

The logarithmic equation for the decay of centres implies that the rate of decay is inversely proportional to time. This is the type of relationship that would be expected when pairs of defects mutually annihilate each other with a probability that decreases exponentially with the distance separating the pair (Delbecq *et al.*, 1974). Such a situation would be expected if the orbitals of the unpaired electrons were able to overlap and interact directly, without the requirement that one of the electrons be excited into the conduction band—in other words, the type of mechanism that is

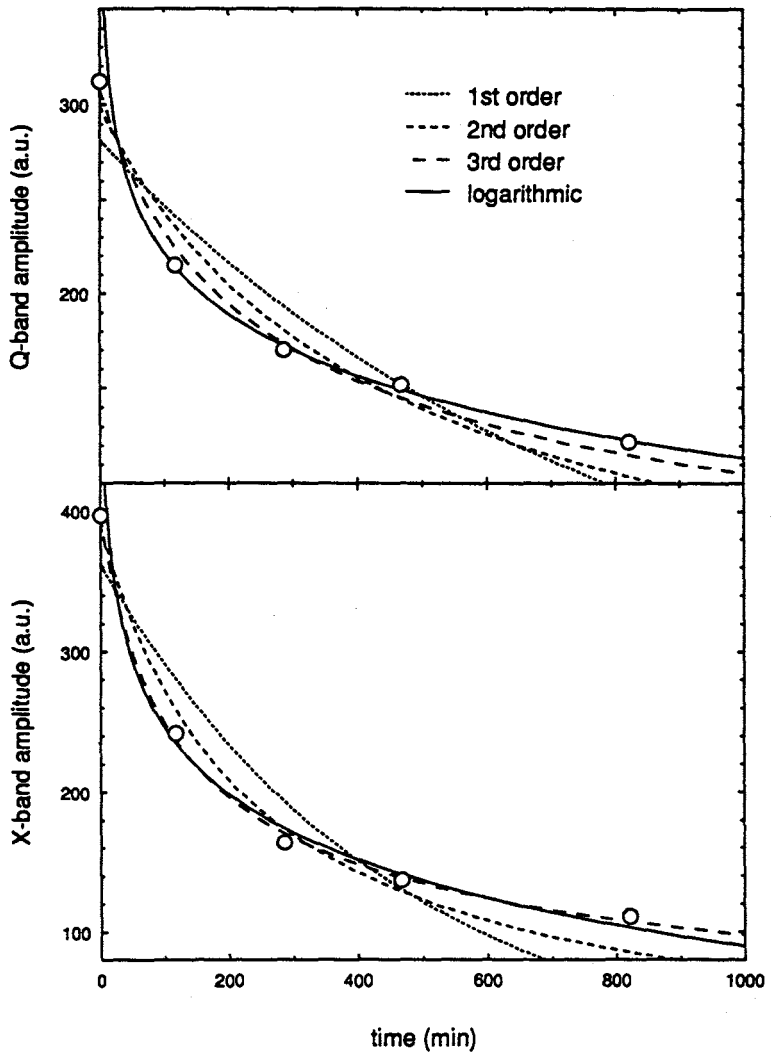

Fig. 2. Decay of the $g = 2.0020$ ESR signal at 110°C, monitored at Q-band (above) and X-band (below) microwave frequencies.

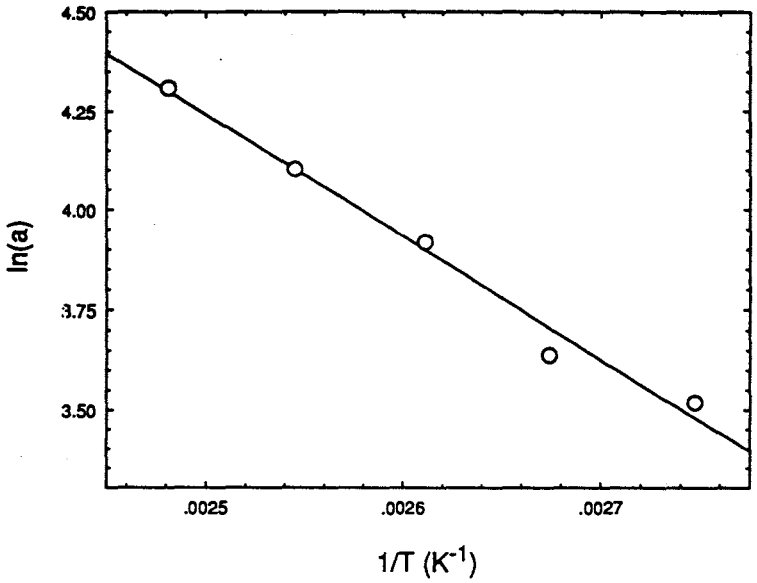

Fig. 3. Arrhenius plot of $\ln(a)$ against $1/T$, where values of a were determined by least squares fitting of the $g = 2.0020$ Q-band decay curves to the equation $y = b - a \ln(t)$.

usually known as quantum mechanical tunnelling. However, the temperature dependence of the decay rate does not appear to be consistent with this mechanism. Figure 3 shows an Arrhenius plot in which the parameter a, estimated by fitting the decay curves to the logarithmic equation, is used as a rate constant. The plot is linear within the experimental uncertainties and indicates an activation energy of (26.1 ± 1.5) kJ mol^{-1}, or (0.271 ± 0.016) eV. It does not show evidence of decreasing gradient with decreasing temperature, which is the expected behaviour when quantum mechanical tunnelling is important. Other mechanisms for decay that are equally consistent with the observed logarithmic relationship, but appear to be in better agreement with the temperature dependence of the decay, are the localised transition model (Templer, 1986) and a mechanism in which pairs of defects annihilate each other when they diffuse together (Kotomin and Kusovkov, 1992). It is not clear how one could distinguish between these possibilities.

It was shown by Debuyst *et al.* (1984) that an unstable ESR signal which decays with 1st-order kinetics could in principle be used to estimate the dose rate to which the sample has been exposed in nature. Grün (1985) considered that the $g = 2.0020$ signal of mollusc shell could be used in this way, but the present work shows that the requirement of 1st-order kinetics is not satisfied. The question arises as to whether the unstable $g = 2.0020$ signal can be used to estimate dose rates even though its decay is not 1st order. In an exact sense, the answer is no, because the type of distribution of defects under the conditions of the annealing experiments is different from the type of distribution reached in nature in the steady state, when the formation of defects is equal to the rate of their annihilation. Therefore, the parameter a, even if extrapolated to the appropriate temperature, is not strictly relevant to the steady-state situation. Nevertheless, it is possible that with simplifying assumptions useful information can be extracted, and we intend to investigate this in future work.

The $g = 2.0058$ signal

The line at $g = 2.0058$ approximates to an isotropic Lorentzian, and has been attributed (Barabas, 1992; Kai and Miki, 1992) to freely rotating SO_2^- radical anions.

At all temperatures, it was found that the increase in amplitude of the signal with time could be fitted to the 1st-order equation, $y = b - a \exp(-kt)$. Typical results, again at 110°C, are shown in Fig. 4. An Arrhenius plot of the rate data is shown in Fig. 5. For the X-band data, a pre-exponential factor of approx. 2.8×10^{13} min^{-1} and an activation energy of (117.1 ± 2.7) kJ mol^{-1} (i.e. 1.214 ± 0.028 eV) was found. The Q-band data were more scattered, but probably not significantly different from the X-band data.

Yokoyama *et al.* (1985) noted a decrease in the width of the $g = 2.0058$ signal in calcite on thermal pre-treatment. We estimated the width of the $g = 2.0058$ signal by numerically fitting a Lorentzian function to the experimental data. The results for an annealing temperature of 110°C are shown in Table 1. For the X-band spectra there was a small but significant decrease in linewidth on annealing, but for the Q-band spectra no significant change could be detected. It, therefore, seemed possible that our rate constants based on the X-band spectra might be overestimated, and to investigate this we computed

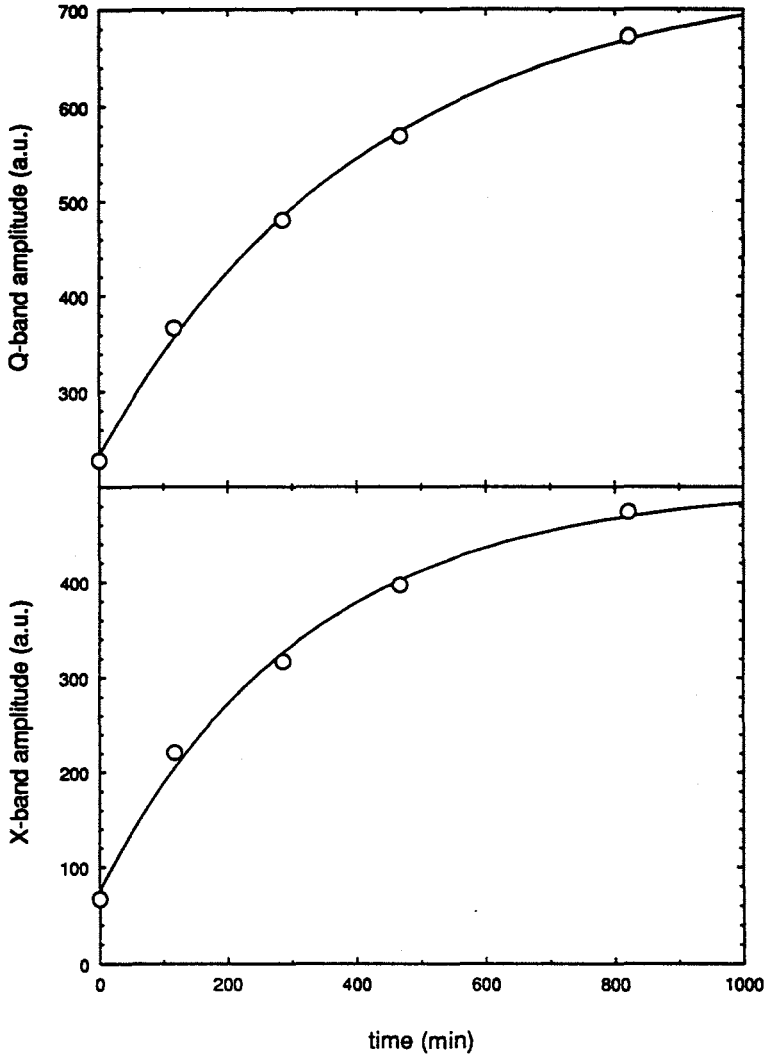

Fig. 4. Build-up of the $g = 2.0058$ signal at 110°C, monitored at Q- and X-band. The continuous curves correspond to 1st-order kinetic equations with rate constants 2.38×10^{-3} min^{-1} and 3.10×10^{-3} min^{-1} for Q- and X-band, respectively.

the area under the absorption signal via the double-integrated first derivative spectra. The rate constants calculated from these areas were consistently larger, by about 40% than from those based on the X-band amplitudes. The explanation for this unexpected result became apparent when the X-band $g = 2.0058$ signals were fitted with excellent agreement to the sums of two superimposed Gaussian lines. The broader of the two Gaussian lines did not greatly influence the peak-to-peak linewidths, but made a major contribution to the integrated areas.

Previously, we proposed (Brumby and Yoshida, 1994) that the $g = 2.0058$ signal may arise by thermal decomposition of SO_3^- radical ions, which contribute to the signal at $g = 2.0032$. This proposal differs from earlier suggestions that the $g = 2.0058$ signals in corals might arise by thermal annealing of the $g = 2.0006$ signal (Yokoyama *et al.*, 1982), or that the same signal might arise in calcite and aragonite by thermal decomposition of diamagnetic SO_3^{2-} ions (Kai and Miki, 1992).

Our suggestion (Brumby and Yoshida, 1994) that the $g = 2.0058$ signal may be worth consideration for dating was based on the idea that SO_3^- radical ions are formed on exposure to ionizing radiation, and

Table 1. Phenomenological Lorentzian peak-to-peak linewidth of the $g = 2.0058$ ESR signal after annealing at 110°C

Annealing time (min)	Linewidth (gauss)	
	Q-band	X-band
117	0.177 ± 0.005	0.558 ± 0.004
286	0.182 ± 0.004	0.545 ± 0.004
467	0.181 ± 0.005	0.522 ± 0.004
821	0.176 ± 0.004	0.506 ± 0.007

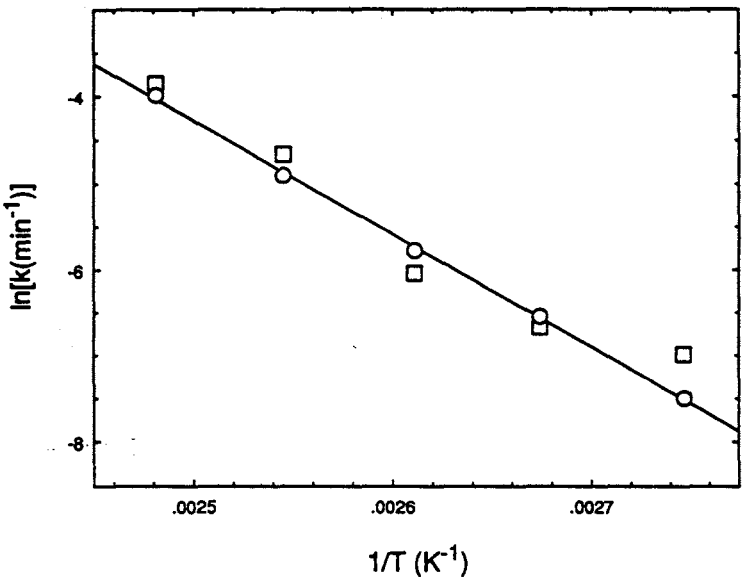

Fig. 5. Arrhenius plot of $\ln(k)$ against $1/T$, where k is the 1st-order rate constant for build-up of the $g = 2.0058$ ESR signal amplitude. Squares—Q-band data; circles—X-band data.

contribute to the signal at $g = 2.0032$. Depending on the storage time, temperature, annual dose and characteristics peculiar to the sample, a variable proportion of these ions decompose to yield (very stable) SO_2^- radical ions. On further irradiation, at room temperature in the laboratory, mostly SO_3^- ions are formed, but a small amount of decomposition to SO_2^- is possible with some samples, and certainly does not invalidate the method. The purpose of the thermal pre-treatment (14 hours at 150°C) is to complete the process requiring thermal activation, thus ensuring that the majority of SO_3^- ions initially formed are converted to SO_2^-. The method does not require 100% efficiency in converting SO_3^- to SO_2^- but does require that the efficiency be approximately the same during both storage and pre-annealing.

We were interested to know whether oxygen influenced the rate of build-up of the $g = 2.0058$ signal. Accordingly, we recorded X-band spectra for two aliquots, and then heated both aliquots for 5 hours at 130°C. During this heating, one of the aliquots was continuously flushed with nitrogen, whereas the other sample was exposed to air in the usual manner. After cooling the spectra were re-recorded. Although the amplitude of the $g = 2.0058$ signal after annealing was slightly smaller for the sample heated in an atmosphere of nitrogen, the difference was not large, and may have been caused by packing errors. Thus, we could find no evidence for the involvement of oxygen in the thermal generation of the $g = 2.0058$ signal.

The $g = 2.0032$ signal

The signal centred at approx. $g = 2.0032$ was considered by Katzenberger *et al.* (1989) to show evidence of a very small axial anisotropy, but it appeared isotropic in our X-band measurements (Fig. 1). At Q-band slight deviations from a symmetric Lorentzian line shape were apparent. While these could be explained in terms of a weakly anisotropic signal, an alternative explanation (Brumby and Yoshida, 1994) is that there are two nearly isotropic signals in close proximity: one of these may be SO_3^- (Barabas, 1992; Kai and Miki, 1992; Miki *et al.*, 1993), and the other, more stable signal, may possibly be related to an organic component (Katzenberger *et al.*, 1989). Therefore, it seemed appropriate to fit the decay curve for this composite signal to the sum of two 1st-order equations. We found that very good agreement with experiment was possible on this basis. However, there are four adjustable parameters which then describe the decay curve, and these parameters are not uniquely defined by the data. Previously, we speculated (Brumby and Yoshida, 1994) that one component of the $g = 2.0032$ signal, due to SO_3^-, might give rise, on annealing, to the signal at 2.0058, due to SO_2^-. Therefore, we wished to determine whether the kinetic evidence was consistent with this hypothesis. To this end, we attempted to fit the $g = 2.0032$ decay curves to the sum of two 1st-order decay expressions, in which one of the two 1st-order decay constants was constrained to be equal to the appropriate 1st-order constant for build-up of the signal at $g = 2.0058$, and the other decay constant was allowed to vary freely. At every temperature, excellent agreement with the experimental data was achieved in this way. Typical results are shown in Fig. 6. Thus the evidence is entirely consistent with our hypothesis. On the other hand, it cannot be said that the evidence unambiguously confirms our hypothesis, because

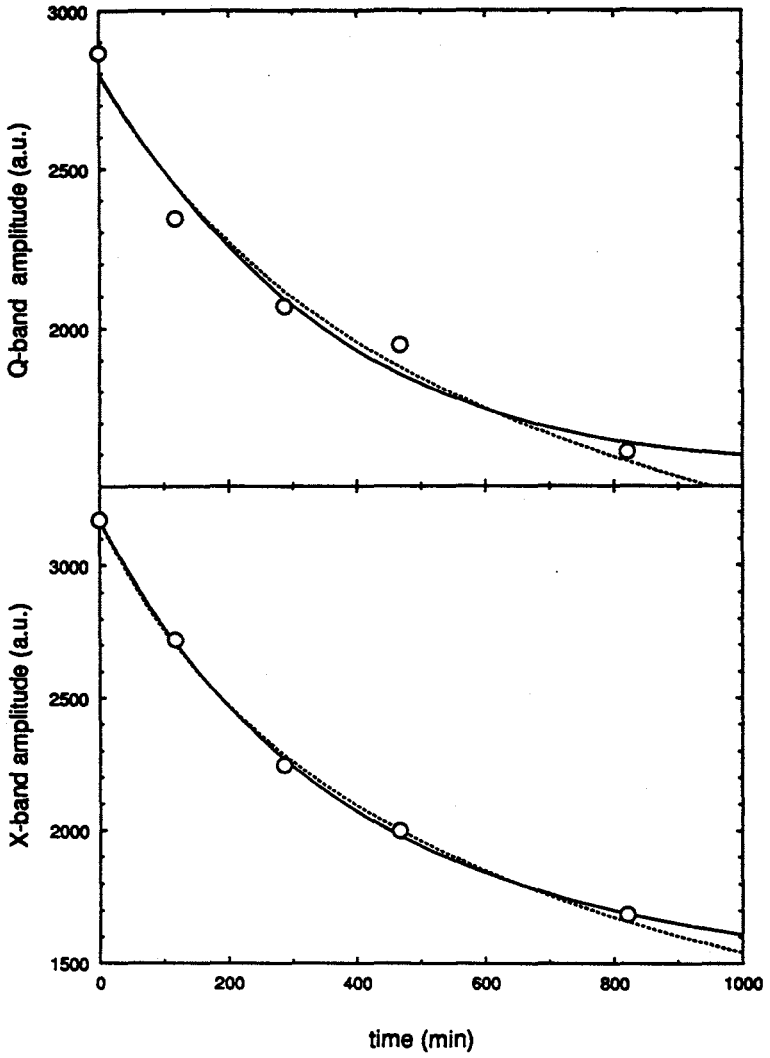

Fig. 6. Decay of the $g = 2.0032$ signal at 110°C, monitored at Q- and X-band. The continuous curves correspond to the sum of two 1st-order kinetic equations, with assumed rate constants for the shorter-lived components of $2.38 \times 10^{-3}\,\mathrm{min}^{-1}$ and $3.10 \times 10^{-3}\,\mathrm{min}^{-1}$ for Q- and X-band, respectively. The broken curves correspond to 3rd-order kinetic equations.

other combinations of parameters allow an equally good fit to the data.

Ikeda *et al.* (1992) pre-annealed a sample of coral at 140°C for various times up to about 16 h, and then applied a saturating γ-dose. The intensity of the $g = 2.0032$ signal, which was a measure of the number of available diamagnetic traps, first increased and then decreased with time. In the region where the signal amplitude decreased, a 3rd-order decay was in best agreement with the measurements. In Fig. 6 curves corresponding to the 3rd-order equation are shown as broken lines, and it may be seen that it can be very hard to distinguish on the basis of experiment between a sum of two 1st-order equations and a 3rd-order equation. However a 3rd-order equation seems harder to justify in principle, for the reasons given above.

The $g = 2.0006$ signal

The signal at $g = 2.0006$ has often been described as the 'dating' signal for carbonates, and there have been a number of studies relating to its stability (Barabas *et al.*, 1992b, and references therein). It has been suggested (e.g. Barabas *et al.*, 1992a) that the signal may be due to freely rotating CO_2^-, probably associated with water of crystallization (Debuyst *et al.*, 1993). Murata *et al.* (1993) and Miki and Kai (1991) considered that thermal annealing of the signal may be linked with loss of water crystallization.

In dating mollusc shell it is not usually considered satisfactory to measure the intensity of the $g = 2.0006$ signal at X-band because of neighbouring signals that interfere. The use of high microwave powers to enhance this signal relative to interfering signals has

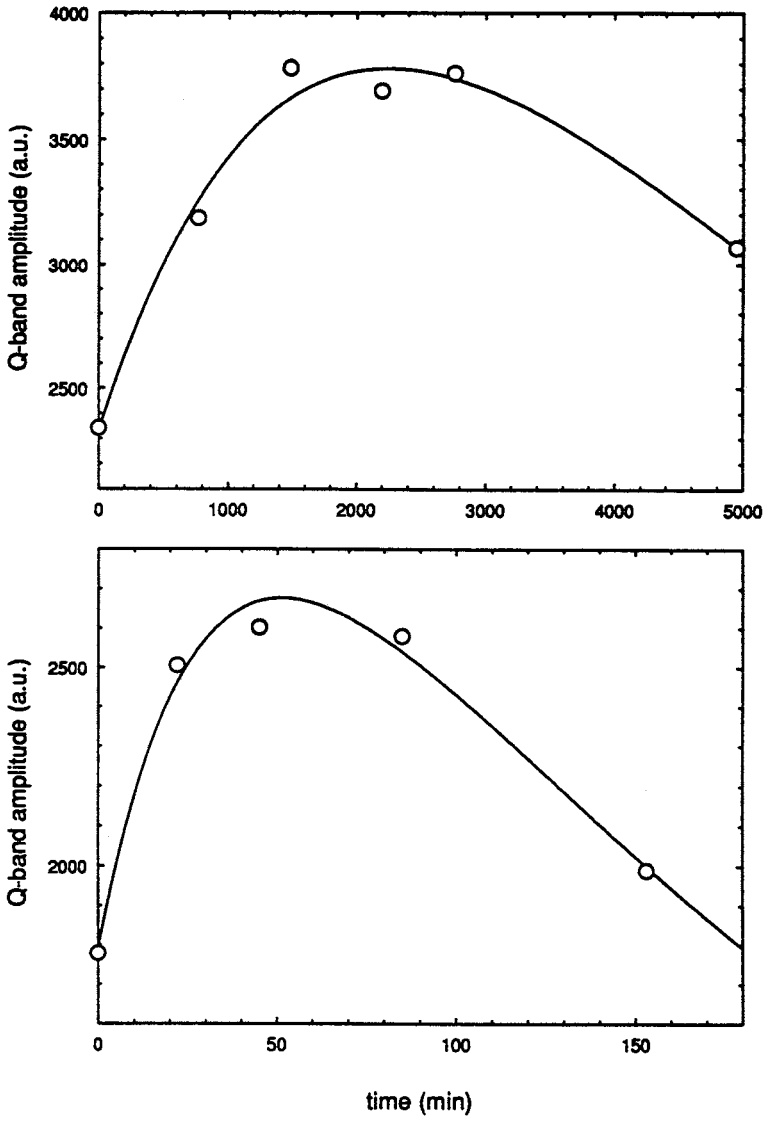

Fig. 7. Evolution of the $g = 2.0006$ Q-band ESR signal at 91°C (above) and 130°C (below). The tentative continuous curves correspond to the sums of a 1st-order build-up and a 1st-order decay term.

been proposed (Barabas *et al.*, 1992b) but the optimum power has not been determined, nor has the effectiveness of the method been convincingly demonstrated (Brumby and Yoshida, 1994). Because of these difficulties, we investigated the amplitude of the signal at Q-band. The amplitude increased and then decreased on annealing. The data seemed to be reasonably well described as the sum of 1st-order build-up and 1st-order decay terms, as illustrated in Fig. 7 for two of the temperatures investigated, but the scatter in the data does not allow detailed analysis. In view of this, it is clear that the use of Q-band techniques has not enabled us to isolate a thermally stable component of the signal.

We believe these observations do not detract from the sizeable body of published dating studies using the $g = 2.0006$ signal at X-band. The $g = 2.0006$ signal is not caused by a single type of paramagnetic centre in mollusc shell (e.g. Barabas *et al.*, 1992a), and we consider that the relative contributions that the different component signals make to the measured amplitudes at $g = 2.0006$ are quite different at X- and Q-band frequencies. This is because of the way in which the measurement frequency influences the effective linewidth, which is different for the different contributing centres. When we investigated (Brumby and Yoshida, 1994) the annealing behaviour of the $g = 2.0006$ signal measured at X-band using the high power technique recommended by Barabas *et al.* (1992b), we reported a small initial increase in intensity, but this was not as large asshown in Fig. 7, and

possibly not large enough to be of serious concern in dating.*

It would be a simple matter to derive Arrhenius parameters based on the interpretation shown in Fig. 7. However, in view of the scatter in the data and the tentative nature of our curve fitting, we do not consider such an analysis to be appropriate.

CONCLUSIONS

The following conclusions are based on measurements with shell of the mollusc *Katelysia scalarina*, and may not apply to other species.

1. The unstable ESR signal at $g = 2.0020$ does not decay with 1st-order kinetics, which raises doubts about its suitability for estimation of the annual dose by the method of Debuyst *et al.* (1984).

2. The kinetic data are consistent with, but do not positively confirm, the hypothesis that a component of the $g = 2.0032$ signal, due to SO_3^-, relaxes on annealing to generate a signal at $g = 2.0058$, due to SO_2^-.

3. At Q-band, the ESR signal at $g = 2.0006$ has thermally unstable components.

REFERENCES

Barabas M. (1992) The nature of the paramagnetic centres at $g = 2.0057$ and $g = 2.0031$ in marine carbonates. *Nucl. Tracks Radiat. Meas.* **20**, 453–464.

Barabas M., Bach A. and Mangini A. (1988) A analytical model for ESR-signals in calcite. *Nucl. Tracks Radiat. Meas.* **14**, 231–235.

Barabas M., Bach A., Mudelsee M. and Mangini A. (1992a) General properties of the paramagnetic centre at $g = 2.0006$ in carbonates. *Quat. Sci. Rev.* **11**, 165–171.

Barabas M., Mudelsee M., Walther R. and Mangini A. (1992b) Dose-response and thermal behaviour of the ESR signal at $g = 2.0006$ in carbonates. *Quat. Sci. Rev.* **11**, 173–179.

Brumby S. and Yoshida H. (1994) ESR dating of mollusc shell: investigations with modern shell of four species. *Quat. Geochron.* **13**, 157–162.

Debuyst R., Dejehet F., Grün R., Apers D. and de Canniére P. (1984) Possibility of ESR-dating without determination of the annual dose-rate. *J. Radioanal. Nucl. Chem. Lett.* **86**, 399–410.

Debuyst R., Dejehet F. and Idrissi S. (1993) Paramagnetic centers in γ-irradiated synthetic monohydrocalcite. *Appl. Rad. Isot.* **44**, 293–297.

Delbecq C. J., Toyazawa Y. and Yuster P. H. (1974) Tunneling recombination of trapped electrons and holes in KCl:AgCl and KCl:TiCl. *Phys. Rev. B* **9**, 4497–4505.

Fischer H. and Paul H. (1987) Rate constants for some prototype radical reactions in liquids by kinetic ESR. *Acc. Chem. Res.* **20**, 200–206.

Grün R. (1985) ESR-dating without determination of annual dose: a first application on dating mollusc shells. In M. Ikeya and T. Miki (Eds) *ESR Dating and Dosimetry*, IONICS, Tokyo, pp. 115–123.

Grün R. (1989) Electron spin resonance (ESR) dating. *Quat. Int.* **1**, 65–109.

Grün R. and de Canniére P. (1984) ESR-dating: problems encountered in the evaluation of the naturally accumulated dose of secondary carbonates. *J. Radioanal. Nucl. Chem. Lett.* **85**, 213–226.

Hennig G. J. and Grün R. (1983) ESR dating in Quaternary geology. *Quat. Sci. Rev.* **2**, 157–238.

Ikeda S., Kasuya M. and Ikeya M. (1992). ESR dating of corals and pre-annealing effects on ESR signals. *Quat. Sci. Rev.* **11**, 203–207.

Katzenberger O., Debuyst R., de Canniére P., Dejehet F., Apers D. and Barabas M. (1989) Temperature experiments on mollusc samples: an approach to ESR signal identification. *Appl. Rad. Isot.* **40**, 1113–1118.

Kai A. and Miki T. (1992) Electron spin resonance of sulfite radicals in irradiated calcite and aragonite. *Radiat. Phys. Chem.* **40**, 469–476.

Kotomin E. and Kusovkov V. (1992) Phenomenological kinetics of Frenkel defect recombination and accumulation in ionic solids. *Rep. Prog. Phys.* **55**, 2079–2188.

Miki T. and Kai A. (1991) Thermal annealing of radicals in aragonitic $CaCO_3$ and $CaHPO_4.2H_2O$. *Jpn. J. Appl. Phys.* **30**, 404–410.

Miki T., Kai A. and Murata T. (1993) Radiation-induced radicals in sulfite-doped $CaCO_3$. *Appl. Rad. Isot.* **44**, 315–319.

Murata T., Kai A. and Miki T. (1993) Hydration effects on CO_2^- radicals in calcium carbonates and hydroxyapatite. *Appl. Rad. Isot.* **44**, 305–309.

Radtke U. and Grün R. (1988) ESR dating of corals. *Quat. Sci. Rev.* **7**, 465–470.

Randall J. T. and Wilkins M. H. F. (1945) Phosphorescence and electron traps. I. The study of trap distributions. *Proc. R. Soc.* **184A**, 366–389.

Strickertsson K. (1985) The thermoluminescence of potassium feldspars—glow curve characteristics and initial rise measurements. *Nucl. Tracks Radiat. Meas.* **10**, 613–617.

Templer R. H. (1986) The localised transition model of anomalous fading. *Rad. Prot. Dos.* **17**, 493–497.

Wintle A. G. (1977) Thermoluminescence dating of minerals—traps for the unwary. *J. Electrostat.* **3**, 281–288.

Yokoyama Y., Quaegebeur J. P., Bibron R. and Leger C. (1983) ESR dating of palaeolithic calcite: thermal annealing experiment and trapped electron lifetime. *PACT* **9**, 371–379.

Yokoyama Y., Bibron R., Leger C. and Quaegebeur J. P. (1985) ESR dating of palaeolithic calcite: fundamental studies. *Nucl. Tracks Radiat. Meas.* **10**, 929–936.

*Two referees argue that annealing studies may not necessarily have direct relevance to dating, because irreversible loss of water occurs at relatively high temperatures, unlike the reversible exchange of water expected under typical storage conditions.

Addendum

FUNDAMENTAL THEORY OF ELECTRON SPIN RESONANCE AND LUMINESCENCE IN MINERALS

When diamagnetic minerals such as calcite and quartz are initially formed all electrons are paired and no positive magnetic susceptibility is present, because the magnetic moments of paired electrons negate one another. Many naturally occurring minerals contain crystal defects which can act as traps for electrons or electron holes. Such electrons/holes are formed on exposure to background ionizing radiation composed of gamma rays, α- and β- particles, and cosmic rays. Some trapped electrons/holes have sufficient thermal stability to survive for thousands of years, and longer, at ambient temperatures. Both ESR and luminescence dating methods depend on the same essential phenomenon - the gradual build-up over time of trapped electrons/holes. An important difference between the two methods is that ESR allows the trapped species to be investigated without disturbing their population, whereas with luminescence methods the electrons are expelled from their traps and a certain proportion recombine with holes at luminescence centres in the mineral, giving rise to the emission of light.

A1 ESR

A1.1 The resonance condition

A trapped (unpaired) electron can be considered as a small magnet, equivalent to a negatively charged rotating sphere. The orientation of the rotation of the electron is random (Figure A.1(a)), but under the influence of an external magnetic field, the direction becomes either parallel or opposite (anti-parallel) to that of the external magnetic field. These states have different energies, as shown in Figure A.1(b). The electron spins in a lower level can be excited to a higher level by absorption of microwave quanta (Figure A.1(c)). After the so called 'spin-lattice relaxation time', the flipped spins drop to the lower level. The flipping of the spins can be induced by microwave radiation.

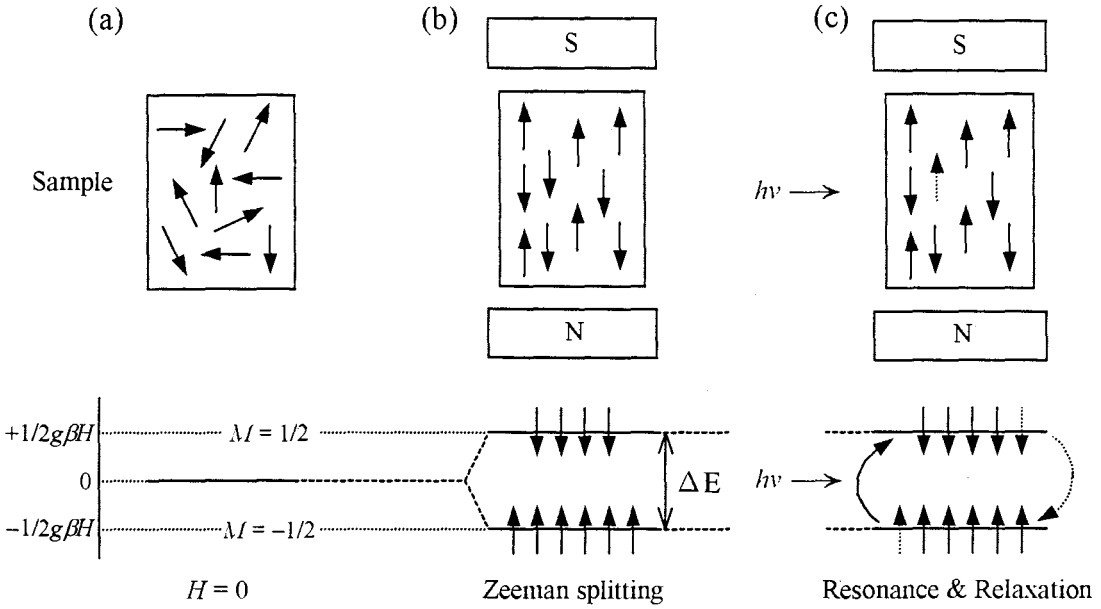

Figure A.1 Orientation of the spin rotation and a two energy level system (Zeeman effect) of an unpaired electron spin (after Ikeya, 1993). (a) Random direction of spins under natural conditions, (b) a parallel or anti-parallel orientation under the external magnetic field and (c) spin transitions by microwave absorption and spin-lattice relaxation.

As shown in Figure A.1(b), the alignment of the spin parallel or anti-parallel with an applied magnetic field may be expressed in terms of a spin quantum number, M, for which values of +1/2 and −1/2 are allowed. The component of the magnetic moment in the direction of the magnetic field is given by the equation

$$\mu_z = - \; g \; \beta \; M$$

where g is a dimensionless number called the electron splitting factor (equal to 2.002322 for a free electron) and β is the electronic Bohr magneton ($9.2740154 \times 10^{-24}$ J T^{-1}).

Under the influence of the external magnetic field, H, there is an energy difference between the spin states, which is known as the Zeeman effect. The Zeeman energy is represented by

$$E_z = - \mu_z H$$

Hence

$$E_z = g \; \beta \; M \; H$$

where H is expressed in Tesla ($1T = 10^4$ gauss).

Transitions between the upper and lower spin states are induced by electromagnetic radiation when the resonance condition is satisfied, i.e. when

$$\Delta E = h \nu = g \beta H$$

Here, ν is the frequency of the radiation and h is Planck's constant ($6.6260755 \times 10^{-34}$ J s^{-1}).

The classical approach outlined above is not strictly applicable to a quantum mechanical problem. For the situation considered, however, it does give the correct result. For more involved problems such as transition element species with more than one unpaired electron, or for species with hyperfine interactions, it may be necessary to write down the spin Hamiltonian, $\mathcal{H}$, and then solve the Schrödinger equation ($\mathcal{H}\phi = E\phi$) to determine the allowed energies.

In ESR spectroscopy, one usually applies a constant electromagnetic radiation field while scanning through the magnetic field. The spectrum is the response recorded as the magnetic field passes through the region in which the resonance condition is satisfied. When the magnetic field is applied but the resonance condition is not satisfied, the populations of the spin states ($N_{+1/2}$ and $N_{-1/2}$) will approach thermal equilibrium, in accordance with Boltzman's Distribution Law:

$$N_{+1/2}/N_{-1/2} = \exp(-\Delta E/kT)$$

Here k represents Boltzman's constant (1.381×10^{-23} J K^{-1}) and T represents temperature (in K). As the field is scanned, when the resonance condition is satisfied the microwave field induces transitions between the spin states. Because of the slight excess population in the state of lower energy, the net effect is that of weak microwave absorption. If the microwave power is low, the populations of the spin states will not be seriously disturbed. But if the power is large, the microwave energy will tend to equalise the populations, by inducing rapid transitions between the spin states. This is termed "saturation" and results in a decrease in the net absorption of microwave energy. Saturation is usually regarded as undesirable and best avoided, but in certain dating applications it may be used as a way of selectively removing interfering signals, when the interfering signal is relatively easily saturated.

A1.2 ESR spectrometer

An X-band spectrometer uses microwave radiation of approximately 9.5 GHz, at which frequency the magnetic field required for resonance is about 0.34 T. A Q-band spectrometer uses microwave radiation of approximately 35 GHz, when the magnetic field required for resonance is about 1.25 T. The most common type of ESR spectrometer uses X-band radiation, and a simplified block diagram is shown in Figure A.2. Microwaves are produced by an oscillator (Klystron) and passed to the resonant reflection cavity through the waveguide. The sample is placed into the resonant transmission cavity which is located between the poles of the electromagnet. The absorption of the microwaves is observed by a detector diode while sweeping the magnetic field. Commonly, a magnetic field modulation frequency of 100 kHz is used to modulate microwave absorption. The spectrum is recorded as the first derivative of the absorption lineshape (Figure A.3.).

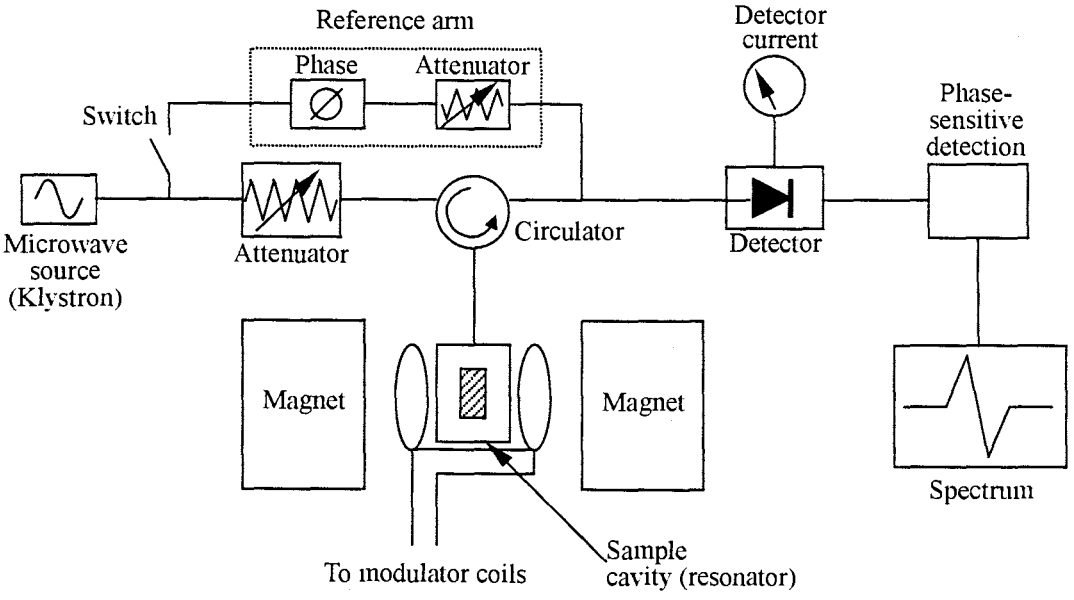

Figure A.2. Block diagram of a modern ESR spectrometer (after Pilbrow, 1990).

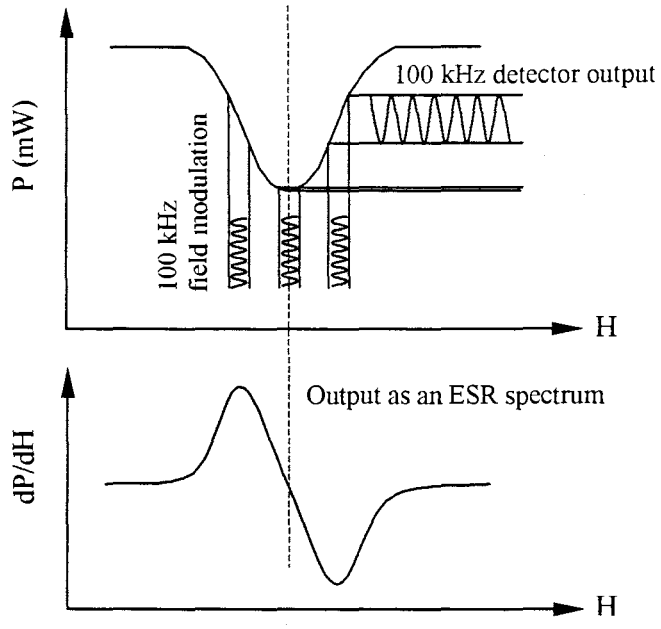

Figure A.3 The microwave absorption curve and the detector output current using 100 kHz magnetic field modulation (after Ikeya, 1993, and Wertz and Bolton, 1972). The ESR spectrum is recorded as the first derivative line of microwave absorption.

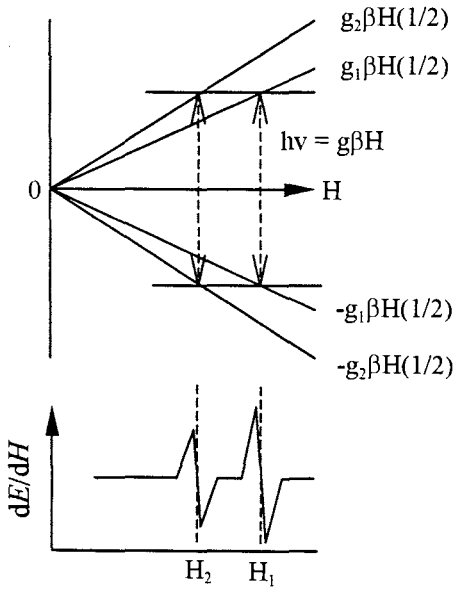

Figure A.4 Spin energy levels as a function of magnetic field at constant microwave frequency (after Ikeya, 1993).

A1.3 g-factor

The electron splitting factor of an ESR signal, the g-factor, is an important quantity since the ESR signal is often identified by this factor. The g-value of a signal can be obtained from the equation

$$g = \frac{h\nu}{\beta H} = 71.455 \times \left(\frac{\nu}{H}\right)$$

where ν is the microwave frequency in GHz and H is the magnetic field in mT (see A.1.1) which can be measured with a frequency counter and a fieldmeter, respectively. This equation indicates that unpaired electrons with different Zeeman energies under the same magnetic field strengths may appear at different g-factors (see Figure A.4). The g-factor differentiation can be explained as the result of so-called 'spin-orbit interaction', a magnetic interaction between the spin magnetic moment and orbital magnetic moment. Figure A.4 shows an example of two types of electron spin that have different energy levels. Since the Zeeman energy is different for each electron spin under the same magnetic field, the slope of the energy level change is also different. The g-factor of an unknown signal can also be determined by using a standard (known) signal from the equation

$$\frac{h\nu}{\beta} = g_1 H_1 = g_2 H_2$$

Hence,

$$g_2 = \frac{g_1 H_1}{H_2} = \frac{g_1 H_1}{(H_1 - \Delta H)} = \frac{g_1}{(1 - \frac{\Delta H}{H_1})}$$

where g_1 and g_2 represent known and unknown g-factors, respectively, and H_1 and H_2 represent their magnetic fields in mT, respectively. ΔH is the magnetic field separation equal to H_1-H_2.

A1.4 Q-band measurement

There may be certain advantages in using a Q-band spectrometer for ESR measurement. Because a Q-band spectrometer employs microwave radiation of frequency

approximately 35 GHz, which is more than 3 times that of an X-band spectrometer, the energy difference between the spin states at resonance is also proportionally greater. This has the beneficial effect of increasing the population difference between the states. Also, if neighbouring signals with g-factors of g_1 and g_2 (see Figure A.4), are measured at X- and Q-band, the magnetic separation, H_1–H_2, monitored by the Q-band is proportionally greater than that measured by X-band. Since the signal widths are the same, more signal resolution is obtained for the Q-band. In the case of tooth enamel, coral, and shell, the X-band dating signals often overlap with others, while the dating signals appear to be isolated at Q-band. The major concern when using a Q-band spectrometer is that a much smaller sample cavity is used than for X-band, and this often introduces considerably poorer reproducibility from sample to sample due to packing and positioning errors (e.g. Barabas *et al.*, 1992).

A2 Luminescence

In a manner similar to the ESR method, thermoluminescence (TL) and optically stimulated luminescence (OSL) utilize trapped electrons/holes at crystal defects, mainly in quartz and various feldspars. Electrons released from traps on heating the sample or exposing it to light recombine with trapped holes, resulting in the emission of light. The TL and OSL methods have, therefore, been used for determining the time since materials such as pottery and burnt flints were subjected to heat, and the time since the last exposure of sediments to sunlight.

A2.1 Physical basis of luminescence

To understand the principles of luminescence, it is necessary to understand the energy states of trapped electrons. In simplified terms, electrons may reside at one of two different energy levels, the valence band (ground state) or the conduction band (see Figure A2.1). Electrons cannot remain between these two levels, a region known as the 'forbidden gap'. However, because of the presence of impurity defects in natural crystals, it is possible for electrons to be trapped within the forbidden gap in minerals such as quartz and feldspar.

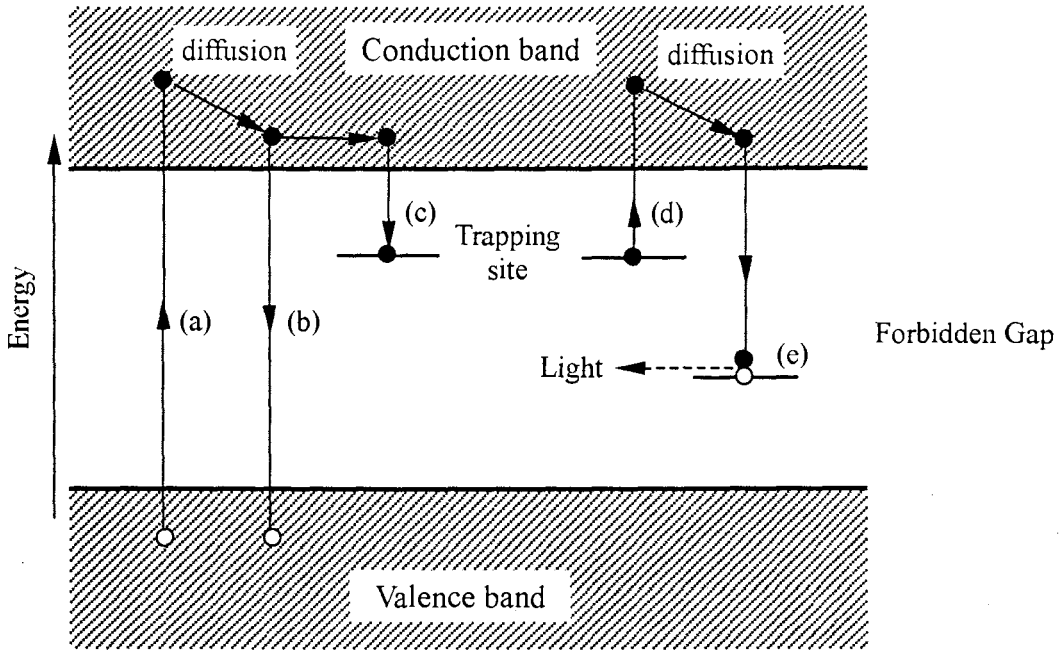

Figure A2.1 Simplified energy-level model of thermoluminescence production (after Duller, 1996, and Aitken, 1985). (a) ionization; (b) direct recombination; (c) electron trapping; (d) electron release; (e) recombination at luminescence centre, with emission of photon.

After a zeroing event, such as crystallization, heating, or exposure to light, the electrons exist at the lowest possible energy level, i.e. within the valence band. When the crystal is exposed to an ionizing radiation field, the electrons may be excited and transferred to the conduction band (see transition (a) in Figure A2.1). After a short period of diffusion, most of the excited electrons may return to the valence band (transition (b)) and recombine with trapped holes. A few electrons, however, may be trapped at impurity defects within the forbidden gap (transition (c)) and could remain there for several millions of years. The trapped electrons can be evicted by heating or by exposure to light (transition (d)). In a similar manner to transition (c), some of the released electrons may recombine with trapped holes (transition (e)) after diffusion in the conduction band. If the trapped hole occurs at a luminescence centre, a photon of light is emitted upon electron/hole recombination. The intensity of light emission from the sample is proportional to the number of electron/hole recombinations.

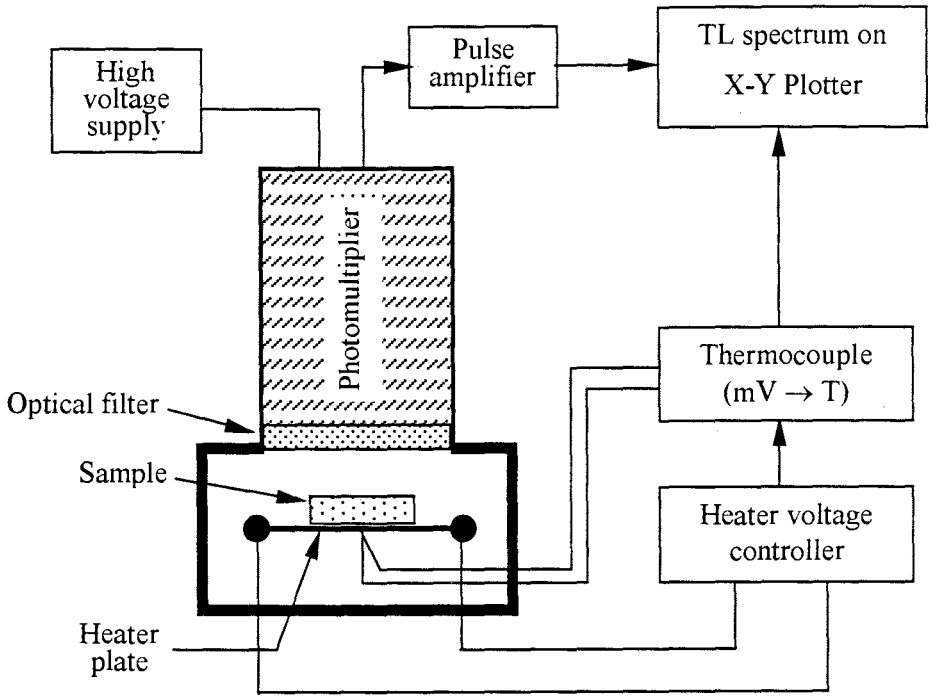

Figure A2.2 Schematic drawing of apparatus for thermoluminescence measurement (after Aitken, 1985).

A2.2 Thermoluminescence

A schematic diagram of the equipment used to induce and detect thermoluminescence is shown in Figure A2.2. The sample is placed on a plate which is heated from room temperature to 500°C at 5 K s^{-1}. The luminescence emitted by the sample is detected by the photomultiplier, after passing through optical filters to select the desired wavelength(s). A plot of photon counts versus temperature (the "glow curve") is recorded on an X-Y plotter. To prevent inadvertent bleaching in the laboratory, samples must be prepared under dim red or orange illumination (>590 nm transmission for quartz).

A2.3 Optically stimulated luminescence

The principles of optically stimulated luminescence (OSL) are closely related to those of the TL method. The major difference is that an OSL signal is induced by sample

exposure to light, such as from an argon laser, green light-emitting diodes, or infrared diodes. OSL dating has been extensively developed during the past decade and has been applied to quartz grains and feldspars from Quaternary deposits (e.g. Huntley *et al.*, 1985; Duller, 1996).

A2.4 OSL and TL signals

A major advantage of the OSL technique over TL is that zeroing of the OSL signal by light occurs much more rapidly. In quartz, two main TL peaks at 325°C and 375°C are observed when the sample is heated at 5 K s^{-1}; these peaks are referred to as the rapidly-bleached peak and the slowly-bleached peak, respectively. The 325°C peak and the OSL signal originate from the same trapped-electron population (Spooner, 1994) and are bleached rapidly (within minutes) and completely by ultraviolet and most visible wavelengths. In contrast, the 375°C peak is bleached only by ultraviolet radiation, and a non-zero (unbleachable) residual level is attained even after several hours of solar illumination (Spooner *et al.*, 1988).

Another advantage of the OSL method is that the observed OSL signal intensity is significantly greater than the TL signal for the same sample. This makes it possible to utilize much smaller amounts of sample for OSL dating. In fact, OSL dating of individual grains of quartz and feldspar have recently been attempted (Lamothe *et al.*, 1994; Murray and Roberts, 1997).

References

Aitken, M.J. (1985). *Thermoluminescence Dating*. Academic Press, London.

Barabas, M., Bach, A., Mudelsee, M. and Mangini, A. (1992). General properties of the paramagnetic centre at g=2.0006 in carbonates. *Quaternary Science Reviews*, **11**, 165-172.

Duller, G.A.T. (1996). Recent developments in luminescence dating of Quaternary sediments. *Progress in Physical Geography*, **20**, 127-145.

Huntley, D.J., Godfrey-Smith, D.I. and Thewalt, M.L.W. (1985). Optical dating of sediments. *Nature*, **313**, 105-107.

Ikeya, M. (1993). *New applications of electron spin resonance*. World Scientific, London.

Lamothe, M., Balescu, S. and Auclair, M. (1994). Natural IRSL intensities and apparent luminescence ages of single feldspar grains extracted from partially bleached sediments. *Radiation Measurements*, **23**, 555-561.

Murray, A.S. and Roberts, R.G. (1997). Determining the burial time of single grains of quartz using optically stimulated luminescence. *Earth and Planetary Science Letters*, **152**, 163-180.

Pilbrow, J.R. (1990). *Transition ion electron paramagnetic resonance*. Clarendon Press, Oxford.

Spooner, N.A. (1994). On the optical dating signal from quartz. *Radiation Measurements*, **23**, 593-600.

Spooner, N.A., Prescott, J.R. and Hutton, J.T. (1988). The effect of illumination wavelength on the bleaching of the thermoluminescence (TL) of quartz. *Quaternary Science Reviews*, 7, 325-329.

Wertz, J.E. and Bolton, J.R. (1972). *Electron Spin Resonance: Elementary Theory and Practical Applications*. McGraw-Hill, New York.